Coherence and Correlation Effects in Coupled Quantum Dot Systems

Zur Erlangung des akademischen Grades eines
DOKTORS DER NATURWISSENSCHAFTEN
der Fakultät für Physik der Universität (TH)
Karlsruhe

genehmigte

DISSERTATION

von

Dipl.-Phys. Stefan Legel
aus Detmold

Contents

Chapter 1

Introduction

The rapid development of fabrication techniques for nanosize structures, the routine availability of low temperatures, and ground-breaking advances in experiments have opened entirely new perspectives on quantum effects in electron transport. Consequences of charge quantization, coherence phenomena and quantum correlations have become observable and give rise to continued fundamental research and new functionalities for technical applications. Theories with high predictive power accelerate the progress and in many cases initiate a new path. Seemingly simple models often yield a rich and unexpected behavior which fertilizes the search for novel physical effects.

Single-electron effects are an invaluable building block in the context of electron transport through nanostructures. In contrast to the common diffusive description of a continuous charge flow in conventional electronics, single-electron devices resolve the charge quantization. Electrons are transported in integer units and interact strongly if they are confined to a small region. In an effective capacitive description the influence of the interaction can be linked to the charging energy associated to a single electron, $E_\mathrm{C} := e^2/2C$, with the capacitance C of the confining structure. Today, controlled fabrication of quantum dots with capacitances of the order of 10^{-16} F and smaller are feasible. This implies a strong dominance of charging effects already in the Kelvin regime.

Quantum dots have attracted a lot of attention in experiment as well as in theory. Due to their well controlled separation from the environment and their broad range of tunability they are regarded as ideal model systems to study quantum effects and the influence of electron-electron interaction. The discrete energy spectrum of the confined semiconductor host establishes a relation to artificial atoms and molecules and opens the horizon to an interdisciplinary field. Moreover, the design of complex geometries which employ one or several quantum dots of various kinds drives vivid branches of ongoing research.

The basic behavior of a single quantum dot which is weakly coupled to electronic reservoirs is often sufficiently described by a classical master equation if the temperature is large compared to the coupling strength (yet small compared to the charging energy) and the transport is dominated by incoherent sequential tunneling of electrons. In this regime the tunnel rates can be calculated with simple Golden Rule arguments. This so-called Orthodox Theory captures the fundamental influence of charging effects. In particular, it

describes the appearance of the Coulomb blockade where sequential transport is exponentially suppressed by the interaction.

However, the limitations of the scheme become apparent as soon as quantum fluctuations, coherence effects and correlation phenomena start to play a decisive role for the properties of a system. Specifically, two kinds of problems are encountered: The first is the order of the perturbation expansion. In the crossover to the Coulomb blockade, for instance, cotunneling processes start to dominate the transport. Here, electrons tunnel in a correlated fashion via a virtual state and may yield coherent contributions. For stronger coupling (or lower temperature), quantum fluctuations lead to renormalization effects which modify the internal structure of the system and, thus, the transport. (For even stronger coupling or lower temperature, in general, processes of arbitrary order have to be taken into account. So-called resonant tunneling, or complicated many-particle correlated states may give rise to a qualitatively new behavior, including so-called Kondo physics.) These problems might be overcome to some (small) extent by incorporating higher orders in the perturbation expansion in the tunneling, but a second problem of conceptual nature remains: A coherent evolution of a general density matrix can not be described with classical master equations.

In the systems considered in this thesis we have to deal with both problems. We use a real-time transport theory to derive kinetic equations for the evolution of the full density matrix of a system of two coherently coupled quantum dots. We are particularly concerned with the behavior in general nonequilibrium situations and the effect of a strong onsite Coulomb interaction. It turns out, that the coherent evolution of the driven system induces quantum correlations between the electron spins on the spatially separated quantum dots, which can be interpreted as the generation of entanglement. We study in detail the precursors of this phenomenon and focus on the coherence signatures in the stationary transport. A systematic expansion up to second order in the coupling strength allows us to regard cotunneling as well as renormalization corrections and analyze how Coulomb interaction affects the coherence of the transport.

To enter the field of electron tunneling through nanostructures we start with a brief introduction of basic concepts in single-electron devices and the phenomenon of Coulomb blockade (chapter 2). Via a capacitive description of a single-electron transistor we motivate the prominent Anderson model for quantum dots. It will serve as a basis for the more complex models discussed in this thesis. With an intuitive picture we contrast the usual sequential tunneling processes with cotunneling and point out the importance of renormalization corrections. Furthermore, the relevance of Aharonov-Bohm interferometry for the identification of quantum coherence is explained.

The scheme of the Real-time Transport Theory presented in chapter 3 allows us to systematically analyze the evolution of the state of a quantum dot system coupled to electron reservoirs. Coulomb interaction and nonequilibrium effects can be rigorously included and transport properties can be studied in detail. We introduce the diagrammatic method for an expansion in the tunnel-coupling strength of a quantum dot system to reservoirs. It enables us to regard sequential tunneling, cotunneling and renormalization processes on the same footing. Anticipating the coherently coupled multi-dot systems considered within

this thesis we particularly emphasize the importance of offdiagonal contributions to the kinetic equations for the determination of the coherent evolution of the density matrix. At the end of chapter 3 we sketch some results for single quantum dots which serve as a reference for the more complex setups.

A system of central concern and one of the main building blocks of this work consists of two quantum dots with strong onsite Coulomb repulsion coherently coupled to a joint reservoir. In chapter 4 we introduce the model and analyze the time evolution of the full reduced density matrix. The most important result is that in nonequilibrium a coherent evolution of the system can induce the generation of spin entanglement between electrons on the spatially separated quantum dots. The underlying mechanism relies on the fact that two electrons in the double-dot form a so-called Werner state with an enhanced singlet probability if the system is charged from the common reservoir. We emphasize that this is a decided nonequilibrium effect which does not require a finite singlet-triplet energy splitting. In a second part we extend the setup with two additional leads and apply a bias voltage to drive the system out of equilibrium. An enhanced probability for spin entanglement is found in the steady state which underlines the dynamical nature of the effect.

A crucial precursor for the generation of spin entanglement in nonequilibrium is the formation of coherent superposition states with a single electron in the double dot. To study the interplay of the coherent evolution of the state of the system with the coherence of the transport we embed two quantum dots in an Aharonov-Bohm interferometer (chapter 5). The stationary density matrix becomes phase dependent which leads to interference signatures in the current already in lowest order tunneling and linear response. We particularly focus on the question how a strong onsite Coulomb interaction affects the coherence of the transport. In this context we suggest an intuitive interpretation of the offdiagonal evolution of the density matrix and its influence on the Aharonov-Bohm signal. We predict clear asymmetries in the differential conductance which can be traced to the Coulomb interaction on the dots. Cotunneling and renormalization effects are discussed, and we identify unexpected conductance contributions which yield qualitative asymmetries.

In chapter 6 we analyze a setup with two spatially separated quantum dots which allows the creation and detection of nonequilibrium spin entanglement. The two dots are coupled coherently to a joint source electrode and to two independent drain reservoirs. An additional joint reservoir closes an Aharonov-Bohm geometry and serves as a probe. By applying a strong bias voltage electrons are driven from the source via the double dot to the drains. Under certain conditions spin entanglement can be created between the electrons in the spatially separated quantum dots which manifests itself in a strong imbalance between singlet and triplet probabilities. We identify regimes in which this imbalance can be detected by the suppression of Aharonov-Bohm oscillations in the probe. The suggested scheme provides a proof of concept for the entanglement generation in coherently coupled, nonequilibrium quantum dots.

Motivated by recent experiments we finally consider two capacitively coupled quantum dots with independent reservoirs (chapter 7). We concentrate on the cotunneling contribution to the conductance in the regime where lowest order tunneling is suppressed by

the interaction between the dots. The effect of low-order quantum fluctuations on the asymmetries of the signal is discussed.

Chapter 2

Basics of Single-Electron Tunneling

In nanostructures the quantum nature of electrons plays a dominant role, and under certain conditions the transport of single electrons can be resolved. The confinement to very small regions leads to a fundamental importance of the electron-electron interaction. This is essential for the behavior of many nanoscale devices. In quantum dots an additional quantization of the electron energies due to the finite size of the constriction can be observed and employed.

2.1   Single-Electron Devices

One of the simplest single-electron devices we can think of is a thin potential barrier between two electrodes: a tunnel junction. Compared to a classical capacitance the insulating layer has to be thin enough such that tunneling of electrons is possible. On the other hand, in contrast to a classical ohmic resistor, charge can cross the barrier only in discrete units of the elementary electron charge $e \approx 1.602 \times 10^{-19}\,\mathrm{C}$. The quantized transport leads to fundamentally new effects as compared to the conventional picture of diffusive transport. The occurence of shot noise, for instance, is by definition a consequence of the discrete current (for review see e.g. Refs. [20, 77]).

Small metallic islands or semiconductor quantum dots, which are among the favorite device components in nano- and mesoscopic electronics, can be realized by confining electrons to small areas wich are coupled to the environment via tunnel junctions. They constitute ideal model systems to study in a controlled way quantum effects and the influence of the Coulomb interaction between the electrons on the transport. Especially semiconductor quantum dots are often considered as tunable toy models for single atoms or molecules. The former have the advantage that the transport properties can be modified in situ by tuning the system's parameters in an adequate geometry. In contrast to metallic islands, which have a quasi continuous spectrum, semiconductor quantum dots show an energy quantization already at a size of the order of $100\,\mathrm{nm}$ due to the large Fermi wavelength of the electrons. The energy spectrum becomes discrete and can be associated to the shell structure of atoms.
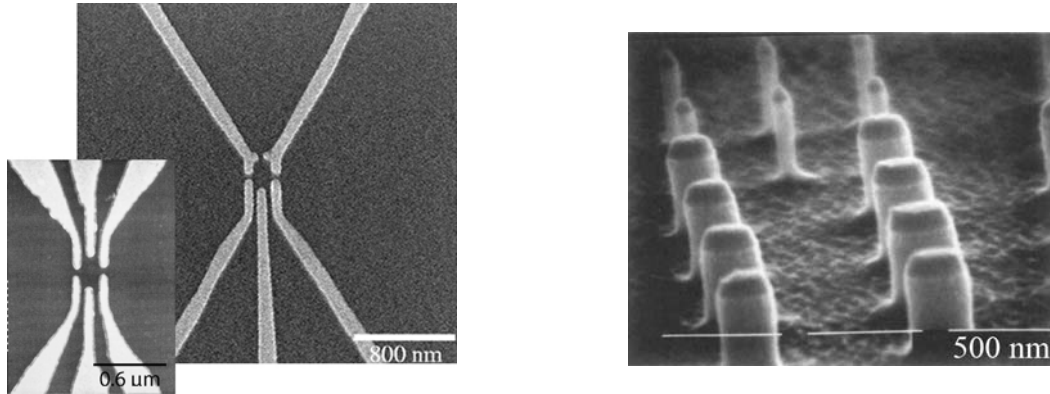
Figure 2.1:   Left picture: Examples of lateral realizations of a quantum dot with metallic gates on top of a GaAs/AlGaAs heterostructure [2]. Right picture: Scanning electron micrograph of one of the first realizations of vertical semiconductor quantum dots [1].

Quantum dots and metallic islands for nano-electronics have been realized in vertical and lateral arrangements based on semiconductor heterostructures, with metallic grains which are contacted e.g. with a scanning tunneling microscope, and ultimately even with molecules. Due to their high degree of tunability lateral setups became very popular for many research applications. Typical lateral quantum dots are realized with lithographically patterned metallic gate electrodes on top of a two-dimensional electron gas (2DEG) which is formed parallel to the surface of a GaAs/AlGaAs heterostructure, for instance. The gate electrodes can be used to electrostatically deplete regions of the 2DEG underneath and to define the geometry of the quantum dot. Furthermore, the tunnel coupling can be tuned by the gate potentials and the energy levels can be shifted. Another often used technique is based on etching a predefined gate geometry into the semiconductor plane. The Coulomb energy of electrons in the confined areas can be characterized by a capacitance which depends on the size of the dot. In recent experiments capacitances of the order of 10^{-16} F and smaller have been documented.

2.2   Charging Effects and Coulomb Blockade

In this section we introduce basic concepts of charging effects in small metallic islands and quantum dots. We focus on the so-called Coulomb blockade which is essential for the considerations within this thesis. It results from a combination of charge quantization and the fundamental importance of the Coulomb interaction between electrons confined to a small region.

Let us consider a small island connected via tunnel junctions to a left and a right reservoir. An additional gate electrode is coupled capacitively and can be used to tune the electrochemical potential of the island. The tunnel junctions can be well characterized by a capacitance and a resistance as sketched in the schematic diagram in Fig. 2.2. The total
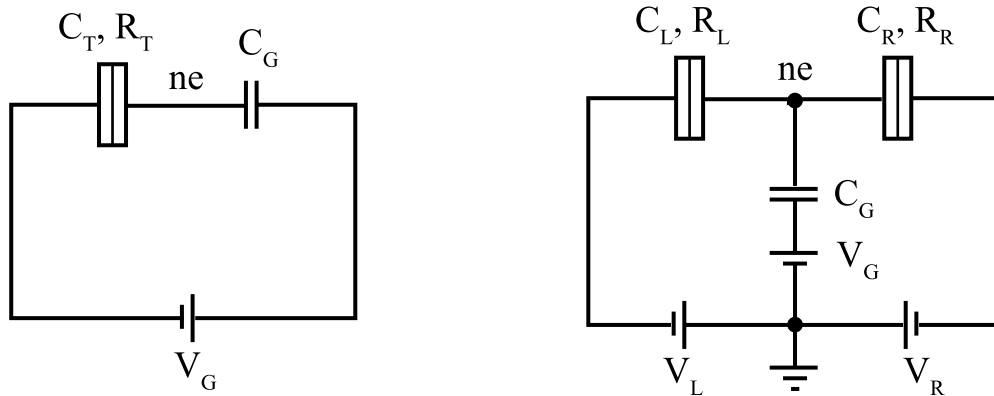
Figure 2.2: Capacitive models of the single-electron box and the single-electron transistor.

capacitance of the island, $C := C_{\mathrm{L}} + C_{\mathrm{R}} + C_{\mathrm{G}}$, introduces an energy scale which is defined by the charging energy associated to a single electron

$$E_{\mathrm{C}} := \frac{e^2}{2C} \, . \tag{2.1}$$

Hence, for n excess electrons on the island and an external charge of $en_x := C_{\mathrm{L}}V_{\mathrm{L}} + C_{\mathrm{R}}V_{\mathrm{R}} + C_{\mathrm{G}}V_{\mathrm{G}}$ the Coulomb interaction is accounted for by the charging energy

$$E_{\mathrm{ch}}(n, n_x) = E_{\mathrm{C}} \left(n - n_x\right)^2 + c(n_x) \, , \tag{2.2}$$

where $c(n_x)$ does not depend on n and is not important for the following reasoning. As function of the external charge, which can be tuned continuously by the gate voltage, the charging energy can be represented by a parabola for each number n of electrons on the island (compare left hand side of Fig. 2.3). For low temperature and small bias voltage,

$$E_{\mathrm{C}} \gg k_{\mathrm{B}}T, eV \, , \tag{2.3}$$

the system can minimize its energy by changing the number of electrons on the island at the degeneracy points given by $E_{\mathrm{ch}}(n, n_x) = E_{\mathrm{ch}}(n+1, n_x)$ (or equivalently $n_x = n + 1/2$). Thus, even for a continuous density of states the island is charged in a steplike fashion with increasing gate voltage. This is the well-known Coulomb staircase of a single-electron box which is equivalent to our island system if we disable one of the tunnel junctions or consider the system simply in equilibrium, $V_{\mathrm{L}} - V_{\mathrm{R}} = 0$.

During a transport cycle from say the left to the right, in which an electron hops from the left lead onto the island and off to the right reservoir (corresponding to the classical picture of sequential tunneling), the number of electrons on the island has to change. Consequently, transport can only occur near the degeneracy points where n_x is half-integer. The resulting periodic structure of the current or the conductance, sketched on the right hand side of Fig. 2.3, is known as Coulomb oscillations. In the region between
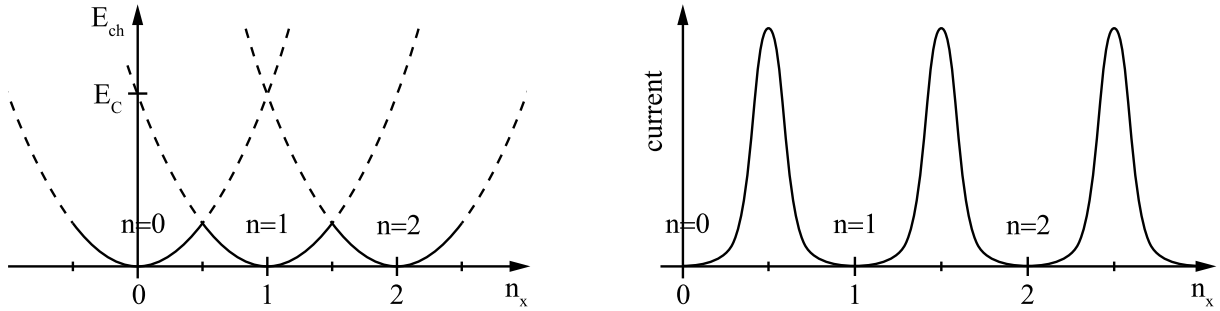
Figure 2.3:   On the left hand side the charging energy is sketched as function of the gate voltage for various numbers n of electrons on the island. The ground state of the system is indicated by the solid line. On the right the corresponding Coulomb oscillations of the electron transport through the island are illustrated.

two subsequent peaks, with a mutual distance corresponding to $2E_C$, we find the so-called Coulomb blockade where the transport is suppressed. The possibility to control the transport through the device in this manner by the gate voltage yields the notion of the single-electron transistor.

2.3   Anderson Model

Additional to the classical concept of the charging energy which explains the appearance of Coulomb oscillations we often might have a level-quantization due to the confinement of electrons to very small regions. This especially applies to semiconductor quantum dots in which the large Fermi wavelength promotes the quantization. In this case the total energy of the dot with n electrons is given by

$$E(n, n_x) = E_{\mathrm{ch}}(n, n_x) + \sum_{i=1}^{n} \tilde{\varepsilon}_j \tag{2.4}$$

where the spin index of the electrons is absorbed in the index j (i.e. the energies have to be counted repeatedly for spin degenerate levels). Denoting the level spacing by $\delta\varepsilon$ the resulting difference between two subsequent resonances at the degeneracy points $E(n, n_x) = E(n+1, n_x)$ becomes $2E_C + \delta\varepsilon$. In the remainder we restrict ourselves to the limiting case of large level spacing, $\delta\varepsilon \to \infty$. (For small level spacing, $\delta\varepsilon \to 0$, the spectrum is quasi continuous and describes a metallic island which is not considered.) Specifically, we express the Hamiltonian $H = H_{\mathrm{res}} + H_{\mathrm{dot}} + H_{\mathrm{t}}$ for a single-level quantum dot tunnel-coupled to a left and a right reservoir by the Anderson model [6]. The electrons in the decoupled, noninteracting reservoirs are described by

$$H_{\mathrm{res}} = \sum_{r} \sum_{k\sigma} \varepsilon_{rk\sigma}\, a_{rk\sigma}^{\dagger} a_{rk\sigma} \,, \tag{2.5}$$

where $a_{rk\sigma}^\dagger$ and $a_{rk\sigma}$ are creation and annihilation operators in the left and right reservoir, $r \in \{\mathrm{L}, \mathrm{R}\}$, respectively. The energies $\varepsilon_{rk\sigma}$ are labeled furthermore with the wave number k and spin σ of the electrons. The decoupled quantum dot is modeled by

$$H_{\mathrm{dot}} = \sum_\sigma \varepsilon_\sigma \, c_\sigma^\dagger c_\sigma + U \, c_\uparrow^\dagger c_\downarrow^\dagger c_\downarrow c_\uparrow \tag{2.6}$$

with the level energy ε_σ and the creation and annihilation operators $c_\sigma^\dagger$ and c_σ. The Coulomb interaction between the electrons on the dot is taken into account in the Hubbard U which is closely related to the former charging energy by $U = 2E_{\mathrm{C}}$. Moreover, the identification $\varepsilon = \tilde{\varepsilon} + E_{\mathrm{C}} \, (1 - n_x)^2$ shows the equivalence to the capacitive model. Thus, the level energy ε can be tuned via the gate voltage. (Effectively, the level position may also be influenced by the bias voltage though.) The quantum dot is coupled to the reservoirs by the tunnel Hamiltonian

$$H_{\mathrm{t}} = \sum_r \sum_{k\sigma} \left(t_{rk\sigma} \, c_\sigma^\dagger a_{rk\sigma} + \mathrm{h.c.} \right) \tag{2.7}$$

with the tunnel matrix elements $t_{rk\sigma}$. The spin of the electrons is conserved during a tunneling process and we usually even assume the tunnel matrix to be completely independent of the spin, $t_{rk\sigma} = t_{rk}$.

The classical rate for electrons tunneling between the dot and the reservoirs can be calculated with simple Golden Rule arguments which yields $2\pi \, \gamma = \hbar \, \Gamma_r(\omega) f_r^\pm(\omega)$ with the coupling strength

$$\Gamma_r(\omega) = 2\pi \sum_k |t_{rk}|^2 \, \delta(\omega - \varepsilon_{rk\sigma}) \,. \tag{2.8}$$

The Fermi distributions of electrons (or holes) in reservoir r are denoted by $f_r^+(\omega) := (\exp[\beta(\omega - \mu_r)] + 1)^{-1}$ and $f_r^-(\omega) := 1 - f_r^+(\omega)$ with the electrochemical potential $\mu_r = -eV_r$. The positive index corresponds to a tunneling into the dot whereas the negative one indicates a leaving electron. In general, the tunneling leads to a finite lifetime τ of a dot state, and consequently, to a broadening $\Gamma = \hbar/\tau$ of the level. If the tunneling is independent of the energy we can identify $\Gamma = \Gamma_{\mathrm{L}} + \Gamma_{\mathrm{R}}$.

The model for the single-level quantum dot is simpel. Nevertheless, it already reveals quite interesting features, especially if the Coulomb interaction plays a role (e.g. compare the last sections of the next chapter). A rich variety of physical effects can be studied in systems consisting of several levels or quantum dots. In general, there is a lot of freedom to imagine sophisticated setups for one or the other purpose. However, the first step in climbing the ladder of complexity is to consider two quantum dots or levels. The gain of effects is enormous and some features may even raise ideas for new functional devices.
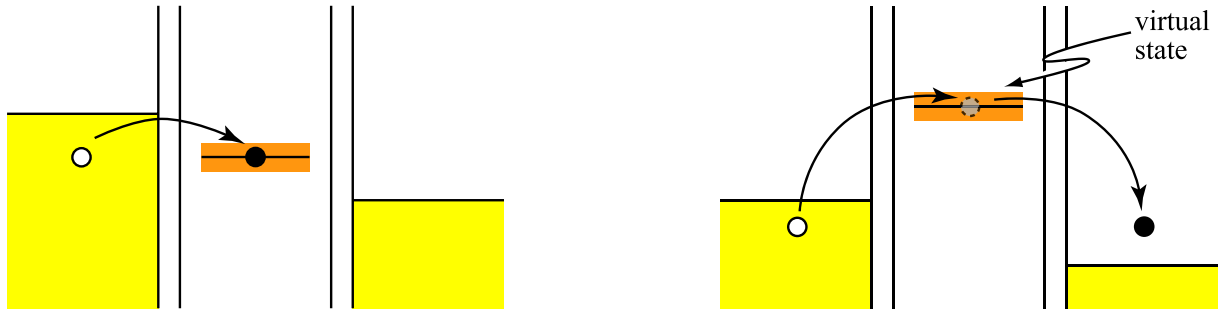
Figure 2.4: Tunneling processes for the single-level quantum dot: sequential tunneling (left sketch) is uncorrelated, the right sketch shows cotunneling via a virtual state.

2.4 Higher Order Tunneling and Renormalization Effects

The current through a driven quantum dot system is large if a dot level lies within the transport window opened by the bias voltage. For weak coupling, $\Gamma \ll k_{\mathrm{B}}T$, sequential tunneling dominates in this situation. Electrons enter the dot and leave it again (or vice versa) one after the other in an uncorrelated manner (see also the left sketch in Fig. 2.4). The differential conductance $\partial I/\partial V$ shows a peak as function of the gate voltage if the bias voltage is small, $eV \ll k_{\mathrm{B}}T, \Gamma$. For a large but fixed bias the current increases if we tune the dot level into the transport window, saturates, and decreases again if the level leaves the window. In the differential conductance two peaks can be resolved, one for each shoulder, if $eV > k_{\mathrm{B}}T, \Gamma$.

A pecularity of a system with two interacting levels which are asymmetrically coupled is the possibility to observe a negative differential conductance. The entrance of a weaker coupled second level into the transport window may suppress the tunneling via a first level due to the interaction between them. Consequently, the current decreases with increasing bias.

In the Coulomb blockade sequential tunneling is energetically forbidden and exponentially suppressed. However, higher order processes such as cotunneling via a virtual state are still possible (see e.g. the right sketch in Fig. 2.4). They give the leading contribution to the current beside the resonance peak [7, 28, 29]. By definition, the cotunneling processes in a single-level quantum dot are elastic, i.e. the energy is conserved. In contrast, cotunneling in a metallic island is most probably inelastic because of the large number of available states.

As mentioned, the tunneling between the reservoirs and the dot system modifies the properties of the bare quantum dot. Quantum fluctuations may lead to a renormalization of the energies and a broadening of the level(s) due to a finite lifetime. This becomes more important for a slightly stronger coupling, $\Gamma \lesssim k_{\mathrm{B}}T$, when quantum fluctuations are enhanced. As a consequence, the position and shape of the conductance peaks change.

It is one of the virtues of the Real-Time Transport Theory introduced in the following chapter which enables us to take these renormalization effects systematically into account. Like cotunneling or higher order transport contributions they show up as correction terms in the expansion for weak coupling.

In the case of strong coupling or very low temperature, $k_\mathrm{B} T \lesssim \Gamma$, the finite width of the dot level due to its coupling to reservoirs can be resolved. In this regime higher order tunneling is very important and resonant tunneling phenomena [8,30,31] and Kondo physics are expected to occur. Especially for temperatures below the Kondo temperature,

$$T_\mathrm{K} \sim \frac{\sqrt{\Gamma U}}{2} \, \exp\left(\frac{\pi \, \varepsilon \, (\varepsilon + U)}{\Gamma U}\right),\tag{2.9}$$

a complicated many-particle groundstate can be formed which gives rise to the Kondo effect [9–16]. If the level of the dot lies well below the Fermi edge of the leads and the onsite Coulomb repulsion U is large, the dot is predominantly occupied with a single spin which acts as a magnetic impurity. For sufficiently strong tunnel coupling spin fluctuations can lead to a correlated state of the localized spin and reservoir electrons. This, in turn, can induce an increase of the density of states at the Fermi edge and an enhancement of the conductance.

In the remainder of this thesis we are mainly concerned with lowest order tunneling, cotunneling and renormalization effects in systems consisting of coherently coupled quantum dots. Throughout the work we assume weak coupling and low temperatures but avoid the regime of resonant tunneling and the Kondo effect.

2.5 Aharonov-Bohm Interferometry

Standard transport experiments are an obligatory tool for the investigation of systems on the meso- and nanoscale. They yield a lot of information about the properties of quantum dot systems and give hints for possible functionalizations. Many important quantum effects have been observed with the help of typical signatures in the I-V characteristics. Nevertheless, the influence on the phase of the electronic wave function during a transport process is not accessible with these measurements. The phase information is yet of major importance if we are aiming at quantum correlation effects, quantum information processing, or simply if we operate a system in a regime in which quantum interference plays a role.

In 1959 Y. Aharonov and D. Bohm [76] prepared the ground for quantum interferometry. They found that an electron wave function encircling an area threaded by a magnetic field accumulates a phase depending on the enclosed magnetic flux. Thus, two partial waves propagating through the arms of an Aharonov-Bohm interferometer undergo a mutual phase shift which can be controlled via the magnetic flux threading the ring structure. At the drain the waves interfere constructively or destructively depending on their phase difference. To gather information about the phase of electrons tunneling through quantum dots and especially for the investigation of the effect of the Coulomb interaction on the
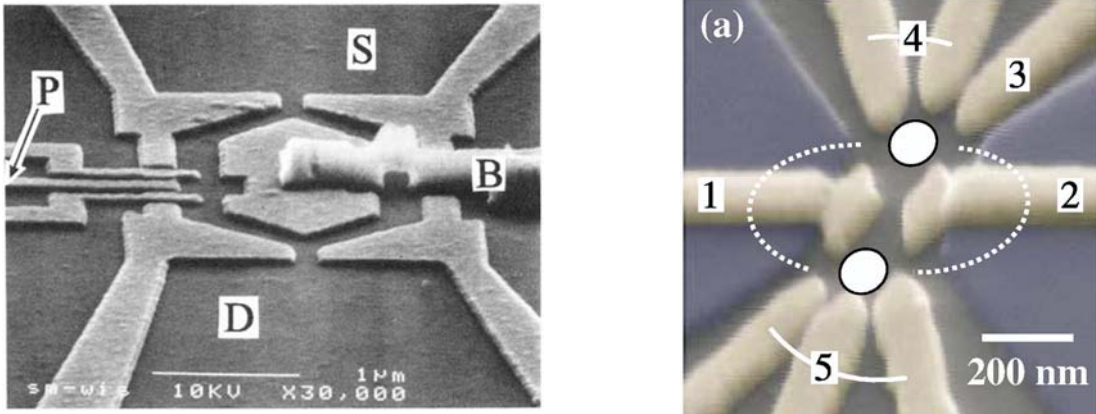
Figure 2.5:   Pioneering experimental realizations of Aharonov-Bohm interferometers with one [79] or two [41] embedded quantum dots.

coherence of the transport, quantum dots have been successfully embedded in Aharonov-Bohm interferometers. After first theoretical works, e.g. [78], pioneering experiments with one [79] and two quantum dots [41] in the arms of an Aharonov-Bohm ring have been realized (compare also Fig. 2.5) (for further references see also chapter 5). Ideas to employ Aharonov-Bohm oscillations to distinguish singlet and triplet states and detect entanglement in double dot systems were first documented in Ref. [91].

In this thesis we will refer several times to quantum dots embedded in an Aharonov-Bohm interferometer. In chapter 5 we investigate how the Coulomb interaction on quantum dots affects the coherence of the transport, and the signatures in the interference pattern of an Aharonov-Bohm interferometer are certainly a main topic. In chapter 4 we are concerned with coherently coupled quantum dots for which Aharonov-Bohm experiments like in Refs. [41, 42] deliver a proof of realizability. Finally, in chapter 6 we use Aharonov-Bohm oscillations to probe the stationary state of a hybrid system in nonequilibrium. Our aim is to find signatures of entanglement in the transport.

Chapter 3

Real-Time Transport Theory

Many transport phenomena in single-electron devices can be understood within a scattering theory or with classical rate equations and Fermi's Golden Rule, for example. Both approaches allow for finite temperature and have a great range of applicability. The scattering approach [22–27], for instance, allows studies of coherent transport through mesoscopic devices with arbitrary tunneling barriers but is restricted to systems with non-interacting particles. Interacting systems, on the other hand, can be treated with classical master equations and transfer rates calculated with Fermi's Golden Rule. The so-called Orthodox Theory is based on a perturbation expansion in the coupling parameter. It is justified if the coupling to the reservoirs is very weak, i.e. the broadening of the spectral density of the system due to tunneling has to be negligable. The lowest order perturbation theory with Fermi's Golden Rule is a well-known standard for incoherent transport. Coherent processes are taken into account in the extension of the expansion to higher orders [28, 29].

Nevertheless, the formalism relies on the calculation of classical probabilities with master equations. It is convenient if the density matrix which describes the general mixed state of the system remains in a diagonal form. The limit of the approach is reached if the evolution of the off-diagonal terms is nontrivial and depends on important transport parameters. In this case we would need to know the basis of the Hilbert space in which the stationary density matrix appears to be diagonal for each set of parameter values. We may set up and solve the master equations in this specific basis and calculate the transport according to the formalism. However, the tricky task is to figure out the appropriate basis. In general, the parametrization of the coordinate system is a complicated problem beyond the accessibility of the rather classical approach.

It is therefore desirable to have a technique which is able to treat nonequilibrium systems with arbitrary interaction and which captures the dynamics of the full density matrix including the evolution of the off-diagonal terms. It should allow a complete and consistent evaluation of all contributions up to a given order in the tunneling. In the following we introduce a diagrammatic approach of the Real-time Transport Theory [30–35] which meets the mentioned requirements and allows a systematic analysis of Coulomb interaction phenomena in general nonequilibrium situations.

3.1 Diagrammatic Expansion

Keeping in mind the problems we would like to address, namely electron transport through quantum dot systems coupled to electron reservoirs, we choose the language for the introduction to the technique accordingly. However, despite the rather specific presentation we do not want to disguise the more general character of the method. The basic idea of the approach is to integrate out the reservoir degrees of freedom and derive an exact kinetic equation for the reduced density matrix of the quantum dot system. The kernel of the integro-differential equation can be calculated in a diagrammatic perturbation expansion in the tunneling.

In the following we will assume a general model Hamiltonian of the form

$$H = H_{\text{res}} + H_{\text{dots}} + H_{\text{t}} \,. \tag{3.1}$$

The leads to which the quantum dot system is coupled via the tunnel Hamiltonian H_{t} are assumed to be large, non-interacting reservoirs in local equilibrium. Typically, they can be expressed by

$$H_{\text{res}} = \sum_r \sum_{k\sigma} \varepsilon_{rk\sigma} \, a_{rk\sigma}^\dagger a_{rk\sigma} \,, \tag{3.2}$$

where $a_{rk\sigma}^\dagger$ and $a_{rk\sigma}$ are creation and annihilation operators of reservoir electrons with energy $\varepsilon_{rk\sigma}$. The individual reservoirs are labeled by r, momenta and channels are summarized in k and the physical spin of an electron is denoted by σ. The quantum dot system can be modeled by

$$H_{\text{dots}} = \sum_i \left[\sum_\sigma \varepsilon_{i\sigma} \, c_{i\sigma}^\dagger c_{i\sigma} + \sum_j U_{ij} \, c_{i\uparrow}^\dagger c_{j\downarrow}^\dagger c_{j\downarrow} c_{i\uparrow} \right], \tag{3.3}$$

where the energy levels are denoted by $\varepsilon_{i\sigma}$, and $c_{i\sigma}^\dagger$ and $c_{i\sigma}$ are the respective creation and annihilation operators of electrons. Possible interactions between the single particles in the dot system are summarized in the matrix U_{ij}. In particular, in the case of single level quantum dots, the diagonal of the interaction matrix describes the Coulomb interaction between the electrons on each individual dot, whereas the interaction between the dots is represented by the off-diagonal. The only term which couples the quantum dot system to the reservoirs is given by the tunnel Hamiltonian

$$H_{\text{t}} = \sum_r \sum_{k\sigma i} \left(t_{rki\sigma} \, c_{i\sigma}^\dagger a_{rk\sigma} + \text{h.c.} \right), \tag{3.4}$$

with the tunnel matrix elements $t_{rki\sigma}$ which may depend in general on all quantum numbers of the complete system.

Equivalently, we can condense the Hamiltonian of the dot system and the tunneling term in the form

$$H_{\text{dots}} = \sum_\chi \varepsilon_\chi |\chi\rangle\langle\chi| \quad \text{and} \quad H_{\text{t}} = \sum_r \sum_{k\sigma,\chi\chi'} \left(t_{rk\sigma,\chi'\chi} \, a_{rk\sigma} \, |\chi'\rangle\langle\chi| + \text{h.c.} \right) \tag{3.5}$$

with the eigenenergies ε_χ of the many-body states $|\chi\rangle$ of the separated, interacting quantum dot system.

We assume the reservoirs and especially the applied bias voltage between the reservoirs to be independent of time, as well as the dot levels in which the gate voltage is absorbed. (This is not a real restriction since by unitary transformations the time dependent part of the gate or bias voltages can be mapped onto an effective time dependency of the tunneling matrix as shown in Ref. [34].) At a time t_0 we switch on the tunneling, i.e. $H_{\mathrm{t}}(t)$ vanishes for times t prior to t_0, and the dot system will be driven out of its static equilibrium. The initial density matrix of the entire system factorizes $\rho_0 := \rho(t_0) = \rho_{\mathrm{res}}^{\mathrm{eq}}(t_0)\,\rho_{\mathrm{dots}}(t_0)$ into the equilibrium density matrix of the reservoirs and the density matrix of the quantum dot system. As mentioned above, we assume the reservoirs to be large enough such that they stay in equilibrium even if we add or remove a few electrons. They can, therefore, be described by a grandcanonical equilibrium density matrix

$$\rho_{\mathrm{res}}^{\mathrm{eq}} = \frac{1}{Z_{\mathrm{res}}}\,\exp\left(-\beta(H_{\mathrm{res}} - \sum_r \mu_r \hat{n}_r)\right) \tag{3.6}$$

with fixed electrochemical potentials μ_r, the number operators $\hat{n}_r := \sum_{k\sigma} a_{rk\sigma}^\dagger a_{rk\sigma}$, and $\beta := 1/(k_{\mathrm{B}}T)$. The normalization condition $\operatorname{tr}\rho_{\mathrm{res}}^{\mathrm{eq}} = 1$ determines the factor Z_{res}.

In general, the diagrammatic approach to the Real-time Transport Theory provides a scheme to calculate the time evolution of the statistical expectation value

$$\langle A(t)\rangle = \operatorname{tr}\left(\rho_0\,A(t)_{\mathrm{H}}\right) \tag{3.7}$$

of a given operator A (here in the Heisenberg picture). For the diagrammatic expansion it is convenient to change to the interaction picture

$$A(t)_{\mathrm{H}} = \widetilde{T}\,\exp\left(-\mathrm{i}\int_t^{t_0} \mathrm{d}t'\,H_{\mathrm{t}}(t')_{\mathrm{I}}\right)\,A(t)_{\mathrm{I}}\,T\,\exp\left(-\mathrm{i}\int_{t_0}^t \mathrm{d}t'\,H_{\mathrm{t}}(t')_{\mathrm{I}}\right), \tag{3.8}$$

where T and $\widetilde{T}$ denote the time- and anti-time-ordering operators, respectively. Here and in the following sections we set $\hbar$ to unity during the calculations, for the sake of transparency. However, in the explicit expressions for the current and conductance of the considered setups we include it again. The operators A and H_{t} are expressed in the interaction picture

$$A(t)_{\mathrm{I}} = \mathrm{e}^{(\mathrm{i}(H_{\mathrm{res}}+H_{\mathrm{dots}})(t-t_0))}\,A\,\mathrm{e}^{(-\mathrm{i}(H_{\mathrm{res}}+H_{\mathrm{dots}})(t-t_0))}\,. \tag{3.9}$$

The time evolution forward in time from t_0 to t, where the operator A_{I} is acting, and then backward from t to the initial time t_0, can be represented by a closed time path, the so-called Keldysh contour [36–38] which is depicted in Fig. 3.1. Formally, we can rewrite the time integrals in the propagators as a single integral over the Keldysh contour

$$A(t)_{\mathrm{H}} = T_{\mathrm{K}}\,\exp\left(-\mathrm{i}\int_{\mathrm{K}} \mathrm{d}t'\,H_{\mathrm{t}}(t')_{\mathrm{I}}\right)\,A(t)_{\mathrm{I}}\,, \tag{3.10}$$
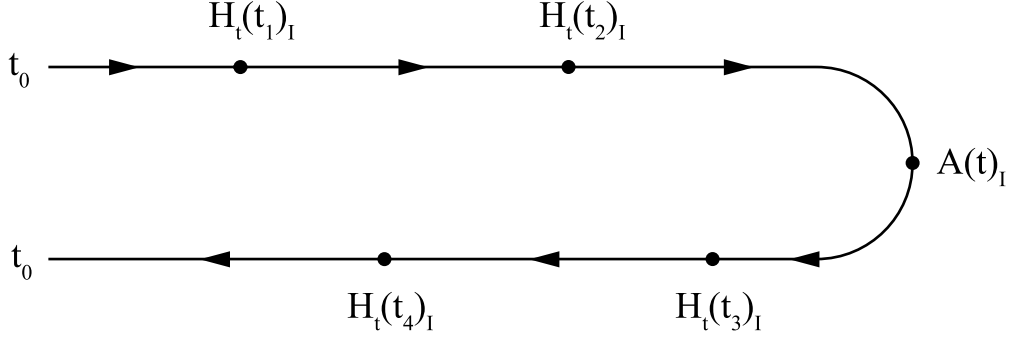
Figure 3.1:   Snapshot of the Keldysh contour for a term of fourth order in H_{t} before the contraction.

where we also introduce the Keldysh time-ordering operator T_{K} which orders all following operators, including $A(t)_{\mathrm{I}}$, along the Keldysh contour. In particular, the operators are rearranged during the integration such that $A(t)_{\mathrm{I}}$ is always acting at the right time.

We can now expand the Keldysh propagator and obtain an expression for the expectation value

$$\langle A(t) \rangle = \mathrm{tr} \left[\rho_0 \sum_{m=0}^{\infty} (-\mathrm{i})^m \int_{\mathrm{K}} \mathrm{d}t_1' \int_{\substack{\mathrm{K} \\ t_1' \geq t_2' \geq \ldots \geq t_m'}} \mathrm{d}t_2' \ldots \int_{\mathrm{K}} \mathrm{d}t_m' \, T_{\mathrm{K}} \left(H_{\mathrm{t}}(t_1')_{\mathrm{I}} \, H_{\mathrm{t}}(t_2')_{\mathrm{I}} \, \ldots \, H_{\mathrm{t}}(t_1')_{\mathrm{I}} \, A(t)_{\mathrm{I}} \right) \right]$$

$$(3.11)$$

in which the integrations are already ordered with respect to the Keldysh contour (see also Fig. 3.1) and all equivalent permutations are identified leading to a factor of $m!$ in the m-th term. Fig. 3.1, for example, depicts a snapshot of the diagrammatic representation of the fourth order term in the tunnel Hamiltonian. Each operator is represented by a vertex at the appropriate time on the contour. In the literature, vertices stemming from the time evolution of the system itself, i.e. vertices from H_{t}, are called internal, whereas vertices arising from external operators like A are called external.

In the next step we trace out the reservoir degrees of freedom. We remember that ρ_0 factorizes, and we know that the propagators from the interaction picture appearing for each operator can also be factorized because they do not include any coupling between the reservoirs and the dot system. This means that the reservoirs and the dot system can be traced independently.

By applying Wick's theorem to the field operators of the non-interacting reservoirs we can perform the trace by summing the contractions of all possible pairings of creation and annihilation operators, regardless their origin (H_{t} or A). Each contraction can be represented by an equilibrium distribution, i.e. in the case of electron reservoirs

$$\left\langle a_{rk\sigma}^{\dagger}(t)_{\mathrm{I}} \, a_{r'k'\sigma'}(t')_{\mathrm{I}} \right\rangle_{\rho_{\mathrm{res}}^{\mathrm{eq}}} = \delta_{rr'} \, \delta_{kk'} \, \delta_{\sigma\sigma'} \, \mathrm{e}^{-\mathrm{i}\varepsilon_{rk\sigma}(t-t')} f_r^+(\varepsilon_{rk\sigma})$$

$$\left\langle a_{rk\sigma}(t)_{\mathrm{I}} \, a_{r'k'\sigma'}^{\dagger}(t')_{\mathrm{I}} \right\rangle_{\rho_{\mathrm{res}}^{\mathrm{eq}}} = \delta_{rr'} \, \delta_{kk'} \, \delta_{\sigma\sigma'} \, \mathrm{e}^{-\mathrm{i}\varepsilon_{rk\sigma}(t-t')} f_r^-(\varepsilon_{rk\sigma}) \,.$$

$$(3.12)$$
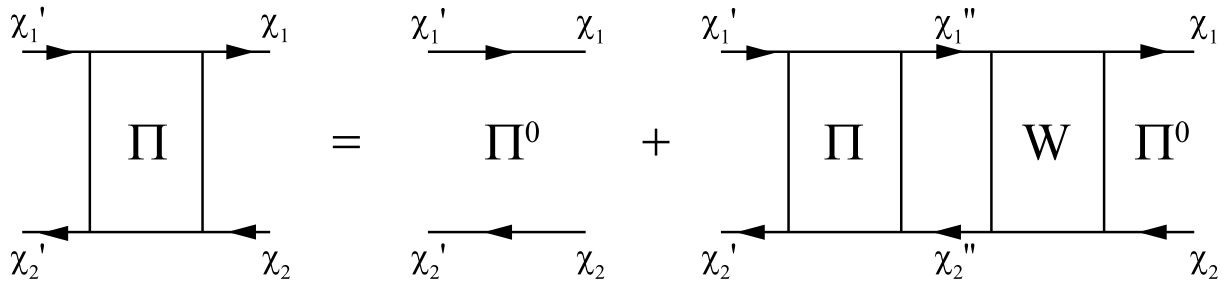
Figure 3.2: Dyson-like equation for the reduced propagator Π with the irreducible kernel **W**.

Diagrammatically the contractions are depicted by directed tunneling lines connecting the corresponding vertices (see e.g. Fig. 3.3). The detailed diagrammatic rules will be introduced in section 3.5.

The creation and annihiliation operators of the dot system appear quadratically in the interaction terms of the Hamiltonian and we can not apply Wick's theorem as long as we want to treat the interaction non-perturbatively. We stress that in the technique which we have already started to introduce we are able to proceed without any restriction to the interaction if we treat the dots' operators explicitly.

3.2 Kinetic Equation

In this section we sketch the derivation (Refs. [34, 35]) of a formally exact kinetic equation for the reduced density operator $\mathbf{p}(t) := \text{tr}_\text{res}\,\rho(t)$ of the coupled quantum dot system (tr_res denotes the trace over the reservoir degrees of freedom). In particular, we place special emphasis on the off-diagonal elements which account for the evolution of coherent superpositions of the many-body states.

The quantum statistical expectation values

$$p_{\chi_2}^{\chi_1}(t) := \left\langle |\chi_2\rangle\langle\chi_1|(t)\right\rangle \tag{3.13}$$

of the operators $\hat{p}_{\chi_2}^{\chi_1} := |\chi_2\rangle\langle\chi_1|$, acting on the reduced many-body system, are identical to the elements of the reduced density matrix,

$$\langle\chi_1|\mathbf{p}(t)|\chi_2\rangle = \text{tr}\left(\rho(t)\,\hat{p}_{\chi_2}^{\chi_1}\right) = p_{\chi_2}^{\chi_1}(t)\,, \tag{3.14}$$

in a given coordinate representation of the many-body Hilbert space. (The invariance of the trace under cyclic permutations of the operators – especially the time evolution operators – allows us to switch to the Heisenberg picture.)

We can express the propagation of the reduced density operator in time,

$$\mathbf{p}(t) = \mathbf{\Pi}(t, t') \cdot \mathbf{p}(t')\,, \tag{3.15}$$
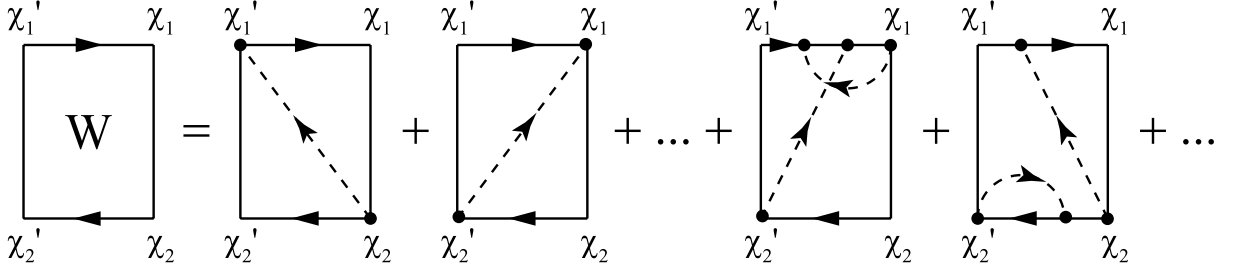
Figure 3.3: Series of irreducible diagrams for the Kernel element $W^{\chi_1\chi_1'}_{\chi_2\chi_2'}$.

with the help of the reduced propagator $\mathbf{\Pi}(t, t')$ which is an operator acting on the space of hermitian operators. It maps the density operator of the reduced system at time t' onto the density operator at time t. By construction it respects the trace, $\mathrm{tr}_{\mathrm{dots}}\left(\mathbf{\Pi}(t, t') \cdot \mathbf{p}(t')\right) = \mathrm{tr}_{\mathrm{dots}} \, \mathbf{p}(t') = 1$. In a coordinate representation we can write Eq. (3.15) for each element of the reduced density matrix,

$$p^{\chi_1}_{\chi_2}(t) = \sum_{\chi_1'\chi_2'} \Pi^{\chi_1\chi_1'}_{\chi_2\chi_2'}(t, t') \, p^{\chi_1'}_{\chi_2'}(t') \,. \tag{3.16}$$

The matrix element of the reduced propagator,

$$\Pi^{\chi_1\chi_1'}_{\chi_2\chi_2'}(t, t') := \langle\chi_2'| \, \mathrm{tr}_{\mathrm{res}} \, \rho^{\mathrm{eq}}_{\mathrm{res}} \, T_{\mathrm{K}} \, \exp\left(-\mathrm{i}\int_{\mathrm{K}} \mathrm{d}t'' \, H_{\mathrm{t}}(t'')\right) |\chi_2\rangle\langle\chi_1|(t)_{\mathrm{I}} \, |\chi_1'\rangle \,, \tag{3.17}$$

propagates from the state χ_1' at time t' along the Keldysh contour to the state χ_1 at time t and then backwards from state χ_2 at time t to the state χ_2' at time t' (see also left part of Fig. 3.2).

Setting $A = |\chi_2\rangle\langle\chi_1|$ in Eq. (3.11) we could start expanding and contracting the reservoir degrees of freedom and calculate the matrix elements of the reduced propagator by the sum of (absolutely) all diagrams with the respective many-body states at the corners. But fortunately, we have an alternative: we can rearrange the rather unpracticable sum such that we collect only all irreducible diagrams in the kernel $\mathbf{W}(t, t')$. A diagram is called irreducible if any vertical cut crosses at least one tunneling line (see e.g. Fig. 3.3). The reduced propagator can then be expressed in an iterative fashion in the style of a Dyson equation (Fig. 3.2),

$$\mathbf{\Pi}(t, t') = \mathbf{\Pi}^{(0)}(t, t') + \int_{t'}^{t} \mathrm{d}t''' \int_{t'}^{t'''} \mathrm{d}t'' \, \mathbf{\Pi}^{(0)}(t, t''') \cdot \mathbf{W}(t''', t'') \cdot \mathbf{\Pi}(t'', t') \,. \tag{3.18}$$

The bare propagator $\mathbf{\Pi}^{(0)}(t, t') = \exp(-\mathrm{i}\mathbf{\Delta}\,(t - t'))$ denotes the time evolution of the isolated dot system due to H_{dots} forward and backward on the Keldysh contour and include no contractions or tunneling lines (compare also Fig. 3.2). The energies of the many-body

states are encoded in the operator $\boldsymbol{\Delta}$. In a coordinate representation we can write

$$\Pi^{\chi_1 \chi_1'}_{\chi_2 \chi_2'}(t, t') = \Pi^{(0)\chi_1 \chi_1'}_{\chi_2 \chi_2'}(t, t') +$$
$$+ \sum_{\chi_1''' \chi_2'''} \sum_{\chi_1' \chi_2''} \int_{t'}^{t} \mathrm{d}t''' \int_{t'}^{t'''} \mathrm{d}t'' \, \Pi^{(0)\chi_1 \chi_1'''}_{\chi_2 \chi_2'''}(t, t''') \, W^{\chi_1''' \chi_1''}_{\chi_2''' \chi_2''}(t''', t'') \, \Pi^{\chi_1'' \chi_1'}_{\chi_2'' \chi_2'}(t'', t') \quad (3.19)$$

with the elements of the bare propagator, $\Pi^{(0)\chi_1 \chi_1'}_{\chi_2 \chi_2'}(t, t') := \exp(-\mathrm{i}(\varepsilon_{\chi_1} - \varepsilon_{\chi_2})(t - t')) \, \delta_{\chi_1 \chi_1'} \, \delta_{\chi_2 \chi_2'}$, and $\Delta^{\chi_1 \chi_1'}_{\chi_2 \chi_2'} := (\varepsilon_{\chi_1} - \varepsilon_{\chi_2}) \, \delta_{\chi_1 \chi_1'} \, \delta_{\chi_2 \chi_2'}$ with the energy differences of the many-body states on the diagonal. (Remark: For the sake of a simple coordinate-free representation we have chosen the notation slightly different from the original literature.)

Starting from the initial time $t' = t_0$ we plug Eq. (3.18) into Eq. (3.15) and differentiate with respect to the time t to arrive at the general and formally exact kinetic equation,

$$\frac{\mathrm{d}}{\mathrm{d}t} \mathbf{p}(t) + \mathrm{i} \boldsymbol{\Delta} \cdot \mathbf{p}(t) = \int_{t_0}^{t} \mathrm{d}t' \, \mathbf{W}(t, t') \cdot \mathbf{p}(t') \,, \tag{3.20}$$

which reads in coordinates

$$\frac{\mathrm{d}}{\mathrm{d}t} p^{\chi_1}_{\chi_2}(t) + \mathrm{i}(\varepsilon_{\chi_1} - \varepsilon_{\chi_2}) \, p^{\chi_1}_{\chi_2}(t) = \sum_{\chi_1' \chi_2'} \int_{t_0}^{t} \mathrm{d}t' \, W^{\chi_1 \chi_1'}_{\chi_2 \chi_2'}(t, t') \, p^{\chi_1'}_{\chi_2'}(t') \,. \tag{3.21}$$

The second term on the left hand side leads to coherent oscillations of the off-diagonal terms of the reduced density matrix in time. They govern the evolution in the absence of tunneling and may be interpreted similar to a precession of a spin around its quantization axis. The dissipative source term on the right hand side accounts for the effects caused by tunneling and describes the dissemination of the probability amplitudes. It induces a relaxation of the reduced density matrix of the uncoupled system to the coupled one. Due to the convolution it is nonlocal in time and respects the full memory of the system. We stress that, at this stage, no further assumptions concerning the properties of the reduced density matrix, neither for the initial conditions nor for the evolution, are needed. The general formula (3.21) describes the dynamics of the full reduced density matrix, including all off-diagonal terms.

In the special case if all quantum numbers of the system are conserved during tunneling the kinetic equations can be simplified considerably. Without loss of generality we can choose the basis such that the density matrix of the initial system is diagonal. If all quantum numbers are conserved during each tunneling event the density matrix remains diagonal for all times. The off-diagonal terms, or their amplitudes, can not grow because each element decouples completely from the rest of the system.

However, in the remainder of this work, we are concerned with effects which arise from the fact that not all quantum numbers of the system are conserved. Thus, we are particularly interested in the evolution of the off-diagonal terms of the density matrix. This
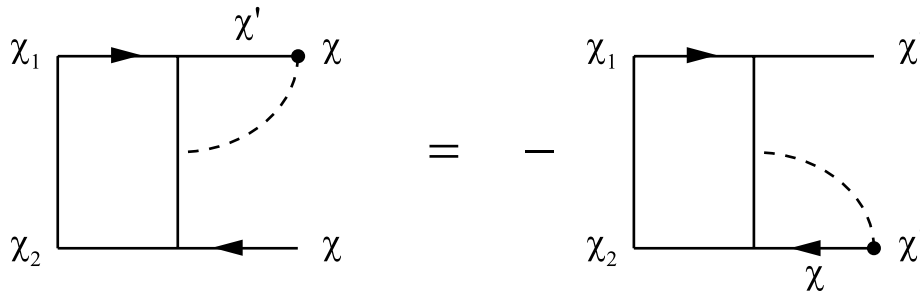
Figure 3.4:   Vertex-shifting yields a minus sign wich ensures probability conservation.

is especially important for coherently coupled quantum systems and marks a fundamental extension to classical master-equation approaches.

Assuming an N-dimensional Hilbert space for the reduced many-body system, the density matrix describing its state has $N \times N$ real degrees of freedom (due to hermiticity). Since, additional to the N^2 kinetic equations, we have the condition of conservation (and normalization) of the overall probability $\mathrm{tr}_{\mathrm{dots}}\,\mathbf{p}(t) = \sum_\chi p_\chi^\chi(t) \equiv 1$ we may ask if we are confronted with an overdetermined set of equations? But a preview on the diagrammatic rules given in section 3.5 proofs that the operator $\mathbf{W}$ and therefore $\mathbf{\Pi}$ does indeed respect the trace. By shifting the rightmost vertex of a diagram from the upper to the lower propagator, or vice versa, we get an additional minus sign (Fig. 3.4). (Obviously, this holds only if the states at the ends where we shift the vertex are identical for the upper and lower propagator.) Hence, the sum over symmetric end states of the selfenergy matrix elements vanishes, $\sum_{\chi'} W_{\chi'\chi_2}^{\chi'\chi_1} = 0$. This means, the probability conservation is automatically respected by the kinetic equations which become, in turn, linearly dependent. To determine the density matrix uniquely we have to take into account the probability normalization explicitly.

Fortunately, in many cases the number of degrees of freedom can be decreased considerably by conservation laws and symmetries of the system. In the following chapters we leverage this fact and discuss it in detail.

3.3   Stationary Equations and Markov Approximation

In experiments stationary properties of quantum dot systems such as the conductance are well accessible observables in transport measurements. Therefore, interesting phenomena and new effects arising in complicated nano-scale structures are often investigated by the signatures they leave in the current or the conductance. With one exception in chapter 4 we focus in this thesis on transport properties of driven quantum dot systems and their nonequilibrium state in the stationary limit.

For times $t - t_0$ much larger than the time scale on which the system relaxes due to its coupling to the reservoirs the reduced density matrix approaches a time independent

stationary state,

$$\mathbf{p}^{\mathrm{st}} := \lim_{t \to \infty} \mathbf{p}(t) = \lim_{t_0 \to -\infty} \mathbf{p}(t = 0) \,. \tag{3.22}$$

(The system is assumed to be invariant under time translation.) As long as there is no further driven oscillation, e.g. of the Rabi-kind, also the coherent oscillations of the off-diagonal terms will decay on this scale. For simplicity, we drop the stationary label in the following and refer to the stationary density matrix if no explicit time argument is given or stated otherwise.

We obtain the stationary equations from Eq. (3.20)

$$0 = -\mathrm{i}\boldsymbol{\Delta} \cdot \mathbf{p} + \mathbf{W} \cdot \mathbf{p} \,, \tag{3.23}$$

where we define the Laplace transform $\mathbf{W} := \lim_{\eta \searrow 0} \int_{-\infty}^{0} \mathrm{d}t' \, \exp(\eta\, t') \, \mathbf{W}(0, t')$. The kernel $\mathbf{W}$ can be calculated conveniently in the diagrammatic expansion in energy space.

For a well-defined perturbation expansion in the tunneling the stationary equations have to be satisfied in each order

$$0 = -\mathrm{i}(\varepsilon_{\chi_1} - \varepsilon_{\chi_2})\, p^{(0)\chi_1}_{\chi_2} + \sum_{\chi_1'\chi_2'} W^{(1)\chi_1\chi_1'}_{\chi_2\chi_2'}\, p^{(0)\chi_1'}_{\chi_2'} \tag{3.24a}$$

$$0 = -\mathrm{i}(\varepsilon_{\chi_1} - \varepsilon_{\chi_2})\, p^{(1)\chi_1}_{\chi_2} + \sum_{\chi_1'\chi_2'} \left(W^{(1)\chi_1\chi_1'}_{\chi_2\chi_2'}\, p^{(1)\chi_1'}_{\chi_2'} + W^{(2)\chi_1\chi_1'}_{\chi_2\chi_2'}\, p^{(0)\chi_1'}_{\chi_2'} \right) \tag{3.24b}$$

$$0 = -\mathrm{i}(\varepsilon_{\chi_1} - \varepsilon_{\chi_2})\, p^{(2)\chi_1}_{\chi_2} + \sum_{\chi_1'\chi_2'} \ldots \tag{3.24c}$$

Here we count only every second order in the tunneling elements $t_{rki\sigma}$ because every pairwise contraction leads to a prefactor quadratic in the tunneling elements. This is equivalent to an expansion in the coupling strength

$$\Gamma_{ri\sigma}(\omega) := 2\pi \sum_{k} |t_{rki\sigma}|^2\, \delta(\omega - \varepsilon_{rk\sigma}) \,. \tag{3.25}$$

The stationary equations (3.24) can be solved successively for the reduced density matrix in each order in Γ.

If there is a unique solution for the stationary state of the system, it is independent of the initial conditions of the time evolution. It may happen though, that a low order equation, e.g. Eq. (3.24a), does not determine the corresponding order of the density matrix, here $\mathbf{p}^{(0)}$, uniquely, because the low order tunneling obeys some symmetry. Nevertheless, in some cases the symmetry is broken by higher order tunneling processes and the (low order) stationary density matrix can be determined uniquely if we take these into account additionally.

We note, that for a potential difference between the reservoirs the stationary reduced density matrix is, in general, not identical to the equilibrium one which we would get in the absence of a bias voltage.

If we are interested in the actual time evolution of the reduced density matrix the exact kinetic equations (3.20) can be conveniently simplified with the Markov approximation. The density matrix is assumed to have no memory, i.e. the kinetic equations become local in time and very similar to the stationary equations (3.23),

$$\frac{\mathrm{d}}{\mathrm{d}t}\mathbf{p}(t) = -\mathrm{i}\boldsymbol{\Delta}\cdot\mathbf{p}(t) + \mathbf{W}\cdot\mathbf{p}(t)\,. \tag{3.26}$$

We solve the kinetic equations in the Markov approximation in chapter 4 to follow the evolution of the density matrix of a system of two coherently coupled quantum dots.

3.4   Tunneling Current

A lot of effort in studying quantum dot systems is directed towards the analysis of their transport properties, especially the conductance. As already mentioned, the electrical current is one of the best accessible quantities in experiments and it can tell us a lot about the behavior of the electronic wave functions travelling through the system. On this track, many prominent effects caused by the underlying quantum nature and many-body behavior of quantum dot systems have been observed (e.g. Coulomb blockade, cotunneling, Kondo effect, Aharonov-Bohm oscillations, etc.).

Starting from our general model Hamiltonian (3.1), we can relate the operator of the tunneling current, flowing into reservoir r, to the time derivative of the particle number operator of the respective reservoir,

$$\hat{I}_r(t)_{\mathrm{I}} = e\,\frac{\mathrm{d}}{\mathrm{d}t}\hat{n}_r(t)_{\mathrm{I}} = -\frac{\mathrm{i}e}{\hbar}\,[\hat{n}_r, H](t)_{\mathrm{I}}\,. \tag{3.27}$$

We further simplify the commutator and find an expression for the current operator

$$\hat{I}_r(t)_{\mathrm{I}} = \frac{\mathrm{i}e}{\hbar}\sum_{k\sigma i}\left(t_{rki\sigma}\,(c_{i\sigma}^\dagger a_{k\sigma r})(t)_{\mathrm{I}} - t_{rki\sigma}^*\,(a_{k\sigma r}^\dagger c_{i\sigma})(t)_{\mathrm{I}}\right)\,, \tag{3.28}$$

in which the constituents remind us of the terms of the tunneling Hamiltonian (3.4).

To calculate the expectation value of the current we can now apply the diagrammatic technique introduced in section 3.1. Each term of the current operator in Eq. (3.28) gives rise to an external vertex at time t with the same structure as the internal tunneling vertices from H_{t}, Eq. (3.4). By attaching the external vertices to the upper or lower propagator $((a_{k\sigma r}^\dagger c_{i\sigma})(t)_{\mathrm{I}}$ to the upper and $(c_{i\sigma}^\dagger a_{k\sigma r})(t)_{\mathrm{I}}$ to the lower, or vice versa), we take advantage of this similarity by relating the rightmost irreducible part of the diagram to the kernel $\mathbf{W}(t,t') = \sum_r \mathbf{W}_{r+}(t,t') + \mathbf{W}_{r-}(t,t')$ and calculate the partial rates $\mathbf{W}_{r\pm}(t,t')$ correspondingly. For the expectation value of the current we obtain

$$I_r(t) = \pm\frac{e}{\hbar}\int_{t_0}^t \mathrm{d}t'\sum_{\chi\chi_1'\chi_2'} W_{r\pm}{}^{\chi\chi_1'}_{\chi\chi_2'}(t,t')\,p_{\chi_2'}^{\chi_1'}(t')\,. \tag{3.29}$$
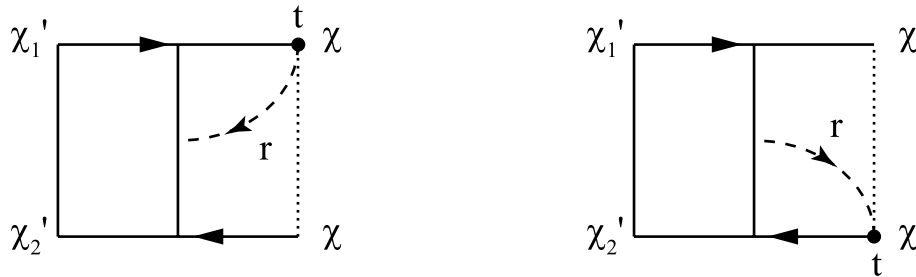
Figure 3.5: Sketch of contributions to the partial rate $W_{r+\chi\chi_2'}^{\chi\chi_1'}$.

The diagrams contributing to $\mathbf{W}_{r+}$ can be obtained by attaching the external vertices of the form $(a_{k\sigma r}^\dagger c_{i\sigma})(t)_\mathrm{I}$ to the upper and $(c_{i\sigma}^\dagger a_{k\sigma r})(t)_\mathrm{I}$ to the lower propagator. They correspond to the diagrams of $\mathbf{W}$ in which the rightmost tunneling line belongs to reservoir r and is outgoing if the rightmost vertex lies on the upper propagator, or incoming if the vertex lies on the lower propagator. Schematically this is sketched in Fig. 3.5. (The direction of the tunneling lines is defined such that an incoming or outgoing tunneling line at a vertex indicates the creation or annihilation of an electronic state in the dot system, respectively.) Vice versa, the diagrams contributing to $\mathbf{W}_{r-}$ can be obtained by attaching vertices of the form $(c_{i\sigma}^\dagger a_{k\sigma r})(t)_\mathrm{I}$ to the upper and $(a_{k\sigma r}^\dagger c_{i\sigma})(t)_\mathrm{I}$ to the lower propagator.

By construction, only diagrams with the same states at the ends at time t contribute to the current in Eq. (3.29). A factor of $-\mathrm{i}$ appearing in the current operator (3.28) but not in the expectation value (3.29) is already taken into account in the diagrammatic rules (see section 3.5) and absorbed in the partial rates $\mathbf{W}_{r\pm}$, similar to the factors from the expansion in Eq. (3.11).

In Refs. [33, 34] the charge conservation law $\sum_r I_r(t) = -e\frac{\mathrm{d}}{\mathrm{d}t}\langle n(t)\rangle$ was proven for the diagrammatic scheme, where the total charge of the quantum dot system is denoted by $-en$. In the stationary limit, or in a general time independent situation this reduces to $\sum_r I_r = 0$.

In combination with the kinetic equation (3.20) which determines the evolution of the reduced density matrix $\mathbf{p}(t)$, the current formula (3.29) allows us to describe general time dependent phenomena of the electron transport through the system. In the present form it comprises all coherent processes including the coherent evolution of the system itself, manifest in the progression of the off-diagonal terms of the reduced density matrix.

For systems invariant under time translation we can write the current formula in the stationary limit

$$I_r := \lim_{t\to\infty} I_r(t) = \pm\frac{e}{\hbar} \sum_{\chi\chi_1'\chi_2'} W_{r\pm\chi\chi_2'}^{\chi\chi_1'} p_{\chi_2'}^{\chi_1'} \tag{3.30}$$

where we defined the Laplace transform of the partial rates $W_{r\pm\chi\chi_2'}^{\chi\chi_1'} := \int_{-\infty}^0 \mathrm{d}t'\, W_{r\pm\chi\chi_2'}^{\chi\chi_1'}(0, t')$, similarly to the kernel $\mathbf{W}$ in the stationary equations (3.23). Again, we simplify the notation such that we do not introduce a new label to indicate the stationary limit, but

just drop the explicit time dependence.

Analogue to the systematic expansion of the stationary equations in the coupling strength (Eqs. (3.24a) and (3.24b)) which allows us to successively determine the contributions to the stationary density matrix, we expand the current in a perturbation series in the tunneling. The first and second order terms read

$$I_r^{(1)} = \frac{e}{\hbar} \sum_{\chi\chi_1'\chi_2'} \pm W_{r\pm}^{(1)\chi\chi_1'} {}_{\chi\chi_2'} p^{(0)\chi_1'} {}_{\chi_2'}, \tag{3.31a}$$

$$I_r^{(2)} = \frac{e}{\hbar} \sum_{\chi\chi_1'\chi_2'} \left(\pm W_{r\pm}^{(1)\chi\chi_1'} {}_{\chi\chi_2'} p^{(1)\chi_1'} {}_{\chi_2'} \pm W_{r\pm}^{(2)\chi\chi_1'} {}_{\chi\chi_2'} p^{(0)\chi_1'} {}_{\chi_2'} \right). \tag{3.31b}$$

In some systems, e.g. a single quantum dot coupled to two reservoirs such that all quantum numbers of the system are conserved during tunneling, the first order contribution to the current is equivalent to the so-called sequential tunneling which can be calculated within the orthodox theory with classical master equations and Fermi's Golden Rule. If all quantum numbers are conserved the off-diagonal elements of the density matrix decouple completely from the diagonal and can be neglected. In other words, if we choose the basis of our system such that the initial density matrix is diagonal, it will remain in a diagonal form during its entire evolution. No superposition states will develop. In this case, the equations for the density matrix as well as the current formula simplify considerably since we can neglect all off-diagonal terms from the beginning.

The second order contribution to the current comprises different kinds of corrections. These are renormalization terms which provide corrections for processes of lower order, but also, in many respects much more important, higher order processes like the so-called cotunneling in which an electron tunnels coherently via a virtual state, or two electrons tunnel together in a correlated fashion.

It is important to note, that for a systematic calculation of the current in higher orders of the coupling strength it is in general not sufficient to restrict ourselves to the lowest order density matrix and second order partial rates, i.e. terms of the form $W_{r\pm\,\dots}^{(1)\,\cdots} p^{(1)\,\cdots}_{\dots}$. It is even not possible to distinguish these contributions clearly in a more physical sense, e.g. interpreting terms of the form $W_{r\pm\,\dots}^{(2)\,\cdots} p^{(0)\,\cdots}_{\dots}$ as cotunneling and $W_{r\pm\,\dots}^{(1)\,\cdots} p^{(1)\,\cdots}_{\dots}$ as renormalization terms, or likewise.

3.5 Diagrammatic Rules

In the preceding sections we referred several times to the diagrammatic rules which we present in the following. We adapt the scheme from the literature [34, 35] to the structure of our general Hamiltonian (3.1) and put special emphasis on the asymmetric diagrams which are important for the evolution of the off-diagonal terms of the density matrix and their coupling to the diagonal elements.

With regard to our aim to study the evolution of the reduced density matrix and the electron transport through the system, we can restrict ourselves here to the diagrammatic

expansion of the kernel $\mathbf{W}(t, t')$ and the current rates $\sum_\chi W_{r\pm}{}^{\chi\chi'_1}_{\chi\chi'_2}(t, t')$. As discussed before, we can therefore assume that all vertices from internal as well as external operators which appear in the expansion (3.11) are of the form $\sum_{k\sigma i} t_{rki\sigma} (c^\dagger_{i\sigma} a_{k\sigma r})(t)_{\mathrm{I}}$ or its hermitian conjugate.

After integrating out the reservoir degrees of freedom, all vertices are connected in pairs by directed tunneling lines. The latter represent transition terms going from time t' to t. They are denoted by $\gamma^+_{ii'r\sigma}(t - t')$ if $t' > t$ and $\gamma^-_{ii'r\sigma}(t - t')$ if $t' < t$ with respect to the Keldysh contour, where

$$\gamma^\pm_{ii'r\sigma}(t) = \int_{-\infty}^{\infty} \mathrm{d}\omega \, \exp(-\mathrm{i}\omega t) \, \gamma^\pm_{ii'r\sigma}(\omega) \tag{3.32}$$

can be calculated with

$$
\begin{aligned}
\gamma^+_{ii'r\sigma}(\omega) &:= \sum_k t_{rki\sigma} t^*_{rki'\sigma} \, \delta(\omega - \varepsilon_{rk\sigma}) \, f^+_r(\omega) \,, \\
\gamma^-_{ii'r\sigma}(\omega) &:= \sum_k t^*_{rki\sigma} t_{rki'\sigma} \, \delta(\omega - \varepsilon_{rk\sigma}) \, f^-_r(\omega)
\end{aligned}
\tag{3.33}
$$

according to the contractions (3.12). If all quantum numbers, especially the dot or level number i in our case, are conserved during tunneling, we can relate the transition terms to the classical tunnel rates obtained from simple Golden Rule arguments, $2\pi \, \gamma^\pm_{ii'r\sigma}(\omega) = \delta_{ii'} \, \Gamma_{ri\sigma}(\omega) \, f^\pm_r(\omega)$, with the coupling strength $\Gamma_{ri\sigma}(\omega)$ and the Fermi functions $f^\pm_r(\omega)$. But as mentioned, we are especially interested in non-conserved quantum numbers and the coherence effects connected with them. Therefore, we stick to the general, more complicated form.

The diagrammatic rules how to calculate all possible terms contributing to the kernel $\mathbf{W}(t, t')$ or the current rates $\sum_\chi W_{r\pm}{}^{\chi\chi'_1}_{\chi\chi'_2}(t, t')$ follow directly from the expansion (3.11). We summarize here the general derivation from Refs. [34, 35] and adapt it to our specific needs.

Rules in Time Space

T1) Find all terms of possible combinations of pairwise contractions. That means: Draw all topologically different diagrams with directed tunneling lines connecting pairs of vertices which contain lead electron operators. To each topological class assign all possible many-body states χ, and the corresponding energy ε_χ to each line between two vertices on the Keldysh contour. Furthermore, assign all possible combinations of reservoir, spin and dot indices, (i, i', r, σ), to each tunneling line.

T2) Each contour line between two vertices corresponds to a free propagation of the dot system from t' to t ($t' < t$) on the Keldysh contour and yields a factor $\exp(-\mathrm{i}\varepsilon_\chi(t-t'))$. (In case the dots' Hamiltonian was not diagonal in the states χ we have to assign a state χ' at t' and a state χ at t to the free contour line and replace the exponential

factor by the matrix element $\langle\chi|U_{\mathrm{dots}}(t,t')|\chi'\rangle$ of the time evolution operator of the bare dot system.)

T3) Each dot operator B of a vertex with an incoming state χ and an outgoing state χ' on the Keldysh contour leads to a matrix element $\langle\chi'|B|\chi\rangle$. In our case, B is either a creation or an annihilation operator of the dot system and the matrix element $\langle\chi'|B|\chi\rangle \in \{0, +1, -1\}$ due to the algebra of Fermi operators.

T4) A directed tunneling line with indices (i, i', r, σ) running from t' to t yields $\gamma^+_{ii'r\sigma}(t-t')$ if $t' > t$ and $\gamma^-_{ii'r\sigma}(t-t')$ if $t' < t$ with respect to the Keldysh contour.

T5) From the expansion of the time evolution with respect to H_{t} each diagram obtains a factor of $(-\mathrm{i})^m$ with the total number m of internal vertices. Furthermore, each crossing of tunneling lines indicates an odd number of transpositions of electron operators and we get a prefactor of $(-1)^c$, with the number c of crossings of tunneling lines.

T6) Finally, integrate over all internal times along the Keldysh contour respecting their order and sum over all remaining internal indices, i.e. reservoir, spin, and dot indices.

With this recipe we can calculate any element of the kernel $W^{\chi_1\chi'_1}_{\chi_2\chi'_2}(t,t')$ by summing the diagrams with the respective many-body states at the ends. Accordingly, we can calculate the constituents $W^{\chi\chi'_1}_{r\pm\chi\chi'_2}(t,t')$ of the current rates by taking the appropriate part of the sum of diagrams.

Rules in Energy Space

Alternatively to the ordering of all times and integrations along the Keldysh contour in rule T6, we can order the times of all vertices along the real axis, irrespective on which branch of the Keldysh contour they are, and label them by τ_i. The time integrations are then performed on the real axis and each internal vertex on the backward propagator gives rise to an additional minus sign. The ordering in real time segments is especially convenient for the calculation of the stationary transport properties. As mentioned before, in this case it proofs favorable to change to an energy representation via a Laplace transform. In the stationary limit we send $t_0 \to -\infty$ and set $t = 0$. Combining the exponentials from $\gamma^\pm_{ii'r\sigma}(t-t') = \int_{-\infty}^{\infty}\mathrm{d}\omega\,\exp(-\mathrm{i}\omega(t-t'))\,\gamma^\pm_{ii'r\sigma}(\omega)$ and the free propagation $\exp(-\mathrm{i}\varepsilon_\chi(t-t'))$ according to rule T2, we obtain expressions of the form

$$\lim_{\eta \searrow 0} \int_{-\infty}^{0}\mathrm{d}\tau_1 \int_{\tau_1}^{0}\mathrm{d}\tau_2 \cdots \int_{\tau_{\widetilde{m}-1}}^{0}\mathrm{d}\tau_{\widetilde{m}}\, \mathrm{e}^{\eta\,\tau_1}\mathrm{e}^{-\mathrm{i}E_1(\tau_1-\tau_2)}\mathrm{e}^{-\mathrm{i}E_2(\tau_2-\tau_3)}\cdots\mathrm{e}^{-\mathrm{i}E_{\widetilde{m}}\tau_{\widetilde{m}}} =$$

$$= \mathrm{i}^{\widetilde{m}}\,\frac{1}{E_1 + \mathrm{i}\eta}\cdot\frac{1}{E_2 + \mathrm{i}\eta}\cdots\frac{1}{E_{\widetilde{m}} + \mathrm{i}\eta}, \quad (3.34)$$

where the energies E_i are given by the sum of all energies in the segment between τ_i and τ_{i+1} (see e.g. Fig. 3.6). The convergence factor $\exp(\eta\,\tau_1)$ with $\eta \searrow 0$ can be related to an
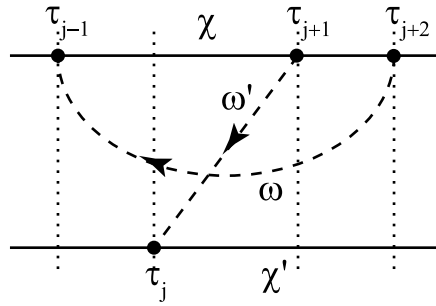
Figure 3.6: A diagram with sketched time segments. The energy resolvent of the central block is $E_j = \varepsilon_{\chi'} + \omega + \omega' - \varepsilon_\chi$.

adiabatic switching of the tunneling H_{t} by inserting unity factors, $1 = \exp(-\eta\,\tau_i)\,\exp(\eta\,\tau_i)$, between the exponentials. (For a detailed discussion of the Laplace transform and the time integration in case of several external vertices, see Ref. [35].) We can translate from the rules in time space:

E1) Take all diagrams as generated according to rule T1 but additionally assign an energy ω to each tunneling line.

E2) Each time segment between τ_i and τ_{i+1}, $i \in \{1, 2, \ldots, m\}$, gives rise to a resolvent $1/(E_i + \mathrm{i}\eta)$, where E_i is given by the sum of all leftgoing energies minus all rightgoing energies (see e.g. Fig. 3.6). (Here, $\tau_{m+1} = 0$ corresponds to the rightmost vertex, which is the external one.)

E3) The factors can be obtained according to rule T3.

E4) A directed tunneling line with indices (i, i', r, σ) and energy ω yields $\gamma^+_{ii'r\sigma}(\omega)$ if the tunneling line is going backward, and $\gamma^-_{ii'r\sigma}(\omega)$ if the tunneling line is going forward with respect to the closed time path.

E5) The total number b of internal vertices on the backward propagator gives a factor $(-1)^b$ and the number of crossings c of tunneling lines an additional factor $(-1)^c$, like in time space. (Additional signs may emerge due to the matrix elements $\langle \chi' | B | \chi \rangle$ in rule T3.)

E6) Finally, integrate over all energies of the tunneling lines, take the limit $\eta \searrow 0$, and sum over all remaining internal indices, i.e. reservoir, spin, and dot indices.

For the calculation of $\mathbf{W}$, or parts of it, in the stationary limit it is important that for m vertices we have only $m - 1$ time-integrations. This is because $\mathbf{W}$ is defined such that two vertices, the leftmost and the rightmost, are always at the very end of a propagator. Hence, there are $m - 1$ resolvents, which gives a factor i^{m-1}. Together with $(-\mathrm{i})^m$ from the expansion, taken into account in rule T5, there is a factor $-\mathrm{i}$ which remains. For the current rates we have one internal vertex less because of the external vertex from the
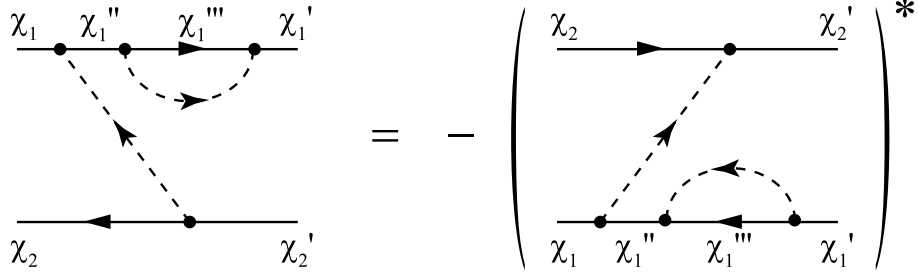
Figure 3.7: Explanatory sketch of an example for the mirror rule. The diagram on the right shows the mirrored counterpart of the original on the left hand side.

current operator. The missing imaginary factor is compensated by including the i from Eq. (3.28) into the definition of the current rates.

The diagrams running from the end state χ_1 to χ_1' on the upper branch and backwards from χ_2' to χ_2 on the lower branch can directly be summed into matrix elements $\Sigma_{\chi_2\chi_2'}^{\chi_1\chi_1'}$ which are related to the kernel $\mathbf{W}$ by the definition $\Sigma_{\chi_2\chi_2'}^{\chi_1\chi_1'} := \mathrm{i}\,W_{\chi_2'\chi_2}^{\chi_1'\chi_1}$. While $\mathbf{\Sigma}$ allows a better relation to a selfenergy (see e.g. Ref. [35]) the matrix elements $W_{\chi_2'\chi_2}^{\chi_1'\chi_1}$ (at least the symmetric terms with $\chi_1 = \chi_2$ and $\chi_1' = \chi_2'$) have the advantage that they can be interpreted as transition rates. For a large number of complicated diagrams, however, the summation of diagrams in $\Sigma_{\chi_2\chi_2'}^{\chi_1\chi_1'}$ can simplify the bookkeeping since all diagrams with the respective end states can be summed directly without transposition.

3.5.1   Mirror Rule

An important symmetry which can be read directly from the diagrammatic recipe can be summarized in the so-called mirror rule. It reduces the number of diagrams which we have to determine by a factor of two and leads in many cases to a considerable simplification of the integrals we actually have to calculate. The main statement of the rule is the following: For any relevant diagram we find a counterpart which can be obtained from the original by mirroring all vertices from the upper branch of the diagram to the lower one and vice versa. Additionally we change the directions of all tunneling lines. (The direction of the tunneling lines with respect to the contour remains.) For an explanatory sketch see Fig. 3.7. In some sense the procedure corresponds to a reversal of time. We first run against the backward propagator and follow the forward propagator to its start. In energy space this is equivalent to changing the signs of all energies. Thus, according to the diagrammatic rules, each resolvent of the mirrored diagram is the negative complex conjugate of its original,

$$\frac{1}{E + \mathrm{i}\eta} \; \longrightarrow \; \frac{1}{-E + \mathrm{i}\eta} = -\left(\frac{1}{E + \mathrm{i}\eta}\right)^* . \tag{3.35}$$

Additionally the indices of the transition functions change, $\gamma_{ii'r\sigma}^{\pm} \longrightarrow \gamma_{i'ir\sigma}^{\pm} = \left(\gamma_{ii'r\sigma}^{\pm}\right)^*$. Consequently the new diagram is given by $(-1)^{\widetilde{m}}$ times the complex conjugate of the
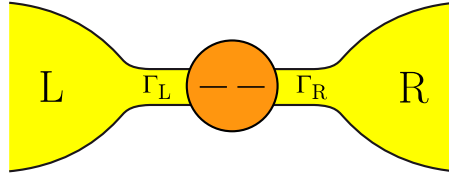
Figure 3.8: Sketch of a single-level quantum dot coupled to a left and a right reservoir.

original where $\widetilde{m}$ is the number of resolvents.

This in mind we can economize the number of diagrams which we have to compute and cut it down by one half. We gain even more for the symmetric kernels $\Sigma_{\chi\chi'}^{\chi\chi'}$ (or $W_{\chi'\chi}^{\chi'\chi}$, respectively) correspondig to the diagonal elements of the density matrix: in many cases the integrals become considerably simpler. Due to the symmetry between the end states of the upper and lower branch the original diagram and its mirrored counterpart contribute to the same kernel element. Thus, each pair can be combined to 2i times the imaginary part of the value of the original diagram. That means, instead of two integrals, consisting of a real and an imaginary part each, it is sufficient to compute only the imaginary part of one of them if the transition functions $\gamma_{ii'r\sigma}^{\pm}$ are real.

3.6 Single Quantum Dot

As a first application and test of the diagrammatic technique we sketch in this section the formalism to determine the stationary density matrix and the stationary current through a single quantum dot weakly coupled to two reservoirs (see Fig. 3.8). The single dot has already been studied extensively in the literature, yet it has some fascinating features we would like to point out. We consider two limiting cases: a quantum dot without interaction between the electrons and a quantum dot with strong onsite Coulomb repulsion. We present results for both of them with a focus on the second, interacting case. The examples may serve as reference points to which we can compare the results for the more complicated quantum dot systems in the remainder.

The Hamiltonian for the dot reads

$$H_{\mathrm{dot}} = \sum_{\sigma} \varepsilon \, c_{\sigma}^{\dagger} c_{\sigma} + U \, c_{\uparrow}^{\dagger} c_{\downarrow}^{\dagger} c_{\downarrow} c_{\uparrow} \,, \tag{3.36}$$

the tunnel coupling is modeled by

$$H_{\mathrm{t}} = \sum_{kr\sigma} (t_r \, c_{\sigma}^{\dagger} a_{kr\sigma} + \mathrm{h.c.}) \,, \tag{3.37}$$

and the Hamiltonian for the reservoirs is defined by $H_{\mathrm{res}} = \sum_{rk\sigma} \varepsilon_{rk} \, a_{rk\sigma}^{\dagger} a_{rk\sigma}$. The Coulomb interaction on the dot is denoted by U. As mentioned, we consider two simple limits, the non-interacting case, $U = 0$, and, on the other hand, strong Coulomb repulsion, i.e. U is
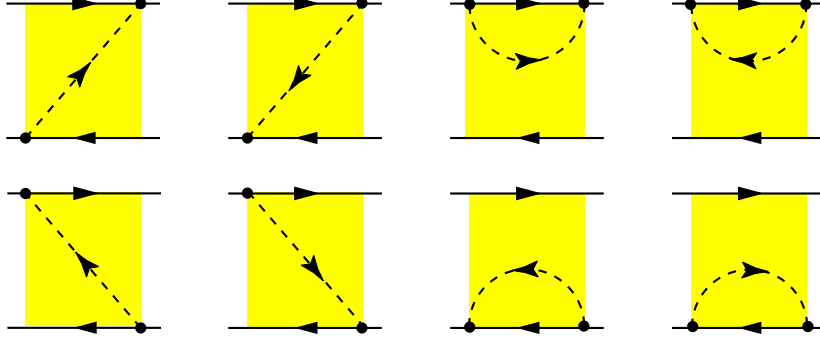
Figure 3.9:   Topological classes of first order diagrams.

much larger than all other energy scales of the system and prohibits double occupancy of the dot. The reservoirs and the dot level are assumed to be spin degenerate.

From Eq. (3.37) we can see that all quantum numbers of the system are conserved during the tunneling and the reduced density matrix will evolve in a diagonal form if we start diagonal initially. We can, therefore, neglect all off-diagonal terms from the beginning which simplifies the consideration significantly. Furthermore, we assume the tunneling independent of spin and energy such that the coupling is completely determined by $\Gamma_r = 2\pi \left|t_r\right|^2 N_r$ with the density of states N_r of reservoir $r \in \{\mathrm{L}, \mathrm{R}\}$.

In the non-interacting case, $U = 0$, the problem can be solved exactly within an equations of motion approach for the Green's function. For comparability we expand anyway and contrast with the results for the interacting case which could equivalently be obtained with Fermi's Golden Rule.

The Hilbert space of the reduced system is spanned by four states and the reduced density matrix is 4×4 with probabilities for the empty dot p_0, the singly occupied dot with spin up or spin down p_σ, and the doubly occupied dot $p_{\sigma\bar{\sigma}}$ on the diagonal. We recognize, that in the non-interacting case the spin summation yields two identical copies of the Hamiltonian for each spin (due to spin degeneracy and spin independent tunneling). Hence, we can regard the system as the sum of two independent, identical, spinless systems. For each of them the probabilities are denoted by $\tilde{p}_0$ for the empty state and $\tilde{p}_1$ for the occupied state. The density matrix of the original system can trivially be regained by the product of the two, $p_0 = \tilde{p}_0 \cdot \tilde{p}_0$, $p_\sigma = \tilde{p}_0 \cdot \tilde{p}_1$ and $p_{\sigma\bar{\sigma}} = \tilde{p}_1 \cdot \tilde{p}_1$.

3.6.1   Lowest Order Transport

The first order diagrams needed to set up the kinetic equations can be grouped in eight topological classes sketched in Fig. 3.9. Each explicit diagram consists of a topological backbone, belonging to one of the eight classes, which is dressed with the corresponding states at the ends, all possible intermediate states and the corresponding energies, and all possible combinations of indices and energies for the tunneling lines. In the simple case of a non-interacting dot, for example, there are only two explicit realizations of each topological

class of first order diagrams. Each class has only one possible combination of the two end states (dot empty or dot occupied) and has two possible tunneling indices, for tunneling on the left or the right hand side. Furthermore, we only have to take into account the coupling between diagonal terms (as concluded above). Hence, according to the mirror rule, it suffices to calculate only the imaginary part of the four diagrams represented by the first row in Fig. 3.9.

The solution of the stationary equations in lowest order tunneling yields

$$\tilde{p}_0^{(0)} = \frac{\sum_r \Gamma_r \left(1 - f_r(\varepsilon)\right)}{\Gamma} \qquad \text{and} \qquad \tilde{p}_1^{(0)} = \frac{\sum_r \Gamma_r f_r(\varepsilon)}{\Gamma} \tag{3.38}$$

with $\Gamma = \sum_r \Gamma_r$ and the Fermi function $f_r(\varepsilon) := f_r^+(\varepsilon)$. In equilibrium, i.e. for zero bias voltage, the probabilities are governed by Boltzmann factors, $\tilde{p}_0^{(0)}|_{V=0} = (1 - f(\varepsilon))$ and $\tilde{p}_1^{(0)}|_{V=0} = f(\varepsilon)$, as expected. The lowest order current through the dot reads

$$I^{(1)} = -2 \frac{e}{\hbar} \frac{\Gamma_\text{L} \Gamma_\text{R}}{\Gamma} \left(f_\text{L}(\varepsilon) - f_\text{R}(\varepsilon)\right) \tag{3.39}$$

and we obtain the linear conductance,

$$G^{(1)} := \left. \frac{\partial I^{(1)}}{\partial V} \right|_{V=0} = -4\pi \frac{e^2}{h} \frac{\Gamma_\text{L} \Gamma_\text{R}}{\Gamma} f'(\varepsilon)|_{V=0} . \tag{3.40}$$

For an interacting quantum dot we can not simplify the Hamiltonian like in the non-interacting case, but for large U we can flatten one dimension of the Hilbert space since double occupancy is prohibited. We now have to distinguish the two spin states of the occupied dot in the diagrams. As a consequence, we have to take into account more explicit realizations of the topological classes, but the simplification due to the mirror rule still applies. The solution of the stationary equations yields

$$p_0^{(0)} = \frac{\sum_r \Gamma_r \left(1 - f_r(\varepsilon)\right)}{\sum_r \Gamma_r \left(1 + f_r(\varepsilon)\right)} \qquad \text{and} \qquad p_\sigma^{(0)} = \frac{\sum_r \Gamma_r f_r(\varepsilon)}{\sum_r \Gamma_r \left(1 + f_r(\varepsilon)\right)} . \tag{3.41}$$

In equilibrium the probabilities are again governed by Boltzmann factors,

$$p_0^{(0)}|_{V=0} = \frac{1 - f(\varepsilon)}{1 + f(\varepsilon)} \qquad \text{and} \qquad p_\sigma^{(0)}|_{V=0} = \frac{f(\varepsilon)}{1 + f(\varepsilon)} . \tag{3.42}$$

We calculate the lowest order current with the diagrammatically obtained partial rates,

$$I^{(1)} = -2 \frac{e}{\hbar} \frac{\Gamma_\text{L} \Gamma_\text{R}}{\sum_r \Gamma_r \left(1 + f_r(\varepsilon)\right)} \left(f_\text{L}(\varepsilon) - f_\text{R}(\varepsilon)\right) , \tag{3.43}$$

which yields the linear conductance

$$G^{(1)} = -4\pi \frac{e^2}{h} \frac{\Gamma_\text{L} \Gamma_\text{R}}{\Gamma} \frac{f'(\varepsilon)|_{V=0}}{1 + f(\varepsilon)|_{V=0}} . \tag{3.44}$$

The linear conductance in the non-interacting case is particle-hole symmetric, i.e. it is invariant under sign change of the dot energy ε. In contrast, the interaction induces an asymmetry between the occupied side, $\varepsilon < 0$, and the unoccupied side, $\varepsilon > 0$, of the conductance peak (see also Fig. 3.12) which manifests itself in the factor $1/(1 + f(\varepsilon))$. To motivate the asymmetry we sketch the possible processes which transport an electron.

For each sequential transport process the number of electrons on the dot has to change by one. If the dot is empty we have two possibilities to charge it, either with spin up or with spin down. If the dot is already occupied with one of the two spins, say σ, there is only one possible process: the electron with spin σ leaves the dot. Summing the probabilities for the conditions that these processes may occur and assuming spin degeneracy we obtain $2\,p_0 + p_\sigma + p_{\bar\sigma} = 2\,(p_0 + p_\sigma)$. The factor

$$p_0^{(0)} + p_\sigma^{(0)} = \frac{1}{\sum_r \Gamma_r \left(1 + f_r(\varepsilon)\right)} \tag{3.45}$$

coincides with the asymmetry in the current. For comparison: without interaction we can restrict our consideration to the spinless system. The dot can be empty or occupied to transport an electron and the probability to find the system in one of these states is $\tilde{p}_0 + \tilde{p}_1 = 1$, always.

The asymmetry between particle- and hole-like processes in the interacting quantum dot is already visible in the linear conductance, as discussed. Even more drastic consequences can be observed for bias voltages beyond linear response. As long as the coupling to the left and the right reservoirs is symmetric, the I-V curve is as well. This changes if we detune the couplings to the reservoirs. For asymmetric coupling the current is not symmetric if we switch the polarity of the bias, i.e. the transport through the interacting, asymmetrically coupled quantum dot has a well-conducting and a poor-conducting direction.

In Fig. 3.10 we show a density plot of the differential conductance vs. the bias voltage, and the position of the dot level with respect to the mean of the electro-chemical potentials of the left and the right reservoir. On the vertical slice through $eV/k_\mathrm{B}T = 0$ we previsit the linear conductance of Fig. 3.12 and recognize that the conductance peak is shifted off the symmetry line to the unoccupied side. Furthermore, we see quite a strong asymmetry between the conductance for leftgoing ($eV/k_\mathrm{B}T < 0$) and rightgoing electrons ($eV/k_\mathrm{B}T > 0$). This behavior becomes most obvious if we tune the dot level off the resonance at $\varepsilon = 0$. In this regime we need a strong bias to drive the transport and the onset of the current for each direction of the transport manifests itself in two well separated conductance peaks. Apparently, the conductance for leftgoing electrons ($eV/k_\mathrm{B}T < 0$) is much weaker than for rightgoing electrons ($eV/k_\mathrm{B}T > 0$).

By investigation of the probabilities for the occupation of the quantum dot we see that for $eV/k_\mathrm{B}T < 0$ the electrons are pressed into the quantum dot where they retain because the drain is comparably weakly coupled. The quantum dot is predominantly occupied and the conductance is weak according to the argumentation above. For $eV/k_\mathrm{B}T > 0$ the electrons run out of the dot to the left side and the recharging from the right is weak such that the quantum dot is predominantly empty. In this case all electrons which overcome
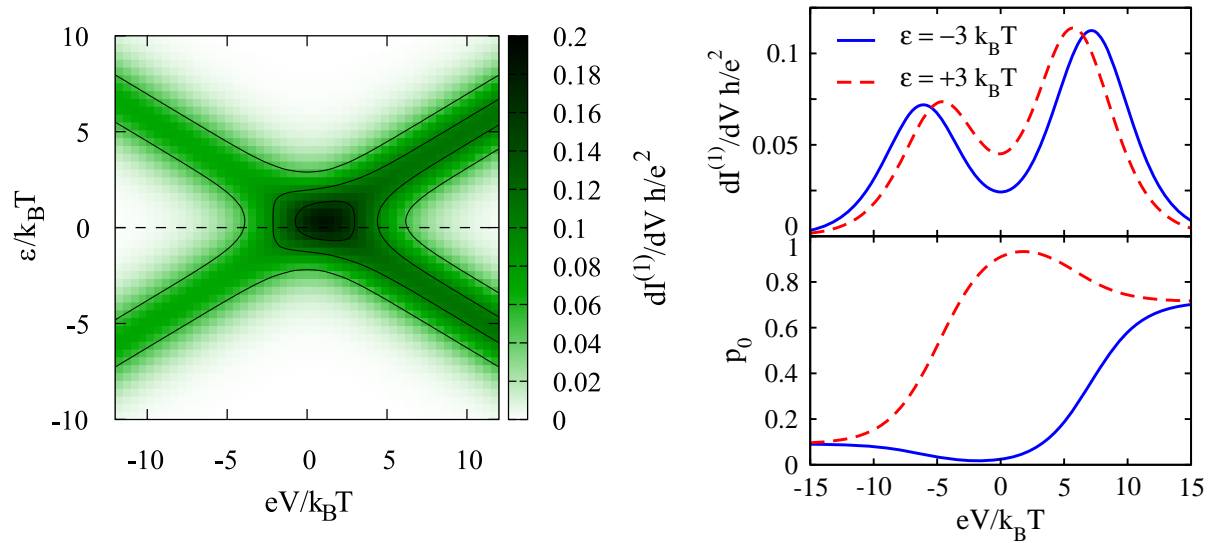
Figure 3.10: Differential conductance and slice of the probability to find the system empty for an asymmetrically coupled, interacting quantum dot. The bias is applied symmetrically, $-\mu_L = eV/2 = \mu_R$, and the dot level is measured with respect to the mean electro-chemical potential. The coupling is chosen to be $\Gamma_L = 0.5 \, k_B T$ for the left and $\Gamma_R = 0.1 \, k_B T$ for the right hand side. The two plots on the right display slices of the density plot and the corresponding probability p_0 for the empty dot at $\varepsilon = -3 \, k_B T$ and $\varepsilon = +3 \, k_B T$.

the right barrier can directly leave the dot through the thin barrier to the left reservoir. The probability to be repelled by some other electron in the dot is small.

3.6.2 Second Order Transport

The tunneling in lowest order gives the main contribution to the transport near the conductance peaks where the dot level is close to resonance with the mean Fermi energy of the leads. In the wider vicinity of the resonance the corresponding current decays exponentially and vanishes in the Coulomb blockade. Equivalently to the real-time diagrammtic technique, the transport through the considered single-level quantum dot in lowest order can be calculated by Fermi's Golden Rule within the orthodox theory. Here the processes are often referred to as sequential tunneling, reflecting the incoherent, sequential hopping of single electrons.

In higher orders the diagrammatic formalism displays its advantages, especially in the interacting case, where e.g. the scattering approach finds its limitations. The real-time diagrammatic technique enables us to perform a systematic expansion up to higher orders in the tunneling. This includes all relevant processes such as cotunneling, but as well corrections like renormalization and broadening of the dot level due to the finite coupling to the leads.

Nevertheless, the price for a systematic expansion is that we have to deal with a quickly
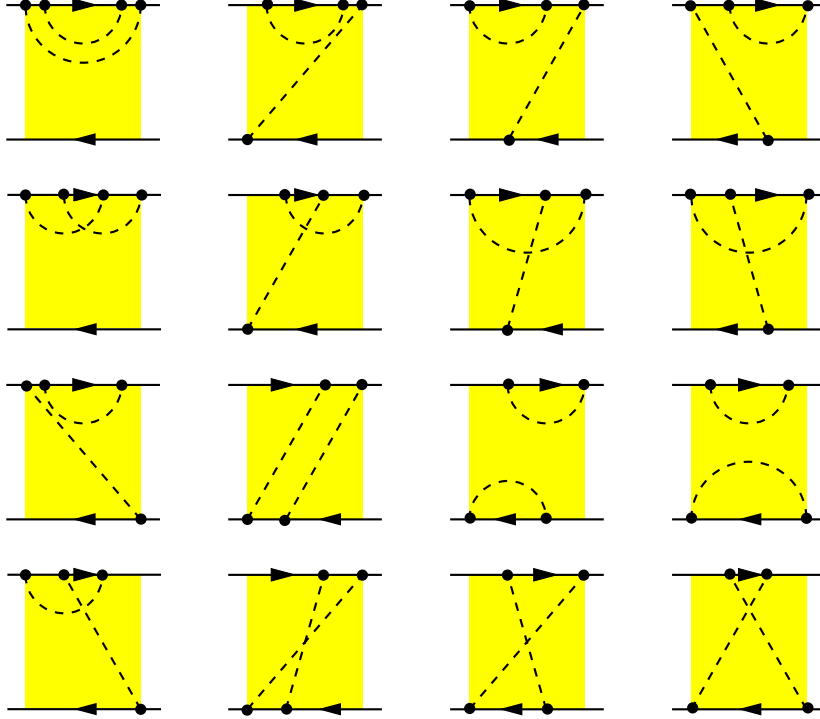
Figure 3.11: Condensed representatives of 128 topological classes of second order diagrams. The directions of the tunneling lines are left out (which reduces the number of representatives by a factor four) and structures which can be obtained by mirroring with respect to a horizontal line are represented by only one original.

increasing number of diagrams which are complicated to evaluate. In second order we already have 128 classes of diagrams which still have to be dressed with all corresponding states, energies and tunneling indices. In Fig. 3.11 we sketched some representatives of the topological classes. We left out all tunneling directions which reduces the number by a factor four and merged all structures which can be obtained by mirroring with respect to a horizontal line (another factor two). Each explicit second order diagram, dressed with all states, energies, indices, etc. is given by a double integral shifted in the complex plane (see e.g. appendix C). Fortunately, we often have some symmetries in the system which help us to simplify the problem considerably (e.g. the mirror rule).

The second order perturbation expansion already comprises fully coherent transport processes, the so-called cotunneling. It manifests itself in the current or conductance by a term qualitatively different from the lower order. While the first order is exponentially suppressed in the Coulomb blockade, the second order survives algebraically and dominates the transport. For the non-interacting dot this can be easily seen in the contribution to the current,

$$I^{(2)} = -2\,\frac{e}{h}\,\Gamma_{\mathrm{L}}\Gamma_{\mathrm{R}}\,\frac{\partial}{\partial\varepsilon} \fint \frac{\mathrm{d}\omega}{\omega - \varepsilon}\left(f_{\mathrm{L}}(\omega) - f_{\mathrm{R}}(\omega)\right), \tag{3.46}$$

where the symbol $\fint \frac{d\omega}{\omega-\varepsilon}$ denotes a principal value integration in the vicinity of the pole at $\omega = \varepsilon$. By introducing a high energy cutoff D, larger than all other energy scales of the system, except for a possibly even larger Coulomb interaction on the dot, the principal value integral of a Fermi function and its derivatives can be calculated analytically with the help of the Digamma or Psi function Ψ and its derivatives (compare appendix C). Without interaction, the complete second order correction to the linear conductance decays algebraically in the Coulomb blockade,

$$G^{(2)} = -2\frac{e^2}{h}\Gamma_{\mathrm{L}}\Gamma_{\mathrm{R}}\frac{\partial^2}{\partial\varepsilon^2}\fint\frac{d\omega}{\omega-\varepsilon}f(\omega)|_{V=0}\,. \tag{3.47}$$

The interacting dot is slightly more complicated because renormalization terms emerge in the second order contribution

$$I^{(2)} = -2\frac{e}{h}\frac{\Gamma_{\mathrm{L}}\Gamma_{\mathrm{R}}\left(\Gamma_{\mathrm{L}}+\Gamma_{\mathrm{R}}\right)}{\sum_r\Gamma_r\left(1+f_r\right)}\left((1+f_{\mathrm{R}})\frac{\partial}{\partial\varepsilon}P(f_{\mathrm{L}},\varepsilon) - (1+f_{\mathrm{L}})\frac{\partial}{\partial\varepsilon}P(f_{\mathrm{R}},\varepsilon)\right) -$$
$$-\frac{\partial I^{(1)}}{\partial\varepsilon}\frac{1}{2\pi}\left(\Gamma_{\mathrm{L}}\,P(f_{\mathrm{L}},\varepsilon) + \Gamma_{\mathrm{R}}\,P(f_{\mathrm{R}},\varepsilon)\right). \tag{3.48}$$

For better readability we dropped the explicit argument ε for all Fermi functions evaluated at the dot's energy and introduced the notation $P(f_r,\varepsilon) := \fint\frac{d\omega}{\omega-\varepsilon}f_r(\omega)$. The second, exponentially decaying term can be directly identified with a renormalization of the level position. It leads to a shift of the conductance peak towards lower energies. The first term contains algebraically as well as exponentially decaying terms. In linear response, all terms can be clearly arranged,

$$G^{(2)} = G_1^{(2)} + G_2^{(2)} + G_3^{(2)}, \tag{3.49}$$

with the algebraically decaying term,

$$G_1^{(2)} = -2\frac{e^2}{h}\Gamma_{\mathrm{L}}\Gamma_{\mathrm{R}}\frac{\partial^2}{\partial\varepsilon^2}P(f|_{V=0},\varepsilon)\,, \tag{3.50}$$

which yields the main broadening of the conductance and the leading contribution in the Coulomb blockade, the renormalization of the level position,

$$G_2^{(2)} = -\frac{\Gamma_{\mathrm{L}}+\Gamma_{\mathrm{R}}}{2\pi}P(f|_{V=0},\varepsilon)\frac{\partial G^{(1)}}{\partial\varepsilon}\,, \tag{3.51}$$

and a further exponentially decaying term,

$$G_3^{(2)} = -G^{(1)}\frac{\Gamma_{\mathrm{L}}+\Gamma_{\mathrm{R}}}{2\pi}\frac{\partial}{\partial\varepsilon}P(f|_{V=0},\varepsilon)\,, \tag{3.52}$$

which in the literature [34,35] is referred to as renormalization of the level broadening.

The notion of renormalization can be motivated by interpreting the conductance as function $G(\tilde{\varepsilon},\tilde{\Gamma})$ of the dot energy and its level width. The uncoupled quantum dot has a sharp level at the eigenenergy ε. Due to the tunnel coupling, however, the lifetime of the
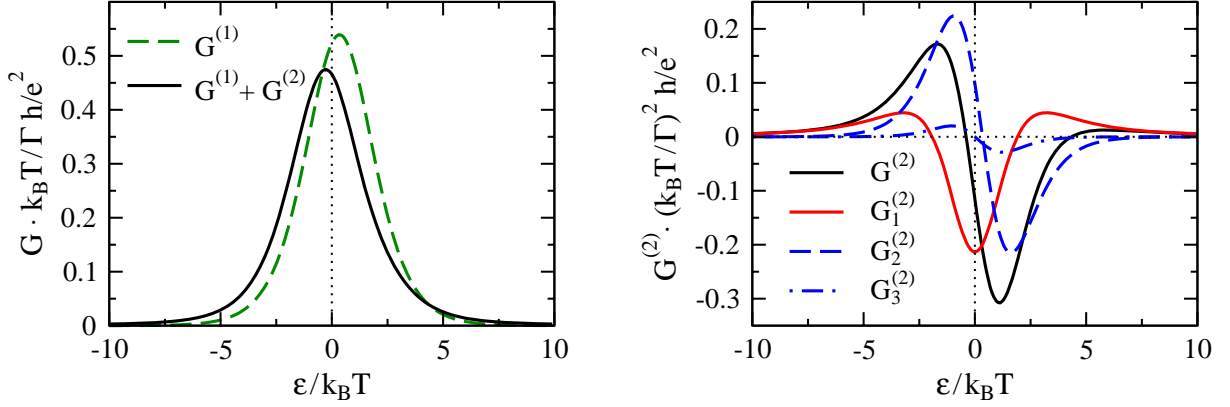
Figure 3.12: Left: Linear conductance in first order in Γ (dashed line) for symmetric coupling $\Gamma_L = \Gamma_R$ and the sum of first and second order linear conductance for the specific case of $\Gamma = 0.5\, k_B T$ (solid line). Right: Second order term of the linear conductance and its contributions $G^{(2)} = G_1^{(2)} + G_2^{(2)} + G_3^{(2)}$. The cutoff was set to $D = 10^3\, k_B T$.

corresponding electronic state becomes finite which can be associated to a level broadening $\tilde{\Gamma}$. Furthermore, the connection of the quantum dot to the reservoirs may lead to quantum fluctuations which influence the eigenenergies of the reduced system as compared to the separate quantum dot. We denote the modified dot energy of the coupled system formally by $\tilde{\varepsilon}$, it depends on the coupling strength. A perturbation expansion of the conductance in the vicinity of the very weakly coupled system yields

$$G(\tilde{\varepsilon}, \tilde{\Gamma}) \approx G(\varepsilon, \Gamma) + (\tilde{\varepsilon} - \varepsilon)\frac{\partial G(\varepsilon, \Gamma)}{\partial \varepsilon} + (\tilde{\Gamma} - \Gamma)\frac{\partial G(\varepsilon, \Gamma)}{\partial \Gamma} + \dots \qquad (3.53)$$

where the renormalization factors of the level position and the level width are indicated by the corresponding lowest order perturbation corrections. By comparison to our result for the linear conductance expanded in orders of the coupling strength (Eq. (3.49) et seq.) we can identify the respective terms, $G_1^{(2)}$, $G_2^{(2)}$ and $G_3^{(2)}$, with the pure correction of the conductance due to cotunneling ($G_1^{(2)}$) the correction due to the renormalization of the dot energy ($G_2^{(2)}$) and the renormalization of the level width ($G_3^{(2)}$).

In Fig. 3.12 we plot the linear conductance of the interacting dot with the second order correction, $G^{(1)} + G^{(2)}$, for the specific case of $\Gamma = 0.5\, k_B T$ and compare it to the first order, $G^{(1)}$. Additionally, we show the three different contributions, $G_1^{(2)}$, $G_2^{(2)}$, and $G_3^{(2)}$, to the second order term $G^{(2)}$. While the corrections $G_2^{(2)}$ and $G_3^{(2)}$ influence the position and the shape of the peak only near the resonance, $G_1^{(2)}$ gives the dominant contribution in the Coulomb blockade.

The renormalization of the level position leaves its trace already in the first correction

to the probabilities

$$p_0^{(1)} = -\frac{2\left(\Gamma_{\mathrm{L}} + \Gamma_{\mathrm{R}}\right)}{\sum_r \Gamma_r \left(1 + f_r(\varepsilon)\right)} \sum_r \frac{\Gamma_r}{2\pi} \frac{\partial}{\partial \varepsilon} P(f_r, \varepsilon) - \frac{\partial p_0^{(0)}}{\partial \varepsilon} \sum_r \frac{\Gamma_r}{2\pi} P(f_r, \varepsilon) \qquad (3.54\text{a})$$

$$p_\sigma^{(1)} = \frac{\Gamma_{\mathrm{L}} + \Gamma_{\mathrm{R}}}{\sum_r \Gamma_r \left(1 + f_r(\varepsilon)\right)} \sum_r \frac{\Gamma_r}{2\pi} \frac{\partial}{\partial \varepsilon} P(f_r, \varepsilon) - \frac{\partial p_\sigma^{(0)}}{\partial \varepsilon} \sum_r \frac{\Gamma_r}{2\pi} P(f_r, \varepsilon). \qquad (3.54\text{b})$$

(The property $p_\sigma^{(1)} = -p_0^{(1)}/2$ is satisfied and ensures the normalization condition $\mathrm{tr}_{\mathrm{dot}}\,\mathbf{p} = p_0 + 2\,p_\sigma = 1$.) The first terms in Eqs. (3.54a) and (3.54b) lead to algebraic tails away from the resonance as we would expect from cotunneling corrections. In contrast, the second terms decay exponentially and shift the probabilities as if the dot level was renormalized to a lower energy.

Chapter 4

Coherent Evolution of Nonequilibrium Quantum Dot Systems

An obvious extension of the well-understood single-level quantum dot is the introduction of a second energy level in the system. The simplest step in such a bottom-up approach is to introduce a second level in a single quantum dot attached to one or several reservoirs. On the other hand, this would be one of the least flexible realizations of a two-level system. Instead, we would like to climb the ladder half a step further.

By introducing the second level in a separate quantum dot which is coupled to the same reservoir as the first one, we gain a lot of freedom for the investigation at a rather low expense. In such a setup we can tune the couplings and the energy-levels separately for each dot and the one- or two-level single quantum dots are included as limiting cases.

A crucial point is in the following that we assume the two dots to be coherently coupled to a joint reservoir. This means, the distance between the two dots, measured through the connection to the joint lead, has to be smaller than the phase coherence length of the electrons in the system. In the remainder, we will call a reservoir a joint or common lead, if and only if it connects two dots in this quantum-mechanically coherent sense. In contrast, we treat reservoirs as separated, if the distance between the two dots is larger than the phase coherence length of the electronic wave function. As consequence, an electron on one dot would not feel the existence of the second dot (unless we introduce a direct interaction between the two dots, which we actually do in chapter 7). In this case, we could treat the system as combination of two independent copies of the well-known single-level quantum dot. A somewhat related system to the coherently coupled double dot was considered by T. V. Shahbazyan and M. E. Raikh [40]. They studied a coherent coupling of two impurities via leads and the effects on the transport.

The advanced fabrication technology of nanoscale devices moves setups with two small quantum dots which are weakly coupled to a joint lead (in the above-named sense) into the range of experimental feasability. Such systems have already been realized in experiments for the investigation of more complicated but related problems [41–43].
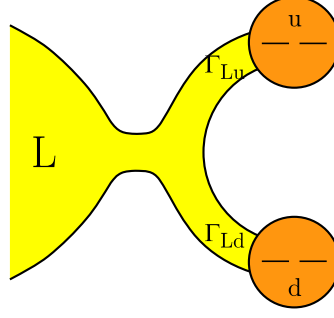
Figure 4.1: Two quantum dots (u and d) are coupled to a joint electron reservoir (L).

In sections 4.4 and 4.6 we show that a setup of the mentioned kind gives rise to new and interesting nonequilibrium physics which bears the potential for functionalization. We explain how the combination of Coulomb interaction on the dots and the coupling to a joint lead can be utilized in a nonequilibrium situation to generate spin entanglement between the spatially separated quantum dots [44].

4.1   Quantum Dots Coupled to a Joint Reservoir

In this section we introduce the basic Hamiltonian that we use to model a system of two single-level quantum dots coupled to a joint electron reservoir as depicted in Fig. 4.1. For simple limiting cases we sketch a heuristic motivation for the results we expect from the formally justified and more general calculation in section 4.2.

Based on the general Anderson-like Hamiltonian $H = H_{\text{res}} + H_{\text{dots}} + H_{\text{t}}$ in section 3.1, we specify the Hamiltonian for the two quantum dots up and down, $i \in \{\text{u}, \text{d}\}$,

$$H_{\text{dots}} = \sum_i \left[\sum_\sigma \varepsilon_i \, c_{i\sigma}^\dagger c_{i\sigma} + U \, c_{i\uparrow}^\dagger c_{i\downarrow}^\dagger c_{i\downarrow} c_{i\uparrow} \right], \qquad (4.1)$$

and the tunneling between the left lead and the dot system

$$H_{\text{t}} = H_{\text{tL}} = \sum_{k\sigma i} \left(t_{\text{L}i} \, c_{i\sigma}^\dagger a_{\text{L}k\sigma} + \text{h.c.} \right). \qquad (4.2)$$

The reservoir is represented by $H_{\text{res}} = \sum_{k\sigma} \varepsilon_{\text{L}k} \, a_{\text{L}k\sigma}^\dagger a_{\text{L}k\sigma}$. Each dot contains a single, spin-degenerate energy level ε_i, which can in general be detuned by $\Delta\varepsilon = \varepsilon_{\text{u}} - \varepsilon_{\text{d}}$. For transparency we focus in the following on a strong intradot Coulomb repulsion, $U \gg k_{\text{B}}T, eV, \Gamma$, which supresses double occupancy of each dot. This is a good approximation as long as the quantum dots are small. Nevertheless, it is not a necessary restriction because our analysis in the following sections can easily be generalized to a finite intradot charging energy, which does not change the conclusions qualitatively. The tunneling is

assumed to be independent of spin and energy and the tunneling strength is parametrized by $\Gamma_{\mathrm{L}i} = 2\pi\, t_{\mathrm{L}i}^2\, N_{\mathrm{L}}$ for the upper ($i = \mathrm{u}$) and the lower dot ($i = \mathrm{d}$), respectively. The density of states of the left reservoir is denoted by N_{L}. (Without loss of generality we can choose the gauge such that the tunneling amplitudes $t_{\mathrm{L}i} \in \mathbb{R}$, as long as the geometry of the setup is simply connected.)

The property of coherent coupling of both dots to the joint left reservoir is reflected in the tunneling Hamiltonian (4.2) by the fact that the creation and annihilation operators $a_{\mathrm{L}k\sigma}$ and $a_{\mathrm{L}k\sigma}^{\dagger}$ for reservoir states do not carry a dot index i. A particle tunneling from the reservoir to the dot system is annihilated in the lead and may either occupy a state in the upper or the lower dot or, if there are no specific energy or tunneling restrictions, it may also end up in a coherent superposition of both states. Vice versa, an electron leaving the dot system and entering the reservoir forgets about where it came from. It just remembers its spin.

The Hilbert space of the dot system is in general 16-dimensional. The prohibition of double occupancy of each dot due to the strong Coulomb repulsion U flattens it to nine dimensions which are spanned by the basis states $|\chi_{\mathrm{u}}, \chi_{\mathrm{d}}\rangle$, with $\chi_i \in \{0, \uparrow, \downarrow\}$ denoting the occupation of dot i.

For degenerate levels, $\Delta\varepsilon = 0$, the singly occupied subspace, in which only one electron is in the dot system, is fourfold degenerate (spin and level symmetry). A finite level-splitting, $\Delta\varepsilon \neq 0$, lifts one degeneracy of the isolated dot system. But on the other hand, the tunnel coupling leads to a broadening of the dot levels of the order of $\Gamma_{\mathrm{L}i}$. Hence, there is still a finite overlap of the energy levels as long as the level-splitting is smaller or of the order of the averaged level-broadening $\Delta\varepsilon \lesssim \Gamma_{\mathrm{L}} := (\Gamma_{\mathrm{L}u} + \Gamma_{\mathrm{L}d})/2$. Similar to the discussion of the distance between the two dots, it is the regime of small level splitting which is the most interesting. For large detuning, $\Delta\varepsilon \gg \Gamma_{\mathrm{L}}$, it is intuitively clear that we can treat the system again as a combination of two independent single-level quantum dots. The doubly occupied subspace, in which both dots are occupied with one electron each, is always fourfold degenerate due to spin symmetry, independent of $\Delta\varepsilon$.

For a discussion in more physical terms it proofs convenient to switch to a basis $\{|\chi\rangle\}$ of the quantum dot system, which reflects the symmetries of the problem. The state of the empty system we denote by $|0\rangle := |0, 0\rangle$. The natural basis states for the doubly occupied subspace, with one electron on each dot, are the spin singlet $|\mathrm{S}\rangle := (|\uparrow, \downarrow\rangle - |\downarrow, \uparrow\rangle)/\sqrt{2}$ and the three triplet states $|\mathrm{T}_+\rangle := |\uparrow, \uparrow\rangle$, $|\mathrm{T}_0\rangle := (|\uparrow, \downarrow\rangle + |\downarrow, \uparrow\rangle)/\sqrt{2}$ and $|\mathrm{T}_-\rangle := |\downarrow, \downarrow\rangle$.

The singly occupied subspace, with only one electron in the double dot system, can be characterized by the physical spin, σ, of the electron, as well as by an isospin defined in the two-dimensional Hilbert space spanned by the two orbital levels. There are two natural choices for the quantization axis for the isospin operator $\mathbf{I}_\sigma$, suggested by the structure of the Hamiltonian. The quantization axis $\mathbf{n}$ in which the eigenstates of $\mathbf{I}_\sigma \cdot \mathbf{n}$ are given by $|+\rangle_{\mathbf{I}_\sigma \cdot \mathbf{n}} := |\sigma, 0\rangle$ and $|-\rangle_{\mathbf{I}_\sigma \cdot \mathbf{n}} := |0, \sigma\rangle$ is motivated by the observation that the Hamiltonian for the dots (4.1) is diagonal in this isospin basis. An alternative quantization axis $\mathbf{m}$,

defined by

$$|+\rangle_{\mathbf{I}_\sigma \cdot \mathbf{m}} := \frac{1}{\sqrt{t_{\mathrm{Lu}}^2 + t_{\mathrm{Ld}}^2}} \left(t_{\mathrm{Lu}} |\sigma, 0\rangle + t_{\mathrm{Ld}} |0, \sigma\rangle \right) \qquad \text{and}$$

$$|-\rangle_{\mathbf{I}_\sigma \cdot \mathbf{m}} := \frac{1}{\sqrt{t_{\mathrm{Lu}}^2 + t_{\mathrm{Ld}}^2}} \left(t_{\mathrm{Ld}} |\sigma, 0\rangle - t_{\mathrm{Lu}} |0, \sigma\rangle \right), \tag{4.3}$$

reflects the structure of the tunnel Hamiltonian (4.2) and accounts for the fact that filling the double dot with an electron, tunneling in from the left reservoir, generates the isospin component $|+\rangle_{\mathbf{I}_\sigma \cdot \mathbf{m}}$, exclusively. Drawing an analogy to magnetism, this can be viewed as if the left reservoir was a fully isospin-polarized lead with only $|+\rangle_{\mathbf{I}_\sigma \cdot \mathbf{m}}$ isospins available.

In general, the two quantization axes $\mathbf{n}$ and $\mathbf{m}$ are neither parallel nor orthogonal. Explicitly, if we choose the coordinate system such that $\mathbf{n} = (0, 0, 1)$ we can deduce from the definitions above:

$$\mathbf{m} = \left(\frac{2\, t_{\mathrm{Lu}}\, t_{\mathrm{Ld}}}{t_{\mathrm{Lu}}^2 + t_{\mathrm{Ld}}^2}, 0, \frac{t_{\mathrm{Lu}}^2 - t_{\mathrm{Ld}}^2}{t_{\mathrm{Lu}}^2 + t_{\mathrm{Ld}}^2} \right). \tag{4.4}$$

Hence, we obtain for the coordinate independent relative orientation

$$\mathbf{n} \cdot \mathbf{m} = \frac{t_{\mathrm{Lu}}^2 - t_{\mathrm{Ld}}^2}{t_{\mathrm{Lu}}^2 + t_{\mathrm{Ld}}^2} = \frac{\Gamma_{\mathrm{Lu}} - \Gamma_{\mathrm{Ld}}}{\Gamma_{\mathrm{Lu}} + \Gamma_{\mathrm{Ld}}}. \tag{4.5}$$

The special case of orthogonal quantization axes is obtained by symmetric coupling, $\Gamma_{\mathrm{Lu}} = \Gamma_{\mathrm{Ld}}$, of the upper and lower dot. The isospin eigenstates $|+\rangle_{\mathbf{I}_\sigma \cdot \mathbf{m}} := (|\sigma, 0\rangle + |0, \sigma\rangle)/\sqrt{2}$ and $|-\rangle_{\mathbf{I}_\sigma \cdot \mathbf{m}} := (|\sigma, 0\rangle - |0, \sigma\rangle)/\sqrt{2}$ are then given by the symmetric and antisymmetric superpositions of the dots' orbital states. The limiting case of $\mathbf{n}$ and $\mathbf{m}$ parallel is represented by a single quantum dot (the other dot is decoupled).

Let us focus for a moment on the idealized system with maximal symmetry between the couplings, $\Gamma_{\mathrm{Lu}} = \Gamma_{\mathrm{Ld}}$, and the dot levels, $\Delta\varepsilon = 0$. With some qualitative and rather naive arguments we can pre-estimate to some degree what kind of behavior we might expect from a detailed and strict analysis given in section 4.2. For $\Gamma_{\mathrm{Lu}} = \Gamma_{\mathrm{Ld}}$ and $\Delta\varepsilon = 0$ we can map the first part of the Hamiltonian 4.1 for the double dot system onto a representation with only symmetric and antisymmetric combinations of creation and annihilation operators of dot states,

$$H_{\mathrm{dots}} = \sum_\sigma \frac{\varepsilon}{2} \left(b_{\mathrm{s}\sigma}^\dagger b_{\mathrm{s}\sigma} + b_{\mathrm{a}\sigma}^\dagger b_{\mathrm{a}\sigma} \right) + \sum_i U\, c_{i\uparrow}^\dagger c_{i\downarrow}^\dagger c_{i\downarrow} c_{i\uparrow}, \tag{4.6}$$

with the annihilation operators for the symmetric, $b_{\mathrm{s}\sigma} := (c_{\mathrm{u}\sigma} + c_{\mathrm{d}\sigma})/\sqrt{2}$, and the antisymmetric superposition states, $b_{\mathrm{a}\sigma} := (c_{\mathrm{u}\sigma} - c_{\mathrm{d}\sigma})/\sqrt{2}$, and the creation operators accordingly. Unfortunately, the interaction term becomes rather intransparent in the new representation, thus we just keep in mind that double occupancy of each dot is prohibited and maintain the original notation. Mapping the tunnel Hamiltonian (4.2),

$$H_{\mathrm{t}} = \sum_{k\sigma} \left(\sqrt{2}\, t_{\mathrm{L}}\, a_{k\mathrm{L}\sigma} b_{\mathrm{s}\sigma}^\dagger + \text{h.c.} \right), \tag{4.7}$$

where $t_{\mathrm{L}} := (t_{\mathrm{Lu}}+t_{\mathrm{Ld}})/2$, it is obvious that the states of the left lead are only coupled to the symmetric combination of the two quantum dots' orbital states. The antisymmetric combination is completely decoupled. This corresponds to the notion of the isospin quantized in the direction of $\mathbf{m}$, perpendicular to $\mathbf{n}$. As already noted, charging the double dot from the joint reservoir can, therefore, generate symmetric states exclusively. Vice versa, if we assume the charged system in an initially antisymmetric state, the dots can not discharge even if we push the dot level well above the Fermi energy of the lead.

We proceed along the same path and include also the transition to the doubly occupied system into our consideration. Charging the dots with two electrons from the reservoir yields the creation of two symmetric combinations $b_{\mathrm{s}\sigma}^{\dagger}b_{\mathrm{s}\sigma'}^{\dagger}|0\rangle = (|\sigma\sigma',0\rangle + |0,\sigma\sigma'\rangle + |\sigma,\sigma'\rangle - |\sigma',\sigma\rangle)/2$. For strong Coulomb repulsion we project out the parts which involve double occupancy of either dot (for $\sigma = \sigma'$ they vanish anyway because of the Pauli exclusion principle). There is only a final state if σ and σ' denote opposite spins, i.e. $\sigma' = \bar{\sigma}$, which results in a spin singlet $|S\rangle$. To generate a triplet component with this procedure it is necessary to apply at least one antisymmetric creation operator or, alternatively, start from a singly occupied system with a finite $|-\rangle_{\mathbf{I}_{\sigma}\cdot\mathbf{m}}$ isospin component. Vice versa, for $\Gamma_{\mathrm{Lu}} = \Gamma_{\mathrm{Ld}}$, a spin singlet state $|S\rangle$ in the doubly occupied subspace discharges to the isospin eigenstate $|+\rangle_{\mathbf{I}_{\sigma}\cdot\mathbf{m}} \propto b_{\mathrm{s}\bar{\sigma}}|S\rangle$ which, for its part, may discharge further to the empty dot system, $b_{\mathrm{s}\sigma}|+\rangle_{\mathbf{I}_{\sigma}\cdot\mathbf{m}} = b_{\mathrm{s}\sigma}b_{\mathrm{s}\bar{\sigma}}^{\dagger}|0\rangle = |0\rangle$. If, for any reason, we have the system in a triplet state, it may discharge to a singly occupied state, but this will have an isospin polarization, $|-\rangle_{\mathbf{I}_{\sigma}\cdot\mathbf{m}} \propto b_{\mathrm{s}\bar{\sigma}}|T_0\rangle$ or $b_{\mathrm{s}\sigma}|T_{\mathrm{sgn}\,\sigma}\rangle$, which can not empty, as discussed before. The system gets stuck between the two possible singly occupied electron spin states with isospin $|-\rangle_{\mathbf{I}_{\sigma}\cdot\mathbf{m}}$ and the three triplet states.

This simplified picture already advises us to be careful with off-diagonal terms in the density matrix. Apparently, it is not only the probabilities but the entire spin-like structure of the singly occupied subspace, in our case, which might become important for the evolution of the system's state. Furthermore, we are inspired to look especially for effects like an asymmetry between singlet and triplet states.

4.2 Evolution of the Density Matrix – Time Resolved

In this section we give a formally justified calculation of the kinetic equations for the reduced density matrix of the double dot system with strong intradot Coulomb repulsion. It is based on the real-time diagrammatic technique introduced in chapter 3 and assumes weak tunnel coupling of the dots to the joint reservoir. In contrast to the heuristic motivation in the preceding section, we extend the consideration also to more realistic situations and allow asymmetric coupling, $\Gamma_{\mathrm{Lu}} \neq \Gamma_{\mathrm{Ld}}$, and finite, yet small detuning, $\Delta\varepsilon \lesssim \Gamma_{\mathrm{L}}$. Although the general calculation for arbitrary $\Delta\varepsilon$ is straight forward, the equations become less transparent and do not yield anything important for the investigation we are focused on.

The density matrix for the nine-dimensional Hilbert space is 9×9, but already with particle number conservation we can reduce it to 33 elements, one for the empty system, 16 for the singly and 16 for the doubly occupied subspace. That means, the density operator

decomposes into a direct product $\rho = \rho_{0e} \otimes \rho_{1e} \otimes \rho_{2e}$ of density operators ρ_{0e}, ρ_{1e} and ρ_{2e} for the empty, the singly and the doubly occupied subspaces, respectively. Furthermore, the total Hamiltonian is invariant under rotations of the electron spin, i.e. spin is a conserved quantum number during tunneling. Thus, we are left with eight elements for the singly and six elements for the doubly occupied subspace. Taking also into account the spin symmetry of the dot Hamiltonian we finally have to determine seven independent real degrees of freedom of the reduced density matrix by solving the kinetic equations.

According to the basis introduced in the preceding section we write the probabilities to find the system empty, p_0, singly occupied, p_1, and both dots occupied forming either a spin singlet with probability p_S, or a triplet state with p_T. We summarize the probabilities in a vector representation $\mathbf{p} = (p_0, p_1, p_S, p_T)$, where the notation for the three triplets $p_T/3 := p_{T_-} = p_{T_0} = p_{T_+}$ is justified by the spin symmetry of the Hamiltonian. The probability for the singly occupied system comprises both dots with either spin, $p_1 := \sum_{i\sigma} p_{i\sigma}$. While the empty and the doubly occupied subspaces are completely determined by the corresponding probabilities, the probability for the singly occupied system has to be supplemented by the quantum statistical expectation value of the isospin, $\mathbf{I}/2 = (I_x, I_y, I_z)/2 := \langle \mathbf{I}_\uparrow \rangle = \langle \mathbf{I}_\downarrow \rangle$, which accounts for possible coherent superposition states in the singly occupied system. The original structure of the singly occupied block of the reduced density matrix might be regained by $\rho_{1e} = (p_1/2\, \mathbb{1}_2 + I_x\, \sigma_x + I_y\, \sigma_y + I_z\, \sigma_z)/2\, \delta_{\sigma\sigma'}$ with the Pauli matrices σ_i acting on the orbital degrees of freedom of the dot system and $\delta_{\sigma\sigma'}$ representing the unity in spin space.

Remembering the two quantization axes $\mathbf{n}$ and $\mathbf{m}$ (see section 4.1), suggested by the structure of the Hamiltonian, we can represent the kinetic equations in lowest order tunneling, i.e. first order in Γ_L, in the Markov approximation,

$$
\frac{\mathrm{d}}{\mathrm{d}t}\mathbf{p} = \Gamma_L \begin{pmatrix} -4\,f_L & 1-f_L & 0 & 0 \\ 4\,f_L & -1-f_L & 2-2\,f_L & 2-2\,f_L \\ 0 & f_L/2 & -2+2\,f_L & 0 \\ 0 & 3\,f_L/2 & 0 & -2+2\,f_L \end{pmatrix} \mathbf{p} +
$$

$$
+\,\Gamma_L \begin{pmatrix} 2-2\,f_L \\ -2+4\,f_L \\ f_L \\ -3\,f_L \end{pmatrix} (\mathbf{I} \cdot \mathbf{m}) + 2\,\Gamma_L\,f_L \begin{pmatrix} 0 \\ 1 \\ -1 \\ 0 \end{pmatrix} (\mathbf{I} \cdot \mathbf{n})(\mathbf{m} \cdot \mathbf{n}) \qquad (4.8)
$$

$$
\frac{\mathrm{d}}{\mathrm{d}t}\mathbf{I} = \Gamma_L \left[2\,f_L\,p_0 + \left(f_L - \frac{1}{2} \right) p_1 + (1-f_L)\,p_S - (1-f_L)\,p_T \right] \mathbf{m} +
$$

$$
+\,\Gamma_L \left[\frac{f_L}{2}\,p_1 - 2\,(1-f_L)\,p_S \right] \mathbf{n}\,(\mathbf{m} \cdot \mathbf{n}) - \Gamma_L\,(1+f_L)\,\mathbf{I} + \Delta\tilde{\varepsilon}\,(\mathbf{n} \times \mathbf{I}), \qquad (4.9)
$$

where we abbreviated the Fermi distribution of the electrons in the left reservoir f_L, evaluated at the mean dot energy $\varepsilon := (\varepsilon_u + \varepsilon_d)/2$. The level detuning $\Delta\varepsilon$ is complemented or

renormalized to an effective detuning

$$\Delta\tilde{\varepsilon} = \Delta\varepsilon + \frac{\Gamma_{\mathrm{Lu}} - \Gamma_{\mathrm{Ld}}}{2\pi} \fint \frac{d\omega}{\omega - \varepsilon} f_{\mathrm{L}}(\omega)$$

$$\approx \Delta\varepsilon - \frac{\Gamma_{\mathrm{Lu}} - \Gamma_{\mathrm{Ld}}}{2\pi} \left[\ln\left(\frac{\beta D}{2\pi}\right) - \mathrm{Re}\,\Psi\left(\frac{1}{2} + i\frac{\beta(\varepsilon - \mu_{\mathrm{L}})}{2\pi}\right) \right], \qquad (4.10)$$

where D is an high-energy cutoff provided by the minimum of either Coulomb interaction U or bandwith of the leads, and Ψ is the digamma function (see also appendix C).

The first block of the equations for $\mathbf{p}$ looks similar to the classical master equations which we could equivalently obtain by Fermi's Golden Rule. But here we also have a nontrivial influence of the isospin which accounts for the coupling to the evolution of the off-diagonal terms in the density matrix. Let us concentrate on three main scenarios to get an impression of the evolution of the density matrix depending on its initial state. We compare

    i. the completely symmetric setup, $\Gamma_{\mathrm{Lu}} = \Gamma_{\mathrm{Ld}}$ and $\Delta\varepsilon = 0$,

    ii. symmetric coupling, $\Gamma_{\mathrm{Lu}} = \Gamma_{\mathrm{Ld}}$, but finite detuning $\Delta\varepsilon$, and

    iii. asymmetric coupling $\Gamma_{\mathrm{Lu}} \neq \Gamma_{\mathrm{Ld}}$

for the initial states $|0\rangle$, $|\mathrm{S}\rangle$ and $|\mathrm{T}\rangle$. Each initial state is assumed to be in a nonequilibrium situation, i.e. we tune the dot levels via the gate voltage such that the system is forced to change its charge state. In particular, for the initial state $|0\rangle$ we pull the dot levels well below the Fermi energy of the lead, $-\varepsilon \ll k_{\mathrm{B}}T, \Gamma_{\mathrm{L}}$, whereas for an initially doubly occupied system, $|\mathrm{S}\rangle$ or $|\mathrm{T}\rangle$, we push them well above, $\varepsilon \gg k_{\mathrm{B}}T, \Gamma_{\mathrm{L}}$.

    i. The kinetic equations (4.9) become most transparent for the completely symmetric setup, $\Gamma_{\mathrm{Lu}} = \Gamma_{\mathrm{Ld}}$ and $\Delta\varepsilon = 0$. In this limit, the quantization axes $\mathbf{n}$ and $\mathbf{m}$ are orthogonal, $\mathbf{n} \cdot \mathbf{m} = 0$. The equation for the triplet $|\mathrm{T}\rangle$,

$$\frac{d}{dt} p_{\mathrm{T}} = 3\,\Gamma_{\mathrm{L}}\, f_{\mathrm{L}}\, p_{|-\rangle_{\mathbf{I}\cdot\mathbf{m}}} - 2\,\Gamma_{\mathrm{L}}\,(1 - f_{\mathrm{L}})\, p_{\mathrm{T}}, \qquad (4.11)$$

and the evolution of the expectation value $p_{|-\rangle_{\mathbf{I}\cdot\mathbf{m}}} := \langle|-\rangle\langle-|_{\mathbf{I}\cdot\mathbf{m}}\rangle = \left(\frac{p_1}{2} - \mathbf{I}\cdot\mathbf{m}\right)$ of the $|-\rangle_{\mathbf{I}\cdot\mathbf{m}}$ eigenstate of the isospin quantized in the direction of $\mathbf{m}$,

$$\frac{d}{dt} p_{|-\rangle_{\mathbf{I}\cdot\mathbf{m}}} = -3\,\Gamma_{\mathrm{L}}\, f_{\mathrm{L}}\, p_{|-\rangle_{\mathbf{I}\cdot\mathbf{m}}} + 2\,\Gamma_{\mathrm{L}}\,(1 - f_{\mathrm{L}})\, p_{\mathrm{T}}, \qquad (4.12)$$

decouple completely from all other equations. Furthermore, there is no isospin component generated which is perpendicular to $\mathbf{m}$. Conversely, if there was such a component initially it would decay exponentially according to

$$\frac{d}{dt} \mathbf{I}_{\perp\mathbf{m}} = -\Gamma_{\mathrm{L}}\,(1 + f_{\mathrm{L}})\, \mathbf{I}_{\perp\mathbf{m}}. \qquad (4.13)$$

Starting with an empty double dot system and charging it subsequently with two electrons, the first electron can only occupy a $|+\rangle_{\mathbf{I \cdot m}}$ state because it is in general exclusively $p_{|+\rangle_{\mathbf{I \cdot m}}} := \langle|+\rangle\langle+|_{\mathbf{I \cdot m}}\rangle = \left(\frac{p_1}{2} + \mathbf{I} \cdot \mathbf{m}\right)$ which couples to p_0. With the next incoming electron a spin singlet, $|S\rangle$, is formed. No triplet (or $|-\rangle_{\mathbf{I \cdot m}}$) component can be generated, although they are energetically degenerate to the singlet (or $|+\rangle_{\mathbf{I \cdot m}}$) component.

Vice versa, starting from an initially doubly occupied system, a singlet can be discharged via a $|+\rangle_{\mathbf{I \cdot m}}$ state to the empty system. In contrast, an initial triplet state may discharge to a $|-\rangle_{\mathbf{I \cdot m}}$ state which, for its part, can not empty further.

In realistic situations there are various mechanisms which weaken the blocking or trapping effect for $|-\rangle_{\mathbf{I \cdot m}}$ and $|T\rangle$ states and lead to a relaxation via a finite coupling of the expectation value $p_{|-\rangle_{\mathbf{I \cdot m}}}$ and the triplet probability p_{T} to other density matrix elements. In the more quantitative analysis of the symmetric, asymmetric and detuned setups in section 4.4 we also include in a phenomenologic way the coupling to an external bath which mediates spin-flip processes or creates a phase difference between the dots' states. An additional tunnel coupling to further reservoirs is discussed in section 4.5.

ii. Compared to the completely symmetric setup, a finite detuning leads even for symmetric tunneling strengths to a finite coupling of $p_{|-\rangle_{\mathbf{I \cdot m}}}$ and p_{T} to other elements of the density matrix. Although it is still only the $|+\rangle_{\mathbf{I \cdot m}}$ component which couples directly to the empty system or the singlet, a precession of the isospin links the $|-\rangle_{\mathbf{I \cdot m}}$ component and the triplet to the rest. The precession takes place in a plane perpendicular to $\mathbf{n}$ and is initiated by the detuning $\Delta\varepsilon$, as soon as the probability to find the system singly occupied becomes finite. Thus, the expectation value $p_{|-\rangle_{\mathbf{I \cdot m}}}$ gains at the expense of $p_{|+\rangle_{\mathbf{I \cdot m}}}$, or vice versa. In the language of the kinetic equations in the original basis, $\{|\chi_{\mathrm{u}}, \chi_{\mathrm{d}}\rangle : \chi_i \in \{0, \uparrow, \downarrow\}\}$, the precession translates to coherent oscillations which become apparent in the off-diagonal terms of the density matrix.

iii. Asymmetric coupling induces rotations of the isospin which are in part similar to the effect of finite detuning but go beyond. The many-particle renormalization term in $\Delta\tilde{\varepsilon}$, to which all possible states in the reservoir contribute, gives rise to a $\Delta\varepsilon$-like precession around the axis $\mathbf{n}$. It reflects the fact, that the stronger coupled level is further renormalized to lower energies than the weaker coupled one. As a consequence, an effective energy difference is generated by the tunneling. In addition, terms appear which lead to a rotation of the isospin out of the plane perpendicular to $\mathbf{n}$. Some of the terms even couple directly to the singlet (accounting for the $|S\rangle \longrightarrow |-\rangle_{\mathbf{I \cdot m}}$ discharging, for example). These rotations are evoked by the fact that the quantization axes $\mathbf{n}$ and $\mathbf{m}$ are not orthogonal for $\Gamma_{\mathrm{Lu}} \neq \Gamma_{\mathrm{Ld}}$. They act more directly than the $\Delta\varepsilon$-like precession and reflect the immediate response of the system to asymmetric coupling.

We summarize the effects of rotations of the isospin described in ii and iii by sketching qualitatively an interpretation of the charging process from the empty system to the doubly

occupied one and, vice versa, the discharging process from doubly occupied to empty. Charging the empty double dot with the first electron, the occupied state is a $|+\rangle_{\mathbf{I\cdot m}}$ eigenstate of the isospin quantized in the direction of $\mathbf{m}$ (so far this is similar to i). In contrast to the symmetric setup, the isospin starts to precess until it is charged with the second electron. Depending on the progress of the precession and the statistical distribution of $|+\rangle_{\mathbf{I\cdot m}}$ and $|-\rangle_{\mathbf{I\cdot m}}$ states, the second electron leads to the formation of a singlet or rather a triplet state. As long as the system is quite close to the symmetric setup, i.e. if the precession is slow compared to the inverse charging rate, we expect the singlet to outbalance the triplet.

Now the other direction: The initially doubly occupied system can either be in a singlet or in a triplet state. Discharging a triplet leads to a singly occupied state with polarization $|-\rangle_{\mathbf{I\cdot m}}$ which starts to precess and empties little by little as the rotation progresses. For an initial singlet we distinguish the two scenarios ii, with finite detuning $\Delta\varepsilon$ but symmetric coupling, $\Gamma_{\mathrm{Lu}} = \Gamma_{\mathrm{Ld}}$, and iii, with asymmetric coupling, $\Gamma_{\mathrm{Lu}} \neq \Gamma_{\mathrm{Ld}}$, and arbitrary detuning $\Delta\varepsilon$ (but still small compared to Γ). In scenario ii the singlet discharges to a $|+\rangle_{\mathbf{I\cdot m}}$ state and empties further in the usual way, equivalent to the perfectly symmetric setup in i. In scenario iii the singlet discharges to a singly occupied state with a more complicated isospin than just $|+\rangle_{\mathbf{I\cdot m}}$. Anyway, it kicks the precession of the isospin and empties, even if the process is presumably not as fast as in the symmetric setup.

Recapitulating, we remark that the isospin, or in other words, the off-diagonal of the density matrix, is crucially important for the evolution of a system with two nonequilibrium quantum dots which are coherently coupled to a joint reservoir and subject to an onsite Coulomb interaction. In particular, it seems possible to create an imbalance between singlet and triplet states, although they are energetically degenerate.

In contrast, if we do not allow the evolution of superposition states for some reason (e.g. the dots are much further apart than the phase coherence length, the level detuning is much larger than the level broadening, intermediate measurement or projection on a dot takes place, etc.), i.e. if we neglect the isospin structure, the evolution of the singlet and triplet is nicely balanced. The probability to find a singlet or one of the triplets is exactly the same at any time and the system behaves as if it was a combination of two independent copies of a single level quantum dot.

4.3 Werner States and Entanglement

The observation that it is possible to create an imbalance between singlet and triplet, although they are energetically degenerate, is already fascinating in its own right. Yet, it raises two important questions. Is the effect realizable in an experiment and how may a measurement give evidence for the predicted behavior? And secondly, does the system bear any potential for a functional device? While we enter into the discussion of the first question in the next section by a quantitative analysis of the influence of asymmetric tunnel coupling, detuning, finite spin-flip relaxation and dephasing on the singlet-triplet asymmetry, we motivate in this section the functional potential of the system.

Entanglement of quantum states is one of the most fascinating features of quantum mechanics and one of the cornerstones of quantum information processing [45, 46]. Entangled photons have already been used in various experiments in quantum communication and cryptography [47]. For electrons in a solid-state environment recent progress can be linked to the advancing fabrication technology for nano-scale devices [48, 49]. The availability of an electron spin entangler would allow the implementation of quantum information schemes with electron spins [50, 51]. There is a strong experimental evidence that the spin degree of freedom of electrons in a semiconductor is very well protected from the environment. Dephasing times approaching microseconds and phase coherent transport over distances exceeding $100\,\mu m$ have been reported [52–54]. Therefore, electron spins are promising candidates for carriers in quantum information processing devices. Several schemes have been suggested for the production of spatially separated entangled electrons in solid state systems. Many of them rely on extracting the entangled electrons of a Cooper pair from a superconductor and separate them into two normal leads [55], Luttinger liquids [56, 57], or to two leads via two quantum dots [58]. Others are based on separating the electrons forming a spin singlet on a double quantum dot [59], using interference effects in a quantum dot in the cotunneling regime [60], separating a pair of entangled electrons from a singlet state by a triple quantum dot [61], or scattering off magnetic impurities [62].

In this section we summarize some basic facts about entanglement and introduce in particular the notion of entanglement for mixed states, which builds the foundation for the discussion of the generation of spin entanglement in nonequilibrium quantum dots coherently coupled to a joint reservoir, presented in the following sections.

4.3.1   Separability and Bell Inequalitites

Let us assume a bipartite system with a Hilbert space $H = H_A \otimes H_B$ as a direct product of two qubit Hilbert spaces (i.e. two-level systems) H_A and H_B, respectively. In the spin language, where the two possible projections of a qubit on a certain basis $\{|0\rangle_i, |1\rangle_i\}$, with $i \in \{A, B\}$, are denoted by the spin degree of freedom, $|0\rangle_i = |\uparrow\rangle_i$ and $|1\rangle_i = |\downarrow\rangle_i$, we can write an arbitrary pure state of a single qubit in the form $|\psi\rangle_i = a|\uparrow\rangle_i + b|\downarrow\rangle_i$, $a, b \in \mathbb{C}$, where $|a|^2 + |b|^2 = 1$ ensures normalization. More general, we can represent any pure or mixed state of a part-system by a density operator ρ_i defined on the corresponding Hilbert space H_i. In case of a pure state, $|\psi\rangle_i$, the density operator is simply given by the projector $\rho_i = |\psi\rangle_i\langle\psi|_i$. A state of the bipartite system, pure or mixed, can be described by a density operator ρ defined on the product space $H = H_A \otimes H_B$. It is called separable if and only if it can be decomposed in a convex sum $\rho = \sum_k p_k\,\rho_{Ak} \otimes \rho_{Bk}$ of product states of the subsystems A and B, described by the operators ρ_{Ak}, ρ_{Bk} on H_A and H_B, respectively [65, 66]. For a pure state $|\Psi\rangle$ with $\rho = |\Psi\rangle\langle\Psi|$ the notation simplifies and the above definition implies that $|\Psi\rangle$ is separable iff $|\Psi\rangle = |\psi\rangle_A \otimes |\psi\rangle_B$, i.e. if $|\Psi\rangle$ can be represented by a product of pure states of the two subsystems. A state in the Hilbert space H is called entangled if and only if it is not separable. We note that the properties entangled or separable are not affected by local unitary transformations $U = U_A \otimes U_B$. In turn, this means that any product state can not become entangled just by acting locally

on one or the other qubit, we rather have to introduce some nonlocal interaction between the two qubits at some point. One of the most popular maximally entangled pure states is a spin singlet

$$|\mathrm{S}\rangle = \frac{1}{\sqrt{2}}(|\uparrow\rangle_\mathrm{A} \otimes |\downarrow\rangle_\mathrm{B} - |\downarrow\rangle_\mathrm{A} \otimes |\uparrow\rangle_\mathrm{B}) \tag{4.14}$$

which is equivalent to our former notation, $|\mathrm{S}\rangle = (|\uparrow,\downarrow\rangle - |\downarrow,\uparrow\rangle)/\sqrt{2}$ with $|\sigma,\tilde{\sigma}\rangle := |\sigma\rangle_\mathrm{A} \otimes |\tilde{\sigma}\rangle_\mathrm{B}$. It is part of the basis of the four maximally entangled, so-called Bell states $\{|\psi_-\rangle, |\psi_+\rangle, |\phi_-\rangle, |\phi_+\rangle\}$ which consists of the singlet $|\psi_-\rangle = |\mathrm{S}\rangle$ and the three triplets $|\psi_+\rangle = |T_0\rangle$ and $|\phi_\pm\rangle = (|T_+\rangle \pm |T_-\rangle)/\sqrt{2}$. The spins of the subsystems A and B in a maximally entangled state are maximally quantum mechanically correlated. A spin measurement in either subsystem on the singlet state, for example, yields a spin up or a spin down with equal probability. But the instant we perfom the measurement on one subsystem, say A, with outcome σ, the state of subsystem B is immediately projected to the opposite spin $\bar{\sigma}$, which we will then detect with certainty.

The situation is similar for a mixed state described by a density matrix

$$\begin{aligned}\rho_\mathrm{classic} &= \frac{1}{2}\left(|\uparrow\rangle\langle\uparrow|_\mathrm{A} \otimes |\downarrow\rangle\langle\downarrow|_\mathrm{B} + |\downarrow\rangle\langle\downarrow|_\mathrm{A} \otimes |\uparrow\rangle\langle\uparrow|_\mathrm{B}\right) \\ &= \frac{1}{2}\left(|\uparrow,\downarrow\rangle\langle\uparrow,\downarrow| + |\downarrow,\uparrow\rangle\langle\downarrow,\uparrow|\right).\end{aligned} \tag{4.15}$$

But in contrast to the quantum correlation which persists under local unitary transformations, the classical stochastic correlation of the mixed state decreases if we rotate the basis.

A more quantitative test to distinguish quantum from classical correlation is provided by the Bell inequalities [63], in which the correlations along different directions are compared. The spin of A is measured in direction of a vector $\mathbf{a}$ and the spin of B in direction of a vector $\mathbf{b}$, the correlator $C_{\mathbf{ab}}$ is then defined as the expectation value

$$C_{\mathbf{ab}} := \langle(\mathbf{a}\cdot\boldsymbol{\sigma})_\mathrm{A} \otimes (\mathbf{b}\cdot\boldsymbol{\sigma})_\mathrm{B}\rangle = \mathrm{tr}\left(\rho\cdot(\mathbf{a}\cdot\boldsymbol{\sigma})_\mathrm{A} \otimes (\mathbf{b}\cdot\boldsymbol{\sigma})_\mathrm{B}\right) \tag{4.16}$$

with $\boldsymbol{\sigma} = (\sigma_x, \sigma_y, \sigma_z)$, the vector of Pauli matrices

$$\sigma_x = \begin{pmatrix} 0 & 1 \\ 1 & 0 \end{pmatrix}, \quad \sigma_y = \begin{pmatrix} 0 & -i \\ i & 0 \end{pmatrix}, \quad \sigma_z = \begin{pmatrix} 1 & 0 \\ 0 & -1 \end{pmatrix}. \tag{4.17}$$

The common Bell inequalities derived by Clauser, Horne, Shimony and Holt [64] is given in the (CHSH) form by

$$\mathrm{tr}\,\rho\,\mathcal{B} = C_{\mathbf{ab}} + C_{\mathbf{a'b}} + C_{\mathbf{ab'}} - C_{\mathbf{a'b'}} \leq 2 \tag{4.18}$$

with arbitrary vectors $\mathbf{a}, \mathbf{a'}, \mathbf{b}, \mathbf{b'} \in \mathbb{R}^3$ and the Bell operator

$$\mathcal{B} := \mathbf{a}\cdot\boldsymbol{\sigma} \otimes (\mathbf{b}+\mathbf{b}')\cdot\boldsymbol{\sigma} + \mathbf{a}'\cdot\boldsymbol{\sigma} \otimes (\mathbf{b}-\mathbf{b}')\cdot\boldsymbol{\sigma}. \tag{4.19}$$

If the Bell inequalities are violated for some choice of the vectors $\mathbf{a}, \mathbf{a}', \mathbf{b}, \mathbf{b}'$, the state of the system described by ρ is not separable. Thus, it is entangled and is, beyond any classical correlation, quantum correlated. Vice versa, separable states may be classically correlated, which means that they may be correlated in a stochastic sense, but they always respect all possible forms of Bell-type inequalities [68]. Thus, entanglement is a necessary condition for the violation of the CHSH Bell inequalities, but it is not sufficient. In other words, there exist mixed states that are entangled in the sense that they can not be decomposed into a convex sum of product states, but $\operatorname{tr} \rho \, \mathcal{B} \leq 2$ holds for all sets of unit vectors.

4.3.2 Entanglement Measures for Pure States

It is obvious that not every quantum correlated state is maximally entangled, and it is, therefore, desirable to quantify the degree to which a state is entangled. For pure states' entanglement a convenient measure is the entropy of entanglement or the so-called entanglement of formation [72],

$$\mathcal{E}(\Psi) := \mathcal{S}(\rho_{\mathrm{A}}) = \mathcal{S}(\rho_{\mathrm{B}}). \tag{4.20}$$

The notation for the system's state, $|\Psi\rangle \in H$, shall emphasize that it is a pure state, described by $\rho = |\Psi\rangle\langle\Psi|$, and $\rho_{\mathrm{A}} := \operatorname{tr}_{\mathrm{B}} \rho$ is the reduced density matrix of subsystem A, obtained by tracing out the degrees of freedom of subsystem B. Similarly, $\rho_{\mathrm{B}} := \operatorname{tr}_{\mathrm{A}} \rho$ is a partial trace over the degrees of freedom of subsystem A. The function

$$\mathcal{S}(\rho) := -\operatorname{tr} \rho \, \log_2 \rho \tag{4.21}$$

denotes the von Neumann entropy. The values of $\mathcal{E}$ range from zero for a product state to one for a maximally entangled state of two qubits.

In this special case, in which both subsystems contain only a single qubit, an often used equivalent measure of entanglement is the so-called concurrence [72],

$$\mathcal{C} := 2 \, \sqrt{\det \rho} \, . \tag{4.22}$$

Similar to the entropy it ranges from zero to one. A relation of the concurrence to the Bell inequalities, which are from an experimental point of view the most direct way to probe entanglement, can be established by searching for the set of unit vectors, $\{\mathbf{a}, \mathbf{a}', \mathbf{b}, \mathbf{b}'\}$, which maximizes the Bell parameter [70],

$$\max_{\mathbf{a}, \mathbf{a}', \mathbf{b}, \mathbf{b}'} \operatorname{tr} (\rho \mathcal{B}) = 2 \, \sqrt{1 + \mathcal{C}^2} \, . \tag{4.23}$$

Hence, for any pure state we find an equivalence of the violation of the Bell inequalities and a concurrence larger than zero,

$$\max_{\mathbf{a}, \mathbf{a}', \mathbf{b}, \mathbf{b}'} \operatorname{tr} (\rho \mathcal{B}) > 2 \qquad \Longleftrightarrow \qquad \mathcal{C} > 0 \, . \tag{4.24}$$

4.3.3 Entanglement Measures for Mixed States

For mixed states it is more complicated to quantify the degree of entanglement. It is even qualitatively more difficult to judge if a mixed state is entangled or not. It follows from the spectral theorem for compact self-adjoint operators, that every mixed state can be represented by a convex sum of pure states,

$$\rho = \sum_n p_n \, |\Psi_n\rangle\langle\Psi_n| \,, \tag{4.25}$$

but this representation is in general not unique, because the states $|\Psi_n\rangle$ need not be orthogonal (maybe there is a degenerate subspace of dim > 1). Guided by the definition of separability, we call the mixed state entangled if we can not find any decomposition into pure product states, $|\Psi_n\rangle = |\psi_n\rangle_{\mathrm{A}}|\psi_n\rangle_{\mathrm{B}}$. Corresponding to pure states, the entanglement of formation for a mixed state is defined [72] as the minimum entanglement of all possible mixtures of pure states which represent ρ in a decomposition,

$$\mathcal{E} := \min_{\{p_n, |\Psi_n\rangle\}} \sum_n p_n \, \mathcal{E}(\Psi_n) \,. \tag{4.26}$$

The calculation of the entanglement of formation for a general bipartite mixed state is more complicated than for a pure state, because we have to minimize over all possible convex sum decompositions which are in general hard or even impossible to find. However, in the case of two two-state systems, i.e. two entangled qubits, S. Hill and W. K. Wootters [69, 71] derived an explicit expression for the entanglement of formation,

$$\mathcal{E}(\rho) := h\left(\frac{1}{2}(1 + \sqrt{1 - \mathcal{C}^2}) \right), \tag{4.27}$$

with the function $h(x) := -x \log_2 x - (1 - x) \log_2(1 - x)$ and the concurrence

$$\mathcal{C}(\rho) := \max\{0, \sqrt{\lambda_1} - \sqrt{\lambda_2} - \sqrt{\lambda_3} - \sqrt{\lambda_4}\} \,. \tag{4.28}$$

The eigenvalues λ_i of the matrix product $\rho \cdot (\sigma_y \otimes \sigma_y) \cdot \rho^* \cdot (\sigma_y \otimes \sigma_y)$ are numbered in decreasing order $\lambda_1 \geq \lambda_2 \geq \lambda_3 \geq \lambda_4$. The entanglement of formation, $\mathcal{E}$, is a strictly monotonic function of the concurrence, $\mathcal{C}$, with $0 \leq \mathcal{C} \leq 1$, so that both can be viewed as equivalent measures of entanglement. If ρ describes a pure state, both definitions coincide with the corresponding definitions originally introduced for pure states. Following from the definition (4.26), the entanglement of formation and, equivalently, the concurrence is zero for a separable state, whereas $\mathcal{E} > 0$ or $\mathcal{C} > 0$ indicate an entangled mixed state.

4.3.4 Werner States

A special class of mixed states of a bipartite system is given by states that are diagonal in the Bell basis $\{\psi_-, \psi_+, \phi_-, \phi_+\}$. In the theory of quantum information and, more

specifically, in the discussion of entanglement purification from mixed states and quantum error correction [72,73] the even more restricted family of spin-rotation invariant, so-called Werner states [68] play an important role. Werner states can be parametrized in the form

$$W(F) := F \, |\mathrm{S}\rangle\langle\mathrm{S}| + \frac{1-F}{3} \left(\mathbb{1}_4 - |\mathrm{S}\rangle\langle\mathrm{S}| \right), \tag{4.29}$$

consisting of F parts pure singlet and $(1-F)/3$ parts of each of the other Bell states or triplets. Here, $|\mathrm{S}\rangle\langle\mathrm{S}|$ is the projector onto the singlet state, $|\mathrm{S}\rangle$, which is equivalent to the Bell state $|\psi_-\rangle$. The parameter F is the so-called Werner- or singlet fidelity and ranges from zero to one, $0 \leq F \leq 1$. The concurrence of a Werner state is given by

$$\mathcal{C}(W(F)) = \max\{0, 2\,F - 1\}. \tag{4.30}$$

Hence, it is entangled in the sense that it can not be decomposed into a convex sum of product states if $F > 1/2$. On the other hand, R. F. Werner was the first who showed that, although a mixed state like $W(F)$ with $F > 1/2$ is entangled, it does not necessarily violate the Bell inequalities in the CHSH form [68]. In particular, it has been shown [74] that the maximal CHSH-Bell parameter for Werner states is given by

$$\max_{\mathbf{a},\mathbf{a}',\mathbf{b},\mathbf{b}'} \operatorname{tr}(\rho\mathcal{B}) = \frac{2\sqrt{2}}{3} \left(2\,\mathcal{C} + 1 \right) = \frac{2\sqrt{2}}{3} \left(4\,F - 1 \right). \tag{4.31}$$

That means, in a range of $1 < F \leq (3 + \sqrt{2})/(4\sqrt{2})$ the Werner fidelity F parametrizes mixed states which are entangled without violating the Bell inequalities in the CHSH form. But, nevertheless, Werner states with a fidelity $F > 1/2$ are entangled and there exist entanglement purification protocols to destill arbitrarily entangled states, e.g. maximally entangled pure singlets, from an ensemble of entangled mixed states [72,73].

   In the next section we will see in detail how two quantum dots with a strong on-site Coulomb repulsion and a coherent coupling to a joint reservoir can be driven into a nonequilibrium situation such that the mixed state of the doubly occupied system is a Werner state with fidelity $F > 1/2$, indicating the generation of entanglement.

4.4   Generation of Spin Entanglement in Nonequilibrium – Part 1

Motivated by the possibility to create an imbalance between the singlet and triplet probabilities in the driven double dot system, which we discussed formally in section 4.2, we examine in this section quantitatively how robust the effect is under realistic conditions. Furthermore, we suggest a measurement scheme which may give evidence for the predicted behavior.

   Focused on the observation that the mixed state of the doubly occupied quantum dot system is a Werner state, we concentrate on the fact that the creation of a singlet probability

outbalancing the probability for triplets by a certain amount can be viewed as generation of spin entanglement between the electrons on the two spatially separated quantum dots.

A general state of the reduced system can be described by the two vectors $\mathbf{p} = (p_0, p_1, p_S, p_T)$ and $\mathbf{I} = (I_x, I_y, I_z)$ summarizing all degrees of freedom if the symmetries of the Hamiltonian, especially the spin symmetry, are taken into account. The doubly occupied system is then completely determined by the singlet and triplet probabilities p_S and p_T such that the block of the reduced density matrix for the doubly occupied subspace has Werner form

$$\rho_{2e} = \frac{p_S}{p_S + p_T}\, |S\rangle\langle S| + \frac{p_T}{3\,(p_S + p_T)}\,(\mathbb{1}_4 - |S\rangle\langle S|)\,, \tag{4.32}$$

and the Werner parameter given by

$$F = \frac{p_S}{p_S + p_T}\,. \tag{4.33}$$

Recalling the property of entanglement of a Werner state if $F > 1/2$, we conclude that we can consider our double dot system as an nonequilibrium entangler if we are able to generate an imbalance between the singlet and triplet probabilities such that more than every second doubly occupied state is a singlet, i.e. $p_S > p_T$. We note that in an equilibrium situation the probabilities are governed by Boltzmann factors and in particular singlet and triplets are equally distributed, $p_S = p_T/3$.

Let us reconsider the charging scheme from section 4.2, i.e. we are starting with an initially empty system and pull the dot levels down quickly, well below the Fermi energy of the lead. In the case of the perfectly symmetric setup, $\Gamma_{Lu} = \Gamma_{Ld}$ and $\Delta\varepsilon = 0$, the system will be charged subsequently with two electrons forming a pure singlet state, because, as we have seen in section 4.2, the evolution of the triplet decouples completely from the probability of the empty system. Thus, we obtain a fidelity $F = 1$ and the electrons are maximally entangled.

In realistic situations, however, various mechanisms will relax the imbalance between the population of spin singlet and triplet states. In section 4.2 we already discussed qualitatively how the isospin rotation, induced by asymmetric coupling or finite detuning, affects the imbalance between singlet and triplet probabilities. Here we analyze more quantitatively the influence on the ability to generate spin entanglement. In Fig. 4.2 we plot the time evolution of the Werner fidelity in lowest order in the tunneling, corresponding to the solution of the kinetic equations (4.9), and compare four different scenarios. The curve for the symmetric setup shows the formation of the maximally entangled, pure singlet state with F identical to unity. To mark a frame of accessibility of $F > 1/2$, we plot two further curves for which we assumed quite strong asymmetries. One is calculated with a detuning $\Delta\varepsilon$ of the order of the level broadening Γ_L, the other with one order of magnitude between the coupling strengths of the upper and lower dot. In both cases we still find a considerable imbalance between singlet and triplet probabilities and a Werner fidelity well exceeding the threshold of entanglement at one half.
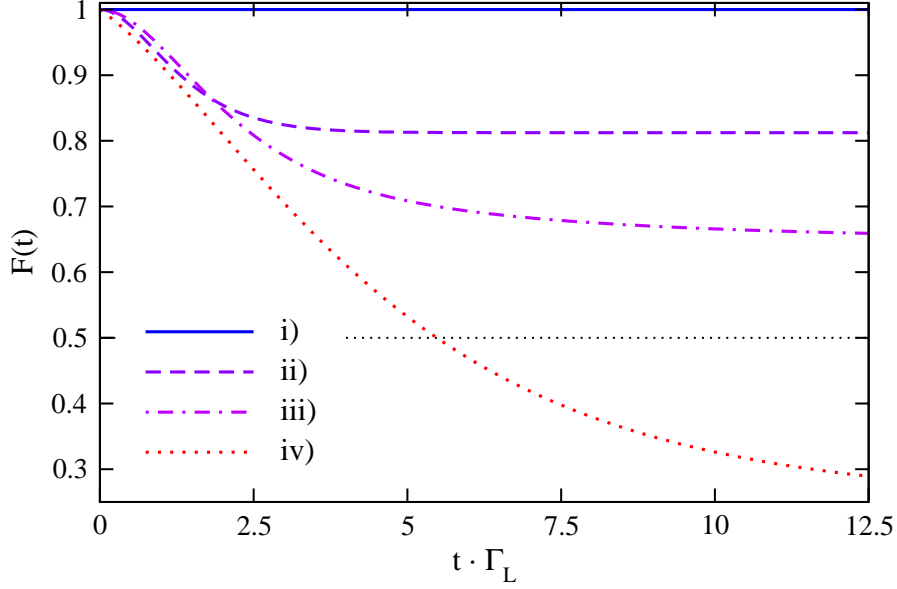
Figure 4.2:   The evolution of the Werner fidelity. For the perfectly symmetric setup, $\Delta\varepsilon = 0$, $\Gamma_{\mathrm{Lu}} = \Gamma_{\mathrm{Ld}}$, in the absence of spin relaxation, $\Gamma_{\mathrm{S}\to\mathrm{T}} = 0$, curve i), we find $F \equiv 1$. The Werner fidelity is reduced for either ii) nondegenerate dot energy levels, $\Delta\varepsilon = \Gamma_{\mathrm{L}}$, iii) asymmetric coupling $\Gamma_{\mathrm{Ld}} = 0.1\,\Gamma_{\mathrm{Lu}}$, iv) a finite spin relaxation rate $\Gamma_{\mathrm{S}\to\mathrm{T}} = 0.2\,\Gamma_{\mathrm{L}}$. The high-energy cutoff is set to $D = 100\,\mathrm{k_B}T$.

If we concentrate on the case of finite detuning but symmetric coupling of the two levels, the triplet probability saturates at

$$p_{\mathrm{T}} = \frac{3\,\Delta\varepsilon^2\,(\Gamma_{\mathrm{L}}^2 - \Delta\varepsilon^2)}{4\,(4\,\Gamma_{\mathrm{L}}^4 - (\Gamma_{\mathrm{L}}^2 + \Delta\varepsilon^2)^2)} \tag{4.34}$$

which scales with $p_{\mathrm{T}} \approx \left(\frac{\Delta\varepsilon}{2\,\Gamma_{\mathrm{L}}}\right)^2$ for weak detuning. Schematically we can motivate that with the kinetic equations (4.9) at hand: For $\Gamma_{\mathrm{Lu}} = \Gamma_{\mathrm{Ld}}$ the quantization axes **n** and **m** are perpendicular. The detuning $\Delta\varepsilon$ leads to a rotation of the isospin around **n** with a frequency $\Delta\varepsilon$. Hence, the isospin, which we would get for $\Delta\varepsilon = 0$, rotates out of the **m**-direction, in which the triplet was blocked, until a second electron enters the system. In average this happens after a time $1/\Gamma_{\mathrm{L}}$. The further the isospin is rotated away from the **m**-direction, the higher the probability that an entering electron may generate a triplet. Because of symmetry reasons, the lowest order correction due to a finite detuning has to be quadratic. Thus, the scaling behavior of the triplet probability for weak detuning seems reasonable. Remark: The asymptotic behavior (4.34) even holds for strong detuning $\Delta\varepsilon \gg \Gamma_{\mathrm{L}}$, as long as both dot levels are well below the Fermi energy of the lead, $\varepsilon \ll -|\Delta\varepsilon|, \Gamma_{\mathrm{L}}, k_{\mathrm{B}}T$. If the splitting is much larger than the level broadening of the dots, the isospin will be polarized during the charging process, i.e. an electron enters either the upper or the lower dot, depending on which energy is lower. The second electron then occupies the opposite

dot. That way, neither superposition states of the upper and lower dot are formed nor an imbalance between singlet and triplet. This is reflected in the limit of the asymptotic behavior for strong detuning, $p_T \approx 3/4$, which is the equilibrium value.

Additionally to the curves which stem directly from the systematic derivation of the kinetic equations (4.9) from the Hamiltonian of our system, we include a further curve for which we extend the kinetic equations by a phenomenologic block which accounts for spin flip processes and dephasing, mediated by a possible coupling to an external bath. We introduce phenomenologic transition rates between singlet and triplets as well as between the different triplets and summarize them in matrix form in the general basis $\{p_S, p_{T_0}, p_{T_\pm}\}$ for the doubly occupied subspace,

$$\mathbf{M} := \begin{pmatrix} -\Gamma_{S \to T_0} - 2\,\Gamma_{S \to T_\pm} & \Gamma_{T_0 \to S} & 2\,\Gamma_{T_\pm \to S} \\ \Gamma_{S \to T_0} & -\Gamma_{T_0 \to S} - 2\,\Gamma_{T_0 \to T_\pm} & 2\,\Gamma_{T_\pm \to T_0} \\ \Gamma_{S \to T_\pm} & \Gamma_{T_0 \to T_\pm} & -\Gamma_{T_\pm \to S} - \Gamma_{T_\pm \to T_0} \end{pmatrix}. \tag{4.35}$$

Spin flip processes induce transitions beween $|S\rangle$ and $|T_\pm\rangle$, as well as between $|T_0\rangle$ and $|T_\pm\rangle$, whereas $\Gamma_{S \to T_0}$ and $\Gamma_{T_0 \to s}$ account for the appearance of a relative phase between $|\uparrow, \downarrow\rangle$ and $|\downarrow, \uparrow\rangle$ caused by dephasing. For the plot we specifically choose all rates to be equal to preserve the spin symmetry apparent in the equivalence of the three triplet probabilities in the kinetic equations (4.9) and in the form of the Werner state (4.29). We simplify the basis again to $\{p_S, p_T\}$ and obtain the matrix

$$\mathbf{M}_{S \leftrightarrow T} := \begin{pmatrix} -\Gamma_{S \to T} & \Gamma_{T \to S}/3 \\ \Gamma_{S \to T} & -\Gamma_{T \to S}/3 \end{pmatrix} \tag{4.36}$$

with the effective transition rate $\Gamma_{S \to T} = \Gamma_{T \to S}/3$ (which ensures probability conservation). (A different choice of these parameters does not change the conclusions concerning the perturbation of the singlet-triplet imbalance qualitatively, but we would have to generalize the form of the doubly occupied mixed state. Instead of a Werner state with equal weights for the three triplets, we would have to deal with a more general state which were still diagonal in the singlet-triplet basis, $\{|S\rangle, |T_0\rangle, |T_+\rangle, |T_-\rangle\}$ (and in the Bell basis), but the weights for the triplets were not necessarily equivalent.)

We incorporate the singlet-triplet relaxation in the kinetic equations and solve for the reduced density matrix. In Fig. 4.2 we plot the corresponding curve which quickly approaches the equilibrium between singlet and triplet at $F = 1/4$ (or $p_S = 1/4$ and $p_T = 3/4$, respectively). The formation of an enhanced singlet probability or even a Werner fidelity $F > 1/2$ therefore requires tunneling rates larger than the spin decoherence rate. Reported values of T_2^* of the order of $10\,\mathrm{ns}$ [48,49] (at temperatures of the order of $100\,\mathrm{mK}$) correspond to a lower limit of the coupling strength Γ_L of the order of μeV. For strong tunnel coupling higher-order processes such as cotunneling become important. These are neglected in our quantitative analysis but they do not change our prediction qualitatively. In fact, for symmetric tunnel coupling the Hamiltonian acquires a block structure and the Hilbert subspace containing the triplet states decouples completely from the one for the empty dot. It is only for an assumed asymmetry in the system that higher order processes
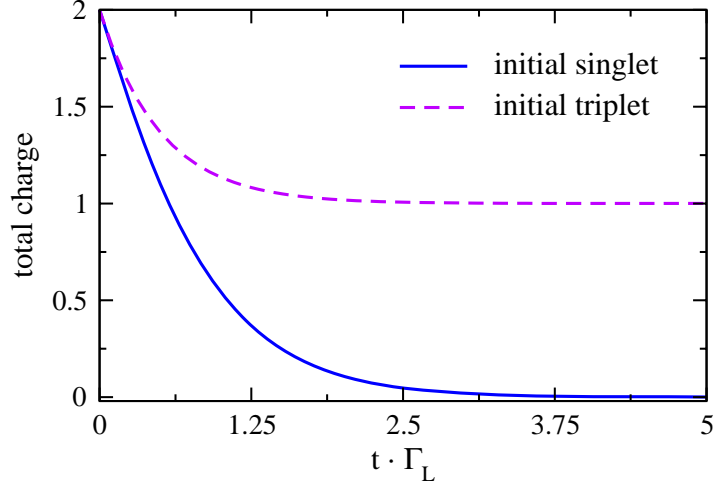
Figure 4.3:   Time evolution of the total charge during the discharging of an initial singlet state compared to an initial triplet state. The system is assumed to b perfectly symmetric, $\Gamma_{\mathrm{Lu}} = \Gamma_{\mathrm{Ld}}$, $\Delta\varepsilon = 0$. Starting from a singlet the system empties quickly, whereas it remains singly occupied if we start from a triplet state.

induce a relaxation of the singlet-triplet imbalance. This equilibration takes place with a comparably small rate if the dots are weakly coupled to the reservoir, $\Gamma_{\mathrm{Lu}}, \Gamma_{\mathrm{Ld}} \ll k_{\mathrm{B}}T$. Hence, the corresponding time scale is much larger than the time scale for the formation of the singlet state. (For a temperature of the order of $100\,\mathrm{mK}$ an upper bound of the coupling strength might be of the order of $10\,\mu eV$.)

To create and detect an enhanced spin-singlet fidelity and to measure the relaxation time between singlet and triplet, we propose the following scheme that is similar to the experiment performed in Ref. [48]. It is based on the observation that just like charging the double dot predominantly yields singlet states, the converse process, the discharging, is easy if the initial state is a spin singlet. An initial triplet state may get stuck in a singly occupied state with an isospin component antiparallel to **m** (as discussed in detail in section 4.2). The complete discharging of a triplet to an empty state, therefore, takes on average a longer time than the transition from the singlet to the empty system. We illustrate this for the ideal system in Fig. 4.3. The total charge of the double dot is plotted versus the discharging time for an initial singlet and an initial triplet state, respectively.

The suggested measurement scheme consists of an entire cycle:

1. Prepare the system in an empty state.

2. Pull the dot levels down quickly (i.e. faster than the time scales for the relaxation of the isospin polarization and the singlet-triplet transitions), well below the Fermi energy of the lead. The double dot will be charged with two electrons which preferably form a spin singlet state, as explained above.

3. Wait some given time t_{w}. During this time the imbalance between singlet and triplet

decays exponentially on a time scale given by the relaxation rate. The Werner fidelity is reduced.

4. Now we start to analyze how the double dot is depleted. Depending on whether the initial state is a singlet or a triplet, it is possible or impossible to extract both electrons to the joint lead. We continue the scheme in the following way: Push the dot levels up quickly (i.e. faster than the relaxation for the isospin polarization), well above the Fermi energy of the lead.

5. Wait some time longer than $1/\Gamma_\mathrm{L}$ but shorter than the relaxation time of the isospin-polarized state.

6. Measure the total charge on the double dot.

If the charge is zero, the doubly-occupied state was a spin singlet, whereas it was a triplet if one electron remains in the system. The measurement of the total charge on the double dot could be performed by a close-by quantum point contact. This does not introduce an additional relaxation mechanism for either the isospin or the singlet and triplet states because the quantum-point contact is only sensitive to the total charge.

4.5 Bias Voltage Driven Quantum Dots

An important building block for the conclusions in section 4.4 was the nonequilibrium situation, in which the double dot system was driven by quickly moving the level positions of the dots with respect to the Fermi energy of the reservoir. This way the system was forced to change its charge state, which facilitated the generation of an isospin polarization and an imbalance between singlet and triplet probabilities. In the present and in the following section we extend the previous consideration to a driving by an applied bias voltage and analyze the stationary state of the double dot. Based on the introduced model for two quantum dots coherently coupled to one joint reservoir in section 4.1, we attach additional leads to each of the dots as depicted in Fig. 4.4. This enables us to apply a bias voltage between the joint left and the two independent right reservoirs.

Corresponding to the Hamiltonian in section 4.1 the system is modeled by $H = H_\mathrm{res} + H_\mathrm{dots} + H_\mathrm{t}$, consisting of the term for the leads, $H_\mathrm{res} = \sum_r \sum_{k\sigma} \varepsilon_{rk}\, a^\dagger_{rk\sigma} a_{rk\sigma}$, with a joint left ($r = \mathrm{L}$) and two independent right reservoirs ($r = \mathrm{R_u}, \mathrm{R_d}$), the part for the double dot system which is equivalent to Eq. (4.1), and the tunnel Hamiltonian

$$H_\mathrm{t} = \sum_r \sum_{k\sigma i} \left(t_{ri}\, c^\dagger_{i\sigma} a_{rk\sigma} + \mathrm{h.c.} \right). \tag{4.37}$$

We assume that the upper right reservoir ($r = \mathrm{R_u}$) couples exclusively to the upper dot ($i = \mathrm{u}$), whereas the lower right reservoir ($r = \mathrm{R_d}$) couples exclusively to the lower dot ($i = \mathrm{d}$). Thus, the off-diagonal tunneling elements vanish, $t_{\mathrm{R_u}\mathrm{d}} = t_{\mathrm{R_d}\mathrm{u}} = 0$, and we can simplify the notation, $t_{\mathrm{R}i} := t_{\mathrm{R}_i i}$. In particular, there is no explicit coupling of electrons
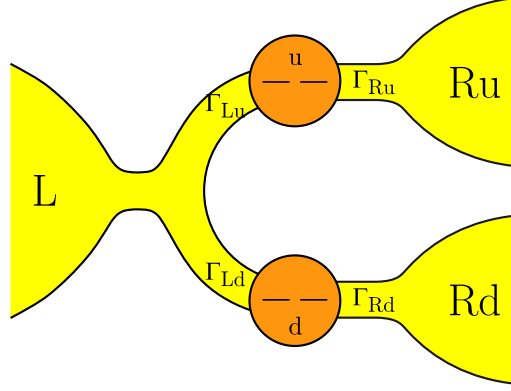
Figure 4.4:   Two quantum dots (u and d) are coupled to a joint electron reservoir on the left (L) and to two additional independent reservoirs (R_u and R_d) on the right.

from the right reservoirs to superposition states. Each level in one of the right leads couples unambiguously to one corresponding dot level. This becomes more obvious if we rearrange the tunnel Hamiltonian and write $H_t = H_{tL} + H_{tR}$ with the coupling to the left reservoir equivalent to Eq. (4.2),

$$H_{tL} = \sum_{k\sigma} \left[\left(t_{Lu}\, c_{u\sigma}^\dagger + t_{Ld}\, c_{d\sigma}^\dagger \right) a_{Lk\sigma} + \text{h.c.} \right], \tag{4.38}$$

and the coupling to the additional right reservoirs,

$$H_{tR} = \sum_{k\sigma i} \left[t_{Ri}\, c_{i\sigma}^\dagger a_{Rik\sigma} + \text{h.c.} \right], \tag{4.39}$$

where the index i of the annihilation operators $a_{Rik\sigma}$ (as well as the creation operators $a_{Rik\sigma}^\dagger$) for electron states in the right reservoirs explicitly indicates the upper ($i = u$) or the lower dot ($i = d$).

   As in Eq. (4.2), the tunneling is assumed to be independent of spin and energy. The tunneling strength is parametrized by $\Gamma_{ri} = 2\pi\, t_{ri}^2\, N_r$ for the upper ($i = u$) and the lower dot ($i = d$), respectively, and depends on the reservoir the electron tunnels to or from ($r \in \{L, R_u, R_d\}$). The density of states of the respective reservoir is denoted by N_r. (Since the geometry of the setup is simply connected we can choose the gauge such that the tunneling amplitudes t_{ri} are real.) The leads serve again as equilibrium reservoirs with spin degenerate energies ε_{rk}. Their electrochemical potentials μ_r are not necessarily equivalent and allow for a finite potential difference between the left and the right side.

   We choose the basis as explained in section 4.2 and express the degrees of freedom of the reduced density matrix in a vector representation for the probabilities, $\mathbf{p} = (p_0, p_1, p_S, p_T)$, and the isospin, $\mathbf{I} = (I_x, I_y, I_z)$. Applying the real-time diagrammatic technique, we set up the kinetic equations governing the evolution of the reduced density matrix. Similar to

Eqs. (4.9) we obtain

$$
\frac{\mathrm{d}}{\mathrm{d}t}\mathbf{p} = \sum_{ri}\Gamma_{ri}
\begin{pmatrix}
-2\,f_r & (1-f_r)/2 & 0 & 0 \\
2\,f_r & -(1+f_r)/2 & 1-f_r & 1-f_r \\
0 & f_r/4 & -1+f_r & 0 \\
0 & 3\,f_r/4 & 0 & -1+f_r
\end{pmatrix}
\mathbf{p} + \Gamma_{\mathrm{L}}
\begin{pmatrix}
2-2\,f_{\mathrm{L}} \\
-2+4\,f_{\mathrm{L}} \\
f_{\mathrm{L}} \\
-3\,f_{\mathrm{L}}
\end{pmatrix}
(\mathbf{I}\cdot\mathbf{m}) +
$$

$$
+
\begin{pmatrix}
\Gamma_{\mathrm{Ru}}\left(1-f_{\mathrm{R_u}}\right) - \Gamma_{\mathrm{Rd}}\left(1-f_{\mathrm{R_d}}\right) \\
-\Gamma_{\mathrm{Ru}}\left(1+3\,f_{\mathrm{R_u}}\right) + \Gamma_{\mathrm{Rd}}\left(1+3\,f_{\mathrm{R_d}}\right) \\
-(\Gamma_{\mathrm{Ru}}\,f_{\mathrm{R_u}} - \Gamma_{\mathrm{Rd}}\,f_{\mathrm{R_d}})/2 \\
-3\left(\Gamma_{\mathrm{Ru}}\,f_{\mathrm{R_u}} - \Gamma_{\mathrm{Rd}}\,f_{\mathrm{R_d}}\right)/2
\end{pmatrix}
(\mathbf{I}\cdot\mathbf{n}) + 2\,\Gamma_{\mathrm{L}}\,f_{\mathrm{L}}
\begin{pmatrix}
0 \\
1 \\
-1 \\
0
\end{pmatrix}
(\mathbf{I}\cdot\mathbf{n})(\mathbf{m}\cdot\mathbf{n})
\tag{4.40}
$$

for the probabilities, where $r \in \{\mathrm{L},\mathrm{R_u},\mathrm{R_d}\}$, $i \in \{\mathrm{u},\mathrm{d}\}$ and $\Gamma_{\mathrm{L}} := (\Gamma_{\mathrm{u}} + \Gamma_{\mathrm{d}})/2$. The quantization axes $\mathbf{n}$ and $\mathbf{m}$ are familiar from section 4.2, and we abbreviate the Fermi distribution of the electrons in the left and the right reservoirs by $f_r \to [1 + \exp(\beta\,(\varepsilon - \mu_r))]^{-1}$, evaluated at the mean dot energy $\varepsilon := (\varepsilon_{\mathrm{u}} + \varepsilon_{\mathrm{d}})/2$. The equations for the isospin read

$$
\frac{\mathrm{d}}{\mathrm{d}t}\mathbf{I} = \Gamma_{\mathrm{L}}\left[2\,f_{\mathrm{L}}\,p_0 + \left(f_{\mathrm{L}} - \frac{1}{2}\right)p_1 + (1-f_{\mathrm{L}})\,p_{\mathrm{S}} - (1-f_{\mathrm{L}})\,p_{\mathrm{T}}\right]\mathbf{m} +
$$

$$
+ \left[\Gamma_{\mathrm{Ru}}\,f_{\mathrm{R_u}}\,p_0 + \frac{1}{4}\,\Gamma_{\mathrm{Ru}}\left(-1+3\,f_{\mathrm{R_u}}\right)p_1 - \frac{1}{2}\,\Gamma_{\mathrm{Ru}}\left(1-f_{\mathrm{R_u}}\right)(p_{\mathrm{S}}+p_{\mathrm{T}})\right]\mathbf{n} -
$$

$$
- \left[\Gamma_{\mathrm{Rd}}\,f_{\mathrm{R_d}}\,p_0 + \frac{1}{4}\,\Gamma_{\mathrm{Rd}}\left(-1+3\,f_{\mathrm{R_d}}\right)p_1 - \frac{1}{2}\,\Gamma_{\mathrm{Rd}}\left(1-f_{\mathrm{R_d}}\right)(p_{\mathrm{S}}+p_{\mathrm{T}})\right]\mathbf{n} +
$$

$$
+ \Gamma_{\mathrm{L}}\left[\frac{f_{\mathrm{L}}}{2}\,p_1 - 2\,(1-f_{\mathrm{L}})\,p_{\mathrm{S}}\right]\mathbf{n}\,(\mathbf{m}\cdot\mathbf{n}) - \sum_{ri}\Gamma_{ri}\frac{1+f_r}{2}\,\mathbf{I} + \Delta\tilde{\varepsilon}\,(\mathbf{n}\times\mathbf{I}).
\tag{4.41}
$$

The level detuning $\Delta\varepsilon$ is mapped onto a renormalized, effective detuning

$$
\Delta\tilde{\varepsilon} = \Delta\varepsilon + \frac{\Gamma_{\mathrm{Lu}} - \Gamma_{\mathrm{Ld}}}{2\pi}\fint\frac{\mathrm{d}\omega}{\omega - \varepsilon}\,f_{\mathrm{L}}(\omega) - \frac{1}{2\pi}\fint\frac{\mathrm{d}\omega}{\omega - \varepsilon}\left(\Gamma_{\mathrm{Ru}}\,f_{\mathrm{R_u}}(\omega) - \Gamma_{\mathrm{Rd}}\,f_{\mathrm{R_d}}(\omega)\right).
\tag{4.42}
$$

To keep the discussion transparent we assume in the following symmetric couplings on the left, $\Gamma_{\mathrm{Lu}} = \Gamma_{\mathrm{Ld}} = \Gamma_{\mathrm{L}}$, as well as on the right side, $\Gamma_{\mathrm{Ru}} = \Gamma_{\mathrm{Rd}} =: \Gamma_{\mathrm{R}}$, and degenerate dot levels, $\Delta\varepsilon = 0$. Furthermore, we take the electrochemical potentials for the two right reservoirs to be equal $\mu_{\mathrm{R_u}} = \mu_{\mathrm{R_d}} =: \mu_{\mathrm{R}}$. With these assumptions the kinetic equations

simplify considerably,

$$\frac{\mathrm{d}}{\mathrm{d}t}\mathbf{p} = \sum_{r=\mathrm{L},\mathrm{R}} \Gamma_r \begin{pmatrix} -4\,f_r & 1-f_r & 0 & 0 \\ 4\,f_r & -1-f_r & 2-2\,f_r & 2-2\,f_r \\ 0 & f_r/2 & -2+2\,f_r & 0 \\ 0 & 3\,f_r/2 & 0 & -2+2\,f_r \end{pmatrix} \mathbf{p} + \Gamma_{\mathrm{L}} \begin{pmatrix} 2-2\,f_{\mathrm{L}} \\ -2+4\,f_{\mathrm{L}} \\ f_{\mathrm{L}} \\ -3\,f_{\mathrm{L}} \end{pmatrix} (\mathbf{I} \cdot \mathbf{m})$$

$$\frac{\mathrm{d}}{\mathrm{d}t}\mathbf{I} = \Gamma_{\mathrm{L}} \left[2\,f_{\mathrm{L}}\,p_0 + \left(f_{\mathrm{L}} - \frac{1}{2} \right) p_1 + (1-f_{\mathrm{L}})\,p_{\mathrm{S}} - (1-f_{\mathrm{L}})\,p_{\mathrm{T}} \right] \mathbf{m} - \sum_{r=\mathrm{L},\mathrm{R}} \Gamma_r\,(1+f_r)\,\mathbf{I}\,.$$

$$(4.43)$$

We compare the kinetic equations (4.43) to Eqs. (4.9) and note that the generation of an isospin polarization is governed solely by the coupling to the joint left reservoir. The two independent right reservoirs couple to all isospin components in the same way. Specifically, they contribute only to the decay of the isospin, and influence the evolution of the probabilites in the same way classical rates do. That means, we can not expect any isospin polarization or generation of a singlet-triplet imbalance by the independent right reservoirs. Quite the contrary, the coupling to the right reservoirs seems to diminish the effect induced by the coherent coupling to the joint left lead.

The generalization to asymmetric couplings on the left as well as on the right side and to arbitrary electrochemical potentials for the upper and the lower right reservoir is straightforward. Similar to the consideration in section 4.4 such asymmetries lead to a rotation of the isospin. However, the corresponding expressions (Eqs. 4.43) are less transparent and do not enlighten the discussion of generation of spin entanglement in nonequilibrium quantum dots, which we envisage in the next section. Nevertheless, asymmetries are always present in an experimental situation and yield a perturbation of the predicted behavior. Therefore it seems worthwhile to keep in mind the sources of possible distortions and render the examination more precisely if required.

4.6   Generation of Spin Entanglement in Nonequilibrium – Part 2

Related to the discussion in section 4.4, in which we drove the double dot system into a nonequilibrium situation by moving the dot levels with respect to the Fermi energy of the reservoir, the additional leads on the right hand side enable us to drive the system by an applied bias voltage. In the preceding section we set up the kinetic equations governing the evolution of the reduced density matrix, and we have seen that an isospin polarization can only emerge due to the coupling to the joint left reservoir. The leads on the right hand side couple to all isospin components in the same way. In a magnetic analogue such a situation is similar to a dot coupled to one ferromagnetic and one nonmagnetic lead, for which, at large bias voltage, spin accumulation occurs.
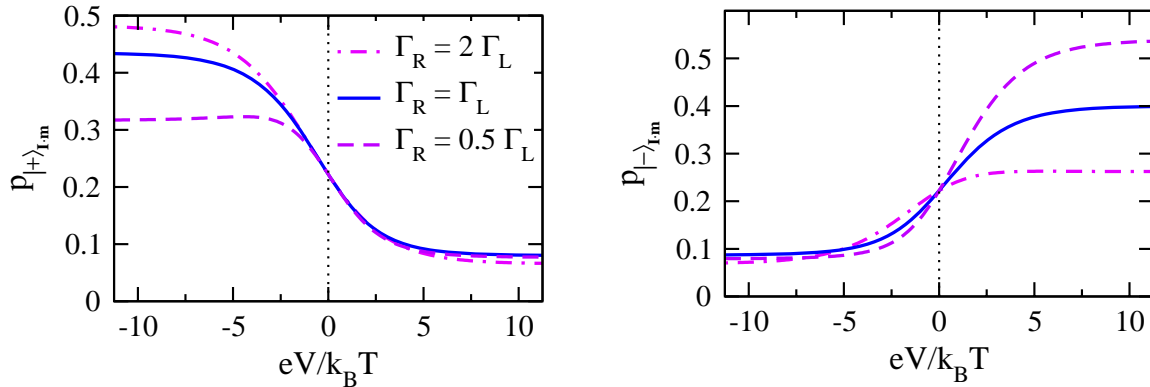
Figure 4.5: The stationary probabilities for the $|+\rangle_{\mathbf{I}\cdot\mathbf{m}}$ and $|-\rangle_{\mathbf{I}\cdot\mathbf{m}}$ state plotted vs. the bias voltage for $\varepsilon = 0$ and different ratios of the coupling strengths, $\Gamma_R/\Gamma_L = 2, 1, 0.5$. The bias is applied symmetrically, $-\mu_L = eV/2 = \mu_{R_u} = \mu_{R_d}$.

For the present model we solve the kinetic equations (4.40) and (4.41) in the stationary limit, where we assume a vanishing detuning of the dot levels, $\Delta\varepsilon = 0$, for simplicity. Depending on the polarity of the bias voltage, a finite isospin is accumulated in the double dot, as depicted in Fig. 4.5. We can interpret the curves in the following three scenarios:

i. For zero bias voltage the system is in equilibrium, and the probabilities to find a $|+\rangle_{\mathbf{I}\cdot\mathbf{m}}$ or a $|-\rangle_{\mathbf{I}\cdot\mathbf{m}}$ state are equivalent. This indicates that no isospin direction is preferred, there is no polarization.

ii. If the bias is applied such that the double dot is charged from the joint left and discharged to the right leads, the isospin is polarized in the positive $\mathbf{m}$ direction, and the probability to find the singly occupied system in a superposition state $|+\rangle_{\mathbf{I}\cdot\mathbf{m}}$ is high. On first sight, the modification for different relative couplings Γ_L/Γ_R looks counterintuitive, we might have expected a strong polarization for a strong coupling to the joint left reservoir. However, if we crank up Γ_L with respect to Γ_R, the probability that two electrons are pressed into the double dot increases (compare also the inset of Fig. 4.6). Therefore, the isospin polarization and the overall probability to find the double dot singly occupied decreases for $\Gamma_L > \Gamma_R$, in favor of the generation of singlet states. In the meanwhile the probability for $|-\rangle_{\mathbf{I}\cdot\mathbf{m}}$ stays more or less constant for different ratios Γ_L/Γ_R.

iii. If the bias is applied such that the double dot is discharged to the joint left and charged from the right leads, the induced doubly occupied states (for strong bias) are equally distributed between the singlet and the three triplets. As discussed in section 4.1, the singlet empties easily via a $|+\rangle_{\mathbf{I}\cdot\mathbf{m}}$ state to $|0\rangle$ during the discharging to the joint left reservoir, whereas the triplets decay to a $|-\rangle_{\mathbf{I}\cdot\mathbf{m}}$ state and might get stuck. Therefore, we accumulate an isospin in negative $\mathbf{m}$ direction as leftover.
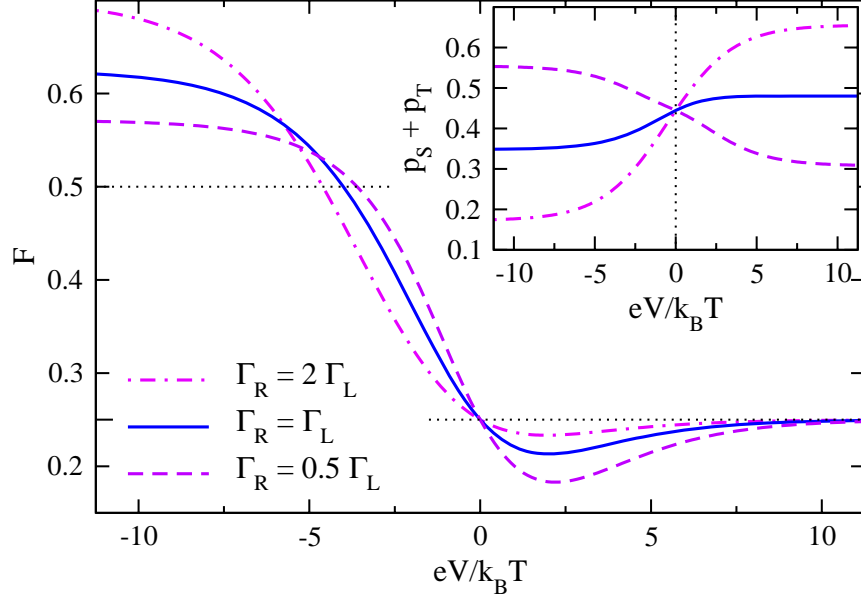
Figure 4.6: The stationary Werner fidelity F vs. bias voltage for $\varepsilon = 0$ and different ratios of the coupling strengths, $\Gamma_R/\Gamma_L = 2, 1, 0.5$. The bias is applied symmetrically, $-\mu_L = eV/2 = \mu_{R_u} = \mu_{R_d}$. The inset shows the corresponding stationary overall probabilities $p_S + p_T$ to find the system doubly occupied.

The induced imbalance between singlet- and triplet-state probabilities are shown in Fig. 4.6. Similar to the results in section 4.4 we find regimes with an enhanced singlet probability, culminating in a Werner fidelity $F > 1/2$ which indicates the generation of spin entanglement between the two spatially separated quantum dots. Hooked to the scenarios sketched above we can distinguish

i. In equilibrium the Werner fidelity $F = 1/4$, as expected for equally distributed singlet and triplet states.

ii. If we charge the double dot predominantly from the joint left reservoir the isospin becomes polarized and the singlet probability increases. In this regime the Werner fidelity saturates at

$$F = \frac{3\,\Gamma_L + 2\,\Gamma_R}{6\,\Gamma_L + 2\,\Gamma_R} \tag{4.44}$$

which ranges from $1/2$ for $\Gamma_L \gg \Gamma_R$ to 1 for $\Gamma_L \ll \Gamma_R$. Unfortunately, at the same time the Werner fidelity approaches 1 linearly for $\Gamma_L \ll \Gamma_R$, the overall probability to find the quantum dot system doubly occupied vanishes quadratically according to $p_S + p_T \approx 2\,(\Gamma_L/\Gamma_R)^2$. Hence, there is a tradeoff between finding singlets dominating over triplets and the probability to find a doubly occupied state at all (compare the inset of Fig. 4.6). Nevertheless, for the considered specifications with reasonable coupling to the left and right reservoirs, a Werner fidelity $1/2 < F < 1$, indicating

the generation of spin entanglement, is accessible for a (rather strong) bias voltage applied such that the electrons enter the system from the joint left lead.

iii. If the bias voltage is applied in the opposite direction, triplets are more likely. The system is charged from the right side, and the singlet and the three triplets are equally distributed ($F = 1/4$). The singlet is easily discharged to the left reservoir, whereas the discharging of the triplets yields $|-\rangle_{\mathbf{l \cdot m}}$ leftovers. As a consequence, the easy decay of $|+\rangle_{\mathbf{l \cdot m}}$ leads to a lack of singlets, apparent in the Werner fidelity $F < 1/4$, unless the recharging from the right reservoirs is strong and causes a saturation at $F = 1/4$.

4.7 Chapter Summary

In this chapter we studied two spatially separated quantum dots with an onsite Coulomb repulsion coherently coupled to a joint reservoir. We showed that a pair of entangled electrons can be created by driving the system out of equilibrium. The offdiagonal evolution of the reduced density matrix in a nonequilibrium situation indicates that electrons occupy coherent superposition states of the double dot's orbitals. In combination with a strong Coulomb interaction which prevents double occupancy of each individual dot, two excess electrons in the system form a so-called Werner state, a mixture of a singlet and three equiprobable triplets. If the double dot is coherently charged from a joint reservoir the singlet probability is enhanced, an imbalance is formed between the singlet and triplet states. In the framework of the discussion of entanglement of mixed states this can be related to the generation of spin-entanglement between the electrons on the spatially separated dots. The underlying mechanism is fundamentally different from those that rely on a singlet-triplet energy splitting, where entanglement is generated by a relaxation of the system to the spin-entangled ground state.

We suggested two schemes in which entanglement is a consequence of the coherent coupling of two quantum dots to a joint lead in combination with a strong onsite Coulomb interaction. In the first setup we studied the transient behavior after qickly pushing the dot levels from above to below the Fermi energy of the lead and the system starts to charge subsequently with two electrons. In the second setup we drive the system out of equilibrium by applying a bias voltage between the leads in a fork-like geometry. Depending on the polarity of the bias, we find in the steady state an enhanced probability of either the singlet or the triplet states. In both systems a strong singlet overweight is feasible under certain conditions. We emphasize that our proposal is based on a decided nonequilibrium effect and, in particular, does not require a finite singlet-triplet splitting.

The spatial separation of the two dots is only limited by the phase-coherence length, which can be several micrometer in typical semiconductor structures. Experimental realizations of quantum dots coherently coupled to a joint reservoir have already been demonstrated, e.g. [41–43].

In our quantitative analysis we neglected higher-order processes such as cotunneling and

Kondo-assisted tunneling, which become important for tunnel couplings Γ larger than $k_\mathrm{B}T$. However, these do not change our predictions qualitatively. In fact, for symmetric tunnel coupling, the Hamiltonian acquires a block structure and the Hilbert subspace containing the triplet states decouples completely from the one for the emtpy double dot.

Chapter 5

Aharonov-Bohm Interferometry with Quantum Dots

Quantum coherence is one of the fundamental building blocks in the physics of mesoscopic systems and is often a key for the understanding of phenomena in nanosize devices. In chapter 4 we discussed how a coupling of two quantum dots to a joint reservoir can lead to the formation of quantum mechanically coherent states and subsequent correlations. A naturally arising question is which effect coherent states and quantum correlations have on the transport properties of the system? The problem if and to which extent the transport through quantum dots is phase coherent is closely related but transcending. In the following we try to tackle both questions on the same footing. We have seen that Coulomb interaction on quantum dots plays a crucial role for the behavior of the system. Thus, we focus especially on the issue how Coulomb interaction affects the coherence of the transport and examine in detail possible signatures in the current or the conductance.

5.1 General Setup

In general, the current through a quantum dot does not provide any information about the coherence of the transport. We rather have to study interference experiments to approach this question. A convenient method is to embed quantum dots in an Aharonov-Bohm ring structure [76] (compare also Fig. 5.1). Similar to a double-slit experiment an electron which enters the interferometer splits into two partial waves propagating through the upper or the lower arm, respectively. By encircling the magnetic flux Φ threading the ring, the partial waves accumulate a mutual phase difference of $\varphi = 2\pi\,\Phi/\Phi_0$ which leads to an interference pattern at the drain. The periodicity is given by the flux quantum $\Phi_0 = e/h$.

Electrons are driven from say the left to the right reservoir by an applying a bias voltage across the Aharonov-Bohm interferometer. For (at least partially) coherent transport through the quantum dots we expect manifestations of interference in the current, i.e. periodic signatures depending on the magnetic flux. We can conclude that the transport through the system is entirely coherent if the current at a given bias voltage can be com-
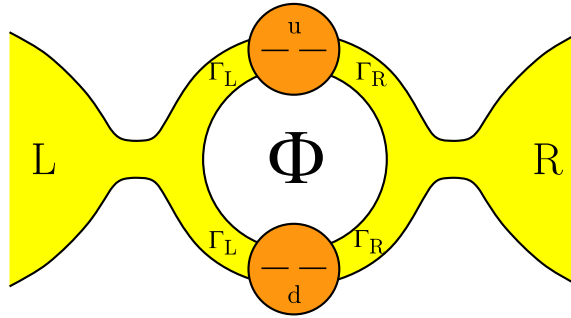
Figure 5.1:   Two quantum dots (u and d) embedded in an Aharonov-Bohm interferometer.

pletely blocked by tuning the magnetic flux, or in other words, if the interference pattern displays fully destructive interference. This is a sufficient indicator for total coherence but it is not a necessary one. In general, there are several mechanisms which can spoil fully destructive interference:

i. Each arm of the Aharonov-Bohm interferometer can be imagined as bunch of transmission channels with transmission probabilities $T_\sigma(\omega)$ for incoming electrons with spin σ and energy ω. If there is a mismatch between the sets of transmission channels of the upper and the lower arm, for example if the number of channels differs, we can not expect destructive interference for the unmatching channels even though the transport through each individual one is coherent.

ii. Provided a transmission channel, characterized by σ and ω, exists in both arms of the interferometer, an asymmetry between the corresponding transmission probabilities leads to a finite background even if the transport is fully coherent.

iii. A coupling of transmitted electrons to additional degrees of freedom can lead to dephasing. If the coupling is uncorrelated for the upper and lower arm of the interferometer the coherence, and therefore the possibility for interference, is destroyed (at least partially).

The first two mechanisms are qualitatively different from the third. They disturb the fully destructive interference, although the actual coherence is not affected. By optimizing the configuration of the setup, e.g. choose symmetric transmission probabilities for the upper and the lower arm and care for equivalent transmission channels, the influence of them can be minimized. In contrast, the third mechanism indeed destroys coherence. It is an inherent effect of the properties of the system we probe.

To meet the demands for the reduction of the influence of the first two mechanisms we consider in the following two nearly identical quantum dots embedded in an Aharonov-Bohm interferometer (Fig. 5.1). Due to tunneling the dot levels broaden to a width given by the coupling strength. If the dots are coupled equivalently to the reservoirs, the broadening of both is the same. If the dot levels are additionally degenerate, they filter out the same

fraction of incoming electrons in both arms, even at high temperature, high bias voltage and arbitrary level position.

In many experimental works Aharonov-Bohm interferometers with one [79, 84, 86, 89, 90, 99] or two quantum dots [41, 42, 103] have been realized, and a magnetic flux sensitivity of the total current and interference effects have been observed. This indicates that the current through quantum dots has at least phase coherent contributions. A fundamental challenge and achievement of the experiments lies in the focus on setups in which the role of electron-electron interaction is emphasized and investigated in a controlled way.

Our goal is to analyze in detail how Coulomb interaction on the dots can affect the coherence of the transport. We proceed on a path initiated in Refs. [96, 98] and take into account the full dynamics of the reduced density matrix, including all off-diagonal terms in first and second order tunneling. Furthermore, we go beyond the linear response regime and discuss nonequilibrium properties of the stationary state and the transport in the interplay of interaction and coherence effects.

We model the system sketched in Fig. 5.1 with a Hamiltonian $H = H_{\text{res}} + H_{\text{dots}} + H_{\text{t}}$ consisting of the term for the leads,

$$H_{\text{res}} = \sum_r \sum_{k\sigma} \varepsilon_{rk} \, a^{\dagger}_{rk\sigma} a_{rk\sigma}, \tag{5.1}$$

with a joint left and right reservoir ($r \in \{\text{L}, \text{R}\}$), the familiar part for the double dot system,

$$H_{\text{dots}} = \sum_i \left[\sum_\sigma \varepsilon_i \, c^{\dagger}_{i\sigma} c_{i\sigma} + U \, c^{\dagger}_{i\uparrow} c^{\dagger}_{i\downarrow} c_{i\downarrow} c_{i\uparrow} \right], \tag{5.2}$$

comprising the quantum dots up and down, $i \in \{\text{u}, \text{d}\}$, with the onsite Coulomb repulsion U, and the tunnel Hamiltonian $H_{\text{t}} = H_{\text{tL}} + H_{\text{tR}}$ which couples the double dot system to the reservoirs on the left and the right hand side. For reasons explained above we restrict ourselves to a small detuning $\Delta\varepsilon := \varepsilon_{\text{u}} - \varepsilon_{\text{d}}$ which is at most of the order of the level broadening implied by the tunneling, or, in the majority of cases, even to degenerate dot energies $\Delta\varepsilon = 0$. We define the mean of the spin degenerate dot energies by $\varepsilon := (\varepsilon_{\text{u}} + \varepsilon_{\text{d}})/2$. The phase which an electron accumulates while it is travelling through the ring is taken into account by attaching phase factors to each tunnel barrier. The gauge invariance allows us to choose a symmetric gauge, which proofs expedient for the bookkeeping, especially in higher order tunneling. We write the coupling to the left reservoir specifically

$$H_{\text{tL}} = \sum_{k\sigma} \left[t_{\text{L}} \left(\mathrm{e}^{-i\frac{\varphi}{4}} \, c^{\dagger}_{\text{u}\sigma} + \mathrm{e}^{+i\frac{\varphi}{4}} \, c^{\dagger}_{\text{d}\sigma} \right) a_{\text{L}k\sigma} + \text{h.c.} \right] \tag{5.3}$$

and for the right reservoir correspondingly

$$H_{\text{tR}} = \sum_{k\sigma} \left[t_{\text{R}} \left(\mathrm{e}^{+i\frac{\varphi}{4}} \, c^{\dagger}_{\text{u}\sigma} + \mathrm{e}^{-i\frac{\varphi}{4}} \, c^{\dagger}_{\text{d}\sigma} \right) a_{\text{R}k\sigma} + \text{h.c.} \right], \tag{5.4}$$

where $t_r \in \mathbb{R}^+$. We emphasize that for the determination of the functions $\gamma^{\pm}_{ii'r\sigma}$ in the diagrammatic technique (compare Eq. (3.33) in section 3.5) it is not merely t_r which has to

be taken into account, but the entire tunnel matrix element. In case of the Aharonov-Bohm interferometer it comprises in particular a phase factor which depends on the reservoir and dot index.

For transparency and reasons explained above, we restrict ourselves to a symmetric coupling strength of the upper and lower dot, but we explicitly allow for an asymmetry between the left and the right reservoir. Furthermore, the tunneling is assumed to be independent of spin and energy and we parametrize its strength by $\Gamma_r = 2\pi\, t_r^2\, N_r$. The density of states of the respective reservoir is denoted by N_r. The reservoirs are assumed to be large and in local equilibrium, with spin degenerate energies ε_{rk}. Their electrochemical potentials μ_r are not necessarily equivalent and allow for a finite potential difference between the left and the right hand side.

Our setup of an Aharonov-Bohm interferometer with embedded quantum dots can be considered as a closed two terminal device in which each electron which enters the system from the source reservoir is either transmitted to the drain or reflected back to the source. There is no way to escape to the environment in an uncontrolled way like in an open geometry (e.g. a usual double-slit experiment). Consequently, the Onsager relations yield a symmetry in the linear conductance which is known as phase locking [25,77]. In particular, the linear conductance $G = \partial I/\partial V|_{V=0}$ is symmetric under reversal of the magnetic flux $G(\varphi) = G(-\varphi)$. For higher bias voltage, i.e. if we are leaving the linear response regime, the Onsager relations do not enforce this symmetry anymore. However, the idealized setup with degenerate dot levels and equivalent couplings in the upper and the lower arm of the ring possesses a mirror symmetry with respect to a horizontal axis. For this special case the spatial symmetry implies

$$I(V,\varphi) = I(V, -\varphi) \tag{5.5}$$

in general, and phase locking occurs even for high bias voltage. This is not necessarily the case if we break the spatial symmetry, for instance by a finite detuning $\Delta\varepsilon$, and drive the system into a nonequilibrium situation beyond the validity of linear response. For an Aharonov-Bohm interferometer containing a single quantum dot with onsite Coulomb interaction this has been demonstrated explicitly in Refs. [82,98].

5.2   Noninteracting Quantum Dots

As starting point for the discussion of quantum dots embedded in an Aharonov-Bohm interferometer we set $U = 0$ and ignore the Coulomb interaction on the dots. For this simple case we summarize some basic results and sketch properties of the transport in first and second order in the coupling strength. The idea is to provide a reference to which we can contrast the more complicated and multifarious behavior of the system in the presence of strong Coulomb repulsion.

The Hilbert space of the reduced system has in general $2^4 = 16$ dimensions. Each of the dots can be empty, occupied with either spin, or both spins at the same time. Similar to the discussion of the noninteracting single quantum dot in section 3.6, we can decompose the Hamiltonian into two identical copies for each spin (if $U = 0$). Thus, the entire information

of the system can be condensed into a four-dimensional, spinless Hilbert space in which the states describe the empty system, one electron either on the upper or the lower dot, and both dots occupied. All other states can be reconstructed by products of these.

In contrast to a single dot the reduced density matrix does not stay diagonal during its evolution. According to the discussion of two quantum dots coupled to a joint lead in chapter 4, the electrons may occupy coherent superposition states which, in the case of an Aharonov-Bohm interferometer, may even be influenced by the phase induced by the magnetic flux threading the ring. We would have a hard time trying to solve the problem with a classical master-equation approach and Fermi's Golden Rule, because we do not know the basis in which the density matrix becomes diagonal at the instant of time we are interested in. Instead, we have to follow the full dynamics, including all off-diagonal terms.

According to the four dimensions of the Hilbert space, the reduced density matrix is 4×4, but similar to the discussion in section 4.2, the density operator decomposes due to particle number conservation into a direct product $\rho = \rho_{0e} \otimes \rho_{1e} \otimes \rho_{2e}$ of density operators ρ_{0e}, ρ_{1e} and ρ_{2e} for the empty, the singly and the doubly occupied subspaces, respectively. The singly and doubly occupied subspaces are completely determined by the diagonal terms or probabilities p_0 and p_2, respectively. The singly occupied subspace is spanned by the states $|1, 0\rangle$ and $|0, 1\rangle$ representing the occupation of the upper or the lower dot. Besides the corresponding diagonal probabilities p_{u} and p_{d} we have to respect the fact that the dots are coupled to joint reservoirs on either side, which yields the possibility for coherent superposition states, reflected in nonvanishing off-diagonal elements $p_{\mathrm{d}}^{\mathrm{u}} := \langle |0, 1\rangle\langle 1, 0| \rangle$ and $p_{\mathrm{u}}^{\mathrm{d}} := \langle |1, 0\rangle\langle 0, 1| \rangle$.

We set up the kinetic equations for the reduced density matrix according to the diagrammatic rules in section 3.5. In first order we take into account all diagram classes of the form depicted in Fig. 3.9. The solution of the equations in the stationary limit is straightforward except for two cases: if the dot levels are degenerate (i.e. $\Delta \varepsilon = 0$) and, at the same time, either $\varphi = 0$ or the coupling to one of the reservoirs vanishes, the solution is not unambiguously determinate. Fortunately, it is possible to solve the system in the vicinity of these points and perform an analytical continuation. For brevity, we write the lowest order solution of the stationary density matrix for $\Delta \varepsilon = 0$ and linear response:

$$p_0^{(0)} = (1 - f)^2 + \mathcal{O}(V^2), \qquad p_{\mathrm{u}}^{(0)} = p_{\mathrm{d}}^{(0)} = (1 - f)\, f + \mathcal{O}(V^2), \qquad p_2^{(0)} = f^2 + \mathcal{O}(V^2) \quad (5.6)$$

for the probabilities on the diagonal, and

$$p_{\mathrm{d}}^{\mathrm{u}(0)} = \frac{eV}{2} \frac{\Gamma_{\mathrm{L}}\, \mathrm{e}^{-i\frac{\varphi}{2}} - \Gamma_{\mathrm{R}}\, \mathrm{e}^{+i\frac{\varphi}{2}}}{\Gamma_{\mathrm{L}} + \Gamma_{\mathrm{R}}} f' + \mathcal{O}(V^2) \qquad \text{and} \qquad p_{\mathrm{u}}^{\mathrm{d}} = (p_{\mathrm{d}}^{\mathrm{u}})^* \qquad (5.7)$$

for the off-diagonal elements, where the Fermi function f and its derivative f' are evaluated at the dots' energy ε. We note that in the linear response regime the density matrix is not simply given by an equilibrium distribution. While the diagonal probabilities are actually determined by their equilibrium values, the off-diagonals are not. The elements which might appoint a designated direction in the singly occupied Hilbert subspace (even for

$\Delta\varepsilon = 0$), $p_{\rm d}^{{\rm u}(0)}$ and $p_{\rm u}^{{\rm d}(0)}$, vanish in equilibrium. However, they can give a finite contribution to the transport in linear response (the corresponding current rates contain a term which is constant in the bias voltage V). Furthermore, these are the only elements which actually depend on the phase φ. For finite detuning, $\Delta\varepsilon \neq 0$, or higher bias voltage, i.e. beyond linear response, all matrix elements become phase dependent. This is an effect of the coherent coupling to the joint reservoirs and possible quantum fluctuations between the upper and the lower dot.

The total current through the device is given by

$$I^{(1)} = -4 \, \frac{e}{\hbar} \, \frac{\Gamma_{\rm L}\Gamma_{\rm R}}{\Gamma} \, \frac{\Delta\varepsilon^2 + \Gamma_{\rm L}\Gamma_{\rm R} \, \sin^2\varphi}{\Delta\varepsilon^2 + 4\,\Gamma_{\rm L}\Gamma_{\rm R} \, \sin^2(\varphi/2)} \, (f_{\rm L} - f_{\rm R}) \tag{5.8}$$

which reduces to

$$I^{(1)} = -2 \, \frac{e}{\hbar} \, \frac{\Gamma_{\rm L}\Gamma_{\rm R}}{\Gamma} \, (1 + \cos\varphi) \, (f_{\rm L} - f_{\rm R}) \tag{5.9}$$

for $\Delta\varepsilon = 0$. As usual we define the total coupling strength $\Gamma := \Gamma_{\rm L} + \Gamma_{\rm R}$ and the Fermi functions in the left, $f_{\rm L}$, and the right reservoir, $f_{\rm R}$, are evaluated at the mean dot energy ε. We stress that even in lowest order in the coupling, which is often referred to as sequential tunneling, the transport is sensitive to the magnetic flux threading the ring. Moreover, complete destructive interference is feasible for a phase of odd multiples of π, which indicates fully coherent transport. Inspection of the current rates yields that in linear response the phase dependence originates solely from the off-diagonal terms. More drastically speaking, without the possibility to occupy superposition states we would not have any interference.

Heuristically we might draw a picture in which an electron from the left reservoir splits into two partial waves. These enter the upper and the lower dot and form a superposition state. As long as there is no dephasing during the delay of the partial waves until they tunnel out to the right reservoir, they keep the information of their relative phase. If they actually enter the right reservoir they circled a not simply-connected region which encloses a magnetic flux. This gives rise to a relative phase φ, and the waves interfere with each other. In our case there is no dephasing included in the model, such that an electron sitting on one of the dots keeps its phase information for a much longer time than it takes to complete two subsequent sequential tunneling processes.

One might argue that this picture contradicts the results for an Aharonov-Bohm interferometer with just one embedded quantum dot. Also in that case interference signals were found already in lowest order transport through the dot [96, 98]. However, it was as well assumed that the tunneling processes through the dot and the reference arm were correlated and there was no dephasing bath coupled to the system. If the partial wave traveling through the reference arm is delayed, such that it has a finite overlap with the wave tunneling (sequentially) through the dot, the stage is set for interference already in lowest order. In case of an Aharonov-Bohm interferometer containing only one quantum dot, the comparison of the current or conductance amplitudes for the entire system, and the quantum dot and the reference arm taken apart is not that straightforward as in the
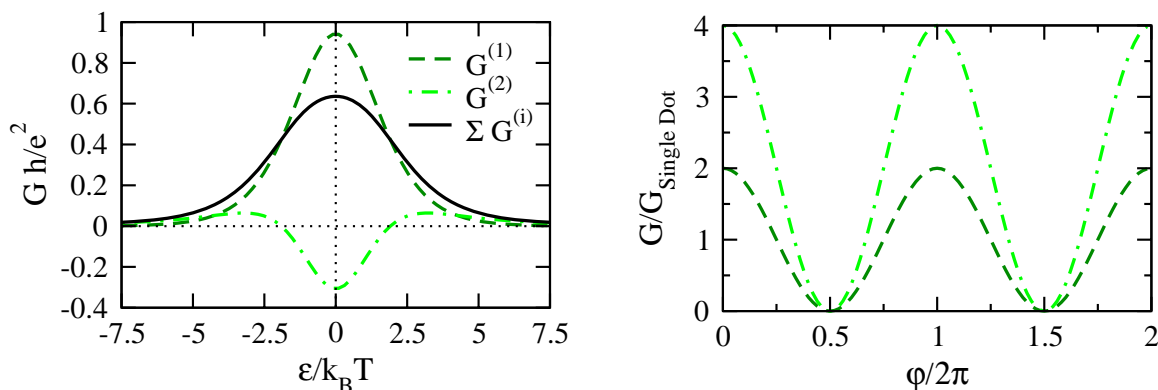
Figure 5.2: The linear conductance $G := \mathrm{d}I/\mathrm{d}V|_{V=0}$ is plotted in first and second order for $\Gamma_\mathrm{L} = \Gamma_\mathrm{R} = 0.3\,k_\mathrm{B}T$. The plots on the left show the maximal conductance for $\varphi = n\,2\pi$, $n \in \mathbb{Z}$ versus the dot energy ε. On the right hand side the interference oscillations are plotted for a fixed dot energy in comparison to the linear conductance of a single dot.

double-dot interferometer because the orders in the tunneling strength are kind of hard to compare.

Comparison of Eq. (5.9) with the corresponding result for a single quantum dot (Eq. (3.39)) shows that the maximal current, obtained for $\varphi = n\,2\pi$ where n is an integer, is equal to the current through two quantum dots taken apart, i.e. it corresponds to the sum of two independent channels. In particular, there is no additional factor two which we might expect from constructive interference, familiar from the double-slit experiment (compare also Fig. 5.2). Formally this puzzle can be solved (see e.g. Ref. [101]) by recognizing that in the Hamiltonian for $\varphi = n\,2\pi$, rewritten in terms of symmetric and antisymmetric combinations of dot operators, the antisymmetric superposition decouples completely, whereas the coupling of the symmetric superposition is increased by a factor $\sqrt{2}$. Consequently, we can map the system onto a single-level quantum dot with coupling strenghts $2\,\Gamma_\mathrm{L}$ and $2\,\Gamma_\mathrm{R}$, twice as big as the original coupling strengths. Thus, in first order we gain just a factor of two as compared to the original single dot. It is not until the second order where a factor of four is feasible,

$$I^{(2)} = -4\,\frac{e}{h}\,\Gamma_\mathrm{L}\Gamma_\mathrm{R}\,(1 + \cos\varphi)\,\frac{\partial}{\partial\varepsilon}\fint \frac{\mathrm{d}\omega}{\omega - \varepsilon}\,(f_\mathrm{L}(\omega) - f_\mathrm{R}(\omega)) \tag{5.10}$$

(compare also to Eq. (3.46)). Remark: For the second order current in Eq. (5.10) we did not set $\Delta\varepsilon = 0$ explicitly. In the case of symmetrically chosen dot energies $\varepsilon_\mathrm{u} = \varepsilon + \Delta\varepsilon/2$ and $\varepsilon_\mathrm{d} = \varepsilon - \Delta\varepsilon/2$ as defined above, the second order current becomes independent of the small detuning $\Delta\varepsilon$.

The transport through the system without interaction can actually be calculated exactly. The electrical current is in general given by

$$I = \frac{e}{h}\,\sum_\sigma \int \mathrm{d}\omega\,T_\sigma(\omega)\,(f_\mathrm{L}(\omega) - f_\mathrm{R}(\omega))\,. \tag{5.11}$$

The transmission probability $T_\sigma(\omega)$, which we already met in section 5.1, in the discussion of transmission channels, denotes the probability for an incoming electron with spin σ and energy ω to be transmitted through the device. In the noninteracting case the transmission probability can be calculated according to the Landauer-Büttiker or scattering formalism [22–24] by the modulus squared of the total transmission amplitude for each spin channel and given energy ω. On the other hand, it can be obtained in the tunneling picture with single-particle (retarded) Green's functions [39] which can be determined in equilibrium with equations of motion, for example [101]. Both approaches have been proven to be equivalent for an Aharonov-Bohm interferometer containing two noninteracting quantum dots [101, 102] in the sense that they yield the same total transmission. Furthermore, it turns out that for $U = 0$ phase locking appears even at finite bias voltage.

5.3   Quantum Dots with Interaction

The technological progress in confinement of electrons into small quantum dots and realizations of sophisticated experiments emphasizing the rich physics induced by interacting electrons strengthen the desire for a theoretical formulation focusing on the effects of electron-electron interaction and its influence on transport properties. From this point of view, the virtue of the tunneling picture as compared to the scattering approach lies in the fact that many-body effects, which enter the scene in the presence of Coulomb interaction on the quantum dots, can be included in a straightforward way. On the basis of the Anderson-like model introduced in section 5.1 we study the stationary state and transport properties of the weakly coupled double-dot Aharonov-Bohm interferometer in the case of strong Coulomb repulsion on the dots by means of the real-time diagrammatic technique. Regarding the evolution of the full reduced density matrix, including all off-diagonal terms, we calculate the current in general nonequilibrium situations beyond linear response. A systematic expansion in the coupling strength of the dots to the leads allows us to extend the calculation of lowest order tunneling to higher orders to include cotunneling and renormalization effects.

5.3.1   Isospin

As mentioned, we choose for the interacting case a strong onsite Coulomb repulsion, $U \gg k_\mathrm{B}T, eV, \Gamma_\mathrm{L}, \Gamma_\mathrm{R}$, which supresses double occupancy of each dot. This keeps the discussion transparent and simplifies the bookkeeping considerably without undermining the relevant physics. However, it is not a fundamental restriction and the generalization to arbitrary U is straightforward. In contrast to the noninteracting case the Hamiltonian can not be mapped onto a spinless system because of the coupling contained in the interaction term. Hence, we have to treat the electron spins explicitly. Nevertheless, the invariance of the total Hamiltonian under rotations in spin space implies an equivalence of elements of the reduced density matrix which can be obtained by flipping all spins. This reduces the number of independent density matrix elements which we actually have to calculate. Furthermore,

the prohibition of double occupancy of each dot allows us to flatten immediately seven of the generally sixteen dimensions of the Hilbert space of the double-dot system which is then spanned by nine basis states $|\chi_u, \chi_d\rangle$ with $\chi_i \in \{0, \uparrow, \downarrow\}$ denoting the occupation of dot i.

Instead of an examination in the original basis like in the noninteracting case, we proceed with the introduction of an isospin and switch to a more physical basis $\{|\chi\rangle\}$ which is tailored to describe the symmetries implied by the tunneling. Similar to section 4.1, the state of the empty system is denoted by $|0\rangle := |0, 0\rangle$. The doubly occupied subspace with one electron on each dot is naturally spanned by the spin singlet $|S\rangle := (|\uparrow, \downarrow\rangle - |\downarrow, \uparrow\rangle)/\sqrt{2}$ and the three triplet states $|T_+\rangle := |\uparrow, \uparrow\rangle$, $|T_0\rangle := (|\uparrow, \downarrow\rangle + |\downarrow, \uparrow\rangle)/\sqrt{2}$ and $|T_-\rangle := |\downarrow, \downarrow\rangle$. The corresponding probabilities which enter in the diagonal of the reduced density matrix are denoted by $p_0 := \langle|0\rangle\langle0|\rangle$, $p_S := \langle|S\rangle\langle S|\rangle$ and $p_T/3 := \langle|T_0\rangle\langle T_0|\rangle = \langle|T_\pm\rangle\langle T_\pm|\rangle$, where the spin symmetry of the Hamiltonian implies the equivalence of the three triplet states.

The structure of the singly occupied subspace can be described by an isospin $\mathbf{I}_\sigma$ for each electron spin σ. It accounts for all possible rotations of orbital states, or in other words: all possible superposition states, within the subspace spanned by $|\sigma, 0\rangle$ and $|0, \sigma\rangle$. Additionally to the quantization axis $\mathbf{n}$ which is defined by the eigenstates of $\mathbf{I}_\sigma \cdot \mathbf{n}$, given by $|+\rangle_{\mathbf{I}_\sigma \cdot \mathbf{n}} := |\sigma, 0\rangle$ and $|-\rangle_{\mathbf{I}_\sigma \cdot \mathbf{n}} := |0, \sigma\rangle$, there are two further quantization axes $\mathbf{m}_L$ and $\mathbf{m}_R$ suggested by the structure of the tunnel Hamiltonians for the left and the right side, Eqs. (5.3) and (5.4). The corresponding isospin eigenstates are given by

$$|+\rangle_{\mathbf{I}_\sigma \cdot \mathbf{m}_L} := \frac{1}{\sqrt{2}} \left(e^{-i\frac{\varphi}{4}} |\sigma, 0\rangle + e^{+i\frac{\varphi}{4}} |0, \sigma\rangle \right),$$
$$|-\rangle_{\mathbf{I}_\sigma \cdot \mathbf{m}_L} := \frac{1}{\sqrt{2}} \left(e^{+i\frac{\varphi}{4}} |\sigma, 0\rangle - e^{-i\frac{\varphi}{4}} |0, \sigma\rangle \right) \tag{5.12}$$

for the left, and for the right accordingly

$$|+\rangle_{\mathbf{I}_\sigma \cdot \mathbf{m}_R} := \frac{1}{\sqrt{2}} \left(e^{+i\frac{\varphi}{4}} |\sigma, 0\rangle + e^{-i\frac{\varphi}{4}} |0, \sigma\rangle \right),$$
$$|-\rangle_{\mathbf{I}_\sigma \cdot \mathbf{m}_R} := \frac{1}{\sqrt{2}} \left(e^{-i\frac{\varphi}{4}} |\sigma, 0\rangle - e^{+i\frac{\varphi}{4}} |0, \sigma\rangle \right). \tag{5.13}$$

They reflect the formation of coherent superposition states and account for the accumulation of a phase difference between the upper and the lower arm of the interferometer at the same time. Electrons which enter the double-dot from the left reservoir generate an isospin polarization in direction of $\mathbf{m}_L$, whereas electrons from the right are polarized in $\mathbf{m}_R$-direction. Both axes are perpendicular to $\mathbf{n}$ and enclose an angle of φ, given by the phase difference which is accumulated after encircling the magnetic flux threading the ring once (compare also Fig. 5.3). For exemplification, we can choose our coordinate system such that $\mathbf{n} = (0, 0, 1)$. In this representation the quantization axes are consequently given by $\mathbf{m}_L = (\cos(\varphi/2), \sin(\varphi/2), 0)$ and $\mathbf{m}_R = (\cos(\varphi/2), -\sin(\varphi/2), 0)$.

Taking advantage of the symmetry of the Hamiltonian under rotations of the electron spin, we summarize the isospin structure in the notion of the quantum statistical expectation value $\mathbf{I}/2 = (I_x, I_y, I_z)/2 := \langle\mathbf{I}_\uparrow\rangle = \langle\mathbf{I}_\downarrow\rangle$, like in section 4.2. The singly occupied
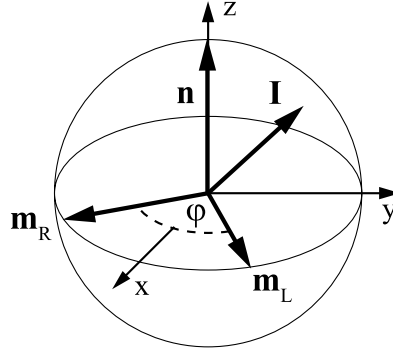
Figure 5.3: The quantization axes $\mathbf{m}_L$ and $\mathbf{m}_R$ are suggested by the symmetries of the tunnel Hamiltonian for electrons entering the double-dot system from the left or the right reservoir. They enclose an angle φ given by the magnetic flux threading the Aharonov-Bohm ring. For symmetric coupling of the upper and lower dot to either side, $\mathbf{m}_L$ and $\mathbf{m}_R$ are perpendicular to the axis $\mathbf{n}$.

subspace is then sufficiently determined by the overall probability p_1 to find one electron in the double-dot system and the isospin $\mathbf{I}$ for the structure imposed by superpositions of the dots' orbital states.

5.3.2   Meir-Wingreen formula

For quantum dots without interaction we mentioned in section 5.2 the equivalence of the total transmission probability $T_\sigma(\omega)$ from Eq. (5.11) in the tunneling picture and in the scattering approach. In the presence of interaction, however, the scattering approach is not applicable, and it has been shown, that the transmission probability or the current can not in general be recast in terms of modulus squared transmission amplitudes. Moreover, it seems that there is no direct physical meaning of the latter, e.g. in the sense of a transmission probability for a specified channel. (Compare Ref. [39] and in particular for quantum dot systems Refs. [96, 98].)

   The tunneling picture turns out to be suitable for the incorporation of many-body effects and the treatment of interacting systems. In a seminal paper Y. Meir and N. S. Wingreen [39] derived a Landauer formula for the current through a region of interacting electrons by using the nonequilibrium Keldysh formalism. Adapted to our model system, which consists of two interacting quantum dots embedded in an Aharonov-Bohm ring structure, the current can be written in the form

$$I = \frac{ie}{h} \frac{1}{\Gamma_L + \Gamma_R} \int d\omega \, \mathrm{tr}\Big[(\Gamma_R \boldsymbol{\Gamma}_L \, f_L - \Gamma_L \boldsymbol{\Gamma}_R \, f_R) \cdot (\mathbf{G}^> - \mathbf{G}^<) + (\Gamma_R \boldsymbol{\Gamma}_L - \Gamma_L \boldsymbol{\Gamma}_R) \cdot \mathbf{G}^< \Big] \quad (5.14)$$

where current conservation, $I_L + I_R = 0$, of electrons leaving or entering the left or the right reservoir allows us to symmetrize, $I := (\Gamma_R \, I_L - \Gamma_L \, I_R)/(\Gamma_L + \Gamma_R)$. For the sake of

compactness we use a matrix notation for the tunnel coupling,

$$\mathbf{\Gamma}_{\mathrm{L}} := \Gamma_{\mathrm{L}} \begin{pmatrix} 1 & \mathrm{e}^{+\mathrm{i}\frac{\varphi}{2}} \\ \mathrm{e}^{-\mathrm{i}\frac{\varphi}{2}} & 1 \end{pmatrix} \delta_{\sigma\sigma'} \qquad \text{and} \qquad \mathbf{\Gamma}_{\mathrm{R}} := \Gamma_{\mathrm{R}} \begin{pmatrix} 1 & \mathrm{e}^{-\mathrm{i}\frac{\varphi}{2}} \\ \mathrm{e}^{+\mathrm{i}\frac{\varphi}{2}} & 1 \end{pmatrix} \delta_{\sigma\sigma'} , \qquad (5.15)$$

which reflects the spin conservation during tunneling (via the diagonal structure in spin space), and the Green's functions

$$\mathbf{G} := \begin{pmatrix} \mathbf{G}_{\uparrow,\uparrow} & \mathbf{G}_{\uparrow,\downarrow} \\ \mathbf{G}_{\downarrow,\uparrow} & \mathbf{G}_{\downarrow,\downarrow} \end{pmatrix} \qquad \text{with} \qquad \mathbf{G}_{\sigma,\sigma'} := \begin{pmatrix} G_{\mathrm{u}\sigma,\mathrm{u}\sigma'} & G_{\mathrm{u}\sigma,\mathrm{d}\sigma'} \\ G_{\mathrm{d}\sigma,\mathrm{u}\sigma'} & G_{\mathrm{d}\sigma,\mathrm{d}\sigma'} \end{pmatrix} . \qquad (5.16)$$

The Keldysh Green's functions of the dot system are defined according to Refs. [36, 37, 39], $G^{<}_{i\sigma,j\sigma'}(t) := \mathrm{i}\langle c^{\dagger}_{j\sigma'}(0)c_{i\sigma}(t)\rangle$ and $G^{>}_{i\sigma,j\sigma'}(t) := -\mathrm{i}\langle c_{i\sigma}(t)c^{\dagger}_{j\sigma'}(0)\rangle$ with the corresponding Fourier transforms. To emphasize the complexity of the residual problem (the leads are already assumed to be in local equilibrium) we remark, that all Green's functions are influenced by both dots. In particular, the diagonal Green's functions, $G^{\gtrless}_{i\sigma,i\sigma}$, are not simply given by the single dots' Green's functions. Instead, they have to be calculated in the presence of the entire system. We perform the trace over the spin degrees of freedom and the 2×2 matrices and obtain as general result

$$I = 4\frac{e}{h}\frac{\Gamma_{\mathrm{L}}\Gamma_{\mathrm{R}}}{\Gamma_{\mathrm{L}} + \Gamma_{\mathrm{R}}} \int \mathrm{d}\omega \Big[(\operatorname{Im} G^{\mathrm{r}}_{\mathrm{uu}} + \operatorname{Im} G^{\mathrm{r}}_{\mathrm{dd}}) (f_{\mathrm{L}} - f_{\mathrm{R}}) +$$

$$+ \frac{\mathrm{i}}{2} \cos\frac{\varphi}{2} (G^{>}_{\mathrm{ud}} - G^{<}_{\mathrm{ud}} + G^{>}_{\mathrm{du}} - G^{<}_{\mathrm{du}}) (f_{\mathrm{L}} - f_{\mathrm{R}}) +$$

$$+ \frac{1}{2} \sin\frac{\varphi}{2} ((G^{>}_{\mathrm{ud}} - G^{<}_{\mathrm{ud}}) - (G^{>}_{\mathrm{du}} - G^{<}_{\mathrm{du}})) (f_{\mathrm{L}} + f_{\mathrm{R}}) +$$

$$+ \sin\frac{\varphi}{2} (G^{<}_{\mathrm{ud}} - G^{<}_{\mathrm{du}}) \Big] , \qquad (5.17)$$

where we use the spin symmetry, $G^{\gtrless}_{ij} := G^{\gtrless}_{i\uparrow,j\uparrow} = G^{\gtrless}_{i\downarrow,j\downarrow}$, and the relation of the greater and lesser diagonal Green's functions to the usual retarded Green's functions or the corresponding spectral densities, $G^{>}_{ii} - G^{<}_{ii} = -2\mathrm{i}\operatorname{Im} G^{\mathrm{r}}_{ii}$.

The correlators of the dot operators can be calculated systematically within the diagrammatic scheme in the real-time formulation. For the transport in lowest order in the coupling we need the Green's functions in zeroth order in Γ only. It turns out that the off-diagonal greater and lesser Green's functions in lowest order are determined by the off-diagonal terms of the density matrix for each spin, multiplied with the free propagators between the creation and annihilation operators at times $t_0 = 0$ and t. After transformation into energy space we obtain $G^{> \, (0)}_{\mathrm{ud}} = G^{< \, (0)}_{\mathrm{ud}} = 2\pi\mathrm{i}\,p^{\mathrm{u}\sigma(0)}_{\mathrm{d}\sigma}\,\delta(\omega - \varepsilon)$ and $G^{\gtrless \, (0)}_{\mathrm{du}} = 2\pi\mathrm{i}\,p^{\mathrm{d}\sigma(0)}_{\mathrm{u}\sigma}\,\delta(\omega - \varepsilon)$, correspondingly. By way of exception we use here for a moment the off-diagonal elements in the original basis $p^{\mathrm{u}\sigma}_{\mathrm{d}\sigma} := \langle|0,\sigma\rangle\langle\sigma,0|\rangle$ and $p^{\mathrm{d}\sigma}_{\mathrm{u}\sigma} := \langle|\sigma,0\rangle\langle0,\sigma|\rangle$.

As consequence of the equivalence of the off-diagonal greater and lesser Green's functions in lowest order in the coupling strength Γ, the second and third term in the general current formula, Eq. (5.17), vanish. The imaginary part of the retarded Green's functions

(or the spectral functions) in zeroth order is given by a product of a sum of diagonal elements of the reduced density matrix, and the imaginary part of the resolvent stemming from the free propagator, $\operatorname{Im} G_{ii}^{r,(0)} = -\pi \left(p_0^{(0)} + 3/4\, p_1^{(0)} + 1/3\, p_T^{(0)} + 1/2\, p_S^{(0)} \right) \delta(\omega - \varepsilon)$.

Applying the isospin notation we can express the lowest order current in the form

$$I^{(1)} = 4\pi \frac{e}{h} \frac{\Gamma_L \Gamma_R}{\Gamma_L + \Gamma_R} \left[-2 \left(p_0^{(0)} + \frac{3}{4} p_1^{(0)} + \frac{1}{3} p_T^{(0)} + \frac{1}{2} p_S^{(0)} \right) (f_L - f_R) - \right.$$
$$\left. - \mathbf{I}^{(0)} \cdot (\mathbf{m}_L - \mathbf{m}_R) \right] \tag{5.18}$$

where $\mathbf{m}_L$ and $\mathbf{m}_R$ denote the isospin directions of electrons entering from the left or the right reservoir, and the respective Fermi functions are evaluated at the dots' mean energy ε.

In linear response only equilibrium values of the diagonal elements, and first order terms (in V) of the isospin enter the current formula or the linear conductance $G^{(1)} := \partial I^{(1)}/\partial V|_{V=0}$, respectively. In equilibrium we expect the density matrix to be diagonal with probabilities given by Boltzmann weights, all off-diagonal matrix elements are supposed to vanish (we will verify this rigorously in the next subsection). Thus, the first term is given by

$$\left(p_0^{(0)} + 3/4\, p_1^{(0)} + 1/3\, p_T^{(0)} + 1/2\, p_S^{(0)} \right) \Big|_{V=0} = \frac{1}{1+f} , \tag{5.19}$$

where the Fermi function is again evaluated at the dots' mean energy ε. The resulting contribution to the linear conductance represents the sum of two independent quantum dot channels, e.g. the sum of the upper and the lower dot taken apart.

In contrast, the isospin in the second term of Eq. (5.18) contributes with a nonequilibrium value even in linear response. Anticipating a part of the results of the following section we give the solution of the kinetic equations for the isospin

$$\mathbf{I}^{(0)} \cdot (\mathbf{m}_L - \mathbf{m}_R) = -\frac{eV f'}{(1+f)^3} \sin^2 \frac{\varphi}{2} + \mathcal{O}(V^2) . \tag{5.20}$$

Hence, the isospin, which accounts for the possibility to develop coherent superposition states, induces a phase dependence of the transport even in lowest order tunneling and linear response,

$$G^{(1)} = -8\pi \frac{e^2}{h} \frac{\Gamma_L \Gamma_R}{\Gamma_L + \Gamma_R} \frac{f'}{1+f} \left(1 - \frac{\sin^2(\varphi/2)}{(1+f)^2} \right) . \tag{5.21}$$

For φ equal to an integer multiple of 2π the isospin contribution vanishes. The linear conductance shows a maximum which resembles the conductance of the sum of the two quantum dots taken apart, as mentioned (compare also the result for a single dot, Eq. (3.44)). Like in first order in the noninteracting case, we do not get an additional factor two from constructive interference. The maximal destructive interference is obtained at odd multiples of π. In contrast to the noninteracting case, complete destructive interference is not feasible. The factor $1/(1+f)^2$ is always smaller than unity (or equal) and indicates an
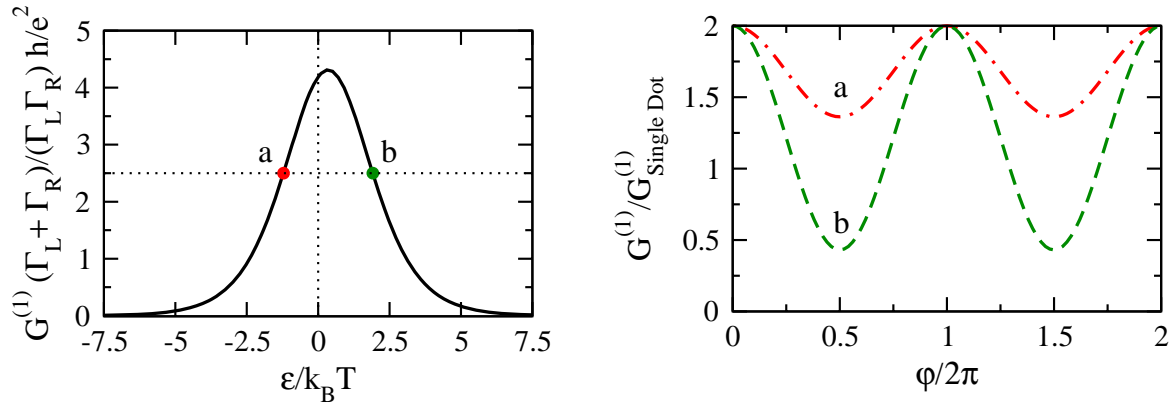
Figure 5.4:   The first order linear conductance, $G^{(1)}$, is asymmetric with respect to $\varepsilon = 0$ due to the particle-hole asymmetry of the interacting system (left plot). Furthermore, the coherent contributions to the transport show a strong asymmetry between the occupied ($\varepsilon < 0$) and the unoccupied side ($\varepsilon > 0$) of the conductance peak. In the regime in which the double dot is predominantly occupied, the destructive interference is much weaker than for the empty system. This indicates a relatively strong incoherent contribution to the transport through the occupied system as compared to the empty one.

incoherent part of the transport which can not be suppressed by interference. Furthermore, it induces an asymmetry of the interference signal between the occupied ($\varepsilon < 0$) and the unoccupied side ($\varepsilon > 0$) of the conductance resonance, which is displayed in Fig. 5.4. This kind of asymmetry was first predicted by J. König and Y. Gefen [96, 98] and has been confirmed experimentally by K. Kobayashi and coworkers [99] in an Aharonov-Bohm interferometer with a single embedded quantum dot.

Heuristically, the difference between the coherent contributions on either side of the conductance resonance can be motivated with incoherent processes, e.g. spin-flip processes [96, 98], which take place only if at least one of the dots is occupied.

Let us consider an incident electron with say spin up. An interference effect at the drain is possible if the electron does not leave a trace in the setup which allows us to judge which path the electron has taken. Specifically, a spin-flip, which might occur if one of the dots is occupied with a spin down, destroys the coherence as well as a switching of the occupancy of the upper and the lower dot. Even if one of the dots is occupied with a spin down and remains the same (i.e. no spin-flip) it is possible to tell afterwards that the electron traveled through the other dot and interference is not possible. In Fig. 5.5 we sketch hopping processes which allow for interference because the path a transported electron has taken is uncertain. The probability for one of these possibly interfering processes is proportional to $p_0 + 1/2\,p_1 + 1/3\,p_T$ which, in lowest order tunneling and equilibrium, is identical to the asymmetry factor $1/(1 + f)^2$.

In this framework it is intuitively clear that the coherence on the occupied side of the conductance resonance is weaker than on the unoccupied side. If the double dot system is basically empty, a major part of the transport is supported by processes of the first kind
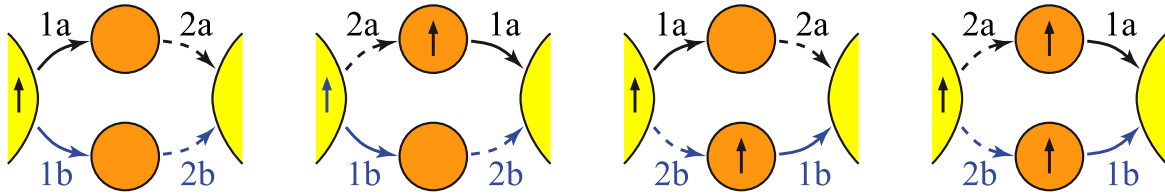
Figure 5.5:   Hopping processes are sketched which allow for coherent transport of an incident electron with spin up. The first part of each process is indicated by a solid line with index 1. The subsequent part, completing the process, is indicated by a dashed line with index 2. Indices a and b distinguish two possibly interfering paths which leave the respective initial state of the double dot system unchanged. All processes which flip the spin of the transported electron or of one of the dots can be considered as incoherent, as well as processes which switch the occupation of the upper and the lower dot.

in Fig. 5.5, there are no incoherent processes possible (in the above named sense) which start and end with an empty state. In contrast, if the system is predominantly occupied with two electrons, a part of the transport is supported by coherent processes of the fourth kind in Fig. 5.5, but additionally there is a strong incoherent contribution since there are three further doubly occupied states (the singlet, the T_0 and the spin-down triplets) which the electron can not pass traceless.

(Remark: The same consideration for $U = 0$ yields a factor of one instead of an asymmetry factor, which is consistent with our previous results of fully coherent transport. Even if one of the dots is occupied with a spin down, a spin up electron can be transferred through the same dot in the noninteracting case. Thus, a which-path argumentation does not apply. On the occupied side of the conductance peak the dominating state is occupied with four electrons, $|\uparrow\downarrow, \uparrow\downarrow\rangle$, and obviously allows for full interference of transfered electrons. The respective hole-like processes are symmetric to their particle-like counterparts on the unoccupied side of the resonance. Hence, the transport is equivalent on both sides of the conductance peak.)

5.3.3   Stationary Equations for the Reduced Density Matrix – Lowest Order Transport

The current formula (5.17) is convenient for transport calculations and one can extract immediately what kind of Green's functions play a role. The Green's functions themselves can be determined via the real-time diagrammatic technique by computing systematically all contributions to the correlations of creation and annihilation operators. However, the procedure explained in section 3.4 yields equivalent results, but, as a matter of taste, the bookeeping displays some advantages, especially beyond linear response and if we extend the consideration to higher order tunneling. To calculate the expectation value of the stationary current through the system we determine the reduced density matrix up to a given order via the solution of the kinetic equations in the stationary limit and perfom

the trace with the current operator. A detailed comparison of the system's state and its transport properties allows us to find relations between evolved peculiarities of the density matrix and signatures in the current or the conductance. Furthermore, with the kinetic equations at hand we may even catch a glimpse of the dynamics of the system and get an idea of the processes governing the evolution. Summarized, the named procedure promises the yield of a more comprehensive insight and a better understanding of the behavior of the considered system.

In lowest order the diagrammatic formulation is quite concise and transparent. We have to regard eight topological classes of first order diagrams (see also Fig. 3.9 on page 34) to set up the kinetic equations governing the evolution of the reduced density matrix. In combination with the nine possible basis states at the ends and between the vertices we obtain 416 possible explicit realizations, where we already used particle conservation and spin conservation during tunneling, i.e. we have to consider only density matrix elements which are diagonal in the particle number and the total spin. In addition, the spin symmetry of the system halves the number of diagrams we have to calculate and the symmetries between upper and lower dot, left and right reservoir, and the mirror properties of the diagrams imply further simplifications which we can use on the fly.

After summation of all diagrams in the appropriate element of the kernel the kinetic equations become surprisingly simple. In the basis introduced above, collecting all probabilities in the vector $\mathbf{p} = (p_0, p_1, p_S, p_T)$, we can write

$$\frac{\mathrm{d}}{\mathrm{d}t}\mathbf{p} = \sum_{r=\mathrm{L,R}} \Gamma_r \begin{pmatrix} -4\,f_r & 1-f_r & 0 & 0 \\ 4\,f_r & -1-f_r & 2-2\,f_r & 2-2\,f_r \\ 0 & f_r/2 & -2+2\,f_r & 0 \\ 0 & 3\,f_r/2 & 0 & -2+2\,f_r \end{pmatrix} \mathbf{p} + \sum_{r=\mathrm{L,R}} \Gamma_r \begin{pmatrix} 2-2\,f_r \\ -2+4\,f_r \\ f_r \\ -3\,f_r \end{pmatrix} (\mathbf{I}\cdot\mathbf{m}_r)$$

$$\frac{\mathrm{d}}{\mathrm{d}t}\mathbf{I} = \sum_{r=\mathrm{L,R}} \Gamma_r \left[2\,f_r\,p_0 + \left(f_r - \frac{1}{2}\right) p_1 + (1-f_r)\,p_S - (1-f_r)\,p_T \right] \mathbf{m}_r - $$
$$ - \sum_{r=\mathrm{L,R}} \Gamma_r\,(1+f_r)\,\mathbf{I} + \Delta\varepsilon\,(\mathbf{n}\times\mathbf{I}), \tag{5.22}$$

with the quantization axes $\mathbf{m}_r$, $r \in \{\mathrm{L,R}\}$, and $\mathbf{n}$ as explained above. As usual, we abbreviate the Fermi distributions f_r of the electrons in the left and the right reservoir, evaluated at the mean dots' energy ε and the electrochemical potential of the left or right reservoir μ_r, respectively. The detuning $\Delta\varepsilon$ is assumed to be smaller or of the order of the level broadening Γ.

Most of the time we do not spotlight the detuning, because as long as it stays among the smallest energy scales of our system, $\Delta\varepsilon < \Gamma_\mathrm{L}, \Gamma_\mathrm{R}$, it is of minor importance for the quality of the coherence. So why do we take it into account at all and make the calculations more complicated than necessary? The simple answer is: we would like to minimize the risk to run into a singularity caused by an oversimplified symmetry of the idealized setup. In a realistic situation there is always a small detuning. The cost of a bit more complexity

during the calculation pays off if we are able to describe the properties of the system in the vicinity of vanishing detuning and ensure a controlled behavior and an experimental relevance of the effects we discuss. Indeed we find, that a detuning up to the order of the level broadening gives a small correction, but does not change our results qualitatively, as far as only the coherence is concerned. Actually, there is a symmetry broken if the detuning is finite. As a consequence, the geometry of the setup does not yield the necessity of phase locking beyond linear response. We place a discussion of this in a subsection on its own and focus here on the coherence in general.

As a matter of principle, the form of the kinetic Eqs. (5.22) is very similar to Eqs. (4.9) and (4.43). The setup consists of two quantum dots coupled to joint reservoirs on the left and on the right hand side. Thus, we expect the isospin to play an important role for the behavior of the system, as we have already anticipated in the preceding section. The difference and extension of the Aharonov-Bohm ring structure compared to the fork-like geometries in chapter 4 is the interplay of the two not necessarily parallel isospin directions of electrons from the left and the right lead. A major advantage of the notion of the isospin is the suggestion of quite an intuitive picture in analogy to magnetism. In this sense we can view the left and the right lead as fully polarized in the respective isospin direction, i.e. in the left resevoir there are exclusively isospins in $\mathbf{m}_\mathrm{L}$ and in the right reservoir exclusively isospins in $\mathbf{m}_\mathrm{R}$ direction available. Thus, we expect a large transmission probability if the isospins of source and drain are aligned, and a weak transmission if they are contrary. In fact, this qualitative picture is supported by a rigorous calculation. The alignment of the isospins is controlled via the magnetic flux or the induced phase, and a comparison to Eq. (5.18) or (5.21), for example, yields the mentioned behavior. Fortunately, a closer look reveals more complicated characteristics and a detailed analysis seems rewarding.

The full analytic solution of the kinetic equations in first order, Eqs. (5.22), is lengthy and not very transparent. The yield of information that we can extract from the formulas is limited. Thus, we give here only a simplified version for $\Delta\varepsilon = 0$ and expand up to linear order in the bias voltage. The lowest order probabilities read

$$p_0^{(0)} = \frac{(1-f)^2}{(1+f)^2} - eV \frac{\Gamma_\mathrm{L} - \Gamma_\mathrm{R}}{\Gamma_\mathrm{L} + \Gamma_\mathrm{R}} \frac{f' f (3 - f - 2 f^2)}{(1+f)^5} + \mathcal{O}(V^2), \tag{5.23a}$$

$$p_1^{(0)} = \frac{4 (1-f) f}{(1+f)^2} + eV \frac{\Gamma_\mathrm{L} - \Gamma_\mathrm{R}}{\Gamma_\mathrm{L} + \Gamma_\mathrm{R}} \frac{2 f' f (1 - 4 f - 3 f^2)}{(1+f)^5} + \mathcal{O}(V^2), \tag{5.23b}$$

$$p_\mathrm{S}^{(0)} = \frac{f^2}{(1+f)^2} + eV \frac{\Gamma_\mathrm{L} - \Gamma_\mathrm{R}}{\Gamma_\mathrm{L} + \Gamma_\mathrm{R}} \frac{f' f (1 + 3 f - f^3)}{(1-f)(1+f)^5} + \mathcal{O}(V^2), \tag{5.23c}$$

$$p_\mathrm{T}^{(0)} = \frac{3 f^2}{(1+f)^2} + eV \frac{\Gamma_\mathrm{L} - \Gamma_\mathrm{R}}{\Gamma_\mathrm{L} + \Gamma_\mathrm{R}} \frac{3 f' f^2 (1 - f - f^2)}{(1-f)(1+f)^5} + \mathcal{O}(V^2). \tag{5.23d}$$

Choosing the coordinate system like in the example in subsection 5.3.1 we can represent

the isospin by its components

$$I_x^{(0)} = eV \frac{\Gamma_{\mathrm{L}} - \Gamma_{\mathrm{R}}}{\Gamma_{\mathrm{L}} + \Gamma_{\mathrm{R}}} \frac{f' \cos(\varphi/2)}{(1+f)^3} + \mathcal{O}(V^2) \,, \tag{5.24a}$$

$$I_y^{(0)} = eV \frac{f' \sin(\varphi/2)}{(1+f)^3} + \mathcal{O}(V^2) \,. \tag{5.24b}$$

The $I_z^{(0)}$ component vanishes in all orders of V.

For zero bias voltage we obtain, as expected, the equilibrium density matrix governed by Boltzmann factors. The isospin of an individual electron, which is not driven, may point in any direction and the quantum statistical expectation value averages to zero. Already in first order in the bias voltage an isospin is accumulated and an imbalance between singlet and triplet becomes apparent. Similar to the discussion in section 4.5, the bias drives the electrons in a defined direction and leads under certain conditions to a favored isospin polarization. The probability that two subsequent electrons from the same reservoir (and the same isospin) form a singlet state rises. Nevertheless, the imbalance between singlet and triplet probabilities does not affect the transport in lowest order in Γ neither in linear response nor beyond. The first order current rates, with which the density matrix has to be multiplied before taking the trace, is symmetric for singlet and triplet states. Hence, the lowest order current depends only on the sum $p_{\mathrm{S}}^{(0)} + p_{\mathrm{T}}^{(0)}$ (i.e. the overall probability to find the system doubly occupied) and is not sensitive to any imbalance between singlet and triplet.

In the coordinate representation of our choice we read directly from Eq. (5.18) that the only isospin component which enters the first order current is the $I_y^{(0)}$ component. Employing the picture of the isospin-polarized leads we can interpret that as if on average only the component of incoming isospins is transported which is parallel to the drain's polarization. The perpendicular component, represented by $I_y^{(0)}$, constitutes a measure for the part of electrons which can not be transferred because of destructive interference. The corresponding contribution to the transport diminishes the current supported by $p_1^{(0)}$.

5.3.4 Singularities of the Stationary Equations

Like in the noninteracting case, the solution of the kinetic equations in the stationary limit is in general straightforward, but there are a few regions in the parameter space in which the first order equations can not determine the system unambiguously, even if we additionally take into account the normalization condition, $\mathrm{tr}\,\rho = 1$. One of these regions is characterized by a complete symmetry of the upper and lower arm of the interferometer, i.e. degenerate dot levels, $\Delta\varepsilon = 0$, and, at the same time, no phase difference, $\varphi = n\,2\pi$, $n \in \mathbb{Z}$. In this case the isospin of electrons from the left and the right side are parallel, and the isospin remains in the direction $\mathbf{m} := \mathbf{m}_{\mathrm{L}} = \mathbf{m}_{\mathrm{R}}$, perpendicular to $\mathbf{n}$, for all times. The reduced Hilbert space decomposes into two decoupled parts, which we will emphasize in a reformulated version of the kinetic equations (see Eqs. (5.27) on page 90). Consequently,

the stationary state is not independent of the initial conditions in this regime and, therefore, not unambiguously defined. We can circumvent this problem easily by introducing a small coupling between the two parts of the Hilbert space. We solve the system, for instance, in the vicinity of $\Delta\varepsilon = 0$ and $\varphi = n\,2\pi$ and perform an analytic continuation.

Another ambiguity appears deep inside the occupied Coulomb Blockade, formally designated by $-\varepsilon \gg \Gamma_{\mathrm{L}}, \Gamma_{\mathrm{R}}, |\mu_{\mathrm{L}}|, |\mu_{\mathrm{R}}|, k_{\mathrm{B}}T$. (On the unoccupied side, $\varepsilon > 0$, there is no problem like this.) In the occupied blockade we have effectively two possible states, the singlet and a triplet. (These are actually four states since the triplet is threefold, but spin symmetry ensures equivalent probabilities for all triplets.) The doubly occupied state generated by two electrons from the same reservoir is always a singlet,

$$(\mathrm{e}^{\pm\mathrm{i}\frac{\varphi}{4}}\,c_{\mathrm{u}\sigma'}^{\dagger} + \mathrm{e}^{\mp\mathrm{i}\frac{\varphi}{4}}\,c_{\mathrm{d}\sigma'}^{\dagger})(\mathrm{e}^{\pm\mathrm{i}\frac{\varphi}{4}}\,c_{\mathrm{u}\sigma}^{\dagger} + \mathrm{e}^{\mp\mathrm{i}\frac{\varphi}{4}}\,c_{\mathrm{d}\sigma}^{\dagger})|0\rangle \sim \delta_{\sigma'\bar{\sigma}}\,|\mathrm{S}\rangle\,. \tag{5.25}$$

This is exactly the argument which we used to motivate the formation of the singlet-triplet imbalance in the fork-like systems in chapter 4. If the upper and lower dot are identical (i.e. coupling and energy are equivalent) we necessarily need the second reservoir to generate a triplet. In that sense a triplet is of a combined form, in which both reservoirs play a role.

Let us now assume that the system is initially in a singlet state and the dot energies are well below the Fermi energy of the leads, $-\varepsilon \gg \Gamma_{\mathrm{L}}, \Gamma_{\mathrm{R}}, |\mu_{\mathrm{L}}|, |\mu_{\mathrm{R}}|, k_{\mathrm{B}}T$. In this regime the system has no chance to relax if we only take into account first order tunneling. Thus, the system remains in the singlet state for any time. The same applies to an initial triplet. In the stationary limit, however, the density matrix should be independent of the initial conditions if it is well defined. Hence, lowest order tunneling in the system under consideration is not sufficient for a well defined stationary state deep in the occupied Coulomb blockade. A simple analytical continuation like in the preceding case does not yield a solution.

To get rid of this more fundamental problem we have to include higher order tunneling. In our case, cotunneling through the doubly occupied state does the job. The initial state can evolve and in the stationary limit the system relaxes to a uniform distribution of the singlet and the three triplets. Technically we have to solve a combined set of equations of first and second order,

$$0 = \frac{\mathrm{d}}{\mathrm{d}t}\begin{pmatrix}\mathbf{p}\\\mathbf{I}\end{pmatrix} = (\mathbf{W}^{(1)} + \mathbf{W}^{(2)})\cdot\begin{pmatrix}\mathbf{p}\\\mathbf{I}\end{pmatrix}. \tag{5.26}$$

(The situation is similar to the treatment of a quantum dot coupled to ferromagnetic leads in the Coulomb blockade in Ref. [106].) We obtain the reduced density matrix in lowest order, determined by the equilibrium values $p_{\mathrm{S}}^{(0)} = 1/4$ and $p_{\mathrm{T}}^{(0)} = 3/4$, as long as the modulus of the bias voltage is small compared to the absolute dot energy ($-\varepsilon \gg \Gamma_{\mathrm{L}}, \Gamma_{\mathrm{R}}, |\mu_{\mathrm{L}}|, |\mu_{\mathrm{R}}|, k_{\mathrm{B}}T$). However, for the extreme case, deep inside the Coulomb blockade regime, there are much simpler schemes to describe the behavior of the system in an adequate way, compare for instance Ref. [78].

Our goal is to address the transport regimes in the vicinity of the resonance, where first order tunneling dominates, and the crossover to the Coulomb blockade, where cotunneling
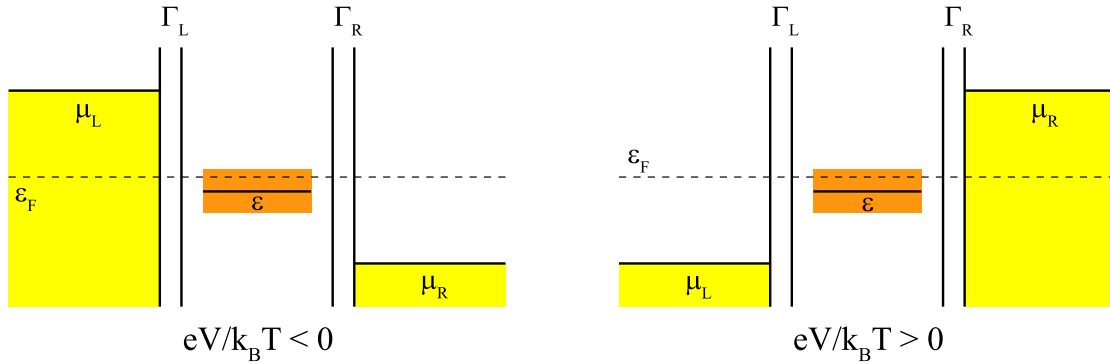
Figure 5.6: The sketch visualizes how the bias voltage is applied. We measure all energy levels with respect to the mean Fermi energy of the leads ε_F. The bias is applied symmetrically such that $eV/k_B T < 0$ drives electrons from left to right and vice versa.

starts to play a major role. We do not concentrate on the behavior deep inside the Coulomb blockade in the following, we just set the frame and make sure that the asymptotic behavior is consistent.

5.3.5 Coherence Asymmetries in Strong Nonequilibrium

Because of symmetry reasons, the terms of the density matrix linear in V (Eqs. 5.23a et seq.) have to be antisymmetric in the coupling to the left and the right lead if they depend on the coupling at all (in our choice of the coordinate system, the y-component of the isospin, for instance, which is responsible for a current contribution in linear response, Eq. (5.21), is in first order in V independent of the coupling strength to the left and the right reservoir (compare Eq. 5.24b)). For symmetric coupling the antisymmetric terms vanish but they do not if the couplings to the left and the right lead are different. In the linear conductance, Eq. (5.21), effects of asymmetric coupling do not become visible. As seen in subsection 5.3.2 only equilibrium probabilities and a coupling-strength independent isospin term enter the formula, thus there is only a symmetric overall factor of $\Gamma_L \Gamma_R / (\Gamma_L + \Gamma_R)$.

Nevertheless, beyond linear response we find a striking difference between the transport through a symmetrically and an asymmetrically coupled system. While the differential conductance of the symmetrically coupled system is by construction invariant under reversal of the current which is driven by the bias voltage (at least for $\Delta\varepsilon = 0$), the asymmetrically coupled system does not have this property. (However, phase locking according to Eq. (5.5) still holds as long as the detuning of the dots vanishes.) In Fig. 5.7 we give an example how a difference between the couplings of source and drain becomes evident in the transport properties of the system. Both plots show the first order differential conductance $dI^{(1)}/dV$ versus bias voltage and phase. For the left plot the coupling to the left and the right reservoir is equivalent, $\Gamma_L = \Gamma_R$. Phase locking is apparent for all voltages and the transport is symmetric under reversal of the current. For the right plot we decreased the coupling to the right reservoir, $\Gamma_R = 0.2\,\Gamma_L$. Obviously, the interference becomes weak if
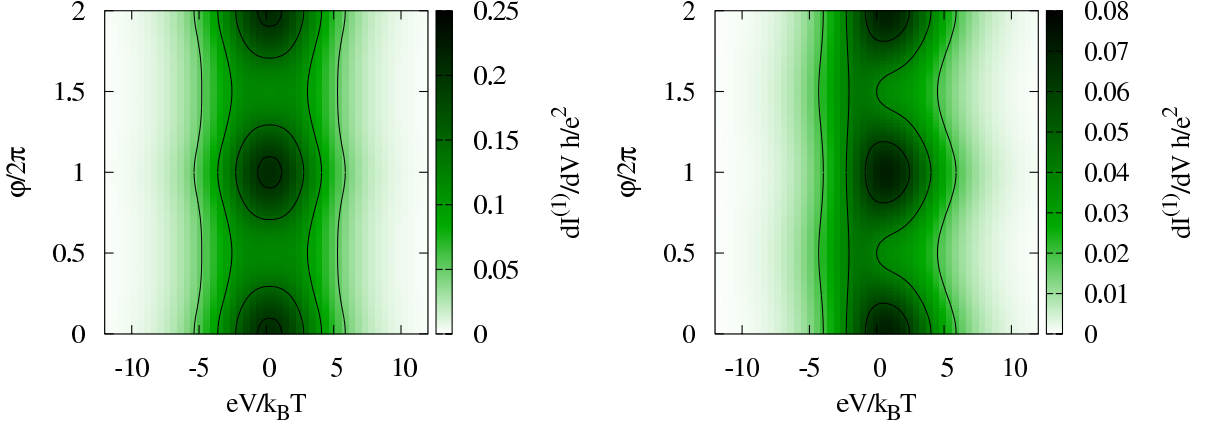
Figure 5.7:   The first order differential conductance $dI^{(1)}/dV$ is plotted versus the bias voltage and the phase for a symmetrically and an asymmetrically coupled system at resonance, $\varepsilon = 0$. For the symmetric setup (left plot) the coupling strength is $\Gamma_L = \Gamma_R = 0.1 \, k_B T$. For the right plot we assume an asymmetry in the coupling of $\Gamma_L = 0.1 \, k_B T$ and $\Gamma_R = 0.2 \, \Gamma_L$. The interference in the asymmetric setup decreases considerably if electrons are pressed into the system ($eV/k_B T < 0$). (To clarify how the bias is applied Fig. 5.6 may help.)

the electrons are driven from the left to the right ($eV/k_B T < 0$), whereas the oscillations (depending on the phase φ) have a large amplitude if the electrons are driven from the right to the left ($eV/k_B T > 0$). There is even a hint for a phase switch (in the region $-3 > eV/k_B T > -4$). This indicates that the interference signal in the current first grows if the driving is increased, but decreases under certain conditions if we crank up the voltage further. The current averaged over a period of the oscillation is always monotonous and saturates at high bias.

To gain an intuitive understanding of the behavior of the system we compare the transport properties, especially the interference signal, with the stationary state of the system. By applying the isospin picture we draw a physical interpretation which allows us to predict qualitative pecularities, especially the effect of asymmetric coupling on the interference signal. The latter is expected to be well accessible via experimental transport investigations.

Let us first concentrate on the suppression of the coherence indicated by the comparably small oscillations if the electrons are driven from the better coupled source to the worse coupled drain. For comparison we plot in Fig. 5.8 the lowest order probabilities versus the bias voltage for a fixed phase, and, in the lower plots, the phase dependence for a selected driving. We contrast the results for the symmetric setup and the asymmetric setup to find relevant differences connected to the suppressed coherence. We start with the focus on the plots for $\Gamma_L = \Gamma_R$ on the left hand side. As expected from the geometric symmetry of the system all physical quantities, such as the probabilities and the conductance, are invariant under reversal of the bias voltage. Nevertheless, an interesting feature is the fact that the probability for the singlet state inreases with the voltage, whereas the triplet
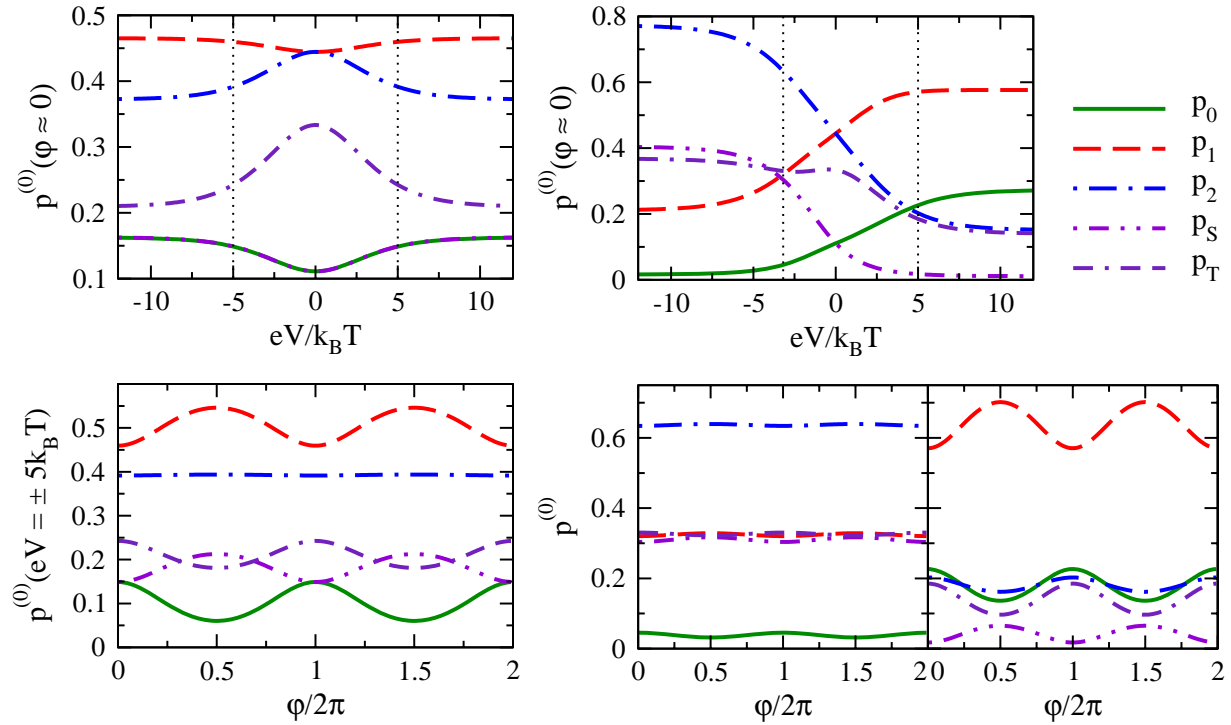
Figure 5.8: The zeroth order probabilities $\mathbf{p}^{(0)}$ and $p_2^{(0)} = p_S^{(0)} + p_T^{(0)}$ are plotted versus the bias voltage (upper plots) and the phase (lower plots) for symmetric (left plots) and asymmetric coupling (rigth plots) at resonance, $\varepsilon = 0$. For asymmetric coupling we assume $\Gamma_R = 0.2\,\Gamma_L$. The bias voltages for the phase dependent plots are selected such that $\mathrm{d}I^{(1)}/\mathrm{d}V(V_1) = \mathrm{d}I^{(1)}/\mathrm{d}V(V_2)$, V_1 and V_2 are indicated in the upper, voltage dependent plots by dotted lines.

probability decreases, i.e. a stationary imbalance between singlet and triplet is generated in a nonequilibrium situation. This reminds us of the similar behavior in the fork system with two quantum dots coupled to one joint source and two separate drains in sections 4.5 and 4.6. In contrast to the fork system, the quantum dots in the Aharonov-Bohm interferometer are coupled to a joint source as well as to a joint drain, which leads to a phase sensitivity of the imbalance between singlet and triplet. That means, in the Aharonov-Bohm interferometer the phase is an additional parameter to control the difference between singlet and triplet probabilities in a certain range. However, as argued above, the generated imbalance can not affect the lowest order transport in any way.

The overall probability for the doubly occupied system decreases if we open the transport window by increasing the voltage. At the same time the probability for the singly occupied system rises. The occupation of the empty system at $\varepsilon = 0$ depends strongly on the phase. While the other probabilities show on (phase) average the same qualitative behavior as plotted for the fixed phase $\varphi \approx 0$, the probability for the empty system actually decreases on average very slightly (at most 10% of its equilibrium value) but oscillates strongly around the mean such that, depending on the actual phase, the probability for

the empty system either increases or decreases with the driving.

The flux dependence of the probabilities in nonequilibrium is displayed in the lower plots in Fig. 5.8. The singlet probability oscillates in phase with the probability to find the system singly occupied, they become minimal for $\varphi = n\,2\pi$. In contrast, the probabilities for the empty system and the triplet become maximal for $\varphi = n\,2\pi$. A quite interesting detail is, that the only difference between the singlet and empty state probabilities is the opposite phase. For $\varphi = n\,2\pi$ they are equivalent. From the kinetic equations (5.22) we can read that all oscillations (as well as the imbalance between singlet and triplet) are evoked by the isospin, i.e. they depend strongly on the structure of the singly occupied state.

Employing the intuitive picture of aligned and misaligned isospins we draw two limiting cases: $\varphi = n\,2\pi$ and $\varphi = (2n+1)\,\pi$. For each we compare the equilibrium with a nonequilibrium situation. For $\varphi = n\,2\pi$ the isospin of electrons from the left lead is parallel to the isospin of electrons from the right lead and the transport is not hindered by any antiparallel component, or in other words, by any destructive interference. An electron with spin σ, which enters an initially empty system occupies a $|+\rangle_{\mathbf{I}_\sigma \cdot \mathbf{m}}$ state, where $\mathbf{m} := \mathbf{m}_{\mathrm{L}} = \mathbf{m}_{\mathrm{R}}$ for $\varphi = n\,2\pi$. In the subsequent process the electron either leaves the double dot again, returning the system to the empty state, or, with the same probability, a second electron with the same isospin but opposite physical spin may enter the system, which leads to the formation of a singlet state. In contrast, electrons with the same spin σ are blocked from entering (for $\varphi = 0$, for instance, we obtain $(c_{\mathrm{u}\sigma'}^\dagger + c_{\mathrm{d}\sigma'}^\dagger)(c_{\mathrm{u}\sigma}^\dagger + c_{\mathrm{d}\sigma}^\dagger)|0\rangle \sim (c_{\mathrm{u}\sigma'}^\dagger c_{\mathrm{d}\sigma}^\dagger - c_{\mathrm{u}\sigma}^\dagger c_{\mathrm{d}\sigma'}^\dagger)|0\rangle)$.

The only way to generate a $|-\rangle_{\mathbf{I}_\sigma \cdot \mathbf{m}}$ state at $\varphi = n\,2\pi$ is to empty one of the triplets. Once we have a $|-\rangle_{\mathbf{I}_\sigma \cdot \mathbf{m}}$ state, it can not decay further (similar to the discussion in section 4.1), neither can it lead to the formation of a singlet state. That means, the evolution of triplets and $|-\rangle_{\mathbf{I}_\sigma \cdot \mathbf{m}}$ states decouples from the empty system, the $|+\rangle_{\mathbf{I}_\sigma \cdot \mathbf{m}}$ states and the singlet. This can also be seen directly from the kinetic equations (5.22) which we can rewrite for $\varphi = n\,2\pi$ in the form

$$\frac{\mathrm{d}}{\mathrm{d}t} \begin{pmatrix} p_0 \\ p_{|+\rangle_{\mathbf{I} \cdot \mathbf{m}}} \\ p_{\mathrm{S}} \end{pmatrix} = \sum_r \Gamma_r \begin{pmatrix} -4\,f_r & 2-2\,f_r & 0 \\ 4\,f_r & -2+f_r & 2-2\,f_r \\ 0 & f_r & -2+2\,f_r \end{pmatrix} \begin{pmatrix} p_0 \\ p_{|+\rangle_{\mathbf{I} \cdot \mathbf{m}}} \\ p_{\mathrm{S}} \end{pmatrix}$$
(5.27)

$$\frac{\mathrm{d}}{\mathrm{d}t} \begin{pmatrix} p_{|-\rangle_{\mathbf{I} \cdot \mathbf{m}}} \\ p_{\mathrm{T}} \end{pmatrix} = \sum_r \Gamma_r \begin{pmatrix} -3\,f_r & 2-2\,f_r \\ 3\,f_r & -2+2\,f_r \end{pmatrix} \begin{pmatrix} p_{|-\rangle_{\mathbf{I} \cdot \mathbf{m}}} \\ p_{\mathrm{T}} \end{pmatrix}.$$

In particular, neither the singlet nor the empty state is affected by the triplets or the $|-\rangle_{\mathbf{I}_\sigma \cdot \mathbf{m}}$ state for $\varphi = n\,2\pi$. Furthermore, in the stationary limit the equations for the empty state and the singlet are identical if the dot levels coincide with the mean Fermi energy of the leads, $\varepsilon = 0$, the couplings of source and drain are equivalent, $\Gamma_{\mathrm{L}} = \Gamma_{\mathrm{R}}$, and the bias voltage is applied symmetrically (in this case $f_{\mathrm{source}} = 1 - f_{\mathrm{drain}}$).

For $\varphi \neq n\,2\pi$ the situation is sligthly more complicated since a decoupling of any kind is not apparent. Furthermore, there exists a isospin component of electrons from the source which is opposite to the isospin of electrons which can leave to the drain. Thus, a fraction

of electrons interferes destructively at the drain and a part of the transport is blocked. Similar to $\varphi = n\,2\pi$, an electron with spin σ, which occupies an initially empty system, forms a $|+\rangle_{\mathbf{I}_\sigma \cdot \mathbf{m}_\mathrm{L}}$ state, where we assume the left reservoir to be the source (without loss of generality). Again, the subsequent process either returns the system to the empty state or forms a singlet. But in contrast to $\varphi = n\,2\pi$, the probability to form a singlet is larger than to return to the empty system because only the fraction of the isospin which is parallel to the isospin of the drain can leave the dot. The antiparallel component is blocked, and a finite probability for a singly occupied system remains. A complementing difference is the fact, that for $\varphi \neq n\,2\pi$ the $|-\rangle_{\mathbf{I}_\sigma \cdot \mathbf{m}_\mathrm{R}}$ state, yielded by the decay of a triplet, is not equal to $|-\rangle_{\mathbf{I}_\sigma \cdot \mathbf{m}_\mathrm{L}}$, but is a superposition of $|+\rangle_{\mathbf{I}_\sigma \cdot \mathbf{m}_\mathrm{L}}$ and $|-\rangle_{\mathbf{I}_\sigma \cdot \mathbf{m}_\mathrm{L}}$. Hence, it can not decay further to the empty state, but the probability to form a singlet by the next electron entering from the left becomes finite, and the singlet probability increases on cost of the triplet. A similar discussion of the discharging of the singlet and a subsequent recharging process yields an indirect coupling of the singlet to the triplet. The antiparallel component of the isospin becomes largest for $\varphi = (2n+1)\,\pi$ and therefore also the indirect crossover between singlet and triplet has its maximum there. As a consequence, we can understand intuitively that the probabilities for the empty system and the triplet become small for $\varphi = (2n+1)\,\pi$ while the singlet probability increases.

Let us now turn to the case of asymmetric coupling and focus on the plots on the right hand side of Fig. 5.8. It is obvious from the upper plot, that the probabilities are not symmetric under reversal of the bias voltage any more. (Phase locking is still present though.) If the voltage is applied such that the source is better coupled than the drain electrons are pressed into the double dot system and accumulate. The probabilities for double occupancy increase significantly, whereas the probability for single occupation decreases, and the probability to find the system empty tends towards zero. The sensitivity of the probabilities to the magnetic flux becomes negligible for high voltages in this regime. In contrast, if the coupling of the source is worse than the coupling of the drain, the system tends to empty, because electrons can leave the system easier than the refill process takes place. As a consequence, the probabilities for the empty and the singly occupied system increase, whereas the probability for double occupation decreases. The oscillations of the probabilities are considerably stronger on the predominantly empty or singly occupied side of the conductance peak than on the doubly occupied side.

A comparison of the probability as function of the bias voltage, its phase dependence and, of course, the differential conductance as function of voltage and phase provokes the conjecture that double occupancy leads to a suppression of coherence. This proposition is consistent with our previous observations for the linear conductance depending on the energy of the dots' level and the phase, which we discussed in detail in subsection 5.3.2. It can be backed up by a heuristic argumentation employing the isospin picture.

We have seen before, that transport processes which involve the empty and a singly occupied state set the stage for isospin accumulation and an effective transport barrier caused by interference. As soon as the isospin of electrons which enter from the source has a component antiparallel to the isospin of electrons which can the system to the drain, an isospin is accumulated in the system and the transfer of a fraction of incoming electrons
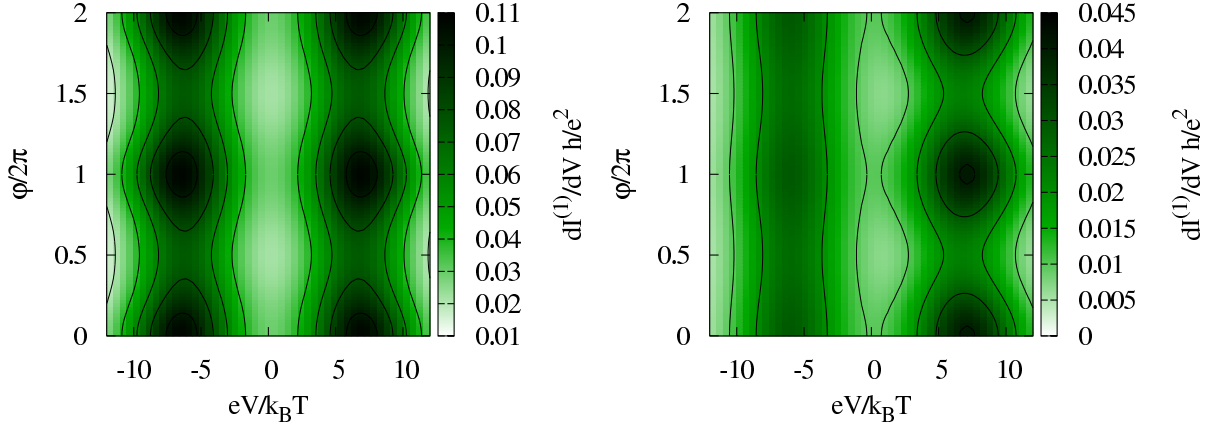
Figure 5.9:   The first order differential conductance $\mathrm{d}I^{(1)}/\mathrm{d}V$ is plotted for dot energies below the mean Fermi energy of the leads, $\varepsilon = -3\,k_\mathrm{B}T$. For the symmetric setup (left plot) the coupling strength is $\Gamma_\mathrm{L} = \Gamma_\mathrm{R} = 0.1\,k_\mathrm{B}T$. For the right plot we assume an asymmetry in the coupling of $\Gamma_\mathrm{L} = 0.1\,k_\mathrm{B}T$ and $\Gamma_\mathrm{R} = 0.2\,\Gamma_\mathrm{L}$.

to the drain is blocked, interference takes place. Considering transport processes which involve only singly and doubly occupied states the behavior is different. Let us assume the system is occupied with two electrons. Since the doubly occupied subspace does not have an isospin structure, one electron can always leave to the drain. The remaining singly occupied state acquires an isospin complementary to the leaving electron. To complete the cycle and return to the initial state we have to recharge the double dot with an electron entering from the source. This is also always possible, no matter which isospin polarization the singly occupied state has, as long as both electron spins are available. It might happen though, that one electron spin is blocked from reentering, but the other spin will fill the gap quickly. Hence, the simplest combinations of processes (in that sense the lowest order processes) which model stationary transport are nearly independent of the phase if they involve exclusively doubly and singly occupied states. From this simple argumentation we conclude that an isospin blockade, i.e. interference, may occur for processes involving the empty and the singly occupied state, but only rarely if exclusively singly and doubly occupied states take part. (This argumentation does not hold if only one kind of electron spin is available at the source, e.g. like in a ferromagnet. But in that case we are anyway more or less back to the discussion of a spinless system which is equivalent to the double dot without interaction. This does not show any asymmetries at all.)

On the same track we can motivate the difference in the amplitude of the probability oscillations on the predominantly occupied side and on the rather unoccupied side of the conductance peak. If the drain is better coupled than the source, electrons can potentially leave the system much faster than the next electron can enter. This is the point where the isospin blockade enters the game. If the isospin of the incoming electrons is nearly aligned to the isospin of the outgoing ones, i.e. $\varphi \approx n\,2\pi$, the isospin filter is open. The electrons can easily leave the system. In the contrary limit the isospin of the incoming electrons
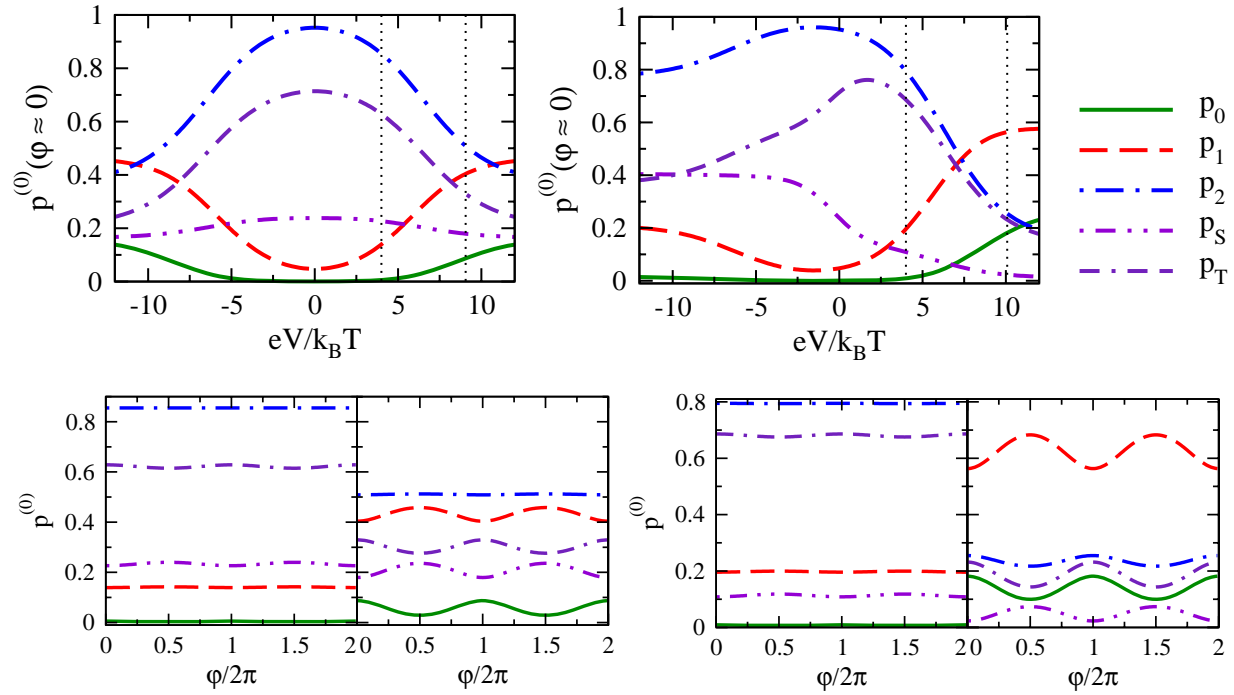
Figure 5.10: The zeroth order probabilities $\mathbf{p}^{(0)}$ and $p_2^{(0)} = p_S^{(0)} + p_T^{(0)}$ are plotted versus the bias voltage (upper plots) and the phase (lower plots) for dot energies below the mean Fermi energy of the leads, $\varepsilon = -3\,k_B T$. The behavior of the symmetric setup is shown in the plots on the left hand side. For the right plots we assume asymmetric coupling, $\Gamma_R = 0.2\,\Gamma_L$.

is antiparallel to the isospin of the outgoing electrons, i.e. $\varphi = (2n+1)\,\pi$. The isospin filter is closed. The electrons can not leave the system easily. In turn, the probability for single occupation rises at cost of the empty system if we compare to $\varphi = n\,2\pi$. Also the chance that a subsequent electron leads to the formation of a singlet increases, and the oscillation is passed to the doubly occupied states. If the source is better coupled than the drain, electrons are pressed into the system faster than they can leave. The probability for double occupancy grows. Consequently, most processes take place between single and double occupation. In this regime the phase dependent isospin blockade does not play a role. Thus, the probabilities are close to phase independent.

One of the main differences of the isospin structure in our system and the electron spin in a quantum dot coupled to magnetic leads is visible here and plays a major role in our argumentation. In both systems a spin or an isospin can be accumulated and the transport may be blocked if the spins or isospins of source and drain are not aligned. In the magnetic case the spin information is conserved even if two spins occupy the system. In contrast, the isospin in our system exists exclusively in the singly occupied subspace. Doubly occupied states (as well as the empty state) do not preserve this structure, the isospin gets sort of initialized. Therefore, we are always careful to distinguish between the pictures of spin polarized leads in the magnetic system and isospin polarized electrons which enter from the

source or leave to the drain. The isospin is a convenient construction to describe a property of the singly occupied state, namely the possibility for coherent superpositions. It can be interpreted as a kind of latent and dynamic property of specified electrons but it is not an inherent attribute of these. Furthermore, the interplay of isospin and physical electron spin is crucially important as far as transitions between the singly and the doubly occupied subspaces are concerned. In particular, the generation of a singlet-triplet imbalance is a consequence of a combination of both structures.

In a second series of exemplary plots, shown in Figures 5.9 and 5.10, we tune the dot energies off resonance, well below the mean Fermi energy of the leads. Close to equilibrium the transport becomes exponentially small. It sets in for high voltages, when the energy levels of the dots come into reach of the transport window opened by the bias. For equal coupling to the left and the right lead we obtain a differential conductance which is symmetric under reversal of the driving. Depending on the phase, maxima of the conductance are located at $\varphi = n\,2\pi$, and destructive interference becomes strong for $\varphi = (2n+1)\,\pi$.

However, the transport for asymmetric coupling is by far more interesting. The induced asymmetry between the two current directions, where either the source is better coupled than the drain or vice versa, is much more pronounced than for the dots at resonance. Like before, we find a strong suppression of the coherence, indicated by suppressed interference oscillations, if the coupling of the source exceeds the coupling of the drain, and rather strong oscillations if the drain is better coupled than the source. The obvious advantage of the system tuned off resonance is, that the incoherent conductance peak for one transport direction is clearly separated from the coherent conductance peak for the other transport direction by a low-bias region where transport is small. From an experimental point of view the feasibility of a measurement which can distinguish the two regimes is strongly enhanced.

A comparison of the plots for the differential conductance and the behavior of the probabilities shown in Fig. 5.10 corroborates our interpretation given above. The conjecture, that an enhanced probability to find the system doubly occupied leads to a suppression of coherence, is confirmed. As expected, the probabilities for the symmetrically coupled system are invariant under reversal of the bias voltage (like the differential conductance). Therefore, they are equivalent for both conductance peaks. The oscillations of the probabilities are negligible as long as the probability for the empty state is vanishingly small. The amplitude rises with increasing p_0, as we would presume from our argumentation above.

The density matrix for unequal coupling is strongly asymmetric with respect to a reversal of the bias voltage. At equilibrium the probabilities for the occupied system are already at a high level because the dot energies are tuned well below the mean Fermi energy of the leads. Driving the system out of equilibrium by an applied bias voltage decreases the overall probability to find the system doubly occupied in favor of single occupation. If the drain is better coupled than the source, the decrease is significant and the system even starts to empty at high voltages because the recharging through the weak tunnel junction to the source is comparably slow. The probabilities start to oscillate, resulting from an enabled isospin blockade. The coherent transport via singly occupied and empty states leads to significant signatures of interference in the differential conductance (left conductance
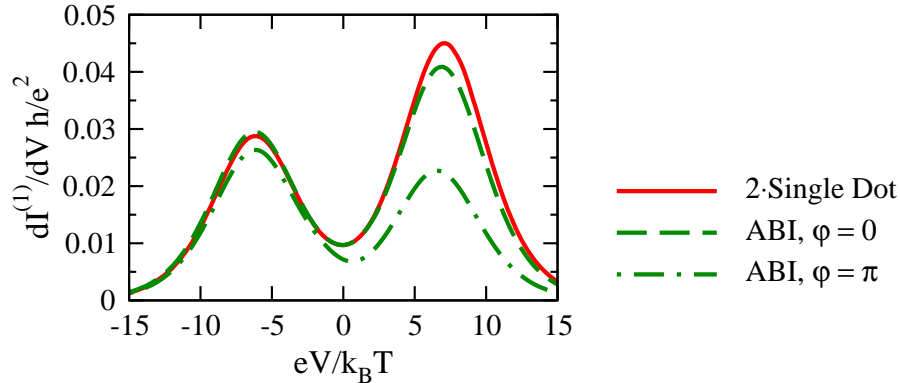
Figure 5.11: The first order differential conductance $dI^{(1)}/dV$ of the Aharonov-Bohm interferometer with dot energies below the mean Fermi energy of the leads, $\varepsilon = -3\,k_{\mathrm{B}}T$, is compared to the conductance of the two arms taken apart. Two slices, $\varphi = 0$ and $\varphi = \pi$, are picked from the contour plot in Fig. 5.9 for asymmetric coupling, $\Gamma_{\mathrm{L}} = 0.1\,k_{\mathrm{B}}T$ and $\Gamma_{\mathrm{R}} = 0.02\,k_{\mathrm{B}}T$.

peak in the right plot of Fig. 5.9). If, on the other hand, the source is better coupled than the drain, the decrease of the overall probability for double occupancy is less pronounced. Electrons can leave the system as soon as the dots' levels are reached by the transport window spanned by the driving, but the recharging takes place quickly. The increase of the empty-state probability is marginal even for high bias. In this regime the isospin blockade is not important, and the diagonal elements of the density matrix are not very sensitive to the magnetic flux. Incoherent processes involving singly and doubly occupied states dominate the transport, such that the interference oscillations in the differential conductance are only small (left conductance peak in the right plot of Fig. 5.9).

From Eq. (5.18) we see that the lowest order current in linear response becomes independent of the isospin if $\mathbf{m}_{\mathrm{L}}$ and $\mathbf{m}_{\mathrm{R}}$ are parallely aligned, i.e. $\varphi = n\,2\pi$. In that case the current is identical to the current through the two arms of the interferometer taken apart. The same conclusion is not valid beyond linear response, because the nonequilibrium density matrix does not decompose into a product of two independent quantum dots, not even for $\varphi = n\,2\pi$. Nevertheless, the presumption, that the conductance of the double-dot system approaches the sum of the conductances of both arms of the interferometer taken apart if the coherence is suppressed, seems to be valid. In Fig. 5.11 we plot two slices of the differential conductance from the right plot in Fig. 5.9 for $\varphi = 0$ and $\varphi = \pi$ and compare them to the sum of the conductances of the two interometer's arms taken apart. The conductance peak for which the coherence is nearly suppressed corresponds pretty well to the result for two independent channels.

5.3.6 Phase Switch in the Conductance Oscillations

Let us now follow the hint for the phase switch in the differential conductance of the asymmetrically coupled system (right plot in Fig. 5.7 in the region $-3 > eV/k_{\mathrm{B}}T > -4$).
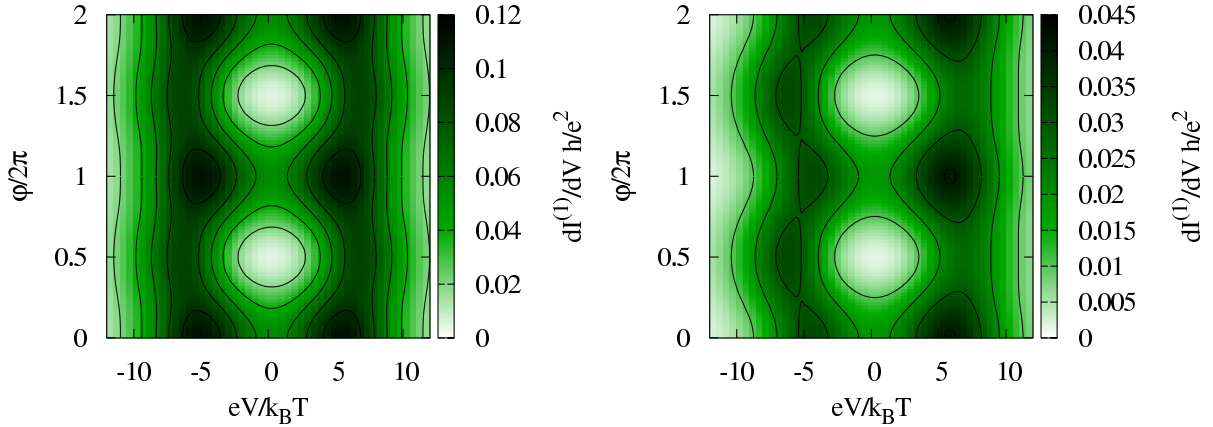
Figure 5.12:   The first order differential conductance $dI^{(1)}/dV$ is plotted for dot energies above the mean Fermi energy of the leads, $\varepsilon = +3\,k_\mathrm{B}T$. For the symmetric setup (left plot) the coupling strength is $\Gamma_\mathrm{L} = \Gamma_\mathrm{R} = 0.1\,k_\mathrm{B}T$. For the right plot we assume an asymmetry in the coupling of $\Gamma_\mathrm{L} = 0.1\,k_\mathrm{B}T$ and $\Gamma_\mathrm{R} = 0.2\,\Gamma_\mathrm{L}$.

In the plots for the dot energies tuned off resonance well below the mean Fermi energy of the leads (Fig. 5.9) there was no evidence for any phase switch. However, pushing the dots' levels off resonance to the other side, well above the mean Fermi energy of the reservoirs, a slight signature of a phase switch becomes visible even in the symmetrically coupled case. For asymmetric coupling though, the phase switch in the differential conductance becomes clear and obvious (compare Fig. 5.12).

How do we have to interpret this behavior? A phase switch in the differential conductance means, that the interference signal in the current has a vertex. Strictly speaking, the amplitude of the current oscillations first increases with enhanced driving, reaches a maximum at a certain bias, and decreases again if we crank up the voltage further. In other words: The coherent part of the current increases with the bias up to a critical voltage beyond which its contribution decreases again. Unfortunately, we can not rephrase the critical value of the voltage in a transparent and physically intuitive manner. In general, the threshold beyond which the transport becomes less coherent with increasing driving even depends on the phase.

Nevertheless, a look at the stationary state (e.g. Fig. 5.13) may motivate and substantiate a physical interpretation. Proceeding along the path which we have already started above, we would expect a transition from increasing to decreasing coherence at the crossover from the transport dominated by processes involving only the empty and a singly occupied state (strong coherence) to the transport predominantly carried by processes via singly and doubly occupied states (weak coherence). We do not have a direct measure for the occurence of processes involving certain states, but the behavior of the probabilities of the density matrix may give us some support for the argumentation. In the vicinity of a phase switch in the conductance we always find the probability for the empty state decreasing with the driving, whereas the probability for double occupation is increasing
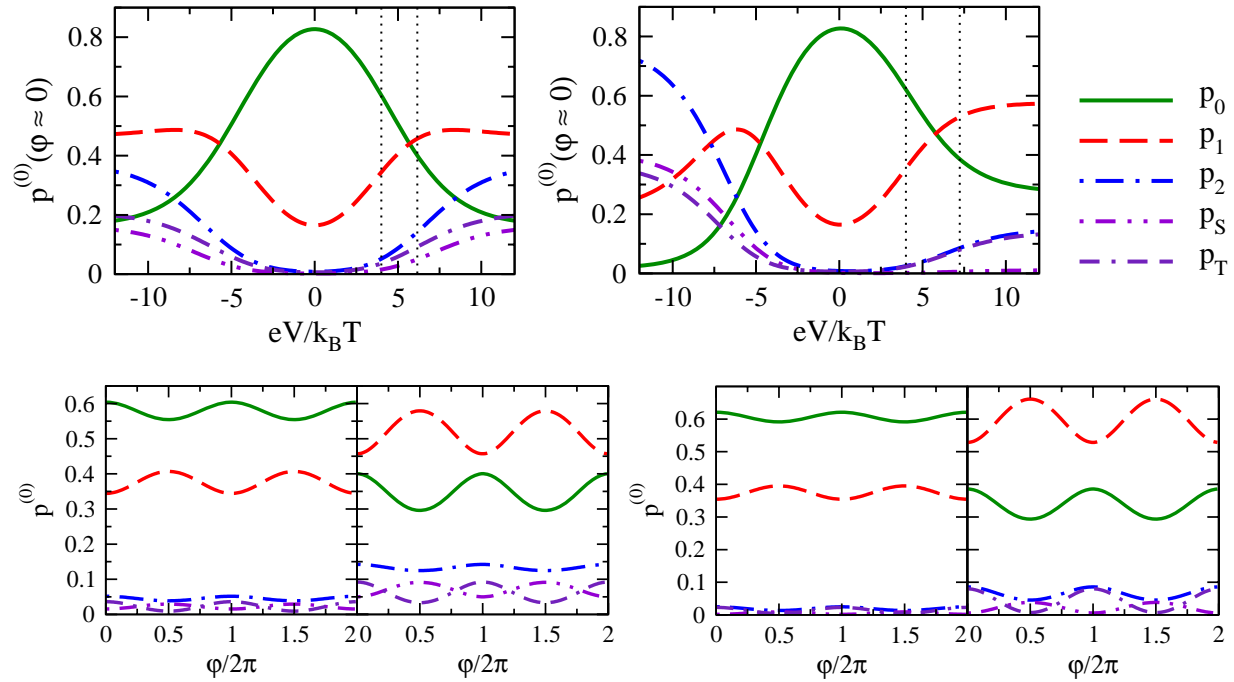
Figure 5.13: The zeroth order probabilities $\mathbf{p}^{(0)}$ and $p_2^{(0)} = p_S^{(0)} + p_T^{(0)}$ are plotted versus the bias voltage (upper plots) and the phase (lower plots) for dot energies above the mean Fermi energy of the leads, $\varepsilon = +3\,k_B T$. The left plots show the behavior of the symmetric setup, $\Gamma_L = \Gamma_R$. For the right plots we assume asymmetric coupling, $\Gamma_R = 0.2\,\Gamma_L$.

and starting to play a dominant role.

A rigorous translation from the composition of the density matrix to the occurance of transport processes is not possible, but we might argue that the current contributions which involve only singly and doubly occupied states increase, while the contributions which involve the empty system and a singly occupied state decrease, if the probability for double occupation rises on cost of the probability to find the system empty. In combination with the conjecture that double occupancy leads to a suppression of coherence we would expect the appearance of a phase switch in the differential conductance.

5.3.7 Cotunneling – Reduced Density Matrix and Second Order Transport

Already the lowest order shows partially coherent transport due to a good separation of the double-dot setup from external dephasing sources. We discussed in detail how this surprising observation can be related to the generation of coherent electronic states in the system, and we exemplified predictions about experimentally well accessible signatures in the conductance. For very weakly coupled quantum dots tuned close to the transport window opened by the bias voltage, $\Gamma_L, \Gamma_R \ll k_B T$ and $|\varepsilon| < \max\{|eV/2|, k_B T\}$, the truncation

of the perturbation expansion after the lowest order is often a sufficiently good approximation. Towards the Coulomb blockade regime, however, the respective contributions to the transport decay exponentially, whereas higher order terms decay only algebraically with ε. Thus, there is a crossover at the shoulder of the resonance peaks beyond which the transport is dominated by second order processes, the so-called cotunneling. Furthermore, if the coupling becomes stronger, higher order corrections modify the lowest order conductance even at the resonance, quantum fluctuations start to play a role and lead to renormalization effects. In this subsection we extend the preceding consideration and include systematically all second order contributions. This comprises cotunneling transport, which dominates in the Coulomb blockade, as well as renormalization effects, which lead to a modification of the position and form of the resonance but decay exponentially.

The stationary equations which we have to solve to determine the first corrections $\mathbf{p}^{(1)}$ and $\mathbf{I}^{(1)}$ to the reduced density matrix have the form

$$0 = \mathbf{W}^{(2)} \cdot \begin{pmatrix} \mathbf{p}^{(0)} \\ \mathbf{I}^{(0)} \end{pmatrix} + (\mathbf{W} - \mathrm{i}\,\boldsymbol{\Delta})^{(1)} \cdot \begin{pmatrix} \mathbf{p}^{(1)} \\ \mathbf{I}^{(1)} \end{pmatrix} \tag{5.28}$$

where we count the orders in Γ and $\Delta\varepsilon$ simultaneously. That means, a first order term may either be a product of first order in Γ and zeroth order in $\Delta\varepsilon$, or vice versa. A second order term may combine second order in Γ and zeroth oder in $\Delta\varepsilon$, or first order in Γ and first order in $\Delta\varepsilon$, a product of zeroth order in Γ and second order in $\Delta\varepsilon$ can not appear. In the preceding subsection we already calculated the kernel $\mathbf{W}$ in first order in the coupling strength which we can (in part) recycle here. (Actually, for the matrix $(\mathbf{W} - \mathrm{i}\,\boldsymbol{\Delta})^{(1)}$, known from the first order equations, the evaluation of the diagrams for $\Delta\varepsilon = 0$ is sufficient. The second order matrix, $\mathbf{W}^{(2)}$, however, contains also first order diagrams with finite detuning.) As a reminder: the eight topological classes of first order diagrams combined with the nine basis states of our Hilbert space gives us 416 possible explicit realizations, where we already took into account particle conservation and spin conservation during tunneling. With the spin symmetry of our system we are left with 208 diagrams which we have to calculate.

In second order in the coupling strength we have to regard 128 topological classes of diagrams (for a compact representation see Fig. 3.11 on page 38). In combination with the nine basis states at the ends and between the vertices we obtain in general 20448(!) possible explicit realizations. Particle conservation and spin conservation during tunneling are already taken into account. The symmetry of the system under rotations of the electron spin halves the number of diagrams we have to calculate (which does not mean that we can ignore the spin within a diagram!). The symmetries between upper and lower dot, left and right reservoir, and the mirror properties of the diagrams imply further simplifications which make the problem treatable. Despite the comment that there is no fundamental technical problem to push the diagrammatic perturbation expansion to higher orders, sometimes the bookkeeping alone reaches a degree of complexity which demands an efficient notation and, besides all convenient simplifications due to symmetries, built-in redundancies which allow for checkups and easy debugging. On top of that, higher order

diagrams represent high-dimensional integrals which are not always easy to treat (see also appendix C.

In view of the large number of complicated diagrams the kinetic equations in second order are already too extended to present in a transparent way. Nevertheless, an analytical solution is feasible for low orders in the bias voltage. Since most parts of the corrections $\mathbf{p}^{(1)}$ and $\mathbf{I}^{(1)}$ are already quite bulky in first order in the voltage, we write only the equilibrium corrections for the probabilities (the isospin corrections follow lateron),

$$p_0^{(1)} = \frac{\Gamma_{\mathrm{L}} + \Gamma_{\mathrm{R}}}{2\pi} \left[-\frac{4\,(1-f)}{(1+f)^2} \fint \frac{\mathrm{d}\omega}{\omega - \varepsilon}\, f'(\omega) - \frac{\partial p_0^{(0)}}{\partial \varepsilon} \fint \frac{\mathrm{d}\omega}{\omega - \varepsilon}\, f(\omega) \right] + \mathcal{O}(V)\,, \quad (5.29\mathrm{a})$$

$$p_1^{(1)} = \frac{\Gamma_{\mathrm{L}} + \Gamma_{\mathrm{R}}}{2\pi} \left[\frac{4\,(1-3\,f)}{(1+f)^2} \fint \frac{\mathrm{d}\omega}{\omega - \varepsilon}\, f'(\omega) - \frac{\partial p_1^{(0)}}{\partial \varepsilon} \fint \frac{\mathrm{d}\omega}{\omega - \varepsilon}\, f(\omega) \right] + \mathcal{O}(V)\,, \quad (5.29\mathrm{b})$$

$$p_{\mathrm{S}}^{(1)} = \frac{\Gamma_{\mathrm{L}} + \Gamma_{\mathrm{R}}}{2\pi} \left[\frac{2\,f}{(1+f)^2} \fint \frac{\mathrm{d}\omega}{\omega - \varepsilon}\, f'(\omega) - \frac{\partial p_{\mathrm{S}}^{(0)}}{\partial \varepsilon} \fint \frac{\mathrm{d}\omega}{\omega - \varepsilon}\, f(\omega) \right] + \mathcal{O}(V)\,, \quad (5.29\mathrm{c})$$

$$p_{\mathrm{T}}^{(1)} = \frac{\Gamma_{\mathrm{L}} + \Gamma_{\mathrm{R}}}{2\pi} \left[\frac{6\,f}{(1+f)^2} \fint \frac{\mathrm{d}\omega}{\omega - \varepsilon}\, f'(\omega) - \frac{\partial p_{\mathrm{T}}^{(0)}}{\partial \varepsilon} \fint \frac{\mathrm{d}\omega}{\omega - \varepsilon}\, f(\omega) \right] + \mathcal{O}(V)\,. \quad (5.29\mathrm{d})$$

The Fermi functions without explicit arguments are, as usual, evaluated at the mean dot energy ε. Each correction consists of a broadening term, which adds algebraic tails and leads to a smoothing of the rather sharp exponential characteristics of $\mathbf{p}^{(0)}$, and a term which indicates a renormalization of the dots' levels. The latter can be expressed by the derivative of the corresponding lower order probability and the renormalization of the energy. It decays exponentially but shifts the probabilities as functions of ε. This correction reflects the influence of the coupling of the dots to the reservoirs and is due to quantum fluctuations. In Fig. 5.14 we plot the equilibrium probabilities and illustrate the influence of the first order corrections. Obviously, all probabilities are shifted systematically to lower energies. Additionally, the curves are broadenend and smoothed. Intuitively, both effects can be linked to a second order tunneling forth and back between reservoirs and double dot system. We can imagine several possible equilibrium processes which neither effectively transport electrons, i.e. they do not give a net current, nor they change the charge or spin state enduringly. Nevertheless, during the process the state is changed for a (virtually) short period of time which can lead to a finite modification of the corresponding probabilities.

The systematic shift to lower energies can be motivated similar to a single dot. We realize that for the empty system a tunneling forth and back of electrons of arbitrary spin is possible for both dots, while for a system occupied with a single electron, say a spin σ, it is only this spin which can leave to one of the reservoirs before the system is recharged again. Thus, the number of processes which may lead to an enhancement of the probability for single occupation at cost of the probability to find the system empty exceeds the number of concurring processes which shift probability from the singly occupied to the empty subspace. Consequently, we expect an increase of the probability to find the
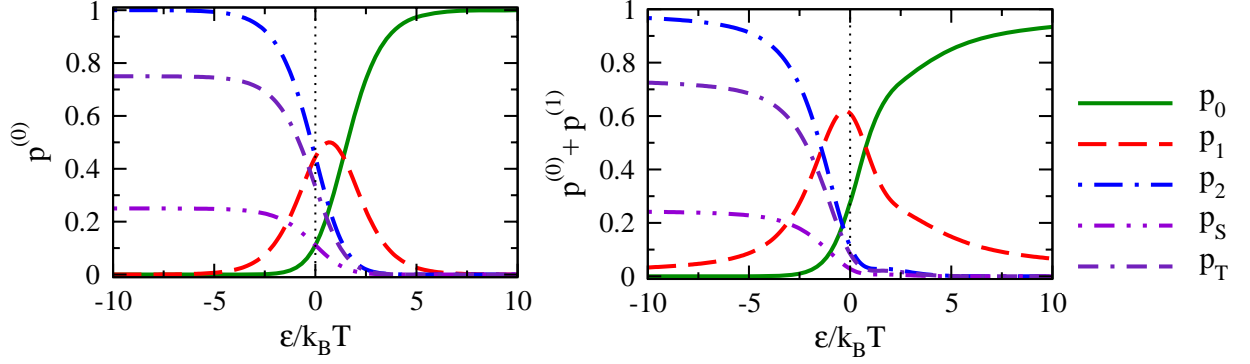
Figure 5.14: The influence of the first correction to the probabilities **p** and $p_2 = p_S + p_T$ are plotted in equilibrium for $\Gamma_L = \Gamma_R = 0.5\,k_B T$. A renormalization of the dots' levels to lower energies (shifting of all probabilities) and a renormalization of the level broadening (smoothing and expansion of the probabilities) are apparent.

system singly occupied at cost of the probability to find the system empty. The competition between single- and double-occupation is more balanced, but if the system is predominantly occupied with two electrons the renormalization tunneling leads as well to an increase of the probability for single occupation at cost of the probability for double occupation.

As expected from the simple picture drawn above, the singlet-triplet imbalance vanishes if there is no defined current direction, even if we take into account the first order correction in Γ. Intuitively it is clear that a tunneling forth and back starting with an doubly occupied state can not change the correlation between the upper and lower dot on average. The operators

$$O_{\mathrm{io}} := (e^{\pm i\frac{\varphi}{4}} c_{u\sigma}^{\dagger} + e^{\mp i\frac{\varphi}{4}} c_{d\sigma}^{\dagger})(e^{\mp i\frac{\varphi}{4}} c_{u\sigma'} + e^{\pm i\frac{\varphi}{4}} c_{d\sigma'}) \,, \tag{5.30}$$

for instance, which represent a tunneling out and subsequent tunneling back into the double dot, do not mix the singlet with the triplets, i.e. the singlet stays invariant. On the other hand, the preferred intermediate (or virtual) state of a process which is composed of an electron tunneling into the system and leaving again to a reservoir,

$$O_{\mathrm{oi}} := (e^{\pm i\frac{\varphi}{4}} c_{u\sigma} + e^{\mp i\frac{\varphi}{4}} c_{d\sigma})(e^{\mp i\frac{\varphi}{4}} c_{u\sigma'}^{\dagger} + e^{\pm i\frac{\varphi}{4}} c_{d\sigma'}^{\dagger}) \,, \tag{5.31}$$

depends on the initial singly occupied state, especially on its isospin polarization. In equilibrium, however, all isospin directions in lowest order are equally distributed and average to zero. Thus, there is no preference of either singlet or triplet correction.

Nevertheless, the first correction of the isospin does not vanish in equilibrium,

$$I_x^{(1)} = 2\,\frac{\Gamma_L + \Gamma_R}{2\pi}\,\frac{\cos(\varphi/2)}{(1+f)^2}\,\fint \frac{d\omega}{\omega - \varepsilon}\,f'(\omega) + \mathcal{O}(V)\,, \tag{5.32a}$$

$$I_y^{(1)} = 2\,\frac{\Gamma_L - \Gamma_R}{2\pi}\,\frac{\sin(\varphi/2)}{(1+f)^2}\,\fint \frac{d\omega}{\omega - \varepsilon}\,f'(\omega) + \mathcal{O}(V)\,, \tag{5.32b}$$

except for the I_z component. The terms in Eqs. (5.32a) and (5.32b) (the coordinate system is chosen like for Eqs. (5.24a), (5.24b)) represent broadening terms which decay algebraically. Hence, beyond lowest order tunneling there is a favored isospin already in equilibrium. That means, coherent superposition states are generated even if the electrons are not driven in a particular direction. In our simple picture with electrons tunneling forth and back between the reservoirs and the double dot system this can be motivated as follows. Assume an electron occupying the double dot system in a localized state, either in the upper or in the lower dot, as suggested by $\mathbf{p}^{(0)}$ and $\mathbf{I}^{(0)}$. It can leave the system to either side. The subsequent recharging generates a superposition state with a preferred isospin in $\mathbf{m}_L$ or $\mathbf{m}_R$ direction, respectively (this is reflected in the structure $\mathbf{I}^{(1)} \sim (\Gamma_L\, \mathbf{m}_L + \Gamma_R\, \mathbf{m}_R)$).

As long as the couplings to the left and the right reservoir are equal, the tunneling forth and back on both sides is balanced and we expect equivalent probabilities for $|+\rangle_{\mathbf{I}_\sigma \cdot \mathbf{m}_L}$ and $|+\rangle_{\mathbf{I}_\sigma \cdot \mathbf{m}_R}$, as well as for $|-\rangle_{\mathbf{I}_\sigma \cdot \mathbf{m}_L}$ and $|-\rangle_{\mathbf{I}_\sigma \cdot \mathbf{m}_R}$ states. Consequently, for our choice of the coordinate system, the $I_y^{(1)}$ component averages to zero. If one of the reservoirs is better coupled than the other, the renormalization processes favor the better coupled side and the probabilities for the respective superposition states are larger, the $I_y^{(1)}$ component becomes finite. However, none of the zero bias isospin corrections in first order show up in the second order transport, it is not before the third order in which a contribution to the current may appear.

For a finite bias voltage we find a noteworthy pecularity of the isospin correction $\mathbf{I}^{(1)}$. Already in first order in the voltage the stationary isospin is rotated out of the plane perpendicular to $\mathbf{n}$, although the coupling of the upper and lower dot is symmetric and the dot levels are degenerate, $\Delta\varepsilon = 0$. In our choice of the coordinate system this is apparent in a non-vanishing I_z-component

$$I_z^{(1)} = eV\,\frac{2\sin\varphi}{\pi^2}\,\frac{\Gamma_L\Gamma_R}{\Gamma_L + \Gamma_R}\left[\frac{1}{(1+f)^3}\,\rlap{\textstyle\int}{\rule[0.3ex]{0.9em}{0.08ex}}\,\frac{\mathrm{d}\omega'}{\omega' - \varepsilon}\,\rlap{\textstyle\int}{\rule[0.3ex]{0.9em}{0.08ex}}\,\frac{\mathrm{d}\omega}{\omega - \omega'}\,f''(\omega)\; - \right.$$

$$\left. - \frac{f'}{(1+f)^4}\,\rlap{\textstyle\int}{\rule[0.3ex]{0.9em}{0.08ex}}\,\frac{\mathrm{d}\omega'}{\omega' - \varepsilon}\,\rlap{\textstyle\int}{\rule[0.3ex]{0.9em}{0.08ex}}\,\frac{\mathrm{d}\omega}{\omega - \omega'}\,f'(\omega)\right] + \mathcal{O}(V^2)\,. \qquad (5.33)$$

This quite surprising feature indicates an interference effect which is generated by directed higher order tunneling. It leads to a phase dependent difference between the occupation probabilities of the upper and the lower dot in a nonequilibrium situation (independent of the detuning). The transport up to third order in Γ is not affected by this pecularity neither in linear response nor beyond.

Actually, we can identify two effective fields which lead to the mentioned stationary behavior of the isospin. They appear in the corresponding second order kinetic equations in the form

$$\frac{\mathrm{d}}{\mathrm{d}t}\mathbf{I} = \ldots + (4\,p_0 - 2\,p_1 - 2\,p_S + p_T)\,\mathbf{S}_I + \mathbf{B}_I \times \mathbf{I}\,. \qquad (5.34)$$

The second term, which is governed by the exchange field

$$\mathbf{B}_I := -2\,\rlap{\textstyle\int}{\rule[0.3ex]{0.9em}{0.08ex}}\,\frac{\mathrm{d}\omega'}{\omega' - \varepsilon}\,\rlap{\textstyle\int}{\rule[0.3ex]{0.9em}{0.08ex}}\,\frac{\mathrm{d}\omega}{\omega - \omega'}\left[\frac{\Gamma_L}{2\pi}\,f_L'(\omega) + \frac{\Gamma_R}{2\pi}\,f_R'(\omega)\right]\left(\frac{\Gamma_L}{2\pi}\,\mathbf{m}_L + \frac{\Gamma_R}{2\pi}\,\mathbf{m}_R\right), \qquad (5.35)$$

leads to the exponentially decaying second term in the stationary solution for $I_z^{(1)}$ (Eq. (5.33)). The field $\mathbf{B}_I$ acts similar to a finite detuning or, partially, like an asymmetric coupling of the upper and the lower dot. It modifies the precession of the isospin and tilts the axis. The direction of the latter is redefined depending on the coupling strenghts to the left and the right reservoir and the phase induced by the magnetic flux threading the Aharonov-Bohm ring.

The first term in the stationary solution for $I_z^{(1)}$ in Eq. (5.33) decays only algebraically in the Coulomb blockade. It originates from the first term in Eq. (5.34), which is governed by a strange field

$$\mathbf{S}_I := -\frac{\Gamma_L \Gamma_R}{(2\pi)^2} \oint \frac{d\omega'}{\omega' - \varepsilon} \oint \frac{d\omega}{\omega - \omega'} \left[f_L'(\omega) - f_R'(\omega) \right] (\mathbf{m}_L \times \mathbf{m}_R) . \qquad (5.36)$$

In contrast to the exchange field $\mathbf{B}_I$, it is always parallel or antiparallel to the quantization axis $\mathbf{n}$ (except for the special situation in which the isospins of the left and the right reservoir are aligned, but in that case its influence, at least on the linear response term of $I_z^{(1)}$, vanishes anyway). Neither its direction nor the amplitude is sensitive to an asymmetry in the coupling. However, the strength of the field varies with the product of the coupling strengths, $\Gamma_L \Gamma_R$, and the magnetic flux. It vanishes for zero bias, i.e. it reflects a pure nonequilibrium property of the system. Surprisingly, the field $\mathbf{S}_I$ does not couple to the isospin but to a combination of diagonal terms of the density matrix. Thus, it does not contribute to a precession of any kind, which could be interpreted as a contribution to a coherent oscillation, instead it leads to a more fundamental rotation of the isospin polarization out of the plane perpendicular to $\mathbf{n}$. An interesting detail is, that it couples to the singlet and the triplet probabilities in a strongly asymmetric fashion.

However, as interesting as these effects are from a theoretical point of view, they do not show up in the transport before the fourth order in the coupling strength. Thus, we leave them for a later discussion and return our focus to the second order.

Despite the large number of diagrams, the calculation yields a surprisingly concise equation for the second order linear conductance. Recalling the first order from Eq. (5.21), we additionally include the detuning and utilize the resulting equation,

$$G^{(1)} = -8\pi \frac{e^2}{h} \frac{\Gamma_L \Gamma_R}{\Gamma_L + \Gamma_R} \frac{f'}{1+f} \frac{\Delta\varepsilon^2 + 4\,\Gamma_L\Gamma_R \left[(1+f)^2 - \sin^2(\varphi/2) \right] \sin^2(\varphi/2)}{\Delta\varepsilon^2 + 4\,\Gamma_L\Gamma_R\,(1+f)^2 \sin^2(\varphi/2)} , \qquad (5.37)$$

for a compact notation of parts of the second order correction.

The linear conductance in second order can be split into several constituents distinguished by their functional properties, $G^{(2)} = G_1^{(2)} + G_2^{(2)} + G_3^{(2)} + G_4^{(2)}$. The first term decays algebraically in the Coulomb blockade and gives the main contribution in the regime in which cotunneling dominates the transport,

$$G_1^{(2)} = -4 \frac{e^2}{h} \Gamma_L \Gamma_R \left(1 + \frac{\cos\varphi}{(1+f)^2} \right) \oint \frac{d\omega}{\omega - \varepsilon} f''(\omega) . \qquad (5.38)$$

Compared to the analogous term for a single quantum dot (Eq. (3.50)), the maximal contribution (for $\varphi = n\,2\pi$) is larger than the corresponding sum of the two arms of the

Aharonov-Bohm interferometer taken apart. Like in the noninteracting case it is the second rather than the first order transport which gives evidence for constructive interference. As a reminder: The first order linear conductance is at most as large as the sum of the two arms taken apart and yields only indicators for destructive interference.

The second and third term, $G_2^{(2)}$ and $G_3^{(2)}$, can be identified with renormalization terms. They are closely related to the first order linear conductance and decay exponentially in the Coulomb blockade. Their main impact is a shift and a quantitative modification of the first order conductance, but they do not add a new qualitative behavior like the algebraically decaying tails of $G_1^{(2)}$. We can summarize the corresponding contributions by recycling the expression for the first order linear conductance (Eq. (5.37)):

$$G_2^{(2)} = -\frac{\partial G^{(1)}}{\partial \varepsilon} \fint \frac{d\omega}{\omega - \varepsilon} \gamma(\omega) \qquad \text{and} \qquad G_3^{(2)} = -G^{(1)} \frac{\partial}{\partial \varepsilon} \fint \frac{d\omega}{\omega - \varepsilon} \gamma(\omega) \qquad (5.39)$$

with $2\pi \gamma := (\Gamma_L + \Gamma_R) f(\omega)$. The correction due to a renormalization of the dots' levels is represented by $G_2^{(2)}$, whereas $G_3^{(2)}$ reflects the renormalization of the level broadening.

The fourth term comprises all remaining contributions and can again be split into three parts,

$$G_4^{(2)} = -4 \frac{e^2}{h} \Gamma_L \Gamma_R (C_1 + C_2 + C_3) \fint \frac{d\omega}{\omega - \varepsilon} \frac{d}{d\omega} \left[f(\omega)(1 - f(\omega)) \right], \qquad (5.40)$$

such that $G_4^{(2)} = G_{C_1}^{(2)} + G_{C_2}^{(2)} + G_{C_3}^{(2)}$. All three contributions are proportional to the derivative of the principal value integral of a product of Fermi functions, and each is proportional to an even power of $\sin^2(\varphi/2)$, i.e. they do not influence the linear conductance if φ equals an even multiple of π (corresponds to aligned isospins). In detail the diverse constituents read

$$C_1 = \frac{\Gamma_L^2 \Gamma_R^2 (\Gamma_L - \Gamma_R)^2}{(\Gamma_L + \Gamma_R)^2} \frac{f'(2 + f)}{1 - f} \frac{16 \sin^6(\varphi/2)}{\left[\Delta\varepsilon^2 + 4\Gamma_L \Gamma_R (1 + f)^2 \sin^2(\varphi/2) \right]^2}, \qquad (5.41)$$

$$C_2 = -\frac{\Gamma_L^2 \Gamma_R^2}{(\Gamma_L + \Gamma_R)^2} \frac{\Delta\varepsilon^2 f'}{(1 - f)(1 + f)^2} \frac{16 \left[2 + f - 3 f \sin^2(\varphi/2) \right] \sin^4(\varphi/2)}{\left[\Delta\varepsilon^2 + 4\Gamma_L \Gamma_R (1 + f)^2 \sin^2(\varphi/2) \right]^2}, \qquad (5.42)$$

$$C_3 = \frac{\Gamma_L^3 \Gamma_R^3}{(\Gamma_L + \Gamma_R)^2} \frac{128 f' \sin^8(\varphi/2)}{\left[\Delta\varepsilon^2 + 4\Gamma_L \Gamma_R (1 + f)^2 \sin^2(\varphi/2) \right]^2}, \qquad (5.43)$$

where the Fermi functions without explicit argument are evaluated at the mean dots' energy ε.

The first conductance contribution, generated by C_1 and denoted by $G_{C_1}^{(2)}$, has very peculiar characteristics. As function of the dots' mean energy it decays algebraically on the occupied side of the conductance resonance, like the cotunneling term $G_1^{(2)}$, but it vanishes exponentially on the unoccupied side, like the first order term or its renormalization
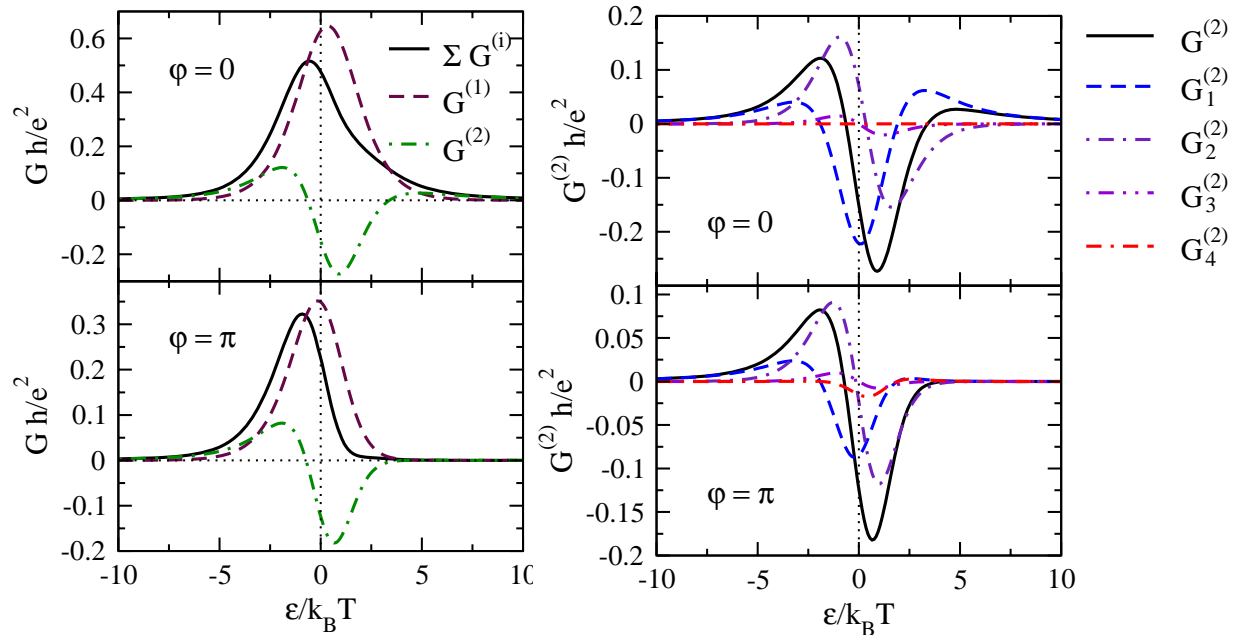
Figure 5.15:   The linear conductance up to second order in the coupling strength and its contributions are plotted for $\Gamma_L = \Gamma_R = 0.3\,k_BT$ and $\Delta\varepsilon = 0$. For the upper plots we assumed $\varphi = 0$ and for the lower plots $\varphi = \pi$. The cutoff is $D = 10^3\,k_BT$.

corrections. Furthermore, it affects the linear conductance only if the coupling to the left and the right reservoir is asymmetric. The second term, $G_{C_2}^{(2)}$, decays algebraically on both sides of the conductance resonance and can be interpreted as a correction to $G_1^{(2)}$ due to a finite detuning. It diminishes the absolute value of $G_1^{(2)}$ at $\varphi = (2n+1)\,\pi$ but leaves it untouched at $\varphi = n\,2\pi$, i.e. destructive interference is enhanced but constructive interference is not affected by a finite detuning. The overall effect of the correction is tiny. For reasonable parameters and a detuning comparable to the level width, the modification of the amplitude of the oscillations is less than one percent. The third term, $G_{C_3}^{(2)}$, is the most inconspicuous. It vanishes exponentially on both sides of the conductance resonance and does not show very noticeable specifics.

In Fig. 5.15 we plot all contributions to the linear conductance up to second order for vanishing detuning. The strong renormalization shift of the first order curve, $G^{(1)}$, to lower energies, which is mainly due to the correction term $G_2^{(2)}$, is clearly visible. The cotunneling term, $G_1^{(2)}$, adds its algebraically decaying tails. Additionally, it diminishes the first order at the resonance and leads to a reduction of the oscillations at the conductance peak. We can already estimate from a comparison of the conductance for $\varphi = 0$ and $\varphi = \pi$ that the oscillation on the unoccupied side of the resonance is a lot stronger than on the side on which the double dot system is predominantly occupied.

The amplitude of the oscillations of the first and second order conductance contributions and their sum as function of the level energies is specifically focused in Fig. 5.16. To keep
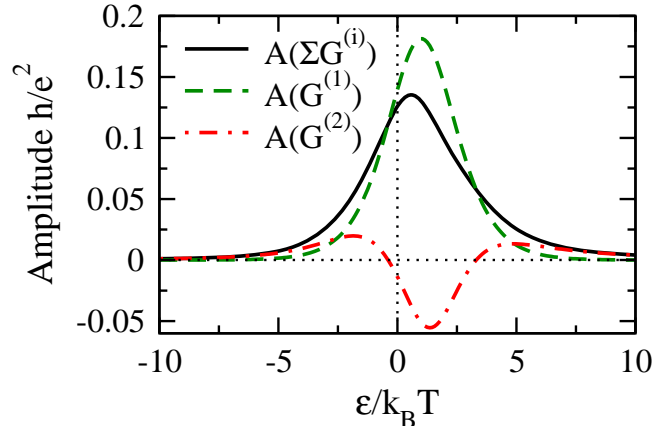
Figure 5.16: The amplitudes of the linear conductance and its first and second order contributions are plotted for $\Gamma_L = \Gamma_R = 0.3\,k_B T$ and $\Delta\varepsilon = 0$. The cutoff is $D = 10^3\,k_B T$.

track if the oscillations of the first and second order are in phase or in mutually opposite phase we define the amplitude of the linear conductance $A[G] := (G|_{\varphi=0} - G|_{\varphi=\pi})/2$ without taking the absolute value. Obviously, the maximum of the oscillations is considerably shifted to the unoccupied side of the averaged conductance resonance which is centered in the vicinity of $\varepsilon \approx -0.75\,k_B T$ (compare Fig. 5.15). Furthermore, a closer look at the shape of the amplitude function of $G^{(1)} + G^{(2)}$ reveals quite a strong asymmetry with respect to the maximum close to $\varepsilon \approx 0.55\,k_B T$. In the Coulomb blockade on the unoccupied side the amplitude approaches a multiple of the linear conductance of a single quantum dot, $G_{\text{dot}}^{(1)} + G_{\text{dot}}^{(2)}$ (compare also Eqs. (3.44) and (3.49) in section 3.6), but only a fraction on the occupied side, $A[G^{(1)} + G^{(2)}] \longrightarrow 2\,G_{\text{dot}}^{(2)}/(1 + f)^2$. (This holds for a symmetrically coupled system, $\Gamma_L = \Gamma_R$. For asymmetric coupling there is an additional contribution from the term $G_{C_1}^{(2)}$ in the crossover regime between occupied side of the resonance and Coulomb blockade. It suppresses the oscillations further, but the overall effect is less than a few percent.) Specifically, for $|\varepsilon| \gg \Gamma_L, \Gamma_R, k_B T$ we expect the amplitude on the unoccupied side to be approximately four times larger than on the occupied side, $A[G^{(1)} + G^{(2)}](|\varepsilon|) \approx 4\,A[G^{(1)} + G^{(2)}](-|\varepsilon|)$.

In the preceding subsection 5.3.3 we discussed in detail how an asymmetry in the coupling affects the state of the system and the signatures of coherence in the transport. In lowest order in Γ we obtain significant characteristics only beyond linear response. Taking into account higher order corrections, we have a conductance contribution in which asymmetric coupling is recognizable already in linear response. To be specific, the term $G_{C_1}^{(2)}$ is finite only if $\Gamma_L \neq \Gamma_R$. It induces an additional asymmetry between the two sides of the conductance resonance. As mentioned, it decays algebraically on the occupied, but exponentially on the unoccupied side of the peak. The phase of its oscillation is opposite to the general cosine-like behavior and leads to a supression of the coherence at the shoulder of the resonance and in the close occupied Coulomb blockade. In general, it
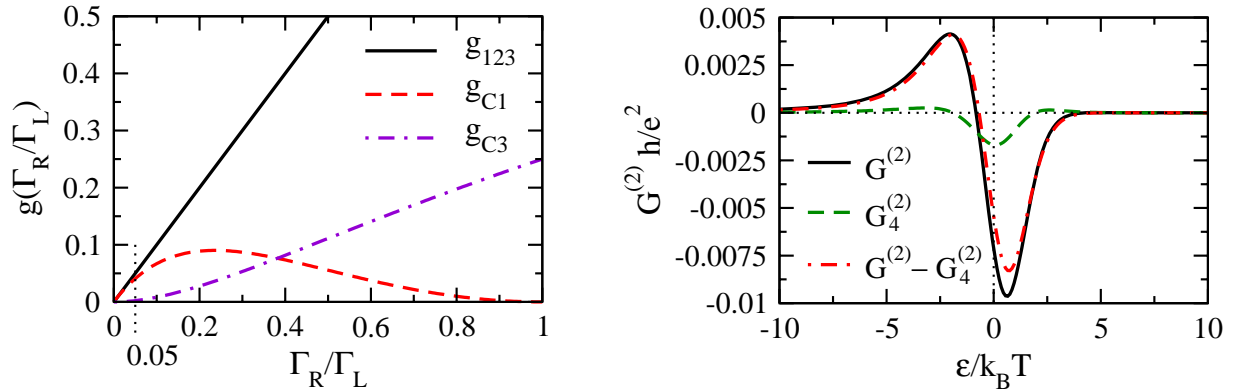
Figure 5.17:   The left plot shows the functions g of the coupling prefactors. As function of the ratio of the couplings, the correction term $G_{C_1}^{(2)}$ is non-monotonic and shows a maximum at $\Gamma_R = (\sqrt{5} - 2)\,\Gamma_L$. The maximal influence of the correction term $G_4^{(2)}$ on the second order linear conductance $G^{(2)}$ can be estimated from the right plot for $\varphi = \pi$, vanishing detuning, $\Delta\varepsilon = 0$, and asymmetric coupling, $\Gamma_L = 0.3\,k_B T$ and $\Gamma_R = 0.05\,\Gamma_L$. The cutoff is $D = 10^3\,k_B T$.

counteracts the interference contribution from the cotunneling term $G_1^{(2)}$, except for the unoccupied blockade where it vanishes exponentially. Hence, the asymmetry between the coherent contributions on both sides of the conductance peak is enhanced qualitatively if the coupling is asymmetric.

To get an idea about the origin of the $G_{C_1}^{(2)}$-term we trace it to the kinetic equations. The first step back tells us that the hybrid algebraically-exponentially decaying term stems exclusively from first order corrections of the reduced density matrix. For $\Delta\varepsilon = 0$ we can encircle the root further and find that only corrections of the singly occupied subspace play a role. The singlet and the triplet contribution to the current contain also an algebraically decaying term of that kind, but in the sum they cancel each other. It is only for $\Delta\varepsilon \neq 0$ where the sum of the relevant contributions from the doubly occupied subspace becomes finite. After the second step back we find, that all respective terms of the first order correction, which may lead to the algebraically-exponentially decaying hybrid, originate from elements of the second order part of the kernel $\mathbf{W}^{(2)}$ which couple only density matrix elements of the doubly occupied subspace, namely singlet and triplet probabilities.

For a quantitative estimate of the impact of the hybrid $G_{C_1}^{(2)}$ term we have to analyze its energy dependence and also the dependence on the asymmetry of the coupling compared to the other contributions. The linear conductance is, in general, invariant under permutation of Γ_L and Γ_R due to the symmetries of the system. Hence, we can assume $\Gamma_L > \Gamma_R \geq 0$ or $\Gamma_L = \Gamma_R \neq 0$, without loss of generality. In second order we can then summarize all coupling parameters in a prefactor of the form $\Gamma_L^2\, g(\Gamma_R/\Gamma_L)$ where the function g has to be specified for each term contributing to the linear conductance. For $G_1^{(2)}$ as well as for $G_2^{(2)}$ and $G_3^{(2)}$, the function g is simply linear, i.e. $g_{123}(x) := x$ for $x \in [0, 1]$. The terms comprised in $G_4^{(2)}$ (for vanishing detuning) are proportional to $g_{C_1}(x) := x\,(1-x)^2/(1+x)^2$

and $g_{C_3}(x) := x^2/(1+x)^2$. The corresponding curves are shown in Fig. 5.17. The term in which we are mainly interested, g_{C_1}, is non-monotonic and has a maximum at $\Gamma_{\mathrm{R}}/\Gamma_{\mathrm{L}} = \sqrt{5} - 2$. With increasing asymmetry in the coupling it rises slowly, reaches the maximum, and approaches for even stronger asymmetries the linear coupling dependence of $G_1^{(2)}$, $G_2^{(2)}$ and $G_3^{(2)}$. Thus, we expect the maximal impact of $G_{C_1}^{(2)}$ on $G^{(2)}$ for quite a strong asymmetry in the coupling, where g_{C_1} approaches g_{123} (and the conductance vanishes). In the second plot in Fig. 5.17 we compare the full second order correction $G^{(2)}$ to the $G_4^{(2)}$ contribution for $\Gamma_{\mathrm{R}} = 0.05\,\Gamma_{\mathrm{L}}$. We are basically concerned with the algebraic decay for $-\varepsilon > \Gamma_{\mathrm{L}}, \Gamma_{\mathrm{R}}, k_{\mathrm{B}}T$ where $G_4^{(2)}$ is essentially given by its $G_{C_1}^{(2)}$ constituent. Obviously, the corresponding correction to $G_1^{(2)}$ is unspectacularly small even for a strong asymmetry in the coupling, although the qualitative behavior is kind of exceptional.

Anyway, deep inside the Coulomb blockade our standard procedure runs into a singularity, and we have to solve combined equations of first and second order simultaneously (Eq. (5.26)). The calculation is straightforward. In the limiting case $-\varepsilon \gg \Gamma_{\mathrm{L}}, \Gamma_{\mathrm{R}}, k_{\mathrm{B}}T$ we obtain the solution for the elements of the stationary density matrix in lowest and, in most cases, also in first order in Γ. The probabilities read

$$p_0^{(0)} + p_0^{(1)} = 0 + \mathcal{O}(V^2)\,, \tag{5.44a}$$

$$p_1^{(0)} + p_1^{(1)} = -2\,\frac{\Gamma_{\mathrm{L}}+\Gamma_{\mathrm{R}}}{2\pi} \fint \frac{\mathrm{d}\omega}{\omega-\varepsilon}\, f'(\omega) - eV\,\frac{\Gamma_{\mathrm{L}}-\Gamma_{\mathrm{R}}}{2\pi} \fint \frac{\mathrm{d}\omega}{\omega-\varepsilon}\, f''(\omega) + \mathcal{O}(V^2)\,, \tag{5.44b}$$

$$p_{\mathrm{S}}^{(0)} = \frac{1}{4} + \mathcal{O}(V^2)\,, \tag{5.44c}$$

$$p_{\mathrm{T}}^{(0)} = \frac{3}{4} + \mathcal{O}(V^2)\,. \tag{5.44d}$$

To determine the first correction of the singlet and triplet probabilities we would have to take into account parts of the kernel in third order in the coupling strength, $\mathbf{W}^{(3)}$. Fortunately, it is only the lowest order terms of the doubly occupied subspace which enter the current formula up to second order in this limit. The first order current rates which are associated to the singlet and triplet contributions vanish for $-\varepsilon \gg \Gamma_{\mathrm{L}}, \Gamma_{\mathrm{R}}, k_{\mathrm{B}}T$. Thus, the first order corrections of the probabilities drop out.

The solution for the stationary isospin is given by

$$I_x^{(0)} + I_x^{(1)} = \frac{\Gamma_{\mathrm{L}}+\Gamma_{\mathrm{R}}}{2\pi}\,\frac{\cos(\varphi/2)}{2} \fint \frac{\mathrm{d}\omega}{\omega-\varepsilon}\, f'(\omega) + \frac{eV}{4}\,\frac{\Gamma_{\mathrm{L}}-\Gamma_{\mathrm{R}}}{2\pi} \fint \frac{\mathrm{d}\omega}{\omega-\varepsilon}\, f''(\omega) + \mathcal{O}(V^2)\,, \tag{5.45a}$$

$$I_y^{(0)} + I_y^{(1)} = \frac{\Gamma_{\mathrm{L}}-\Gamma_{\mathrm{R}}}{2\pi}\,\frac{\sin(\varphi/2)}{2} \fint \frac{\mathrm{d}\omega}{\omega-\varepsilon}\, f'(\omega) + \frac{eV}{4}\,\frac{\Gamma_{\mathrm{L}}-\Gamma_{\mathrm{R}}}{2\pi} \fint \frac{\mathrm{d}\omega}{\omega-\varepsilon}\, f''(\omega) + \mathcal{O}(V^2)\,, \tag{5.45b}$$

$$I_z^{(0)} + I_z^{(1)} = eV\,\frac{\sin\varphi}{(2\pi)^2}\,\frac{\Gamma_{\mathrm{L}}\Gamma_{\mathrm{R}}}{\Gamma_{\mathrm{L}}+\Gamma_{\mathrm{R}}} \fint \frac{\mathrm{d}\omega'}{\omega'-\varepsilon} \fint \frac{\mathrm{d}\omega}{\omega-\omega'}\, f''(\omega) + \mathcal{O}(V^2)\,, \tag{5.45c}$$

where we have choosen the coordinate system like in Fig. 5.3, as usual. The resulting linear conductance,

$$G^{(1)} + G^{(2)} = -4 \frac{e^2}{h} \Gamma_{\mathrm{L}} \Gamma_{\mathrm{R}} \left(1 + \frac{\cos\varphi}{4}\right) \fint \frac{\mathrm{d}\omega}{\omega - \varepsilon} f''(\omega), \qquad (5.46)$$

is identical to the limiting case of the cotunneling contribution $G_1^{(2)}$. It coincides with previous results of a rather phenomenological approach [78]. In particular, the algebraically decaying tail of $G_{C_1}^{(2)}$ does not play a role deep inside the Coulomb blockade. The relevant terms in the correction of the density matrix from which the algebraic-exponential hybrid originated are absent.

Due to the enormous amount of complicated second order diagrams, an analytical solution of the kinetic equations for the reduced density matrix was only feasible in the linear response regime. However, nonequilibrium effects enter via the isospin accumulation already here. We supplement the results of a numerical approach in which all diagrams are generated and computed automatically. This calculation can be extended to arbitrary nonequilibrium situations and, at the same time, provides a check for the bookkeeping in the analytical approach.

Beyond linear response the most apparent impacts of the second order correction to the conductance are induced by the strong broadening due to cotunneling, and the renormalization of the dots' levels. The latter leads to a shift of the conductance to lower energies as already discussed in detail for linear response. Two exemplary plots of the first order differential conductance and the differential conductance including all second order corrections are displayed for comparison in Fig. 5.18 for a fixed magnetic flux.

The phase dependence of the differential conductance at the resonance is not changed significantly by the second order correction (see also Fig. 5.19). Very close to the conductance peaks the amplitude of the oscillations is sligthly diminished, but the specific behavior at the shoulders is supported and continued with an algebraically decaying envelope. The discussed suppression of coherence by double occupancy is still feasible and well visible at the conductance peaks for asymmetric coupling of the left and the right reservoir. Besides the peaks, especially outside the current window opened by the bias voltage, however, the transport in second order shows coherent oscillations even if the system is predominantly doubly occupied. This can be read from the partial rates which are necessary for the calculation of the current. While for the first order only the current rates corresponding to the singly occupied subspace are phase dependent, which reflects the mechanism of the isospin blockade, in second order also the current rates corresponding to the empty and the doubly occupied subspace depend on the phase. Consequently, the coherent contributions to the transport away from the resonance are more complex than the isospin blockade at the resonance. They contain also correlated tunneling and the coherent transfer of electrons via virtual states, i.e. actual cotunneling.

A major difficulty in the Aharonov-Bohm ring setup is to distinguish between the different signatures of coherence in the current. The stationary state, which in general depends on the phase and comprises the possibility for coherent superpositions and quantum correlations (entanglement), is prepared at the same time as the stationary transport
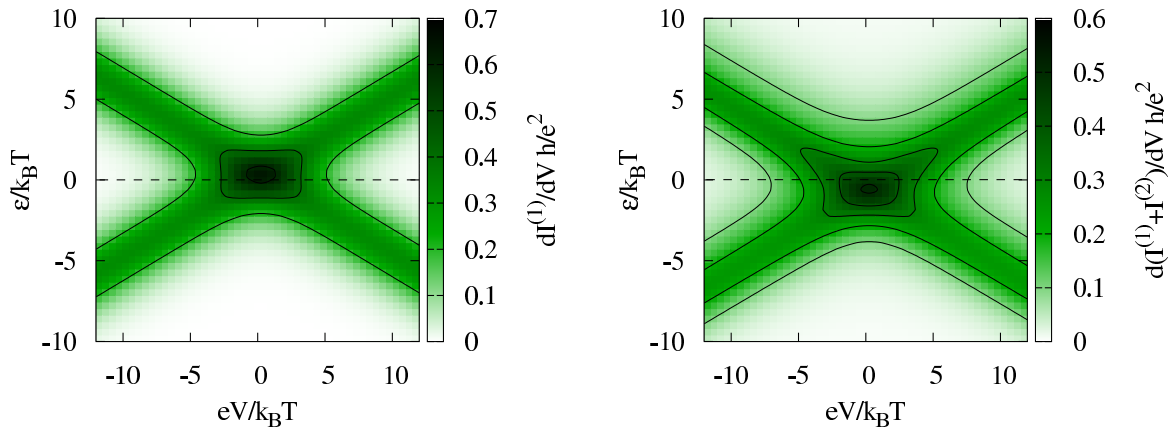
Figure 5.18: The first and second order differential conductance $\mathrm{d}(I^{(1)} + I^{(2)})/\mathrm{d}V$ is plotted on the right hand side versus bias voltage and the mean level energy of the dots for symmetric coupling $\Gamma_\mathrm{L} = \Gamma_\mathrm{R} = 0.3\,k_\mathrm{B}T$, $\varphi \approx 0$ and vanishing detuning. The cutoff is $D = 10^3\,k_\mathrm{B}T$. For comparison we plot on the left hand side only the first order term $\mathrm{d}I^{(1)}/\mathrm{d}V$. The overall renormalization shift to lower energies is clearly visible. Furthermore, we see an asymmetry in the broadening as function of the dots' energy, which is a consequence of the Coulomb interaction.

establishes. The strong mutual cross-link between the state of the system and the flow of electrons does not allow a reliable estimate of the current contribution of a certain fixed state. For a proper modeling of the evolution and the properties in the stationary limit we always have to consider the entire compound as a dynamical system. A possible setup to gain more independence between the preparation of the steady state and the probed current is introduced in the following chapter.

The plots in Fig. 5.19 give an exemplary overview and visualize how the oscillations change for different polarities of the bias voltage. We have chosen similar parameters as for the lowest order differential conductance in Figs. 5.7, 5.9 and 5.12 to allow for a better comparison. The only difference is in the overall coupling strength: for the plots of the first order differential conductance in Figs. 5.7, 5.9 and 5.12 the coupling strength is small enough such that higher order corrections play a minor role. For the plots in Figs. 5.18 and 5.19 we increased the coupling slightly for an enhanced importance of the second order correction. The most eye-catching difference to the first order plots is the increase or decrease of the distance between the two conductance peaks for dot energies above or below the mean Fermi energy of the leads, respectively. This is an effect of the renormalization of the dot energy which is pointed out in Fig. 5.18.

5.4   Chapter Summary

In this chapter we focused on signatures of coherence in an Aharonov-Bohm interferometer with two embedded quantum dots. We investigated the steady state and the stationary transport through the system. All contributions of first and second order tunneling were
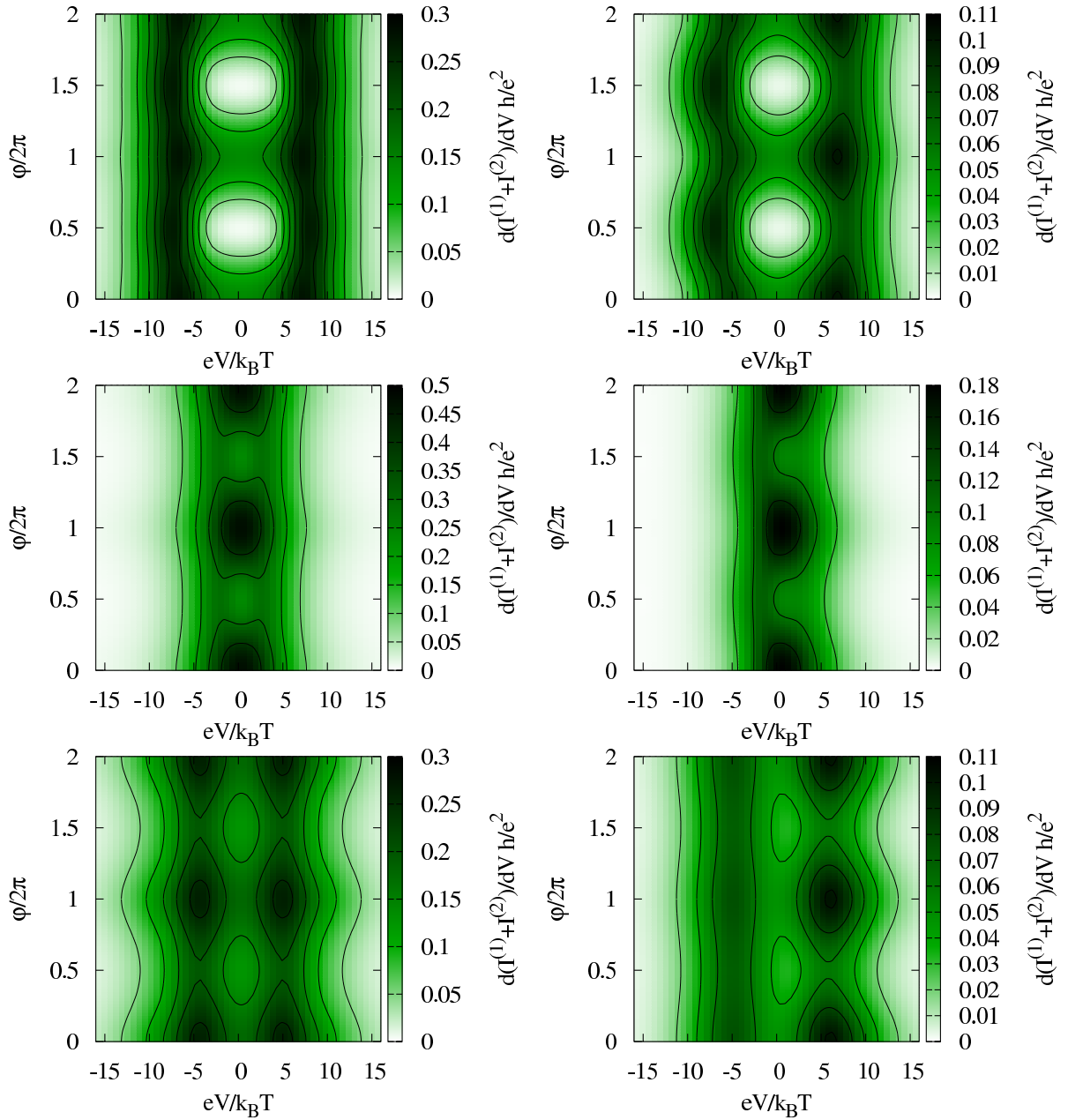
Figure 5.19: The first and second order differential conductance $d(I^{(1)}+I^{(2)})/dV$ is plotted for dot energies above the mean Fermi energy of the leads, $\varepsilon = +3\,k_\mathrm{B}T$ (first row), at the resonance, $\varepsilon = 0$ (center row), and below the mean Fermi energy of the leads, $\varepsilon = -3\,k_\mathrm{B}T$ (lower row). For the symmetric setup (left column) the coupling strength is $\Gamma_\mathrm{L} = \Gamma_\mathrm{R} = 0.3\,k_\mathrm{B}T$. For the right column we assume an asymmetry in the coupling of $\Gamma_\mathrm{L} = 0.3\,k_\mathrm{B}T$ and $\Gamma_\mathrm{R} = 0.2\,\Gamma_\mathrm{L}$. The cutoff is $D = 10^3\,k_\mathrm{B}T$.

systematically regarded, including renormalization corrections due to a finite coupling of the dots to the reservoirs. A particular concern was to study how an onsite Coulomb interaction affects the coherence of the transport through the dots.

We discussed in detail in which way interaction induced asymmetries in the interference signal become well visible in an asymmetrically coupled setup in strong nonequilibrium. Compared to numerous advanced experiments with similar setups the conditions to meet the proper regimes are not very demanding. The experimental realization should be feasible with nowadays technology. With the isospin picture we introduced an intuitive interpretation of the relevant physical behavior and the signatures of coherence already in lowest order transport.

Corresponding to the results for coherently coupled quantum dots the generation of a singlet-triplet imbalance is feasible also in the biased Aharonov-Bohm setup. Additional to the driving and the asymmetry in the coupling, the imbalance is sensitive to the Aharonov-Bohm flux. This yields the opportunity to control the Werner fidelity in situ in a certain range by the magnetic flux threading the ring. However, it is not possible to generate and at the same time probe the entanglement in this geometry with the stationary transport up to second order in the tunneling.

The analytical calculations reveal the rich flavor of properties induced by quantum fluctuations and cotunneling in the considered interacting setup. Although many of the (sometimes complex) pecularities give only negligible (or no) contributions to the second order transport, they might be important for higher order corrections, e.g. in case of a stronger coupling. However, fascinating by themselves, they may prove important pieces for a deeper understanding of the underlying physics apart from low order transport.

Chapter 6

Signatures of Entanglement in the Transport

One of the most intriguing nonequilibrium effects within systems of coherently coupled quantum dots we have encountered in this thesis is the possibility to generate spin entanglement between electrons on two spatially separated quantum dots. In chapter 4 we discussed this exciting feature in detail and proposed a scheme in which the entanglement can be created and, in a second step, can be detected by a charge probe. The suggested procedure (compare section 4.4) is based on time resolved manipulation and measurement, which presumably is quite demanding to accomplish in an experimental realization. From this point of view it is desirable to have some clear signatures in easily accessible stationary observables like the transport.

6.1   Setup of a Hybrid System

In section 4.5 we discussed a fork system with two quantum dots coherently coupled to a left reservoir and separate leads on the right hand side. We have seen that driving the electrons by an applied bias voltage in a certain direction can lead to an imbalance between singlet and triplet probabilities in the stationary state. Even a strong dominance of the singlet over the triplet is feasible, with a Werner fidelity $F > 1/2$ indicating entanglement between the spatially separated electrons on the upper and lower quantum dot. As nice as the generation of entanglement works in this setup, the detection of the imbalance between singlet and triplet in the transport is not that straightforward. The corresponding current rates are identical for singlet and triplet states up to second order (and most probably beyond). Thus, the current through the system depends on the overall probability to find the system doubly occupied, but the deviation between singlet and triplet probabilities does not enter.

This is different in the Aharonov-Bohm ring structure discussed in section 5.3. By calculating the current rates in the diagrammatic formalism we find a mismatch between the singlet and the triplet contributions to the second order transport, which depends on
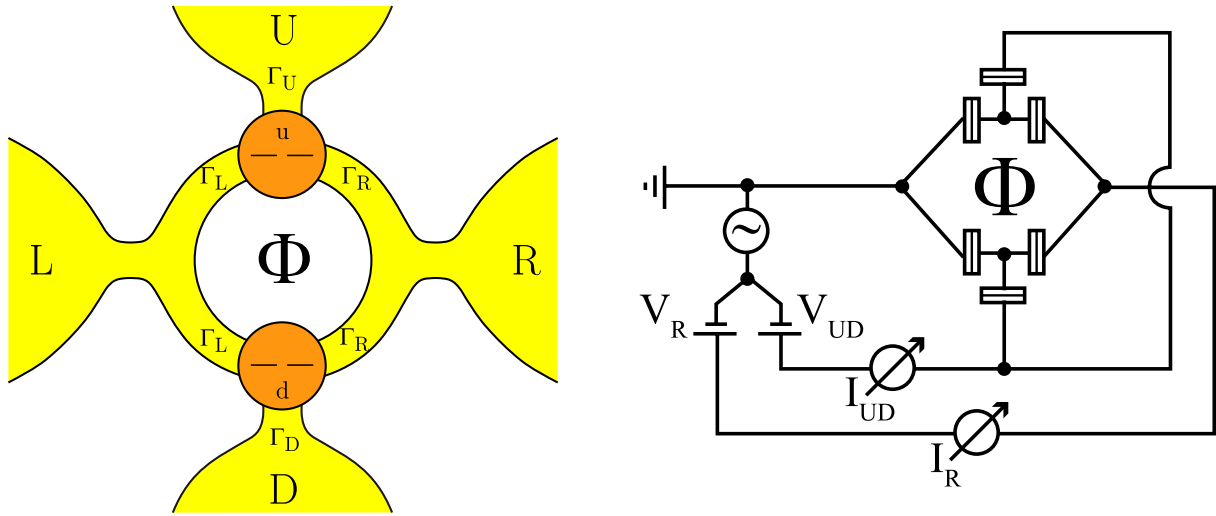
Figure 6.1:   Two quantum dots (u and d) embedded in a fork-like structure with a joint reservoir on the left hand side and two separate leads at the top and the bottom. The second joint reservoir on the right hand side closes the Aharonov-Bohm subsystem and can act as a probe for the state of the system.

the flux threading the ring. Specifically, the second order current rate in first order in the bias voltage and for dot energies well below the Fermi energy of the leads, $\varepsilon \ll -k_{\mathrm{B}}T$, contains a term which is proportional to $eV\,\Gamma_{\mathrm{L}}\Gamma_{\mathrm{R}}\,(2-\cos\varphi)\,\fint \frac{\mathrm{d}\omega}{\omega-\varepsilon}\,f''(\omega)$ for the singlet. The respective triplet rate contains a term which oscillates contrariwise and is proportional to $eV\,\Gamma_{\mathrm{L}}\Gamma_{\mathrm{R}}\,(2+\cos\varphi)\,\fint \frac{\mathrm{d}\omega}{\omega-\varepsilon}\,f''(\omega)$. In lowest order in the coupling strength the current rates are identical for singlet and triplets also in the Aharonov-Bohm setup.

We might conclude that there should be a clear signature of singlet vs. triplet overweight in the interference pattern in second order transport through the Aharonov-Bohm ring (similar to the detection scheme in Ref. [91]). Namely, we would expect a phase switch if we traverse from the unentangled, $F < 1/2$, into the entangled regime, $F > 1/2$, or vice versa. For $F < 1/2$ the triplet component dominates and contributes a $(2 + \cos\varphi)$-like pattern, but for a singlet overweight, $F > 1/2$, we expect a $(2 - \cos\varphi)$-like behavior. At $F = 1/2$ both interference contributions should cancel each other.

However, in general the driven system evolves into a dynamical equilibrium described by a complicated mixed state. The latter comprises probabilities for the empty, the singly and the doubly occupied double dot. Its stationary behavior depends strongly on the parameters which determine the transport through the system. Conversely, the current mirrors pecularities of the steady state (remember the role of coherent superposition states for the oscillations in the lowest order transport). The state of the system and the observable stationary transport reside in a mutual interplay. Thus, it is hard to resolve cause and effect and distinguish between the influence of the properties of the state on the signatures of the current and the evoked feedback. The steady state and the transport are always strongly correlated if we juggle with the parameters of the setup. The conclusion that a

phase switch in the current indicates the existence of entanglement is in general not valid for the pure Aharonov-Bohm interferometer (we discussed counterexamples in chapter 5). (In linear response, where analytical results are feasible even in second order, a singlet triplet imbalance does not show up in the transport anyway.)

To gain a bit more independence between the preparation of the system's state in a nonequilibrium situation and the signatures in the transport, we suggest a hybrid system of a fork-like structure and an Aharonov-Bohm ring as depicted in Fig. 6.1. Based on the fork system with a joint left reservoir and separate upper and lower leads for the upper and lower dot, respectively, we supplement a second joint reservoir on the right, which closes the Aharonov-Bohm ring. The idea is to prepare a stationary state with a bias applied between the joint left reservoir and the separate upper and lower leads. The Aharonov-Bohm ring is used to probe the flux dependence of the transport supported by this state by applying a small bias between the left and the right reservoir.

We model the system by a Hamiltonian $H = H_{\mathrm{res}} + H_{\mathrm{dots}} + H_{\mathrm{t}}$ consisting of a term for the four leads

$$H_{\mathrm{res}} = \sum_{r} \sum_{k\sigma} \varepsilon_{rk}\, a^{\dagger}_{rk\sigma} a_{rk\sigma} \tag{6.1}$$

with $r \in \{\mathrm{L}, \mathrm{U}, \mathrm{D}, \mathrm{R}\}$, the familiar part for the double dot system

$$H_{\mathrm{dots}} = \sum_{i} \left[\sum_{\sigma} \varepsilon_i\, c^{\dagger}_{i\sigma} c_{i\sigma} + U\, c^{\dagger}_{i\uparrow} c^{\dagger}_{i\downarrow} c_{i\downarrow} c_{i\uparrow} \right], \tag{6.2}$$

comprising the quantum dots up and down, $i \in \{\mathrm{u}, \mathrm{d}\}$, with the onsite Coulomb repulsion U, and the tunnel Hamiltonian $H_{\mathrm{t}} = H_{\mathrm{tL}} + H_{\mathrm{U}} + H_{\mathrm{D}} + H_{\mathrm{tR}}$. The tunneling between the dots and the upper or lower reservoir is described by

$$H_{\mathrm{U}} = \sum_{k\sigma} \left[t_{\mathrm{U}}\, c^{\dagger}_{u\sigma} a_{\mathrm{U}k\sigma} + \mathrm{h.c.} \right] \tag{6.3}$$

for the upper dot and reservoir, and H_{D}, respectively, for the lower pair. The coupling to the joint leads on the left and the right side, and the phase an electron may accumulate while traveling through the ring structure is reflected in

$$H_{\mathrm{tL}} = \sum_{k\sigma} \left[t_{\mathrm{L}} \left(\mathrm{e}^{-\mathrm{i}\frac{\varphi}{4}}\, c^{\dagger}_{u\sigma} + \mathrm{e}^{+\mathrm{i}\frac{\varphi}{4}}\, c^{\dagger}_{d\sigma} \right) a_{\mathrm{L}k\sigma} + \mathrm{h.c.} \right], \tag{6.4}$$

and for the right reservoir correspondingly

$$H_{\mathrm{tR}} = \sum_{k\sigma} \left[t_{\mathrm{R}} \left(\mathrm{e}^{+\mathrm{i}\frac{\varphi}{4}}\, c^{\dagger}_{u\sigma} + \mathrm{e}^{-\mathrm{i}\frac{\varphi}{4}}\, c^{\dagger}_{d\sigma} \right) a_{\mathrm{R}k\sigma} + \mathrm{h.c.} \right]. \tag{6.5}$$

There is no direct coupling of the upper dot to the lower lead or vice versa. All tunneling is taken to be independent of spin and energy. Furthermore, we choose a symmetric gauge for the phase, and, without loss of generality, we can assume $t_r \in \mathbb{R}^{+}$ for $r \in \{\mathrm{L}, \mathrm{U}, \mathrm{D}, \mathrm{R}\}$.

The tunneling strength is parametrized by $\Gamma_r = 2\pi\, t_r^2\, N_r$ where N_r denotes the density of states in the respective reservoir. The leads are assumed to be in local equilibrium, with spin degenerate energies ε_{rk}. Their electrochemical potentials μ_r are not necessarily equivalent and allow for a potential difference between each pair of reservoirs.

However, for transparency we assume some symmetries between the upper and the lower dot. Like depicted in the schematic diagram on the right hand side of Fig. 6.1, we set the upper and the lower reservoir to the same potential, $\mu_U = \mu_D =: \mu_{UD}$. Additionally, we restrict ourselves to degenerate dot levels, $\varepsilon_u - \varepsilon_d = 0$, and assume symmetric coupling strengths for the upper and the lower dot, $\Gamma_U = \Gamma_D =: \Gamma_{UD}$. Nevertheless, we explicitly allow for an asymmetry between the diverse couplings of each dot. This gives us enough freedom to tune the system into the desired regime.

6.2   Preparation of Stationary Entangled States

For the specification of the kinetic equations governing the evolution of the reduced density matrix we choose the basis as introduced in subsection 5.3.1 for the Ahronov-Bohm interferometer. We express the matrix elements again in a vector representation where the probabilities are collected in $\mathbf{p} = (p_0, p_1, p_S, p_T)$, and the structure of the singly occupied subspace is specified by the isospin $\mathbf{I} = (I_x, I_y, I_z)$. With the real-time diagrammatic technique we set up the kinetic equations for the hybrid system in lowest order in the coupling. The equations look very similar to the corresponding equations for the bare Aharonov-Bohm interferometer but comprise also the coupling of the upper and lower dot to the separate leads,

$$
\frac{\mathrm{d}}{\mathrm{d}t}\mathbf{p} = \sum_{r=L,UD,R} \Gamma_r \begin{pmatrix} -4\,f_r & 1-f_r & 0 & 0 \\ 4\,f_r & -1-f_r & 2-2\,f_r & 2-2\,f_r \\ 0 & f_r/2 & -2+2\,f_r & 0 \\ 0 & 3\,f_r/2 & 0 & -2+2\,f_r \end{pmatrix} \mathbf{p} + \sum_{r=L,R} \Gamma_r \begin{pmatrix} 2-2\,f_r \\ -2+4\,f_r \\ f_r \\ -3\,f_r \end{pmatrix} (\mathbf{I}\cdot\mathbf{m}_r)
$$

$$
\frac{\mathrm{d}}{\mathrm{d}t}\mathbf{I} = \sum_{r=L,R} \Gamma_r \left[2\,f_r\,p_0 + \left(f_r - \frac{1}{2}\right) p_1 + (1-f_r)\,p_S - (1-f_r)\,p_T \right] \mathbf{m}_r -
$$
$$
- \sum_{r=L,UD,R} \Gamma_r\,(1+f_r)\,\mathbf{I} + \Delta\varepsilon\,(\mathbf{n}\times\mathbf{I}),
\tag{6.6}
$$

with the quantization axes $\mathbf{m}_r$, $r \in \{L, R\}$, and $\mathbf{n}$ as introduced for the Aharonov-Bohm interferometer in subsection 5.3.1. We abbreviate the Fermi distributions of the electrons by f_r which are meant to be evaluated at the dots' mean energy ε. The index for the respective reservoir, $r \in \{L, UD, R\}$, refers to the corresponding electrochemical potential μ_r.

A general analytical solution of the kinetic equations in the stationary limit is feasible but yields quite bulky results which we do not display here. Instead we set up a frame

for the most interesting parameter regimes for our purpose and exemplify the results with specific evaluations.

To generate and detect a singlet-triplet imbalance, the system parameters have to be chosen specifically. As mentioned, we essentially want to use the fork subsystem to prepare the double dot in a stationary state which should only be weakly influenced by the probe via the joint right reservoir. Moreover, the change of the phase behavior of the probe current, which we might expect due to a crossover from a large triplet probability to a dominating singlet and from the consideration of the current rates for the bare Aharonov-Bohm setup, is at least of second order in Γ. Thus, we meet the requirements of the first point with the suggestion of the second and operate the system such that the transport from the joint left source to the separate upper and lower drains is dominated by sequential tunneling, while the Aharonov-Bohm ring is in the Coulomb blockade where second order processes prevail. This is achieved by tuning the dots' energy well below the Fermi energies of the left and the right reservoir, and by applying only a small bias voltage across the Aharonov-Bohm ring. In contrast, a large bias voltage between the left source and the upper and lower drains allows for sequential transport. Furthermore, the tunnel coupling to the right lead should be much weaker than the other ones, $\Gamma_R \ll \Gamma_L, \Gamma_{UD}$, to ensure that the state of the double dot is not affected by the measurement via the interferometer. In order to find with large probability two excess electrons in the system, the rate for charging should be much larger than for discharging, $\Gamma_L \gg \Gamma_{UD}$.

We are basically concerned with the comparison of two scenarios:

i. For vanishing bias voltage between the left and the upper/lower reservoirs the double dot remains in equilibrium, and $F = 1/4$.

ii. By applying a high bias voltage between the left and the upper/lower reservoirs the double dot is driven out of equilibrium and charged from the joint source electrode. A singlet-triplet imbalance with $F > 1/2$ is generated.

From the fork system (sections 4.5 and 4.6, especially Fig. 4.6) we know that the Werner fidelity is larger than $1/2$ as soon as we charge the system from the joint reservoir and the bias is strong enough. Furthermore, there is a tradeoff between strong singlet overweight as compared to the triplet and the overall probability to find the system doubly occupied. For our purpose, we slightly prefer a high probability for double occupancy. The components of the mixed state corresponding to the empty system and occupation with a single electron should be suppressed as far as possible, such that their influence on the signatures in the transport from the left to the right reservoir is controllable and does not mask the effects of the doubly occupied components inextricably.

In contrast to the conventions for the bare fork or the bare Aharonov-Bohm setup (sections 4.5, 4.6 and chapter 5), where we measured dot energies and electrochemical potentials with respect to the mean Fermi energy of the leads and applied the bias voltage symmetrically, we rescale the reference energy as depicted in the circuit scheme in Fig. 6.1. We ground the left reservoir ($\mu_L = 0$) and distinguish the bias voltages $eV_R = \mu_R$ between
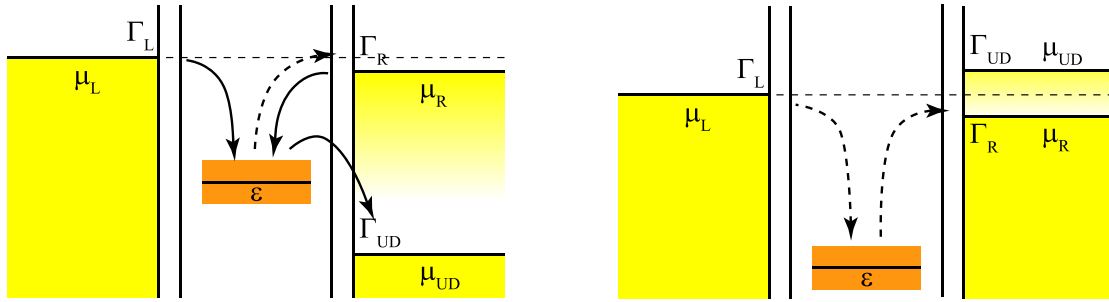
Figure 6.2:   Schematic energy diagrams for the hybrid system are sketched. The adjustment in the left figure yields scenario ii, the right diagram is supposed to be close to the equilibrium situation (scenario i). The arrows indicate expected primary (solid line) and secondary (dashed line) tunneling processes. (The secondary processes are important for the cotunneling transport from the left to the right reservoir.)

the joint right reservoir and ground, and $eV_{UD} = \mu_{UD}$ between the separate leads and the left reservoir.

In Fig. 6.2 we sketch two energy diagrams which depict the two scenarios. The dot energies are tuned well below the Fermi energies of the left and the right reservoir, $-\varepsilon \gg |eV_R|, k_B T, \Gamma_L, \Gamma_R$ such that sequential transport through the ring becomes small. In the left scheme the bias voltage between the left source electrode and the separate upper and lower drains is large enough to allow for sequential tunneling in the fork subsystem which dominates the properties of the stationary state. In particular, electrons from the joint left reservoir induce a high probability for a singlet state as long as the charging from the joint right reservoir is weak due to a weak coupling. The latter ensures that the in principle undesired current from the joint right reservoir to the separate leads is much smaller than the current from the left to the upper and lower drain. This keeps the influence on the state small. However, we should not close the barriers to the right reservoir to far, because we still want to be able to probe the cotunneling current through the ring. For the scheme on the right hand side we switch off the bias voltage in the fork subsystem. In equilibrium singlet and triplets are uniformly distributed. This constitutes the reference to which we compare the results for the nonequilibrium behavior.

The plots in Fig. 6.3 display an exemplary evaluation of the solutions for the stationary probabilities and the Werner fidelity. We sweep from the left scenario in Fig. 6.2 to the right one by changing the bias voltage in the fork subsystem, eV_{UD}. Due to the cascading coupling strength, $\Gamma_L > \Gamma_{UD} > \Gamma_R$, we find a large probability for double occupancy and a small influence of the probe which may introduce a phase dependence of the state. We find a large Werner fidelity for the left scenario and equipartition of singlet and triplets in equilibrium, as expected.

Unfortunately, we can not trust the solution in Fig. 6.3 unconditionally in the entire range. For a small bias voltage or even switched polarity, $\varepsilon \ll eV_{UD}$, the fork subsystem enters the cotunneling regime. Here, a reliable solution of the kinetic equations requires
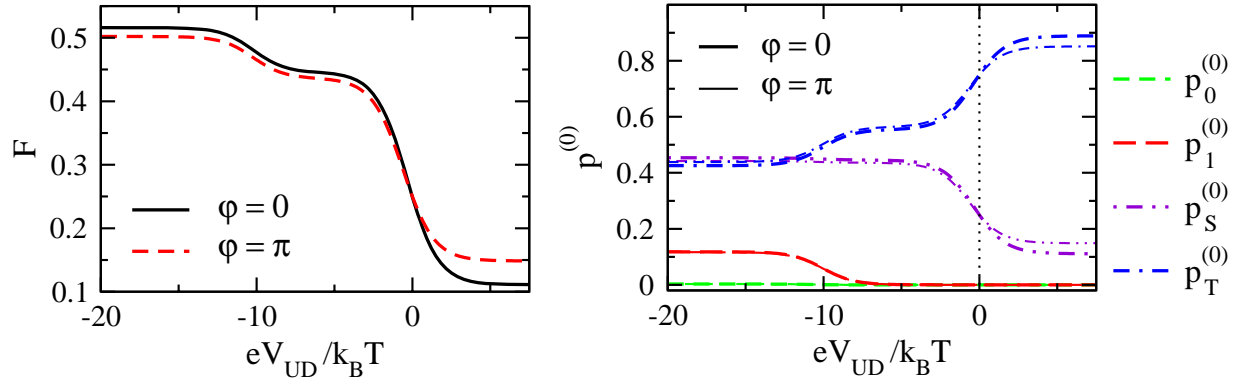
Figure 6.3: The Werner fidelity and the lowest order probabilities for the hybrid system are plotted versus the bias voltage in the fork subsystem. The dot energies are tuned well below the Fermi energies of the left and the right reservoir, $\varepsilon = -10\,k_{\mathrm{B}}T$. According to our argumentation, the coupling strengths are chosen such that $\Gamma_{\mathrm{L}} > \Gamma_{\mathrm{UD}} > \Gamma_{\mathrm{R}}$. Specifically we set $\Gamma_{\mathrm{L}} = 1\,k_{\mathrm{B}}T$, $\Gamma_{\mathrm{UD}} = 0.1\,k_{\mathrm{B}}T$, $\Gamma_{\mathrm{R}} = 0.01\,k_{\mathrm{B}}T$. Since the probabilities are in general phase dependent (due to the coupling of the probe) we pick $\varphi = 0$ and $\varphi = \pi$ for comparison. However, in this regime the flux dependence of the state is nearly negligible and can not even be resolved properly in the plots for the probabilities.

to take into account higher order tunneling rates. However, in equilibrium the solution is correct. Therefore, we restrict ourselves in the following to the comparison of the behavior close to equilibrium and in strong nonequilibrium where the solution is definitely valid (for weak coupling).

6.3 Probing the Singlet-Triplet Imbalance in the Transport

The transport properties of the stationary state are probed with the Aharonov-Bohm interferometer. We are especially interested in signatures which can be related to a singlet-triplet imbalance generated by the driven fork subsystem. We will see that scenarios i) and ii) lead to significantly different interference signatures in the transport through the Aharonov-Bohm ring. While the equilibrium case shows a strong flux dependence and large amplitude of the Aharonov-Bohm oscillations, they are suppressed in the nonequilibrium case, where the Werner fidelity approaches 1/2 if the double dot is predominantly occupied with two electrons.

To operate the Aharonov-Bohm probe in the cotunneling regime, the dot levels are tuned well below the Fermi energies of the left and the right reservoirs, $-\varepsilon \gg |eV_{\mathrm{R}}|, k_{\mathrm{B}}T, \Gamma_{\mathrm{L}}, \Gamma_{\mathrm{R}}$. Thus, we focus on the dominating, algebraically decaying cotunneling contributions to the transport. The exponentially decaying renormalization corrections to the first order terms are of minor importance, and an exhaustive second order calculation within the real-time

diagrammatic technique is not necessary. The strategy is modified such that we employ the full solution of the kinetic equations for the stationary density matrix in lowest order in the coupling strength, as already exemplified in Fig. 6.3, and determine the corresponding second order transition rates for electrons tunneling to the right reservoir within an orthodox perturbation approach. This way we can combine the advantage of taking into account the comprehensive evolution of the density matrix, including all off-diagonal terms within a full-fledged real-time theory, and a less complicated calculation of second order transport within a standard perturbation expansion.

To demonstrate the difference between scenario i) and ii) we calculate the linear conductance through the Aharonov-Bohm interferometer. The contribution to first order in the coupling strength is evaluated within the diagrammatic technique. It turns out to be small due to our choice of parameters (compare also Fig. 6.5). For a controlled calculation of the dominant second-order contribution within an orthodox perturbation expansion we have to choose a coordinate representation in which the stationary density matrix (obtained from (6.6)) is diagonal, with probabilities p_χ for many-body states $|\chi\rangle$. In general, this representation depends on various parameters of the hybrid system, especially on the bias voltage between the left reservoir and the separate upper and lower lead, the dots' energy, and the phase, for example.

Supposed we have found the proper basis, the stationary current from the left to the right reservoir can be expressed by the current formula

$$I_{\mathrm{LR}} = -e \sum_{\chi_1 k_1} \sum_{\chi_2 k_2} [R_{\chi_2 k_2, \chi_1 k_1} \, p_{\chi_1} \, (1 - f_{\mathrm{R}k_2}) f_{\mathrm{L}k_1} - R_{\chi_1 k_1, \chi_2 k_2} \, p_{\chi_2} \, (1 - f_{\mathrm{L}k_1}) f_{\mathrm{R}k_2}] \qquad (6.7)$$

where we sum over all possible intitial and final states of the system. The transition rate between a certain initial state $|\chi_{\mathrm{i}} \, k_{\mathrm{i}}\rangle$, in which the reduced system is in state χ_{i} and an electron in the left reservoir is in state $|k_{\mathrm{i}}\rangle$, to a final state $|\chi_{\mathrm{f}} \, k_{\mathrm{f}}\rangle$, for the double dot in state $|\chi_f\rangle$ and an electron in state $|k_{\mathrm{f}}\rangle$ in the right reservoir, can be expressed in terms of the transition matrix T,

$$R_{\mathrm{f,i}} = \frac{2\pi}{\hbar} \, |\langle \chi_{\mathrm{f}} \, k_{\mathrm{f}} | T | \chi_{\mathrm{i}} \, k_{\mathrm{i}} \rangle|^2 \, \delta(E_{\mathrm{i}} - E_{\mathrm{f}}) \qquad (6.8)$$

which satisfies $R_{\mathrm{f,i}} = R_{\mathrm{i,f}}$ due to detailed balance. The tunneling amplitudes in our setup do not depend on k. We write the sums over the states of the reservoirs in continuous form,

$$I_{\mathrm{LR}} = -\frac{2\pi \, e}{\hbar} \int \mathrm{d}\omega \int \mathrm{d}\omega' \, N_{\mathrm{L}} N_{\mathrm{R}} \sum_{\chi_1, \chi_2} |\langle \chi_2 \, k_2 | T | \chi_1 \, k_1 \rangle|^2 \, p_{\chi_1} \, \delta(\omega - \omega') \, [f_{\mathrm{L}}(\omega) - f_{\mathrm{R}}(\omega')],$$
$$(6.9)$$

with the Fermi functions f_{L} and f_{R} of the left and the right reservoir, respectively, and a potential difference of $\mu_{\mathrm{R}} - \mu_{\mathrm{L}} = eV_{\mathrm{R}}$.

This yields the linear conductance

$$G_{\mathrm{R}} = \left. \frac{\partial I_{\mathrm{LR}}}{\partial V_{\mathrm{R}}} \right|_{V_{\mathrm{R}}=0} = -\frac{e^2}{h} \int \mathrm{d}\omega \, \mathbf{S}(\omega) \cdot \mathbf{p}_{\mathrm{d}} \, f'(\omega) \qquad (6.10)$$

with the vector $\mathbf{p}_\mathrm{d}$ comprising all probabilities of the diagonalized stationary density matrix. The decoration with the index should prevent a confusion with the probability vector $\mathbf{p}$ from the former section(s). In $\mathbf{p}_\mathrm{d}$ the isospin contribution is already included, but the representation is only valid for the very special choice of coordinates in which the density matrix is diagonal. The components of the transfer vector $\mathbf{S}$ are given by

$$S_{\chi_\mathrm{i}}(\omega) = (2\pi)^2 \, N_\mathrm{L} N_\mathrm{R} \sum_{\chi_\mathrm{f}} |\langle \chi_\mathrm{f} \, k_\mathrm{f}|T|\chi_\mathrm{i} \, k_\mathrm{i}\rangle|^2 \ . \tag{6.11}$$

For the second order transport between the left and the right reservoir we expand the transition matrix up to first order in the tunneling amplitudes squared, similar to Refs. [28, 29, 78],

$$\langle \chi_\mathrm{f} \, k_\mathrm{f}|T|\chi_\mathrm{i} \, k_\mathrm{i}\rangle^{(1)} = \sum_n \frac{\langle \chi_\mathrm{f} \, k_\mathrm{f}|H_\mathrm{t}|n\rangle\langle n|H_\mathrm{t}|\chi_\mathrm{i} \, k_\mathrm{i}\rangle}{\omega - E_n} \ . \tag{6.12}$$

The intermediate or virtual state $|n\rangle$ has the energy E_n which is either 0, ε or 2ε, depending on whether $|n\rangle$ belongs to the empty, the singly or the doubly occupied subspace. We sum over all possible final states in Eq. (6.11), i.e. specifically we do not restrict ouselves to any subset of processes. We allow all transitions which are feasible with the given Hamiltonian

In our model the blocks of the density matrix for the empty and the doubly occupied system are always diagonal in the basis states $|0\rangle$, $|S\rangle$, $|T_0\rangle$ and $|T_\pm\rangle$. The corresponding second order current rates can directly be calculated. We obtain

$$S_0^{(2)}(\omega) = \frac{2\,\Gamma_\mathrm{L}\Gamma_\mathrm{R}}{(\omega - \varepsilon)^2} \, (1 + \cos\varphi) \tag{6.13}$$

for the empty system. Its contribution to the transport is negligible for a vanishing probability $p_0^{(0)}$ (compare Fig. 6.3). The most relevant contributions are expected to come from the doubly occupied system. We have to distinguish the rates starting from an initial singlet state and from one of the triplets,

$$S_\mathrm{S}^{(2)}(\omega) = \frac{\Gamma_\mathrm{L}\Gamma_\mathrm{R}}{4\,(\omega - \varepsilon)^2} \, (2 - \cos\varphi) \, , \tag{6.14}$$

$$S_\mathrm{T}^{(2)}(\omega) = \frac{\Gamma_\mathrm{L}\Gamma_\mathrm{R}}{4\,(\omega - \varepsilon)^2} \, (2 + \cos\varphi) \, . \tag{6.15}$$

The three triplet terms are equivalent and simply denoted by S_T. The flux dependence is identical to the results obtained within the full real-time diagrammatic approach for the bare Aharonov-Bohm interferometer. In particular, the singlet and triplet contributions oscillate with opposite phase. We emphasize that these results rely on the degeneracy of singlet and triplets. All four constitute equivalently possible final states of cotunneling processes with an initially doubly occupied system. If there was a large singlet-triplet energy splitting, transitions between singlet and triplet states would be suppressed and $S_\mathrm{S,T}^{(2)}(\omega) = 1/4\,\Gamma_\mathrm{L}\Gamma_\mathrm{R}/(\omega - \varepsilon)^2\,(1 + \cos\varphi)$ without any distinction between the singlet and triplet contributions.

In contrast to the blocks for the empty and the doubly occupied system, the part of the density matrix which describes the singly occupied subspace does evolve also in the off-diagonal. This gave rise to the introduction of the isospin which marks a main source for many coherence effects in the system. In particular, the imbalance between singlet and triplet probabilities finds its root in the isospin polarization. To include the isospin structure into the calculation of the second order transport the corresponding block of the density matrix has to be diagonalized for each parameter set (or point in time). More specifically, for the calculation of the second order current rates for Eq. (6.7) or (6.10) we have to find the coordinate system in which the stationary isospin points in the $\mathbf{e}_z$-direction. Since we do not know the orientation before we have solved the kinetic equations, we start with an arbitrary coordinate system and rotate it afterwards until the isospin direction coincides with the new $\tilde{\mathbf{e}}_z$. In the rotated basis the density matrix is diagonal and the probabilities of the eigenstates $|+\rangle_{\mathbf{I}\cdot\tilde{\mathbf{e}}_z}$ and $|-\rangle_{\mathbf{I}\cdot\tilde{\mathbf{e}}_z}$ are given by

$$p_{|+\rangle_{\mathbf{I}\cdot\tilde{\mathbf{e}}_z}} = p_1/2 + |\mathbf{I}| \qquad \text{and} \qquad p_{|-\rangle_{\mathbf{I}\cdot\tilde{\mathbf{e}}_z}} = p_1/2 - |\mathbf{I}| \,, \tag{6.16}$$

respectively. The current rates for the singly occupied system have to be calculated with the eigenstates.

A convenient first coordinate system is given by the basis in which the Hamiltonian of the double dot is diagonal. This is the canonical basis for the diagrammatic formalism. In our specific case $\{|\sigma,0\rangle, |0,\sigma\rangle\}$ spans the singly occupied subspace. The corresponding second order rates read

$$S^{(2)}_{|\sigma,0\rangle}(\omega) = S^{(2)}_{|0,\sigma\rangle}(\omega) = \frac{2\,\Gamma_{\mathrm{L}}\Gamma_{\mathrm{R}}}{(\omega - \varepsilon)^2}\,(3 - \cos\varphi)\,. \tag{6.17}$$

The transfer vector $\mathbf{S}$ is obviously not linear in the initial states $|\chi_{\mathrm{i}}\rangle$ (compare Eq. (6.11)), nevertheless, we obtain a simple relation for the second order rates,

$$S^{(2)}_{\alpha|a\rangle+\beta|b\rangle} = |\alpha|^2\,S^{(2)}_{|a\rangle} + |\beta|^2\,S^{(2)}_{|b\rangle} +$$
$$+ 2\,(2\pi)^2\,N_{\mathrm{L}}N_{\mathrm{R}}\,\mathrm{Re}\left(\alpha\,\beta^* \sum_{\chi_{\mathrm{f}}}\langle\chi_{\mathrm{f}}\,k_{\mathrm{f}}|T|a\,k_{\mathrm{i}}\rangle^{(1)}\left(\langle\chi_{\mathrm{f}}\,k_{\mathrm{f}}|T|b\,k_{\mathrm{i}}\rangle^{(1)}\right)^*\right)\,. \tag{6.18}$$

Since we already know the quadratic terms in the canonical basis, it is only the mixed term which remains to be determined:

$$(2\pi)^2\,N_{\mathrm{L}}N_{\mathrm{R}}\sum_{\chi_{\mathrm{f}}}\langle\chi_{\mathrm{f}}\,k_{\mathrm{f}}|T|(\sigma,0)\,k_{\mathrm{i}}\rangle^{(1)}\left(\langle\chi_{\mathrm{f}}\,k_{\mathrm{f}}|T|(0,\sigma)\,k_{\mathrm{i}}\rangle^{(1)}\right)^* = -\mathrm{i}\,\frac{8\,\Gamma_{\mathrm{L}}\Gamma_{\mathrm{R}}}{(\omega - \varepsilon)^2}\,\sin(\varphi/2)\,. \tag{6.19}$$

The eigenvectors of the singly occupied block of the reduced density matrix can be represented by

$$|+\rangle_{\mathbf{I}\cdot\tilde{\mathbf{e}}_z} = \frac{1}{\sqrt{2}}\sum_{\sigma}\left(|\sigma,0\rangle + \frac{I_x + \mathrm{i}I_y}{|I_x + \mathrm{i}I_y|}\,|0,\sigma\rangle\right)\,,$$

$$|-\rangle_{\mathbf{I}\cdot\tilde{\mathbf{e}}_z} = \frac{1}{\sqrt{2}}\sum_{\sigma}\left(\frac{I_x - \mathrm{i}I_y}{|I_x + \mathrm{i}I_y|}\,|\sigma,0\rangle - |0,\sigma\rangle\right)\,. \tag{6.20}$$

Hence, using Eq. (6.18) with the expressions in the canonical basis the corresponding second order rates read

$$S^{(2)}_{|+\rangle_{\mathbf{I}\cdot\tilde{\mathbf{e}}_z}}(\omega) = \frac{\Gamma_{\mathrm{L}}\Gamma_{\mathrm{R}}}{(\omega - \varepsilon)^2} \left[6 - 2\cos\varphi + 4\frac{\mathbf{I}}{|\mathbf{I}|}\cdot(\mathbf{m}_{\mathrm{L}} - \mathbf{m}_{\mathrm{R}})\right]$$

$$S^{(2)}_{|-\rangle_{\mathbf{I}\cdot\tilde{\mathbf{e}}_z}}(\omega) = \frac{\Gamma_{\mathrm{L}}\Gamma_{\mathrm{R}}}{(\omega - \varepsilon)^2} \left[6 - 2\cos\varphi - 4\frac{\mathbf{I}}{|\mathbf{I}|}\cdot(\mathbf{m}_{\mathrm{L}} - \mathbf{m}_{\mathrm{R}})\right].$$

(6.21)

The transfer vector $\mathbf{S}^{(2)}$ plugged into the conductance equation (6.10) yields transport terms analogue to those within a rigorous real-time diagrammatic approach up to second order in the coupling strength. Accordingly, we interpret the integrals as principal value integrals, which appear naturally within the diagrammatic technique,

$$\int \mathrm{d}\omega\, \frac{f'(\omega)}{(\omega - \varepsilon)^2} \sim \lim_{\eta\searrow 0} \mathrm{Re} \int \mathrm{d}\omega\, \frac{f'(\omega)}{(\omega - \varepsilon + i\eta)^2} = \fint \frac{\mathrm{d}\omega}{\omega - \varepsilon}\, f''(\omega).$$

(6.22)

Gathering all cotunneling terms corresponding to the states where the dot system is empty, occupied with a single electron with isospin $\mathbf{I}$, or occupied with two electrons either in a singlet or a triplet state, we find the second order contribution to the linear conductance

$$G^{(2)}_{\mathrm{R}} = -\frac{e^2}{h}\, g(\varphi)\, \Gamma_{\mathrm{L}}\Gamma_{\mathrm{R}} \fint \frac{\mathrm{d}\omega}{\omega - \varepsilon}\, f''(\omega).$$

(6.23)

The Aharonov-Bohm flux dependence is included in the dimensionless conductance $g(\varphi) = \sum_\chi g_\chi(\varphi)$, with

$$g_0(\varphi) = 2\,(1 + \cos\varphi)\, p^{(0)}_0(\varphi),$$ (6.24a)

$$g_1(\varphi) = 2\,(3 - \cos\varphi)\, p^{(0)}_1(\varphi) + 8\,(\mathbf{m}_{\mathrm{L}} - \mathbf{m}_{\mathrm{R}})\cdot\mathbf{I}^{(0)},$$ (6.24b)

$$g_{\mathrm{S}}(\varphi) = (\frac{1}{2} - \frac{1}{4}\cos\varphi)\, p^{(0)}_{\mathrm{S}}(\varphi),$$ (6.24c)

$$g_{\mathrm{T}}(\varphi) = (\frac{1}{2} + \frac{1}{4}\cos\varphi)\, p^{(0)}_{\mathrm{T}}(\varphi).$$ (6.24d)

The flux sensitivity of the conductance is twofold. First, the phase factors from the tunneling Hamiltonian are taken into account in the coherent summation of processes in the cotunneling rates, Eq. (6.11). In particular, as discussed in [91], the phase dependence of the contributions from an inital singlet and triplet state (Equations (6.24c) and (6.24d)) are shifted relativ to each other by π. The second kind of flux dependence results from the stationary state of the system. In general nonequilibrium situations, the reduced density matrix, represented by p_0, p_1, $\mathbf{I}$, p_{S}, and p_{T}, is influenced by the Aharonov-Bohm probe and becomes phase sensitive. This effect is weak for weak tunnel coupling $\Gamma_{\mathrm{R}} \ll \Gamma_{\mathrm{L}}, \Gamma_{\mathrm{UD}}$ where the state of the system is only weakly influenced by the Aharonov-Bohm probe. In the limit $\Gamma_{\mathrm{L}} \gg \Gamma_{\mathrm{UD}} \gg \Gamma_{\mathrm{R}}$ and the double dot charged from the left reservoir the isospin points approximately in direction of $\mathbf{m}_{\mathrm{L}}$ such that $g_1(\varphi) \approx 2\,(3 - \cos\varphi)\, p_1 - 8\,(1 - \cos\varphi)\,|\mathbf{I}|$.
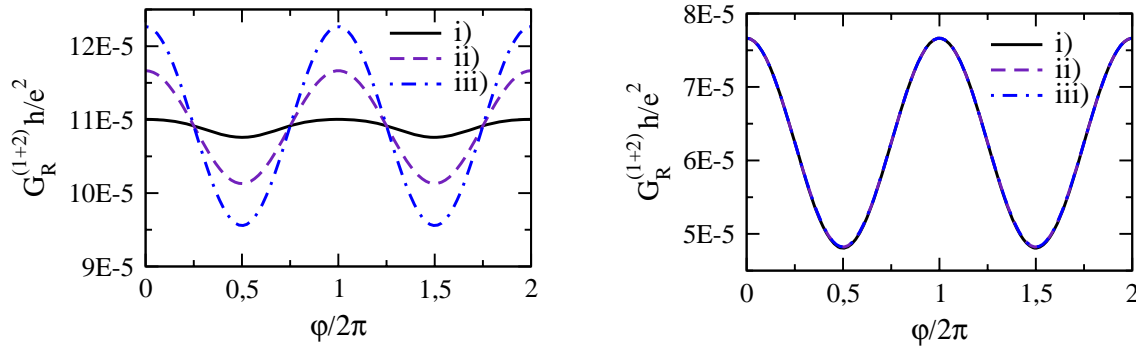
Figure 6.4: The linear conductance of the Aharonov-Bohm subsystem up to second order in the coupling strength is plotted versus the Aharonov-Bohm phase. The parameters are $\Gamma_{\mathrm{L}} = 1\,k_{\mathrm{B}}T$, $\Gamma_{\mathrm{UD}} = 0.1\,k_{\mathrm{B}}T$, $\Gamma_{\mathrm{R}} = 0.01\,k_{\mathrm{B}}T$, $\varepsilon = -10\,k_{\mathrm{B}}T$ and $|eV_{\mathrm{R}}| \ll k_{\mathrm{B}}T$ (equivalent to Fig. 6.3). For both, a strong bias voltage between the left, and the upper and lower reservoirs, $eV_{\mathrm{UD}} = -20\,k_{\mathrm{B}}T$ (left plot) and equilibrium (right plot), the ideal system (i) is compared to results for singlet-triplet decay rates of (ii) $\Gamma_{\mathrm{ST}} = 0.5\,\Gamma_{\mathrm{UD}}$ and (iii) $\Gamma_{\mathrm{ST}} = 10\,\Gamma_{\mathrm{UD}}$.

For low dot energies in an equilibrium situation, $\varepsilon \ll \mu_r$, the double dot is mainly occupied with two electrons with $p_{\mathrm{T}} \approx 3/4$ and $p_{\mathrm{S}} \approx 1/4$. As a consequence, there is a good visibility of the Aharonov-Bohm oscillations in scenario i),

$$g^{(\mathrm{i})}(\varphi) \approx \frac{1}{2} + \frac{1}{8}\cos\varphi \,. \tag{6.25}$$

In contrast, for large bias voltage (scenario ii)), the phase dependence is suppressed. To see this, we expand the density matrix for a strong asymmetry in the coupling to the left, and the upper and lower reservoirs, $x = \Gamma_{\mathrm{UD}}/\Gamma_{\mathrm{L}} \ll 1$, and obtain $p_0 = \mathcal{O}(x^2)$, $p_1 = 4x/3 + \mathcal{O}(x^2)$, $\mathbf{I} \approx x/3\,\mathbf{m}_{\mathrm{L}} + \mathcal{O}(x^2)$, $p_{\mathrm{S}} = 1/2 - x/2 + \mathcal{O}(x^2)$, and $p_{\mathrm{T}} = 1/2 - 5x/6 + \mathcal{O}(x^2)$. Thus, the dimensionless conductance approaches

$$g^{(\mathrm{ii})}(\varphi) \approx \frac{1}{2} + \frac{\Gamma_{\mathrm{UD}}}{\Gamma_{\mathrm{L}}}\left(\frac{14}{3} - \frac{29}{12}\cos\varphi\right) \,. \tag{6.26}$$

For strong asymmetry, $\Gamma_{\mathrm{UD}} \ll \Gamma_{\mathrm{L}}$, the oscillations of the singlet and triplet terms cancel each other and the phase dependence of the conductance vanishes. This suppression of the Aharonov-Bohm amplitude allows us to detect the singlet-triplet asymmetry generated in the system.

The plots in Fig. 6.4 display the linear conductance up to second order in the coupling strength based on a full solution of the stationary equations (6.6). If the system is close to equilibrium, $|eV_{\mathrm{UD}}| \ll k_{\mathrm{B}}T$, the triplet probability is large ($F \approx 1/4$), and the conductance is dominated by a positive $\cos\varphi$ kind of oscillation (compare Eq. (6.25)). In contrast, the interference is suppressed if the system is driven into a singlet-triplet imbalance by charging the double dot from the joint left lead, $F \approx 1/2$.
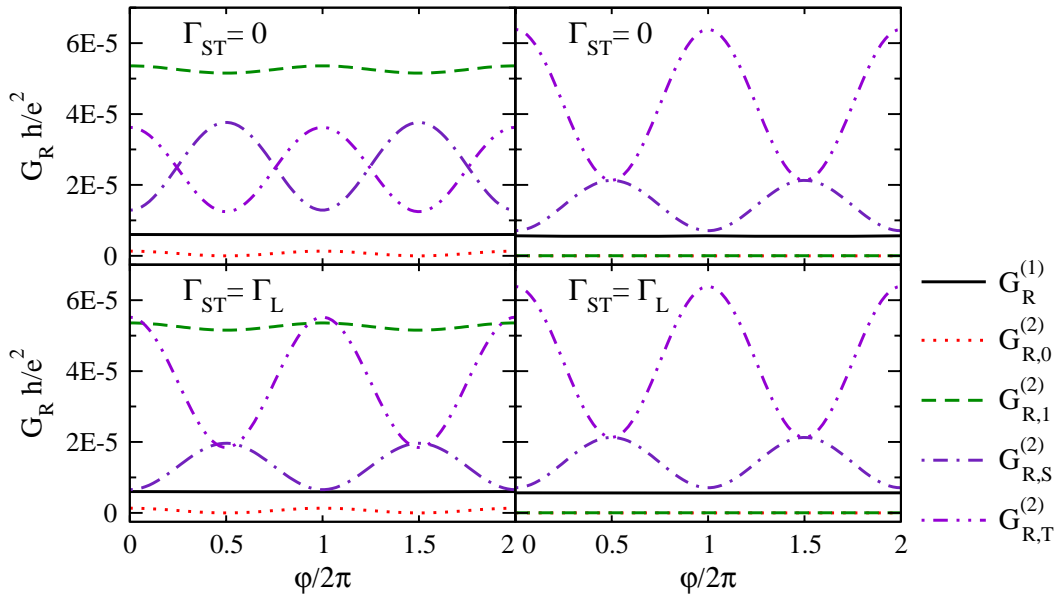
Figure 6.5: The individual contributions to the linear conductance are plotted with and without singlet-triplet relaxation. The first order, $G_R^{(1)}$, and second order terms, $G_{R,\chi}^{(2)}$, are specified for equilibrium (right coloumn) and for strong bias voltage, $eV_{UD} = -20\,k_BT$ (left plots). The parameters are again $\Gamma_L = 1\,k_BT$, $\Gamma_{UD} = 0.1\,k_BT$, $\Gamma_R = 0.01\,k_BT$, $\varepsilon = -10\,k_BT$ and $|eV_R| \ll k_BT$.

A finite singlet-triplet relaxation reduces the imbalance between singlet and triplet in the stationary state, and the Aharonov-Bohm oscillations are restored. To estimate the influence of spin flip and dephasing we introduce phenomenological transition rates between singlet and triplets like in Eq. (4.35) in section 4.4. For simplicity we choose all rates equal to Γ_{ST}. To observe a significant suppression of the Aharonov-Bohm oscillations a relaxation rate smaller than the current rate between source and drain is required, i.e. $\Gamma_{ST} < \Gamma_{UD}$ in our case.

In Fig. 6.5 the first and second order conductance contributions are plotted individually. The transport supported by the equilibrium state is dominated by the second order triplet contribution and the Aharonov-Bohm oscillations are well visible. The singlet-triplet relaxation does not affect the behavior. If the electrons are strongly driven into the double dot from the joint left reservoir, a singlet-triplet imbalance forms and the oscillations of the singlet and triplet contributions cancel each other. A finite relaxation rate partially destroys the imbalance and the cancelation. The conductance supported by the singly occupied states becomes quite strong for a large bias voltage, however, its phase dependence is weak since for strongly asymmetric coupling the isospin is parallel to $\mathbf{m}_L$ with $|\mathbf{I}| \approx 1/4\,p_1$ such that $g_1 \approx 4\,p_1$.

Remark: In the measurement scheme one has to be able to distinguish between the conductance of the fork and the Aharonov-Bohm subsystem(s). In particular, the discus-

sion and the displayed plots focused only on the linear conductance of the Aharonov-Bohm ring as response to a bias voltage between the left and the joint right reservoirs. The current between the separate leads and the right reservoir was only taken into account in the determination of the stationary state and serves only for the preparation of the system. Hence, in the measurement the unavoidable transport between the separate leads and the joint right reservoir has to be filtered out. This problem can be solved by slowly sweeping the voltages eV_R and eV_{UD} simultaneously (this procedure is indicated in the circuit scheme in Fig. 6.1 by the wavy line). A determination of the responding conductances G_R and $\partial I_{UD}/\partial V_{UD}$ with a lock-in technique can be used to separate the influence of electrons transferred between the separate and the joint right reservoirs.

6.4   Phase Switch in the Aharonov-Bohm signal and Flux Sensitivity of the State

In order to spotlight effects which appear in the combined system if the coupling is not tuned extremely asymmetrically we consider the opposite limiting case: symmetric coupling of all reservoirs, $\Gamma_L = \Gamma_{UD} = \Gamma_R$. We focus on two results. First, a phase switch in the Aharonov-Bohm signal can be observed if the bias voltage between the joint left source and the separate upper and lower drains is large enough for sequential tunneling in the fork subsystem. The phase switch is a pure cotunneling effect in the Aharonov-Bohm ring. It allows us to qualitatively estimate the dominance of cotunneling processes over sequential tunneling. Second, a finite coupling of the joint right reservoir, which closes the Aharonov-Bohm geometry, yields a phase dependent stationary state. In turn, the transport from the left source electrode to the separate upper and lower drains becomes flux dependent already in lowest order in the coupling strength.

In Fig. 6.6 we plot the diagonal terms of the density matrix versus the bias voltage in the fork subsystem. Due to the comparatively strong coupling of the joint right reservoir the stationary state of the system is strongly phase dependent. Moreover, in the regime in which the low lying dot levels enter the transport window of the fork subsystem, i.e. $eV_{UD} \lesssim \varepsilon$, the probability to find the double dot singly occupied increases considerably. (In the preceding section we tried to avoid that by choosing a strongly asymmetric coupling in the fork subsystem, $\Gamma_L \gg \Gamma_{UD}$.) Hence, a dominant conductance contribution by g_1 is expected.

A peculiarity of the symmetrically coupled setup is the bias independent ratio of singlet and triplet probabilities for antiparallel isospin axes $\mathbf{m}_L$ and $\mathbf{m}_R$, which becomes apparent in the constant Werner fidelity for $\varphi = \pi$ in Fig. 6.6. It can be understood in the isospin picture. If the double dot is charged from the joint reservoirs ($eV_{UD} \lesssim \varepsilon$) the isospin polarizations in $\mathbf{m}_L$ and $\mathbf{m}_R$ direction are equiprobable since the joint left and the joint right reservoir are coupled equivalently. However, both isospins are antiparallel for $\varphi = \pi$ and average to zero. Consequently the singlet-triplet imbalance vanishes because an essential ingredient, a finite isospin polarization, is absent.
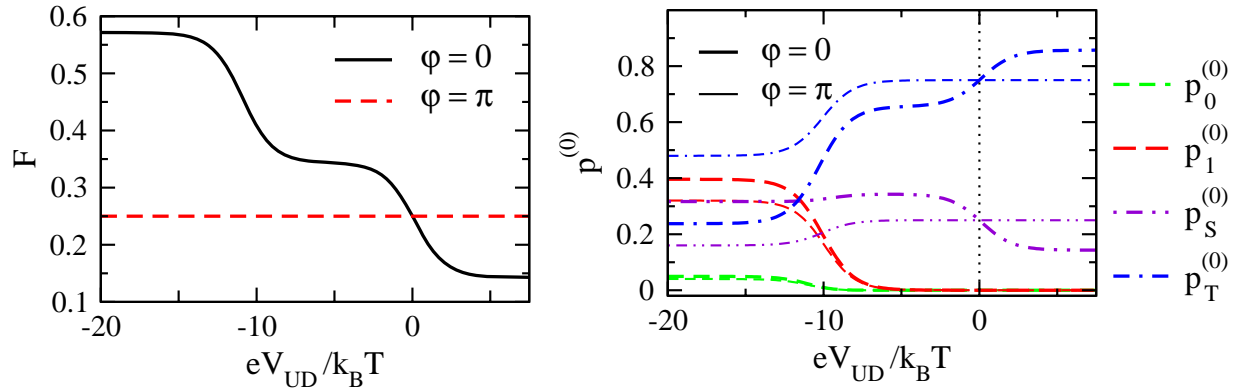
Figure 6.6:   The Werner fidelity and the lowest order probabilities for the hybrid system are plotted versus the bias voltage in the fork subsystem. The dot energies are tuned well below the Fermi energies of the left and the right reservoir, $\varepsilon = -10\,k_B T$. All coupling strengths are chosen to be equivalent, $\Gamma_L = \Gamma_{UD} = \Gamma_R = 0.5\,k_B T$. The phase dependence of the probabilities (due to the coupling of the probe) is illustrated by picking $\varphi = 0$ and $\varphi = \pi$ for comparison.

The increased probability to find only a single electron in the double dot if the bias voltage is large enough leads to a remarkable feature in the linear conductance of the Aharonov-Bohm subsystem. A phase switch can be observed in the second order transport through the Aharonov-Bohm ring as function of the bias voltage between the left source electrode and the separate upper and lower drains (compare Fig. 6.7). The phase switch appears in the vicinity of the onset of the lowest order current in the fork subsystem and allows us to distinguish the first and the second order transport in the Aharonov-Bohm ring. The lowest order transport does not show any phase switch of this kind. That means in particular, if a phase switch is observed in the interference pattern as function of the bias voltage in the fork, we can be sure that the Aharonov-Bohm probe is operated in the cotunneling regime.

Inspection of the individual conductance contributions in Fig. 6.7 reveals that the phase switch can be related to a crossover from a triplet dominated transport to a prevailing conductance contribution from the singly occupied system. As soon as the dots' levels enter the transport regime of the fork, the probability to find the double dot singly occupied increases. Consequently, the corresponding conductance rises and starts to exceed all other contributions. To understand its phase behavior and the influence of the isospin we focus on Eq. (6.24b). For $\varphi = n\,2\pi$ and $\varphi = (2n+1)\pi$ the isospin does not enter the second order conductance of the symmetric setup. Specifically, for $\varphi = n\,2\pi$ the quantization axes $\mathbf{m}_L$ and $\mathbf{m}_R$ are parallel and $\mathbf{m}_L - \mathbf{m}_R = 0$. For $\varphi = (2n+1)\pi$, on the other hand, the expectation value of the isospin itself is zero in the symmetric setup, as discussed above. Thus, in both cases the isospin drops out of the dimensionless conductance term (6.24b) which is then proportional to $p_1^{(0)}$. A phase in between, $n\,2\pi < \varphi < (2n+1)\pi$, yields a finite isospin correction to g_1. Nevertheless, the general behavior is roughly proportional to $(3 - \cos\varphi)$ (the phase dependence of $p_1^{(0)}$ introduces a damping of minor importance).
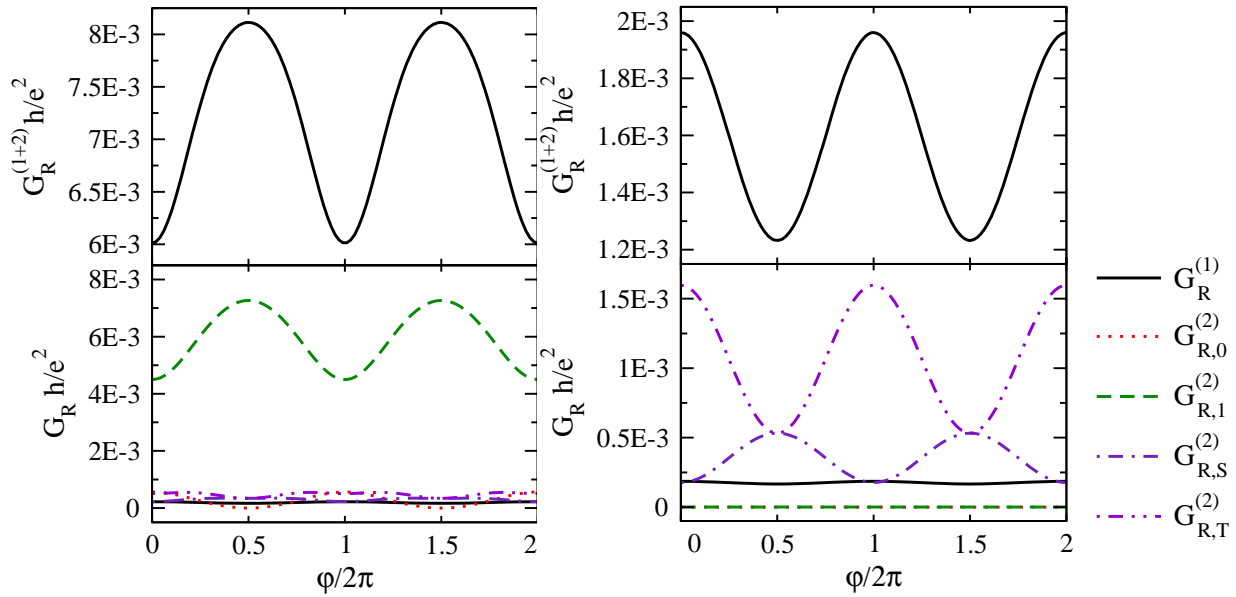
Figure 6.7:   The linear conductance of the Aharonov-Bohm subsystem and its components are plotted versus the phase. Left plot: in nonequilibrium, $eV_{UD} = -20\,k_BT$, the double dot is charged from the joint reservoirs. The electrons can leave the double easily to the separate upper and lower drains. The probability to find the system singly occupied is large, thus, the conductance is dominated by the $G_{R,1}^{(2)}$ term (which is proportional to g_1). Right plot: in equilibrium the system is predominantly doubly occupied with a large triplet probability ($F = 1/4$) which dominates the transport. The parameters are equivalent to Fig. 6.6 ($\Gamma_L = \Gamma_{UD} = \Gamma_R = 0.5\,k_BT$, $\varepsilon = -10\,k_BT$, $eV_R \ll k_BT$).

In contrast, the triplet contribution, which dominates the transport as long as the current through the fork is weak, is roughly proportional to $(2 + \cos \varphi)$ and oscillates contrariwise. Hence, we find a phase switch in the second order conductance of the Aharonov-Bohm subsystem at the crossover from the completely charged double dot to the singly occupied system. This coincides with a bias voltage in the fork subsystem at the onset of sequential transport.

A strong coupling of the second joint reservoir, which closes the Aharonov-Bohm geometry, induces a phase dependence of the state of the system. This is manifest not only in the isospin degree of freedom but also in the diagonal probabilities. The flux dependence of the probabilities can be observed in the lowest order transport through the Ahronov-Bohm ring or, even better, in the lowest order transport between the joint left and the separate upper and lower reservoirs.

In chapter 5 we discussed in detail that an Aharonov-Bohm ring with two embedded quantum dots can be subject to an isospin blockade which yields interference patterns already in the transport in first order in the coupling strength. Therefore it is not very surprising that also the lowest order linear conductance of the Aharonov-Bohm subsystem
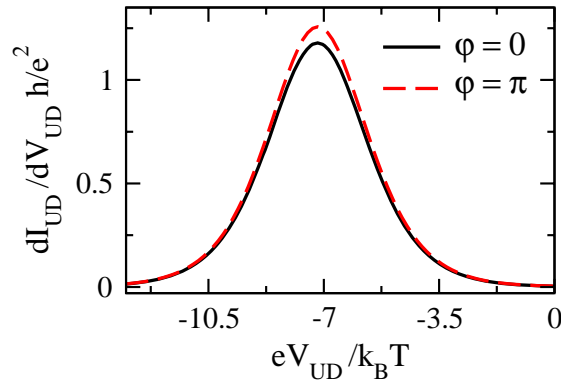
Figure 6.8: The first order differential conductance of the fork subsystem is plotted versus the bias voltage. A comparison of the two curves for $\varphi = 0$ and $\varphi = \pi$ reveals the sensitivity on the magnetic flux threading the ring. The Aharonov-Bohm substructure leads to a phase dependence of the stationary state which is observable in the transport through the fork. The parameters are $\Gamma_\mathrm{L} = \Gamma_\mathrm{UD} = \Gamma_\mathrm{R} = 0.5\,k_\mathrm{B}T$, $\varepsilon = -7\,k_\mathrm{B}T$, $eV_\mathrm{R} \ll k_\mathrm{B}T$.

is sensitive to the phase. To distinguish between a bare isospin effect and the influence of flux dependent probabilities we use the properties of the symmetrically coupled system. In first order the isospin enters the conductance formula (as well as in second order) with a term proportional to $\mathbf{I}^{(0)} \cdot (\mathbf{m}_\mathrm{L} - \mathbf{m}_\mathrm{R})$. (This can be derived with a lowest order perturbation calculation for the transfer rates, similar to the scheme above, or it can be concluded from the Meir-Wingreen formula [39]; compare also Eq. (5.18) on page 80). According to the argumentation above, an isospin term of that form vanishes for the symmetric setup at $\varphi = n\,2\pi$ and $\varphi = (2n+1)\pi$. Thus, the difference between the first order linear conductance for $\varphi = 0$ and $\varphi = \pi$, displayed in the plots in Fig. 6.7, is exclusively due to the oscillation induced by the phase dependent diagonal elements $p_0^{(0)}, p_1^{(0)}, p_\mathrm{S}^{(0)}, p_\mathrm{T}^{(0)}$. Nevertheless, in an experiment it might be difficult to clearly separate the isospin contribution to the transport (e.g. because of asymmetries in the setup, etc.).

The observation of phase dependent transport between a joint lead and the separate upper and lower reservoirs can give less ambiguous evidence for flux dependent probabilities. As consequence of the influence of the Aharonov-Bohm ring on the state of the system, the lowest order transport through the fork subsystem becomes flux sensitive. This interference effect is solely due to the phase dependent diagonal probabilities of the stationary density matrix. In order to sketch the phase dependence we plot the differential conductance of the fork subsystem as function of the bias voltage for $\varphi = 0$ and $\varphi = \pi$ in Fig. 6.8.

Chapter 7

Capacitively Coupled Quantum Dots

Recently, very promising experimental realizations of an arrangement of two parallel quantum dots with a strong capacitive coupling have been performed [107,108]. Similar systems of interacting double-dots have attracted substantial interest in the past decade. Under certain conditions the orbital structure of the wave functions can be expressed in terms of a pseudospin. It has been predicted theoretically and observed experimentally that at low temperature a Kondo correlated state of pseudospins might form. Moreover, the interplay between quantum fluctuations of the spin and pseudospin degrees of freedom may give rise to a SU(4) Kondo effect [109–111].

However, the investigation of interacting double-dot systems reveals many more aspects of many-body physics and correlation effects beside the Kondo regime. Especially for intermediate temperatures for which the Coulomb blockade is fully developed but the Kondo effect is not yet important, or for weak to intermediate coupling of the dots to the leads there is a lot of room beyond standard sequential tunneling. Current and noise correlations of parallel quantum dots are, for instance, studied experimentally [112] and theoretically [114].

In the following we focus on cotunneling and renormalization effects in the region where first order tunneling is suppressed by the interaction between the two quantum dots. We find asymmetries in the linear conductance which are provoked by the strong onsite Coulomb repulsion due to the small size of the dots.

7.1 Setup and Model

Inspired by the experimental activities, especially Ref. [107, 108], we concentrate on two parallel quantum dots with independent leads and capacitive interdot-coupling (see e.g. Fig. 7.1). The model Hamiltonian $H = H_{\mathrm{res}} + H_{\mathrm{dots}} + H_{\mathrm{t}}$ comprises a part for the four reservoirs, a term for the two dots which includes the interactions on each dot as well as between them, and the tunnel Hamiltonian. As usual we assume the four independent leads described by

$$H_{\mathrm{res}} = \sum_r \sum_{k\sigma} \varepsilon_{rk}\, a^\dagger_{rk\sigma} a_{rk\sigma} \tag{7.1}$$
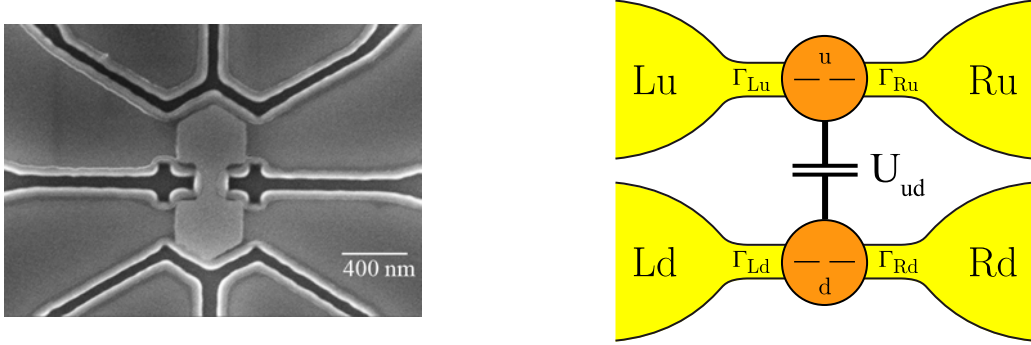
Figure 7.1:   The picture to the left shows a scanning electron micrograph of an experimental setup of two capacitively coupled quantum dots [2, 107, 108]. On the right hand side the model system is sketched schematically.

with $r \in \{\mathrm{Lu, Ld, Ru, Rd}\}$ to be large reservoirs in local equilibrium. Creation and annihilation operators of the respective electrons with spin σ are denoted by $a_{rk\sigma}^\dagger$ and $a_{rk\sigma}$. The double-dot system consists of two small quantum dots which are capacitively coupled. We represent them by the term

$$H_{\mathrm{dots}} = \sum_i \left[\sum_\sigma \varepsilon_i \, c_{i\sigma}^\dagger c_{i\sigma} + U \, c_{i\uparrow}^\dagger c_{i\downarrow}^\dagger c_{i\downarrow} c_{i\uparrow} \right] + \sum_{\sigma\sigma'} U_{\mathrm{ud}} \, c_{\mathrm{u}\sigma}^\dagger c_{\mathrm{d}\sigma'}^\dagger c_{\mathrm{d}\sigma'} c_{\mathrm{u}\sigma} \tag{7.2}$$

where the upper and lower dot are distinguished by the index $i \in \{\mathrm{u, d}\}$ and the spin-degenerate dot levels ε_i can be tuned via gate voltages. Due to the confinement of electrons to the small size of the quantum dots we assume a large onsite Coulomb repulsion U such that double occupancy of each level is suppressed. A central quantity for the experiment and our considerations is the capacitive coupling between the two dots. It is accounted for by the interaction term parametrized by U_{ud}. The tunneling of electrons between dots and reservoirs is summarized in the tunnel Hamiltonian

$$H_{\mathrm{t}} = \sum_{rk\sigma i} \left[t_{ri} \, c_{i\sigma}^\dagger a_{rk\sigma} + \mathrm{h.c.} \right] . \tag{7.3}$$

Since there is no direct coupling of the upper dot to a lower lead or vice versa, i.e. $t_{\mathrm{L}i,j} = 0 = t_{\mathrm{R}i,j}$ for $i \neq j$, we simplify the index notation and define $t_{\mathrm{L}i} := t_{\mathrm{L}i,i}$ and $t_{\mathrm{R}i} := t_{\mathrm{R}i,i}$. Furthermore, we assume the tunneling independent of spin and energy. Hence, the tunneling strengths can be parametrized by $\Gamma_r = 2\pi \, |t_r|^2 \, N_r$ where N_r denotes the density of states of the respective reservoir $r \in \{\mathrm{Lu, Ld, Ru, Rd}\}$.
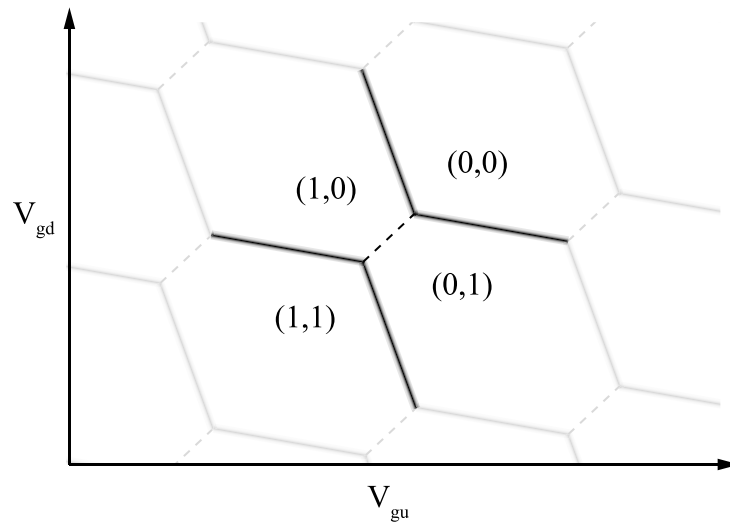
Figure 7.2: Sketch of the charge stability diagram for a double-dot system. By dark lines we emphasize the part which is relevant if we concentrate only on a single level in each dot. The energies can be tuned via the gate voltages V_{gu} and V_{gd}. The charge states of the dots are indicated by tuples of the form ($\#$ of electrons on dot u, $\#$ of electrons on dot d). Along the dashed line transport is suppressed due to the interaction between the upper and lower dot. Here, as well as in the Coulomb blockade valleys between the conductance lines, charge transfer is only possible by cotunneling and higher-order processes. If each dot contains more than a single level the pattern is continued periodically and the well-known honeycomb lattice is formed.

7.2 Cotunneling Bridge in the Charge Stability Diagram

The general structure of the Coulomb oscillation pattern which we expect from a system of two interacting quantum dots is sketched in the charge stability diagram in Fig. 7.2. As function of the dot levels or the corresponding gate voltages we obtain a honeycomb lattice which is composed of Coulomb oscillations of the upper dot (indicated in the figure by the more or less vertical solid lines) and Coulomb oscillations of the lower dot (indicated by the nearly horizontal solid lines). Both conductance lines show a gap (indicated by the dashed line) due to the interdot interaction which suppresses the transport through either dot if the other dot is occupied with an excess electron. In the case of two single-level quantum dots only the emphasized part of the diagram is relevant. The corresponding charge states of the system are indicated tuples containing the number of excess electrons of the upper and lower dot. (In a realistic situation the gate voltage which primarily controls the electrostatic energy of one dot can not be shielded completely from the other dot which is also affected. Consequently the conductance lines do not form a perpendicular lattice. In the following theoretical discussion, however, we assume two independent dot energies which results in a rectangular pattern.)
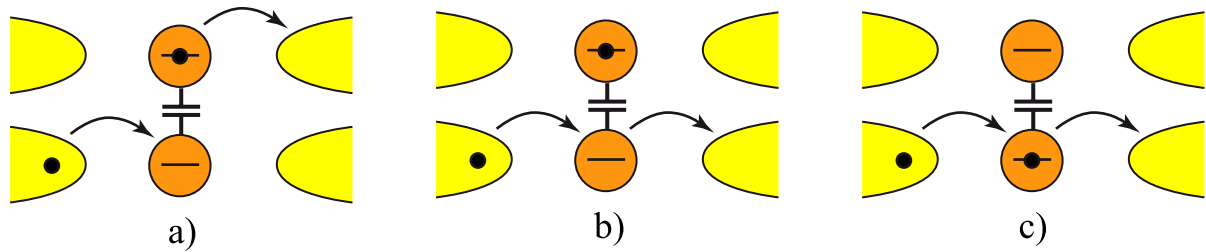
Figure 7.3:   Different kinds of cotunneling processes are sketched. On the right hand side the tunneling of an electron leaving the upper dot is correlated with the tunneling of a second electron onto the lower dot (a). In contrast, the cotunneling processes in figures b) and c) affect only one of the dots at a time.

The solid lines forming the boundaries between the valleys of fixed charge states indicate the regions in which first order transport is possible and a conductance peak develops. In the Coulomb blockade valleys and in the interaction gap, indicated by the dashed line, lowest order tunneling is exponentially suppressed. Nevertheless, cotunneling and higher order processes give finite contributions in this regime and dominate the transport.

We concentrate on the second order corrections of the conductance. In particular we are concerned with the cotunneling contributions in the conductance gap induced by the interdot interaction. Additionally, we take into account all second order renormalization terms which lead to modifications of the shape and position of the conductance peaks. In general we can distinguish two kinds of cotunneling processes:

  i. The first kind is represented by a correlated tunneling of electrons in the upper and lower path, i.e. in both dots tunneling takes place at (nearly) the same time. In Fig. 7.3 this is depicted in sketch a). Each of these processes switches the charge state of the double-dot from $(1,0)$ to $(0,1)$ or vice versa.

 ii. The second kind is depicted in sketches b) and c) in Fig. 7.3. Here only a single dot is affected by a tunneling process at a time. The charge state changes virtually during the process but effectively it remains the same.

While the cotunneling of the second kind is in general not restricted to any region in the charge stability diagram, it is more probable in the vicinity of the conductance peaks though, the processes of the first kind can appear only at the common border of the $(1,0)$ and $(0,1)$ Coulomb blockade cells (in general at the borders between $(n+1,n)$ and $(n, n+1)$), i.e. in the conductance gap caused by the interdot interaction.

To calculate the transport through the double-dot system we employ the real-time diagrammatic technique. We perform an expansion in the coupling strength of the dots to the leads up to second order and respect systematically all contributions, including renormalization terms. Although an analytic solution of the stationary equations for the reduced density matrix and the stationary transport is feasible in lowest order in the coupling strength, the expressions are complicated and not very elucidating. Instead we use
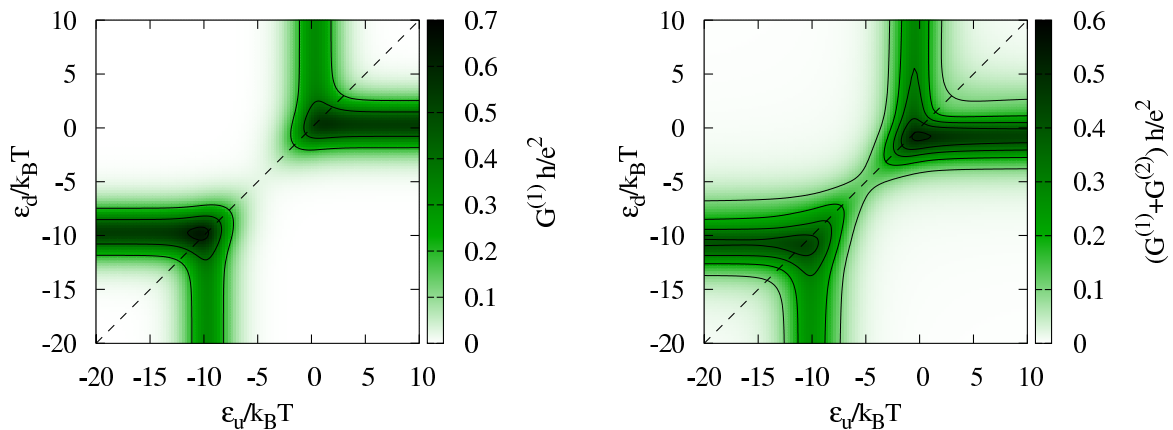
Figure 7.4:   The linear conductance $G(\varepsilon_\mathrm{u}, \varepsilon_\mathrm{d}) := \mathrm{d}I/\mathrm{d}V|_{V=0}$ of the entire double-dot system is plotted in first order in the coupling strength (left plots) and up to second order (right plots) as function of the dot energies ε_u and ε_d. The coupling strengths of the upper dot is chosen symmetrically, $\Gamma_\mathrm{Lu} = \Gamma_\mathrm{Ru} = 0.3\,k_\mathrm{B}T$, a bit weaker than the lower dot, $\Gamma_\mathrm{Ld} = \Gamma_\mathrm{Rd} = 0.5\,k_\mathrm{B}T$. The energy cutoff in the reservoirs is set to $D = 100\,k_\mathrm{B}T$.

a combination of an analytical determination of the kernel **W** (compare section 3.3) and the current rates (section 3.4) but solve the stationary equations numerically. A numerical assistance is anyway inevitable for cotunneling and renormalization corrections. (A fully numerical approach in which all diagrams are generated and calculated automatically confirms the bookkeeping and yields identical results.)

In Fig. 7.4 we plot the linear conductance of the complete system as function of the dot energies ε_u and ε_d. For comparison we show the first order contribution on the left hand side and the first order inclusive the second order correction in the right plot. Beside the broadening and the slight shift of the conductance peaks we find a well pronounced cotunneling bridge which develops in the interaction gap.

For a more detailed view we plot a slice along on the degeneracy line $\varepsilon_\mathrm{u} = \varepsilon_\mathrm{d}$. The peaks are shifted by the renormalization corrections and the algebraically decaying cotunneling tails are clearly visible. In the interaction gap the conductance is considerably increased. However, we find a strong asymmetry in the region between the two peaks.

An analysis of the second order terms for different sets of coupling strenghts reveals a qualitative difference of the cotunneling tails at the shoulders of the conductance peaks and the cotunneling bridge in the interaction gap. The former contributions for say the lower dot are nearly independent of the coupling strength of the upper dot. In contrast, the cotunneling bridge depends strongly on the coupling strength of both dots at the same time as we would expect from processes like sketched in Fig. 7.3 a). A smaller coupling of one of the dots results in a strong decrease of the conductance in the interaction gap for both dots (this can be seen if we consider the conductances of both dots separately like in the plots in Fig. 7.5, for instance). From a phenomenological point of view there is no reason why the cotunneling of type a) depicted in Fig. 7.3 may yield an asymmetry, not
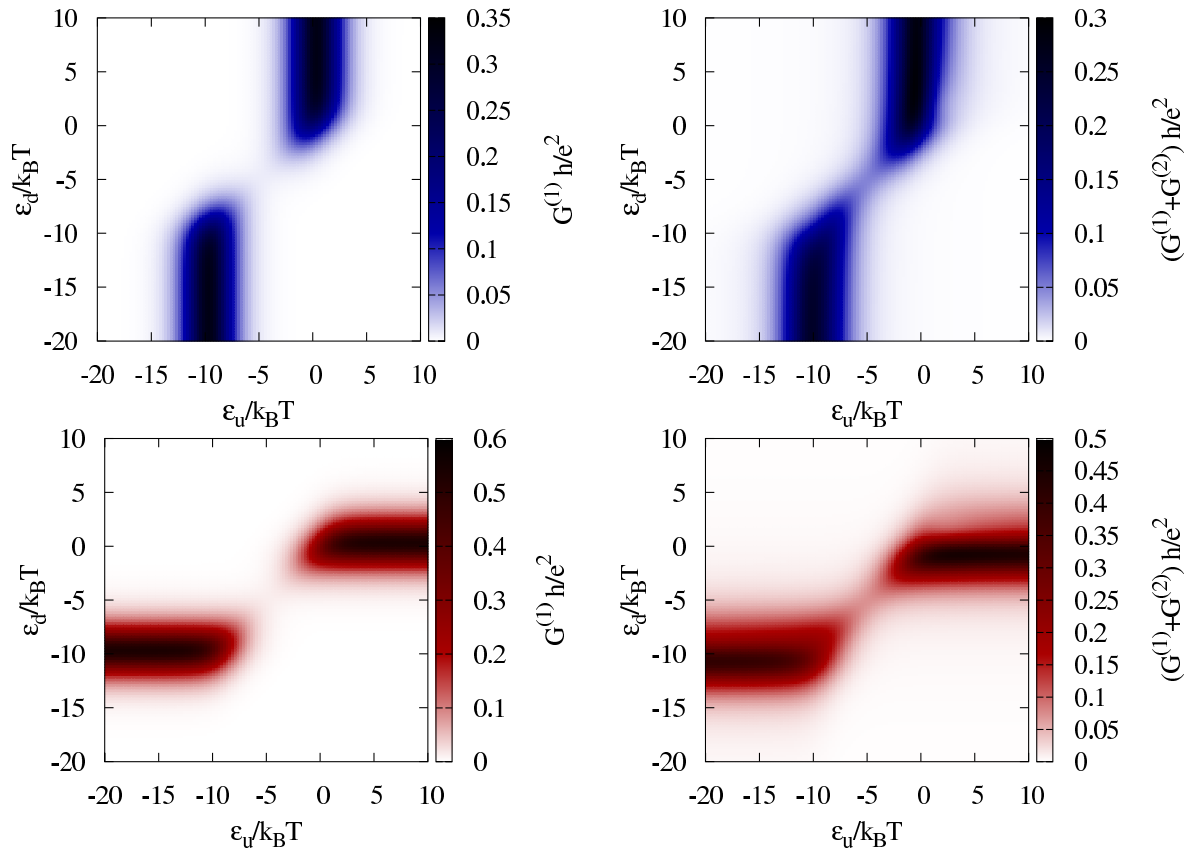
Figure 7.5: The plots show the same data as in Fig. 7.4, but separated for the linear conductance of the upper dot (upper plots) and the lower dot (lower plots). For comparison: The left plots display sequential tunneling. Cotunneling and renormalization effects are regarded in the right plots. The upper dot is slightly weaker coupled than the lower one. Thus, the cotunneling bridge is slightly more pronounced on the scale of the conductance peak.
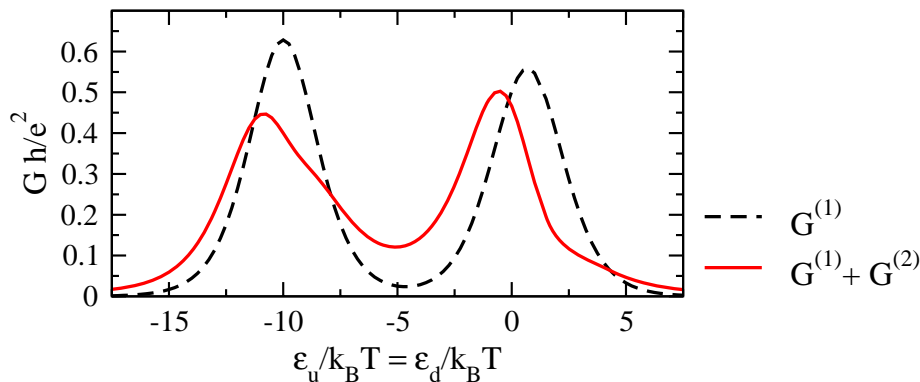
Figure 7.6:   Plot of the linear conductance along the degeneracy line, $\varepsilon_{\mathrm{u}} = \varepsilon_{\mathrm{d}}$, indicated by the dashed diagonal in Fig. 7.4. Correlated tunneling dominates the transport in the interaction gap. Renormalization effects lead to a strong asymmetry due to Coulomb repulsion on the dots.

even for asymmetric coupling.

In the vicinity of the conductance peaks, however, we have additional cotunneling contributions by processes of the kind b) an c) of Fig. 7.3. From a comparison with the corresponding terms for a single quantum dot (see subsection 3.6.2, especially Eq. (3.50) and Fig.3.12) we might conclude that these should be symmetric to their centers at $\varepsilon_i = \varepsilon_{\mathrm{F}i}$ and $\varepsilon_i = \varepsilon_{\mathrm{F}i} - U_{\mathrm{ud}}$ (where $\varepsilon_{\mathrm{F}i}$ denotes the mean Fermi energy of the upper or lower leads, respectively). Nevertheless, they are not symmetric to the center of the conductance peaks. As a consequence, the cotunneling on the unoccupied side of the conductance lines is more pronounced than on the occupied side because the peak is shifted to lower energies by the renormalization correction (a detailed discussion for a single dot can be found in subsection 3.6.2). Hence, the influence of the type b) and c) cotunneling contributions in the $(1, 0)$ and $(0, 1)$ valleys is stronger near the border to the $(1, 1)$ charge state than on the border to the $(0, 0)$ state. In general, this asymmetry can not be compensated by renormalization corrections of the cotunneling which might appear earliest in third order in the coupling strength. The first modification of the cotunneling bridge in the interaction gap where processes of type a) dominate is expected not before the fourth order in Γ.

The experimental data [107, 108, 113] and Fig. 7.7 show a systematic asymmetry of the conductance peaks' shoulders. This is best visible for strongly coupled quantum dots in which cotunneling and higher order terms are expected to play an important role. The asymmetry coincides with our result of a strong cotunneling contribution on the high energy side of the conductance peaks and a weaker cotunneling contribution on the low energy side. Furthermore, from our model we obtain a behavior of the cotunneling bridge which is roughly proportional to the product $\Gamma_{\mathrm{u}}\Gamma_{\mathrm{d}}$ with $\Gamma_i := \Gamma_{\mathrm{L}i} + \Gamma_{\mathrm{R}i}$ for $i \in \{\mathrm{u}, \mathrm{d}\}$ if processes of type a) (sketched in Fig. 7.3) dominate, i.e. apart from the cotunneling through a single dot which is proportional to Γ_i^2. That means by increasing the coupling strength of both dots the conductance at the Coulomb peak grows linearly if it is dominated by first order processes, whereas the cotunneling bridge increases quadratically (compare
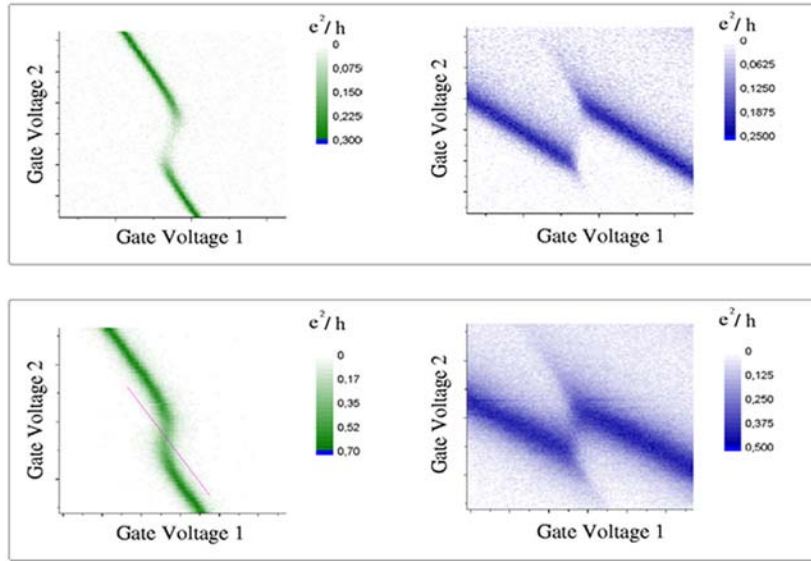
Figure 7.7:   Plots of experimental data [2, 113] for the linear conductance of each dot. From the upper to the lower plots the coupling strength of both dots is increased. The conductance in the interaction gap grows faster than at the resonances.

also the experimental data in Fig. 7.7). If only the coupling of one of the dots is varied, the influence on the cotunneling bridge is linear, but independent of the dot we probe. In contrast, at the conductance peak only the transport of the varied quantum dot is affected. This represents a simple test for the applicability of the considered model.

The computational procedure and our numerical implementation is capable of treating arbitrary interaction between the dots and general nonequilibrium situations. The various tunnel couplings can be varied independently in a wide range. However, the limits of applicability are reached in case of strong coupling of the dots to the leads or for very low temperature. In these cases higher order quantum fluctuations become important which may even lead to Kondo physics.

In the experiments [107, 108] the tunnel coupling was quite strong compared to the temperature. Although there was no clear evidence for a Kondo effect, some important features of the measurements can not be explained with the calculation presented. Further theoretical investigations, e.g. a renormalization group analysis, are under ongoing discussion [115].

Chapter 8

Conclusions

Charging effects based on the quantization of the electronic charge play a fundamental role in single-electron devices. At low temperatures and in nanoscale structures, like quantum dots, they lead to well-known Coulomb blockade phenomena, which are observable in pronounced signatures in transport experiments. In the limit of weak coupling of the dot to the reservoirs these effects can be explained within a perturbation theory. Often a classical master-equation description of sequential tunneling, with rates evaluated in a lowest-order expansion, is already sufficient to capture the main behavior.

However, for stronger coupling or lower temperature quantum fluctuations and correlated tunneling become important. Higher order processes such as cotunneling and renormalization effects start to play a role and give dominant contributions in some regimes. In more complex geometries with directly or indirectly coupled quantum dots the quantum nature of electrons may lead to a coherent evolution of the system's state. This raises the need for a theoretical description beyond classical master equations.

In this thesis we used a real-time transport theory to establish a comprehensive picture of the nonequilibrium behavior of two coherently coupled quantum dots. The time evolution of the entire reduced density matrix, including all off-diagonal terms, was considered within a diagrammatic expansion in the coupling strength. Particular emphasis was put on the effect of strong Coulomb interaction on the dots. We found a surprising feature of the double-dot system: in a nonequilibrium situation quantum correlations develop between electrons on the spatially separated dots. If the system is occupied with two electrons a so-called Werner state is formed which, out of equilibrium, shows an imbalance between its singlet and triplet components. By coherently charging the double dot from a common reservoir the singlet probability is strongly enhanced, indicating the generation of entanglement.

We concentrated on two schemes to investigate this effect. In a setup composed of two quantum dots coherently coupled to one joint reservoir we studied the transient behavior after quickly pushing the dot levels from above to below the Fermi energy of the lead. In a second setup we additionally attached two separate leads to the dots. By applying a bias voltage a current was driven from the joint source electrode via the double dot to the separate drains. In both schemes we found a strongly enhanced singlet probability which

can be linked to the generation of entanglement in nonequilibrium.

An important precursor for this phenomenon is a nontrivial evolution of the off-diagonal elements of the reduced density matrix due to coherent tunneling. We suggested an intuitive interpretation of the offdiagonal evolution by introducing an isospin variable. The influence of the latter on the coherence of the transport was investigated in an Aharonov-Bohm interferometer with embedded quantum dots. The appearance of a phase dependent isospin blockade caused by an onsite Coulomb repulsion yields strong asymmetries in the conductance oscillations. We predicted clear signatures of the isospin blockade in the differential conductance for asymmetrically coupled quantum dots.

By a systematic expansion up to second order in the coupling strength we analytically identified cotunneling terms and renormalization corrections. Moreover, we found unexpected conductance contributions due to exchange interactions, which lead to a qualitative asymmetry between the occupied and the unoccupied side of a conductance peak if the dots are coupled asymmetrically. The analytical calculation which is restricted to the linear response regime was supplemented by a numerical approach in which all diagrams were generated and computed automatically. The goal was the extension of first and second order transport to arbitrary nonequilibrium situations.

Based on our results for entanglement generation in nonequilibrium, and Aharonov-Bohm interferometry with quantum dots, we suggested a combined system which allows the creation and detection of entanglement of spatially separated electron spins in a transport experiment. The setup consists of two spatially separated quantum dots embedded in a fork-like geometry which is supplemented by an Aharonov-Bohm ring. By applying a strong bias voltage between a joint source electrode and separate drain reservoirs in the fork subsystem a strong imbalance between singlet and triplet probabilities, indicating entanglement, is created in the stationary state. We increased the overall probability to find two excess electrons in the double dot by using an asymmetric coupling to source and drain. In order to detect the singlet-triplet imbalance we applied an Aharonov-Bohm probe. The obtained interference pattern depends on the state of the double dot. In particular, the cotunneling transport through the Aharonov-Bohm ring is sensitive to an imbalance in the singlet-triplet distribution. Compared to the equilibrium situation in which singlet and triplets are uniformly distributed, an enhanced singlet probability leads to a suppression of Aharonov-Bohm oscillations. The scheme might provide an experimental proof of concept for the generation of entanglement in nonequilibrium.

Finally, motivated by a promising experiment with two capacitively coupled quantum dots we systematically modeled the transport up to second order, including all cotunneling and renormalization contributions. Our focus was on the enhanced conductance in the interaction gap which in our model is due to correlated tunneling of electrons in both dots. The onsite Coulomb interaction yields an asymmetry of the shoulders of the conductance peaks.

Appendix A

Fork: Lowest Order Density Matrix

The stationary equations (4.43) of the fork system, considered in section 4.5, can be solved analytically in lowest order in the coupling strength of the dots to the leads. In the following we give the full expressions for arbitrary bias voltage. They have been evaluated for the plots in section 4.6.

The probability to find the system empty is given by

$$
p_0^{(0)} = \frac{1}{D}\Big[-(1-f_{\mathrm L})^2(2-f_{\mathrm R}+f_{\mathrm L}-2\,f_{\mathrm L}f_{\mathrm R})\,\Gamma_{\mathrm L}^3 - \\
-5\,(1-f_{\mathrm L})(1-f_{\mathrm R})(1-f_{\mathrm L}f_{\mathrm R})\,\Gamma_{\mathrm L}^2\Gamma_{\mathrm R} + \\
+2\,(1-f_{\mathrm R})^2(-2+f_{\mathrm L}-f_{\mathrm R}+2\,f_{\mathrm L}f_{\mathrm R})\,\Gamma_{\mathrm L}\Gamma_{\mathrm R}^2 - \\
-(1-f_{\mathrm R})^2(1-f_{\mathrm R}^2)\,\Gamma_{\mathrm R}^3 \Big]. \tag{A.1}
$$

The probabilities for the symmetric and antisymmetric superposition states read

$$
p_{|+\rangle_{\mathbf{I}\cdot\mathbf{m}}}^{(0)} = \frac{2}{D}\Big[-\big(f_{\mathrm L}\,(2-f_{\mathrm R}) - f_{\mathrm L}^2\,(1+f_{\mathrm R}) - f_{\mathrm L}^3\,(1-2\,f_{\mathrm R})\big)\,\Gamma_{\mathrm L}^3 - \\
-\big(f_{\mathrm R} + 2\,f_{\mathrm L}\,(2-2\,f_{\mathrm R}-f_{\mathrm R}^2) - f_{\mathrm L}^2\,(1+3\,f_{\mathrm R}-5\,f_{\mathrm R}^2)\big)\,\Gamma_{\mathrm L}^2\Gamma_{\mathrm R} - \\
-\big(f_{\mathrm R}\,(2-f_{\mathrm R}-f_{\mathrm R}^2) + f_{\mathrm L}\,(2-3\,f_{\mathrm R}-3\,f_{\mathrm R}^2+4\,f_{\mathrm R}^3)\big)\,\Gamma_{\mathrm L}\Gamma_{\mathrm R}^2 - \\
-f_{\mathrm R}\,(1-f_{\mathrm R})^2(1+f_{\mathrm R})\,\Gamma_{\mathrm R}^3 \Big], \tag{A.2}
$$

$$
p_{|-\rangle_{\mathbf{I}\cdot\mathbf{m}}}^{(0)} = \frac{2}{D}\Big[-\big(2\,f_{\mathrm R} - 3\,f_{\mathrm L}f_{\mathrm R} + f_{\mathrm L}^2\,(1-f_{\mathrm R}) - f_{\mathrm L}^3\,(1-2\,f_{\mathrm R})\big)\,\Gamma_{\mathrm L}^3 - \\
-\big(f_{\mathrm R}\,(5-2\,f_{\mathrm R}) - 2\,f_{\mathrm L}f_{\mathrm R}\,(2+f_{\mathrm R}) + f_{\mathrm L}^2\,(1-3\,f_{\mathrm R}+5\,f_{\mathrm R}^2)\big)\,\Gamma_{\mathrm L}^2\Gamma_{\mathrm R} - \\
-\big(f_{\mathrm R}\,(4-3\,f_{\mathrm R}-f_{\mathrm R}^2) - f_{\mathrm L}f_{\mathrm R}\,(1+3\,f_{\mathrm R}-4\,f_{\mathrm R}^2)\big)\,\Gamma_{\mathrm L}\Gamma_{\mathrm R}^2 + \\
+(1-f_{\mathrm R})^2(1+f_{\mathrm R})\,\Gamma_{\mathrm R}^3 \Big]. \tag{A.3}
$$

Finally, the doubly occupied subspace is determined by the probabilities to find two elec-

trons in the double dot which either form a spin singlet or a triplet state,

$$
\begin{aligned}
p_{\mathrm{S}}^{(0)} = \frac{1}{D} \Big[&- \left(f_{\mathrm{L}}^2 \left(2 - f_{\mathrm{R}}\right) + f_{\mathrm{L}}^3 \left(1 - 2 f_{\mathrm{R}}\right) \right) \Gamma_{\mathrm{L}}^3 - \\
&- \left(f_{\mathrm{R}}^2 + f_{\mathrm{L}} f_{\mathrm{R}} \left(2 - f_{\mathrm{R}}\right) + f_{\mathrm{L}}^2 \left(2 + f_{\mathrm{R}} - 5 f_{\mathrm{R}}^2\right) \right) \Gamma_{\mathrm{L}}^2 \Gamma_{\mathrm{R}} - \\
&- \left(f_{\mathrm{R}}^2 + 2 f_{\mathrm{L}} f_{\mathrm{R}} \left(1 - 2 f_{\mathrm{R}}^2\right) \right) \Gamma_{\mathrm{L}} \Gamma_{\mathrm{R}}^2 - \\
&- f_{\mathrm{R}}^2 \left(1 - f_{\mathrm{R}}^2\right) \Gamma_{\mathrm{R}}^3 \Big] ,
\end{aligned}
\tag{A.4}
$$

$$
\begin{aligned}
p_{\mathrm{T}}^{(0)} = \frac{3}{D} \Big[&- \left(2 f_{\mathrm{L}} f_{\mathrm{R}} - f_{\mathrm{L}}^2 f_{\mathrm{R}} + f_{\mathrm{L}}^3 \left(1 - 2 f_{\mathrm{R}}\right) \right) \Gamma_{\mathrm{L}}^3 - \\
&- \left(f_{\mathrm{R}}^2 + f_{\mathrm{L}} f_{\mathrm{R}} \left(4 - f_{\mathrm{R}}\right) + f_{\mathrm{L}}^2 f_{\mathrm{R}} \left(1 - 5 f_{\mathrm{R}}\right) \right) \Gamma_{\mathrm{L}}^2 \Gamma_{\mathrm{R}} - \\
&- \left(2 f_{\mathrm{R}}^2 + 2 f_{\mathrm{L}} f_{\mathrm{R}} \left(1 - 2 f_{\mathrm{R}}^2\right) \right) \Gamma_{\mathrm{L}} \Gamma_{\mathrm{R}}^2 - \\
&- f_{\mathrm{R}}^2 \left(1 - f_{\mathrm{R}}^2\right) \Gamma_{\mathrm{R}}^3 \Big] .
\end{aligned}
\tag{A.5}
$$

The general denominator D is given by the determinant of a matrix which can be obtained from the kernel $\mathbf{W}$ by exchanging one of the (necessarily) linear dependent rows by the normalization condition $\mathrm{tr}\,\rho = 1$,

$$
\begin{aligned}
D = &- \left[2 + 3 f_{\mathrm{R}} + f_{\mathrm{L}} \left(1 - 2 f_{\mathrm{R}}\right) + f_{\mathrm{L}}^2 \left(2 - 5 f_{\mathrm{R}}\right) + f_{\mathrm{L}}^3 \left(1 - 2 f_{\mathrm{R}}\right) \right] \Gamma_{\mathrm{L}}^3 - \\
&- \left[5 + 7 f_{\mathrm{R}} + f_{\mathrm{L}} \left(3 - 2 f_{\mathrm{R}} - 7 f_{\mathrm{R}}^2\right) + f_{\mathrm{L}}^2 \left(2 - 3 f_{\mathrm{R}} - 5 f_{\mathrm{R}}^2\right) \right] \Gamma_{\mathrm{L}}^2 \Gamma_{\mathrm{R}} - \\
&- 2 \left[\left(1 + f_{\mathrm{R}}\right)^2 \left(2 - f_{\mathrm{R}}\right) + f_{\mathrm{L}} \left(1 + f_{\mathrm{R}}\right)^2 \left(1 + 2 f_{\mathrm{R}}\right) \right] \Gamma_{\mathrm{L}} \Gamma_{\mathrm{R}}^2 - \\
&- \left(1 - f_{\mathrm{R}}\right) \left(1 + f_{\mathrm{R}}\right)^3 \Gamma_{\mathrm{R}}^3 .
\end{aligned}
\tag{A.6}
$$

Appendix B

Aharonov-Bohm Interferometer: Lowest Order Density Matrix

In lowest order in the coupling strength the stationary equations for the reduced density matrix of the Aharonov-Bohm interferometer with two embedded quantum dots can be solved analytically for arbitrary bias voltage. In second order in Γ we have to restrict ourselves to the linear response regime to obtain analytical results, they are supplemented by numerical calculations for strong nonequilibrium. In the following we give the analytical expressions for $\mathbf{p}^{(0)}$ and $\mathbf{I}^{(0)}$, which were used for the lowest order plots in section 5.3 (the dot levels are assumed to be degenerate, $\Delta\varepsilon = 0$).

The diagonal terms comprised in $\mathbf{p}^{(0)}$ are given by

$$
\begin{aligned}
p_0^{(0)} = \frac{1}{D}\, &\left((1 - f_{\mathrm{L}})\,\Gamma_{\mathrm{L}} + (1 - f_{\mathrm{R}})\,\Gamma_{\mathrm{R}} \right) \cdot \\
&\cdot \Big[(1 - f_{\mathrm{L}}^2)\,(-2 - f_{\mathrm{L}} + f_{\mathrm{R}} + 2\,f_{\mathrm{L}}f_{\mathrm{R}})\,\Gamma_{\mathrm{L}}^2 + (1 - f_{\mathrm{R}}^2)\,(-2 + f_{\mathrm{L}} - f_{\mathrm{R}} + 2\,f_{\mathrm{L}}f_{\mathrm{R}})\,\Gamma_{\mathrm{R}}^2 - \\
&\quad - 4\,(1 - f_{\mathrm{L}}f_{\mathrm{R}})^2\,\Gamma_{\mathrm{L}}\Gamma_{\mathrm{R}} - 2\,(f_{\mathrm{L}} - f_{\mathrm{R}})^2\,\Gamma_{\mathrm{L}}\Gamma_{\mathrm{R}}\,\cos\varphi \Big]
\end{aligned}
\tag{B.1}
$$

$$
\begin{aligned}
p_1^{(0)} = \frac{4}{D}\, &\left((1 - f_{\mathrm{L}})\,\Gamma_{\mathrm{L}} + (1 - f_{\mathrm{R}})\,\Gamma_{\mathrm{R}} \right) \cdot \\
&\cdot \Big[(1 + f_{\mathrm{L}})^2\,(-f_{\mathrm{R}} - f_{\mathrm{L}} + 2\,f_{\mathrm{L}}f_{\mathrm{R}})\,\Gamma_{\mathrm{L}}^2 + (1 + f_{\mathrm{R}})^2\,(-f_{\mathrm{R}} - f_{\mathrm{L}} + 2\,f_{\mathrm{L}}f_{\mathrm{R}})\,\Gamma_{\mathrm{R}}^2 \\
&\quad + 2\,(-1 + f_{\mathrm{L}}f_{\mathrm{R}})\,(f_{\mathrm{L}} + f_{\mathrm{R}} + 2\,f_{\mathrm{L}}f_{\mathrm{R}})\,\Gamma_{\mathrm{L}}\Gamma_{\mathrm{R}} + 2\,(f_{\mathrm{L}} - f_{\mathrm{R}})^2\,\Gamma_{\mathrm{L}}\Gamma_{\mathrm{R}}\,\cos\varphi \Big]
\end{aligned}
\tag{B.2}
$$

$$
\begin{aligned}
p_{\mathrm{S}}^{(0)} = \frac{1}{D} \Big(& (f_{\mathrm{L}} - f_{\mathrm{R}}) \, (\Gamma_{\mathrm{L}} + \Gamma_{\mathrm{R}}) \left[- f_{\mathrm{L}} \, (1 + f_{\mathrm{L}}) \, \Gamma_{\mathrm{L}}^2 + f_{\mathrm{R}} \, (1 + f_{\mathrm{R}}) \, \Gamma_{\mathrm{R}}^2 + (f_{\mathrm{L}} - f_{\mathrm{R}}) \, \Gamma_{\mathrm{L}} \Gamma_{\mathrm{R}} \, \cos \varphi \right] \\
& + (f_{\mathrm{L}} \, \Gamma_{\mathrm{L}} + f_{\mathrm{R}} \, \Gamma_{\mathrm{R}}) \cdot \\
& \quad \cdot \left[(1 + f_{\mathrm{L}})^2 \, (-f_{\mathrm{R}} - f_{\mathrm{L}} + 2 \, f_{\mathrm{L}} f_{\mathrm{R}}) \, \Gamma_{\mathrm{L}}^2 + (1 + f_{\mathrm{R}})^2 \, (-f_{\mathrm{R}} - f_{\mathrm{L}} + 2 \, f_{\mathrm{L}} f_{\mathrm{R}}) \, \Gamma_{\mathrm{R}}^2 - \right. \\
& \quad \left. - 2 \, (1 - f_{\mathrm{L}} f_{\mathrm{R}}) \, (f_{\mathrm{L}} + f_{\mathrm{R}} + 2 \, f_{\mathrm{L}} f_{\mathrm{R}}) \, \Gamma_{\mathrm{L}} \Gamma_{\mathrm{R}} + 2 \, (f_{\mathrm{L}} - f_{\mathrm{R}})^2 \, \Gamma_{\mathrm{L}} \Gamma_{\mathrm{R}} \, \cos \varphi \right] \Big)
\end{aligned}
\tag{B.3}
$$

$$
\begin{aligned}
p_{\mathrm{T}}^{(0)} = \frac{3}{D} \Big(& (f_{\mathrm{L}} - f_{\mathrm{R}}) \, (\Gamma_{\mathrm{L}} + \Gamma_{\mathrm{R}}) \left[f_{\mathrm{L}} \, (1 + f_{\mathrm{L}}) \, \Gamma_{\mathrm{L}}^2 - f_{\mathrm{R}} \, (1 + f_{\mathrm{R}}) \, \Gamma_{\mathrm{R}}^2 - (f_{\mathrm{L}} - f_{\mathrm{R}}) \, \Gamma_{\mathrm{L}} \Gamma_{\mathrm{R}} \, \cos \varphi \right] \\
& + (f_{\mathrm{L}} \, \Gamma_{\mathrm{L}} + f_{\mathrm{R}} \, \Gamma_{\mathrm{R}}) \cdot \\
& \quad \cdot \left[(1 + f_{\mathrm{L}})^2 \, (-f_{\mathrm{R}} - f_{\mathrm{L}} + 2 \, f_{\mathrm{L}} f_{\mathrm{R}}) \, \Gamma_{\mathrm{L}}^2 + (1 + f_{\mathrm{R}})^2 \, (-f_{\mathrm{R}} - f_{\mathrm{L}} + 2 \, f_{\mathrm{L}} f_{\mathrm{R}}) \, \Gamma_{\mathrm{R}}^2 - \right. \\
& \quad \left. - 2 \, (1 - f_{\mathrm{L}} f_{\mathrm{R}}) \, (f_{\mathrm{L}} + f_{\mathrm{R}} + 2 \, f_{\mathrm{L}} f_{\mathrm{R}}) \, \Gamma_{\mathrm{L}} \Gamma_{\mathrm{R}} + 2 \, (f_{\mathrm{L}} - f_{\mathrm{R}})^2 \, \Gamma_{\mathrm{L}} \Gamma_{\mathrm{R}} \, \cos \varphi \right] \Big)
\end{aligned}
\tag{B.4}
$$

To represent the isospin components we choose the coordinate system like in the example in subsection 5.3.1.

$$
\begin{aligned}
I_x^{(0)} = -\frac{2}{D} \, (f_{\mathrm{L}} - f_{\mathrm{R}}) \, (\Gamma_{\mathrm{L}} + \Gamma_{\mathrm{R}}) \left[(1 - f_{\mathrm{L}}) \, \Gamma_{\mathrm{L}} + (1 - f_{\mathrm{R}}) \, \Gamma_{\mathrm{R}} \right] \\
\left[(1 + f_{\mathrm{L}}) \, \Gamma_{\mathrm{L}} - (1 + f_{\mathrm{R}}) \, \Gamma_{\mathrm{R}} \right] \, \cos(\varphi/2)
\end{aligned}
\tag{B.5}
$$

$$
\begin{aligned}
I_y^{(0)} = -\frac{1}{D} \, (f_{\mathrm{L}} - f_{\mathrm{R}}) \, (\Gamma_{\mathrm{L}} + \Gamma_{\mathrm{R}}) \left[(1 - f_{\mathrm{L}}) \, \Gamma_{\mathrm{L}} + (1 - f_{\mathrm{R}}) \, \Gamma_{\mathrm{R}} \right] \\
\left[(1 + f_{\mathrm{L}}) \, \Gamma_{\mathrm{L}} + (1 + f_{\mathrm{R}}) \, \Gamma_{\mathrm{R}} \right] \, \sin(\varphi/2)
\end{aligned}
\tag{B.6}
$$

$$
I_z^{(0)} \equiv 0
\tag{B.7}
$$

The general denominator D is given by the determinant of a matrix which can be obtained from the kernel $\mathbf{W}$ by exchanging one of the (necessarily) linear dependent rows by the normalization condition $\operatorname{tr} \rho = 1$,

$$
\begin{aligned}
D = \; & - (1 + f_{\mathrm{L}}) \left[2 + f_{\mathrm{L}} \, (1 + f_{\mathrm{L}})^2 + f_{\mathrm{R}} \, (3 - 2 \, f_{\mathrm{L}} - 5 \, f_{\mathrm{L}}^2 + 2 \, f_{\mathrm{L}}^4) \right] \Gamma_{\mathrm{L}}^3 - \\
& - (1 + f_{\mathrm{L}}) \left[3 \, (2 + f_{\mathrm{L}}) + f_{\mathrm{R}} \, (9 + f_{\mathrm{R}}) - f_{\mathrm{R}} f_{\mathrm{L}} \, (2 + 7 \, f_{\mathrm{R}}) + (1 + f_{\mathrm{R}}) \, (1 - 6 \, f_{\mathrm{R}}) \, f_{\mathrm{L}}^2 \right] \Gamma_{\mathrm{L}}^2 \Gamma_{\mathrm{R}} - \\
& - (1 + f_{\mathrm{R}}) \left[3 \, (2 + f_{\mathrm{R}}) + f_{\mathrm{L}} \, (9 + f_{\mathrm{L}}) - f_{\mathrm{L}} f_{\mathrm{R}} \, (2 + 7 \, f_{\mathrm{L}}) + (1 + f_{\mathrm{L}}) \, (1 - 6 \, f_{\mathrm{L}}) \, f_{\mathrm{R}}^2 \right] \Gamma_{\mathrm{L}} \Gamma_{\mathrm{R}}^2 - \\
& - (1 + f_{\mathrm{R}}) \left[2 + f_{\mathrm{R}} \, (1 + f_{\mathrm{R}})^2 + f_{\mathrm{L}} \, (3 - 2 \, f_{\mathrm{R}} - 5 \, f_{\mathrm{R}}^2 + 2 \, f_{\mathrm{R}}^4) \right] \Gamma_{\mathrm{R}}^3 + \\
& + 2 \, (f_{\mathrm{L}} - f_{\mathrm{R}})^2 \left[(2 + f_{\mathrm{L}}) \, \Gamma_{\mathrm{L}} + (2 + f_{\mathrm{R}}) \, \Gamma_{\mathrm{R}} \right] \Gamma_{\mathrm{L}} \Gamma_{\mathrm{R}} \, \cos \varphi \, .
\end{aligned}
\tag{B.8}
$$

Appendix C

Calculation of Second Order Diagrams

Every integral of a second order diagram belongs to one of the following types:

$$
\begin{aligned}
I_1 &:= \iint_{-\infty}^{\infty} d\omega \, d\omega' \, \frac{f_r^\tau(\omega) \, f_{r'}^{\tau'}(\omega')}{(\sigma\omega + \Delta_1 + i\eta)(\sigma\omega + \sigma'\omega' + \Delta_{12} + i\eta)(\sigma'\omega' + \Delta_2 + i\eta)} \\
&= \iint_{-\infty}^{\infty} d\omega \, d\omega' \, \frac{f_r^\tau(\sigma\omega) \, f_{r'}^{\tau'}(\sigma'\omega')}{(\omega + \Delta_1 + i\eta)(\omega + \omega' + \Delta_{12} + i\eta)(\omega' + \Delta_2 + i\eta)}
\end{aligned}
\tag{C.1}
$$

$$
\begin{aligned}
I_2 &:= \iint_{-\infty}^{\infty} d\omega \, d\omega' \, \frac{f_r^\tau(\omega) \, f_{r'}^{\tau'}(\omega')}{(\sigma'\omega' + \Delta_2' + i\eta)(\sigma\omega + \sigma'\omega' + \Delta_{12} + i\eta)(\sigma'\omega' + \Delta_2 + i\eta)} \\
&= \iint_{-\infty}^{\infty} d\omega \, d\omega' \, \frac{f_r^\tau(\sigma\omega) \, f_{r'}^{\tau'}(\sigma'\omega')}{(\omega' + \Delta_2' + i\eta)(\omega + \omega' + \Delta_{12} + i\eta)(\omega' + \Delta_2 + i\eta)}
\end{aligned}
\tag{C.2}
$$

with $\sigma, \sigma', \tau, \tau' \in \{+1, -1\}$ and the Fermi functions

$$
f_r^\tau(\omega) := f^\tau(\omega, \mu_r) :=
\begin{cases}
f^+(\omega, \mu_r) := (\exp[\beta(\omega - \mu_r)] + 1)^{-1} & \text{for } \tau = +1 \\
f^-(\omega, \mu_r) := 1 - f^+(\omega, \mu_r) & \text{for } \tau = -1
\end{cases}
\tag{C.3}
$$

for which obviously $f^\tau(\omega, \mu_r) = f^+(\tau\omega, \tau\mu_r)$. In the following we will also use the Bose function $b(x) := (\exp[\beta(\omega - \mu_r)] - 1)^{-1}$ to rewrite a product of Fermi functions

$$
f^\tau(\omega, \mu) \, f^{\tau'}(\omega', \mu') = \delta_{-\tau, \tau'} \, f^\tau(\omega, \mu) + \tau\tau' \, f^\tau(\omega, \mu) +
$$

$$
+ \begin{cases}
\dfrac{\tau'}{\beta} \dfrac{\partial}{\partial \omega} f^\tau(\omega, \mu) & \text{for } \omega - \mu = \omega' - \mu' \\
\tau\tau' \, b(\tau[(\omega - \mu) - (\omega' - \mu')]) \, (f^\tau(\omega, \mu) - f^\tau(\omega', \mu')) & \text{else} .
\end{cases}
\tag{C.4}
$$

The idea is to put all relevant integral terms down to combinations (and maybe functionals) of principal value integrals of the form

$$\fint \frac{\mathrm{d}\omega}{\omega - \varepsilon}\, f_r^\tau(\omega) = \mathrm{Re}\left(-\int \mathrm{d}\omega\, \frac{f_r^\tau(\omega)}{\varepsilon - \omega + \mathrm{i}\eta} \right) . \tag{C.5}$$

and its derivatives. Since the integrand in Eq. C.5 does not decay quickly enough at the boundaries we introduce a smooth cutoff function

$$D_r(\omega) := \frac{D^2}{(\omega - \mu_r)^2 + D^2} \tag{C.6}$$

with the cutoff energy D for an approximate calculation

$$\int_{-\infty}^{\infty} \mathrm{d}\omega\, \frac{f_r^\tau(\omega)}{\varepsilon - \omega + \mathrm{i}\eta} \approx \int_{-\infty}^{\infty} \mathrm{d}\omega\, D_r(\omega)\, \frac{f_r^\tau(\omega)}{\varepsilon - \omega + \mathrm{i}\eta} =$$

$$= D_r(\varepsilon)\left[\tau\,\psi\left(\frac{1}{2} + \frac{\beta D}{2\pi}\right) - \tau\,\mathrm{Re}\left[\psi\left(\frac{1}{2} + \frac{\mathrm{i}\beta(\varepsilon - \mu_r)}{2\pi}\right) \right] + \pi\,\frac{\varepsilon - \mu_r}{2\,D} - \mathrm{i}\pi\, f_r^\tau(\varepsilon) \right] \tag{C.7}$$

with the Digamma function ψ. For a large cutoff energy, $D \gg \varepsilon, k_\mathrm{B}T, \mu_r$, we can approximate further

$$\fint \frac{\mathrm{d}\omega}{\omega - \varepsilon}\, f_r^\tau(\omega) \approx -\tau\,\ln\frac{\beta\,D}{2\pi} + \tau\,\mathrm{Re}\left[\psi\left(\frac{1}{2} + \frac{\mathrm{i}\beta(\varepsilon - \mu_r)}{2\pi}\right) \right] . \tag{C.8}$$

The derivatives can be calculated analogously

$$\frac{\partial^n}{\partial\varepsilon^n} \fint \frac{\mathrm{d}\omega}{\omega - \varepsilon}\, f_r^\tau(\omega) = \mathrm{Re}\left[\left(\frac{\mathrm{i}\beta}{2\pi}\right)^n \psi^{(n)}\left(\frac{1}{2} + \frac{\mathrm{i}\beta(\varepsilon - \mu_r)}{2\pi}\right) \right] \tag{C.9}$$

for $n > 0$ with the polygamma functions $\psi^{(n)}$.

In general, integrals of type I_1 and I_2 consist of a real part and an imaginary part. However, in many cases it is only the imaginary part which is important for the calculation of the kernel. The elements $W_{\chi\chi'}^{\chi\chi'}$, for instance, which correspond to the diagonal terms of the density matrix, contain only imaginary parts of diagrams, due to the mirror rule. If the transition functions $\gamma_{ii'r\sigma}^\pm$ are real, the imaginary part of the integrals is sufficient to determine $W_{\chi\chi'}^{\chi\chi'}$.

An example in which the full integrals have to be taken into account is the Aharonov-Bohm interferometer with embedded quantum dots. For this setup we necessarily have to calculate kernels corresponding to offdiagonal terms of the density matrix. Furthermore, the transition functions can not be gauged to be real. Thus, there are several convenient simplifications which can not be applied a priori, but some of them help a lot during the calculations.

However, it turns out that the real parts of all second order integrals can be expressed, after some algebra, by a combination of terms which stem from integrals of delta functions

and terms which can be reduced to the form of a polygamma function, a product of polygamma functions or a principal value integral of a polygamma function (sometimes additional Fermi functions enter the integrand or factors of logarithms might appear from the cutoff).

In the following we give explicit representations of the usually more important imaginary parts of the integrals I_1 and I_2. Two case can be distinguished for each of them,

$$
\begin{array}{llll}
\text{1a)} & \Delta_1 + \Delta_2 = \Delta_{12} & \text{2a)} & \Delta_2 = \Delta_2' \\
\text{1b)} & \Delta_1 + \Delta_2 \neq \Delta_{12} & \text{2b)} & \Delta_2 \neq \Delta_2' \,.
\end{array}
\tag{C.10}
$$

The imaginary part of integral 1a) can be rewritten in the form

$$
\begin{aligned}
\mathrm{Im}\,(I_{1a}) &= \mathrm{Im}\left[\iint_{-\infty}^{\infty} \mathrm{d}\omega\,\mathrm{d}\omega'\, \frac{f_r^\tau(\sigma\omega)\,f_{r'}^{\tau'}(\sigma'\omega')}{(\omega + \omega' + \Delta_{12} + i\eta)^2}\left(\frac{1}{\omega + \Delta_1 + i\eta} + \frac{1}{\omega' + \Delta_2 + i\eta}\right)\right] \\
&= \mathrm{Im}\left[\iint_{-\infty}^{\infty} \mathrm{d}\omega\,\mathrm{d}\omega'\, \frac{f_r^\tau(\sigma\omega)\,f_{r'}^{\tau'}(\sigma'\omega')}{(\omega + \Delta_1 + i\eta)^2}\left(\frac{1}{\omega' + \Delta_2 + i\eta} - \frac{1}{\omega + \omega' + \Delta_{12} + i\eta}\right)\right] \\
&= \cdots \\
&= \pi\left[-f^{\tau'}(-\sigma'\Delta_2, \mu_{r'}) \left.\frac{\partial}{\partial z}\right|_{z=0} \Xint- \frac{\mathrm{d}\omega}{\omega + \Delta_1 - z}\, f^{\sigma\tau}(\omega, \sigma\mu_r) - \right.\\
&\qquad - f^\tau(-\sigma\Delta_1, \mu_r) \left.\frac{\partial}{\partial z}\right|_{z=0} \Xint- \frac{\mathrm{d}\omega}{\omega + \Delta_2 - z}\, f^{\sigma'\tau'}(\omega, \sigma'\mu_{r'}) + \\
&\qquad + \frac{1 - \sigma\sigma'\tau\tau'}{2} \left.\frac{\partial}{\partial z}\right|_{z=0} \Xint- \frac{\mathrm{d}\omega}{\omega + \Delta_1 - z}\, f^{\sigma\tau}(\omega, \sigma\mu_r) - \\
&\qquad - \left\{\begin{array}{l} \dfrac{\sigma'\tau'}{\beta} \left.\dfrac{\partial^2}{\partial z^2}\right|_{z=0} \Xint- \dfrac{\mathrm{d}\omega}{\omega + \Delta_1 - z}\, f^{\sigma\tau}(\omega, \sigma\mu_r) \qquad \text{for} \quad -\Delta_{12} = \sigma\mu_r + \sigma'\mu_{r'} \\[3ex] \sigma\sigma'\tau\tau'\, b(\sigma\tau[-\Delta_{12} - (\sigma\mu_r + \sigma'\mu_{r'})]) \cdot \\ \qquad \cdot \left[\left.\dfrac{\partial}{\partial z}\right|_{z=0} \Xint- \dfrac{\mathrm{d}\omega}{\omega + \Delta_1 - z}\, f^{\sigma\tau}(\omega, \sigma\mu_r) - \right.\\ \qquad \left.\left. - \left.\dfrac{\partial}{\partial z}\right|_{z=0} \Xint- \dfrac{\mathrm{d}\omega}{\omega - \Delta_2 - z}\, f^{\sigma\tau}(\omega, -\sigma'\mu_{r'})\right] \qquad \text{else} \end{array}\right. \right]
\end{aligned}
\tag{C.11}
$$

For the imaginary part of integral 1b) we obtain

$$
\mathrm{Im}\,(I_{1\mathrm{b}}) = \mathrm{Im}\Bigg[\iint_{-\infty}^{\infty} \mathrm{d}\omega\,\mathrm{d}\omega' \, \frac{f_r^\tau(\sigma\omega)\,f_{r'}^{\tau'}(\sigma'\omega')}{\Delta_1 + \Delta_2 - \Delta_{12}} \,\cdot
$$

$$
\cdot \left(\frac{1}{\omega + \Delta_{12} - \Delta_2 + \mathrm{i}\eta} - \frac{1}{\omega + \Delta_1 + \mathrm{i}\eta} \right) \left(\frac{1}{\omega' + \Delta_2 + \mathrm{i}\eta} - \frac{1}{\omega + \omega' + \Delta_{12} + \mathrm{i}2\eta} \right) \Bigg]
$$

$$
= \cdots
$$

$$
= \frac{\pi}{\Delta_1 + \Delta_2 - \Delta_{12}} \,\cdot
$$

$$
\cdot \Bigg[f^{\tau'}(-\sigma'\Delta_2, \mu_{r'}) \left(\fint \frac{\mathrm{d}\omega}{\omega + \Delta_1} \, f^{\sigma\tau}(\omega, \sigma\mu_r) - \fint \frac{\mathrm{d}\omega}{\omega + \Delta_{12} - \Delta_2} \, f^{\sigma\tau}(\omega, \sigma\mu_r) \right) +
$$

$$
+ f^{\tau}(-\sigma\Delta_1, \mu_r) \left(\fint \frac{\mathrm{d}\omega}{\omega + \Delta_2} \, f^{\sigma'\tau'}(\omega, \sigma'\mu_{r'}) - \fint \frac{\mathrm{d}\omega}{\omega + \Delta_{12} - \Delta_1} \, f^{\sigma'\tau'}(\omega, \sigma'\mu_{r'}) \right) +
$$

$$
+ \frac{1 - \sigma\sigma'\tau\tau'}{2} \left(\fint \frac{\mathrm{d}\omega}{\omega + \Delta_{12} - \Delta_2} \, f^{\sigma\tau}(\omega, \sigma\mu_r) - \fint \frac{\mathrm{d}\omega}{\omega + \Delta_1} \, f^{\sigma\tau}(\omega, \sigma\mu_r) \right) -
$$

$$
- \begin{cases} \dfrac{\sigma'\tau'}{\beta} \dfrac{\partial}{\partial z}\Big|_{z=0} \left(\fint \dfrac{\mathrm{d}\omega}{\omega + \Delta_{12} - \Delta_2 - z} \, f^{\sigma\tau}(\omega, \sigma\mu_r) - \fint \dfrac{\mathrm{d}\omega}{\omega + \Delta_1 - z} \, f^{\sigma\tau}(\omega, \sigma\mu_r) \right) \\[4pt] \text{for} \quad -\Delta_{12} = \sigma\mu_r + \sigma'\mu_{r'} \\[16pt] \sigma\sigma'\tau\tau'\, b(\sigma\tau[-\Delta_{12} - (\sigma\mu_r + \sigma'\mu_{r'})])\,\cdot \\[4pt] \qquad \cdot \left[\left(\fint \dfrac{\mathrm{d}\omega}{\omega + \Delta_{12} - \Delta_2} \, f^{\sigma\tau}(\omega, \sigma\mu_r) - \fint \dfrac{\mathrm{d}\omega}{\omega + \Delta_1} \, f^{\sigma\tau}(\omega, \sigma\mu_r) \right) - \right. \\[4pt] \qquad \left. - \left(\fint \dfrac{\mathrm{d}\omega}{\omega - \Delta_2} \, f^{\sigma\tau}(\omega, -\sigma'\mu_{r'}) - \fint \dfrac{\mathrm{d}\omega}{\omega - \Delta_{12} + \Delta_1} \, f^{\sigma\tau}(\omega, -\sigma'\mu_{r'}) \right) \right] \\[4pt] \text{else} \end{cases}
$$

$$
\tag{C.12}
$$

Similar for the imaginary part of integral 2a)

$$\text{Im}\,(I_{2a}) = \text{Im}\left[\iint_{-\infty}^{\infty} d\omega\, d\omega'\, f_r^{\tau}(\sigma\omega)\, f_{r'}^{\tau'}(\sigma'\omega')\, \frac{1}{(\omega'+\Delta_2+i\eta)^2}\, \frac{1}{\omega+\omega'+\Delta_{12}+i\eta}\right]$$

$$= \cdots$$

$$= \pi\left[f^{\tau}(-\sigma\Delta_2,\mu_r)\, \frac{\partial}{\partial z}\bigg|_{z=0} \fint \frac{d\omega}{\omega+\Delta_{12}-\Delta_2-z}\, f^{\sigma'\tau'}(\omega,\sigma'\mu_{r'}) - \right.$$

$$- \frac{\partial}{\partial z}\bigg|_{z=0} f^{\tau}(-\sigma(\Delta_2-z),\mu_r)\, \fint \frac{d\omega}{\omega+\Delta_{12}-\Delta_2}\, f^{\sigma'\tau'}(\omega,\sigma'\mu_{r'}) -$$

$$- \frac{1-\sigma\sigma'\tau\tau'}{2}\, \frac{\partial}{\partial z}\bigg|_{z=0} \fint \frac{d\omega}{\omega+\Delta_2-z}\, f^{\sigma\tau}(\omega,\sigma\mu_r) +$$

$$+ \left\{ \begin{array}{l} \dfrac{\sigma'\tau'}{\beta}\, \dfrac{\partial^2}{\partial z^2}\bigg|_{z=0} \fint \dfrac{d\omega}{\omega+\Delta_2-z}\, f^{\sigma\tau}(\omega,\sigma\mu_r) \qquad \text{for} \quad -\Delta_{12}=\sigma\mu_r+\sigma'\mu_{r'} \\[2em] \sigma\sigma'\tau\tau'\, b(\sigma\tau[-\Delta_{12}-(\sigma\mu_r+\sigma'\mu_{r'})])\cdot \\[1em] \qquad \cdot\, \dfrac{\partial}{\partial z}\bigg|_{z=0} \fint \dfrac{d\omega}{\omega+\Delta_2-z}\, \big(f^{\sigma\tau}(\omega,\sigma\mu_r)-f^{\sigma\tau}(\omega+\Delta_{12},-\sigma'\mu_{r'})\big) \quad \text{else} \end{array} \right. \Bigg]$$

$$(\text{C.13})$$

Finally we can rewrite the imaginary part of integral 2b)

$$
\begin{aligned}
\mathrm{Im}\,(I_{2\mathrm{b}}) = \mathrm{Im}\Bigg[& \iint_{-\infty}^{\infty} \mathrm{d}\omega\,\mathrm{d}\omega'\, \frac{1}{\Delta_2 - \Delta_2'} \frac{f_r^{\tau}(\sigma\omega)\,f_{r'}^{\tau'}(\sigma'\omega')}{\omega + \omega' + \Delta_{12} + \mathrm{i}\eta} \left(\frac{1}{\omega' + \Delta_2' + \mathrm{i}\eta} - \frac{1}{\omega' + \Delta_2 + \mathrm{i}\eta} \right) \Bigg] \\
= & \cdots \\
= & \frac{\pi}{\Delta_2 + \Delta_2'} \cdot \\
& \cdot \Bigg[-\left\{ f^{\tau}(-\sigma\Delta_2', \mu_r) \,\rlap{\,/}\!\!\oint \frac{\mathrm{d}\omega}{\omega + \Delta_{12} - \Delta_2'}\, f^{\sigma'\tau'}(\omega, \sigma'\mu_{r'}) - \right. \\
& \qquad \left. - f^{\tau}(-\sigma\Delta_2, \mu_r) \,\rlap{\,/}\!\!\oint \frac{\mathrm{d}\omega}{\omega + \Delta_{12} - \Delta_2}\, f^{\sigma'\tau'}(\omega, \sigma'\mu_{r'}) \right\} - \\
& - \frac{1 - \sigma\sigma'\tau\tau'}{2} \left(\rlap{\,/}\!\!\oint \frac{\mathrm{d}\omega}{\omega + \Delta_2'}\, f^{\sigma\tau}(\omega, \sigma\mu_r) - \rlap{\,/}\!\!\oint \frac{\mathrm{d}\omega}{\omega + \Delta_2}\, f^{\sigma\tau}(\omega, \sigma\mu_r) \right) +
\end{aligned}
$$

$$
+ \begin{cases}
\dfrac{\sigma'\tau'}{\beta} \left.\dfrac{\partial}{\partial z}\right|_{z=0} \left(\rlap{\,/}\!\!\oint \dfrac{\mathrm{d}\omega}{\omega + \Delta_2' - z}\, f^{\sigma\tau}(\omega, \sigma\mu_r) - \rlap{\,/}\!\!\oint \dfrac{\mathrm{d}\omega}{\omega + \Delta_2 - z}\, f^{\sigma\tau}(\omega, \sigma\mu_r) \right) \\[4pt]
\text{for} \quad -\Delta_{12} = \sigma\mu_r + \sigma'\mu_{r'} \\[12pt]
\sigma\sigma'\tau\tau'\, b(\sigma\tau[-\Delta_{12} - (\sigma\mu_r + \sigma'\mu_{r'})]) \cdot \\[4pt]
\qquad \cdot \left[\left(\rlap{\,/}\!\!\oint \dfrac{\mathrm{d}\omega}{\omega + \Delta_2'}\, f^{\sigma\tau}(\omega, \sigma\mu_r) - \rlap{\,/}\!\!\oint \dfrac{\mathrm{d}\omega}{\omega + \Delta_2}\, f^{\sigma\tau}(\omega, \sigma\mu_r) \right) - \right. \\[4pt]
\qquad \left. - \left(\rlap{\,/}\!\!\oint \dfrac{\mathrm{d}\omega}{\omega + \Delta_2'}\, f^{\sigma\tau}(\omega + \Delta_{12}, -\sigma'\mu_{r'}) - \rlap{\,/}\!\!\oint \dfrac{\mathrm{d}\omega}{\omega + \Delta_2}\, f^{\sigma\tau}(\omega + \Delta_{12}, -\sigma'\mu_{r'}) \right) \right] \Bigg] \\[4pt]
\text{else}
\end{cases}
$$

$$
\tag{C.14}
$$

Bibliography

[1] M. A. Reed, J. N. Randall, R. J. Aggarwal, R. J. Matyi, R. M. Moore, and A. E. Wetsel, Phys. Rev. Lett. **60**, 535 (1988).

[2] Pictures from the group of J. Weis and K. v. Klitzing, MPI für Festkörperforschung, Stuttgart.

[3] D. V. Averin and K. K. Likharev, in *Mesoscopic Phenomena in Solids*, eds. B. L. Altshuler, P. A. Lee, and R. A. Webb, Elsevier (1991).

[4] *Single Charge Tunneling*, NATO ASI Series **294**, eds. H. Grabert and M. H. Devoret, Plenum Press (1992).

[5] G. Schön, in *Quantum Transport and Dissipation*, eds. T. Dittrich, P. Hänggi, G.-L. Ingold, B. Kramer, G. Schön, and W. Zwerger, Wiley-VCH (1998).

[6] P. W. Anderson, Phys. Rev. **124**, 41 (1961).

[7] D. V. Averin and A. A. Odintsov, Phys. Lett. A **140**, 251 (1989).

[8] J. Könemann, B. Kubala, J. König, and R. J. Haug, Phys. Rev. B **73**, 033313 (2006).

[9] J. Kondo, Progr. Theoret. Phys. (Kyoto) **32**, 37 (1964).

[10] D. C. Ralph and R. A. Buhrman, Phys. Rev. Lett. **72**,3401 (1994).

[11] D. Goldhaber-Gordon, H. Shtrikman, D. Mahalu, D. Abusch-Magder, U. Meirav, and M. A. Kastner, Nature **391**, 156 (1998).

[12] D. Goldhaber-Gordon, G. Göres, M. A. Kastner, H. Shtrikman, D. Mahalu, and U. Meirav, Phys. Rev. Lett. **81**, 5225 (1998).

[13] S. M. Cronenwett, T. H. Oosterkamp, and L. P. Kouwenhoven, Science **281**, 540 (1998).

[14] J. Schmid, J. Weis, K. Eberl, and K. v. Klitzing, Physica B **256-258**, 375 (1998).

[15] F. Simmel, R. H. Blick, J. P. Kotthaus, W. Wegscheider, and M. Bichler, Phys. Rev. Lett. **83**, 804 (1999).

[16] P. Joyez, V. Bouchiat, D. Esteve, C. Urbina, and M. H. Devoret, Phys. Rev. Lett. **79**, 1349 (1997).

[17] J. R. Schrieffer and P. A. Wolff, Phys. Rev. **149**, 491 (1966).

[18] P. Fulde, *Electron Correlations in Molecules and Solids*, Springer Series in Solid-State Sciences, 2nd edition (1993).

[19] A. C. Hewson, *The Kondo Problem to Heavy Fermions*, Cambridge Studies in Magnetism, (1993).

[20] Y. M. Blanter and M. Büttiker, Phys. Rep. **336**, 1 (2000).

[21] R. Landauer. IBM J. Res. Dev. **1**, 233 (1957).

[22] R. Landauer, Philos. Mag. **21**, 863 (1970).

[23] M. Büttiker, Y. Imry, R. Landauer, and S. Pinhas, Phys. Rev. B **31**, 6207 (1985).

[24] Y. Gefen, Y. Imry, and M. Ya. Azbel, Phys. Rev. Lett. **52**, 129 (1984).

[25] M. Büttiker, Phys. Rev. Lett. **57**, 1761 (1986).

[26] M. Büttiker, Phys. Rev. B **46**, 12485 (1992).

[27] Y. M. Blanter and M. Büttiker, Phys. Rep. **336**, 1 (2000).

[28] D. V. Averin and Y. V. Nazarov, Phys. Rev. Lett. **65**, 2446 (1990).

[29] D. V. Averin and Y. V. Nazarov, in *Single Charge Tunneling*, NATO ASI Series **294**, eds. H. Grabert and M. H. Devoret, Plenum Press (1992).

[30] H. Schoeller and G. Schön, Phys. Rev. B **50**, 18436 (1994).

[31] J. König, H. Schoeller, and G. Schön, Europhys. Lett. **31**, 31 (1995).

[32] J. König, H. Schoeller, and G. Schön, Phys. Rev. Lett. **76**, 1715 (1996).

[33] J. König, J. Schmid, H. Schoeller, and G. Schön, Phys. Rev. B **54**, 16820 (1996).

[34] H. Schoeller, in *Mesoscopic Electron Transport*, eds. L. L. Sohn, L. P. Kouwenhoven and G. Schön, NATO ASI Series E **345**, 291, Kluwer (1997); H. Schoeller, Habilitation.

[35] J. König, *Quantum Fluctuations in the Single-Electron Transistor*, Shaker (1999).

[36] L. V. Keldysh, Zh. Eksp. Teor. Fiz. **47**, 1515 (1965); Sov. Phys. JETP **20**, 1018 (1965).

[37] G. D. Mahan, *Many-Particle Physics*, Plenum Press, New York (1990).

[38] J. Rammer and H. Smith, Rev. Mod. Phys. **58**, 323 (1986).

[39] Y. Meir and N. S. Wingreen, Phys. Rev. Lett. **68**, 2512 (1992).

[40] T. V. Shahbazyan and M. E. Raikh, Phys. Rev. B **49**, 17123 (1994).

[41] A. W. Holleitner, C. R. Decker, H. Qin, K. Eberl, and R. H. Blick, Phys. Rev. Lett. **87**, 256802 (2001).

[42] M. Sigrist, T. Ihn, K. Ensslin, D. Loss, M. Reinwald, and W. Wegscheider, Phys. Rev. Lett. **96**, 036804 (2006).

[43] N. J. Craig, J. M. Taylor, E. A. Lester, C. M. Marcus, M. P. Hanson, and A. C. Gossard, Science **304**, 565 (2004).

[44] S. Legel, J. König, G. Burkard, and G. Schön, Phys. Rev. B **76**, 085335 (2007).

[45] A. Einstein, B. Podolsky, N. Rosen, Phys. Rev. **47**, 777 (1935), reprinted in *Quantum Theory and Measurement*, edited by J. A. Wheeler and W. Z. Zurek, Princeton University Press, Princeton (1983).

[46] C. H. Bennett and D. P. DiVincenzo, Nature **404**, 247 (2000).

[47] N. Gisin, G. Ribordy, W. Tittel, and H. Zbinden , Rev. Mod. Phys. **74**, 145 (2002).

[48] J. R. Petta, A. C. Johnson, J. M. Taylor, E. A. Laird, A. Yacoby, M. D. Lukin, C. M. Marcus, M. P. Hanson, and A. C. Gossard, Science **309**, 2180 (2005).

[49] F. H. L. Koppens, C. Buizert, K. J. Tielrooij, I. T. Vink, K. C. Nowack, T. Meunier, L. P. Kouwenhoven, and L. M. K. Vandersypen, Nature **442**, 766 (2006).

[50] G. Burkard, D. Loss, and E. V. Sukhorukov, Phys. Rev. B **61**, R16303 (2000).

[51] G. Burkard and D. Loss, Phys. Rev. Lett. **91**, 087903 (2003).

[52] J. M. Kikkawa, I. P. Smorchkova, N. Samarth, and D. D. Awschalom, Science **277**, 1284 (1997).

[53] J. M. Kikkawa and D. D. Awschalom, Phys. Rev. Lett. **80**, 4313 (1998).

[54] D. D. Awschalom and J. M. Kikkawa, Phys. Today **52**(6), 33 (1999).

[55] G. B. Lesovik, T. Martin, and G. Blatter, Eur. Phys. J. B **24**, 287 (2001).

[56] P. Recher and D. Loss, Phys. Rev. B **65**, 165327 (2002).

[57] C. Bena, S. Vishveshwara, L. Balents, and M. P. A. Fisher, Phys. Rev. Lett. **89**, 037901 (2002).

[58] P. Recher, E. V. Sukhorukov, and D. Loss, Phys. Rev. B **63**, 165314 (2001).

[59] M. Blaauboer and D.P. DiVincenzo, Phys. Rev. Lett. **95**, 160402 (2005).

[60] W. D. Oliver, F. Yamaguchi, and Y. Yamamoto, Phys. Rev. Lett. **88**, 037901 (2002).

[61] D. S. Saraga and D. Loss, Phys. Rev. Lett. **90**, 166803 (2003).

[62] A. T. Costa and S. Bose, Phys. Rev. Lett. **87**, 277901 (2001); F. Ciccarello, G. M. Palma, M. Zarcone, Y. Omar, and V. R. Vieira, J. Phys. A: Math. Theor. **40**, 7993 (2007).

[63] J. S. Bell, Physics **1**, 195 (1964).

[64] J. F. Clauser, M. A. Horne, A. Shimony, and R. A. Holt, Phys. Rev. Lett. **23**, 880 (1969).

[65] V. Vedral and M. Plenio, Phys. Rev. A **57**, 1619 (1998).

[66] P. Horodecki, Phys. Lett. A **232**, 233 (1997).

[67] P. Horodecki, in *Quantum Information*, eds. G. Alber, T. Beth, M. Horodecki, P. Horodecki, R. Horodecki, M. Rötteler, H. Weinfurter, R. Werner, and A. Zeilinger, Springer (2001)

[68] R. F. Werner, Phys. Rev. A, **40**, 4277 (1989).

[69] S. Hill and W. K. Wootters, Phys. Rev. Lett. **78**, 5022 (1997).

[70] N. Gisin, Phys. Lett. A **154**, 201 (1991)

[71] W. K. Wootters, Phys. Rev. Lett. **80**, 2245 (1998).

[72] C. H. Bennett, D. P. DiVincenzo, J. A. Smolin, and W. K. Wootters, Phys. Rev. A **54**, 3824 (1996).

[73] N. Linden, S. Massar, and S. Popescu, Phys. Rev. Lett. **81**, 3279 (1998).

[74] F. Verstraete and M. M. Wolf, Phys. Rev. Lett. **89**, 170401 (2002).

[75] F. H. L. Koppens, J. A. Folk, J. M. Elzerman, R. Hanson, L. H. Willems van Beveren, I. T. Vink, H. P. Tranitz, W. Wegscheider, L. P. Kouwenhoven, and L. M. K. Vandersypen, Science **309**, 1346 (2005).

[76] Y. Aharonov and D. Bohm, Phys. Rev. **115**, 485 (1959).

[77] Y. Imry, *Introduction to Mesoscopic Physics*, Oxford University Press, New York (1997).

[78] H. Akera, Phys. Rev. B **47**, 6835 (1993).

[79] A. Yacoby, M. Heiblum, D. Mahalu, and H. Shtrikman, Phys. Rev. Lett. **74**, 4047 (1995).

[80] A. L. Yeyati and M. Büttiker, Phys. Rev. B **52**, R14360 (1995).

[81] G. Hackenbroich and H. A. Weidenmüller, Phys. Rev. Lett. **76**, 10 (1996).

[82] C. Bruder, R. Fazio, and H. Schoeller, Phys. Rev. Lett. **76**, 114 (1996).

[83] Y. Oreg and Y. Gefen, Phys. Rev. B **55**, 13726 (1997).

[84] R. Schuster, E. Buks, M. Heiblum, D. Mahalu, V. Umansky, and H. Shtrikman, Nature **385**, 417 (1997).

[85] W. Izumida, O. Sakai, and Y. Shimizu, J. Phys. Soc. Jpn. **66**, 717 (1997).

[86] E. Buks, R. Schuster, M. Heiblum, D. Mahalu, and V. Umansky, Nature **391**, 871 (1998).

[87] D. Goldhaber-Gordon, H. Shtrikman, D. Mahalu, D. Abusch-Magder, U. Meirav, and M. A. Kastner, Nature **391**, 156 (1998).

[88] R. Baltin, Y. Gefen, G. Hackenbroich, and H. A. Weidenmüller, Eur. Phys. J. B **10**, 119 (1999).

[89] Y. Ji, M. Heiblum, D. Sprinzak, D. Mahalu, and H. Shtrikman, Science **290**, 779 (2000).

[90] W. G. van der Wiel, S. De Franceschi, T. Fujisawa, J. M. Elzerman, S. Tarucha, and L. P. Kouwenhoven, Science **289**, 2105 (2000).

[91] D. Loss and E. V. Sukhorukov, Phys. Rev. Lett. **84**, 1035 (2000).

[92] U. Gerland, J. v. Delft, T. A. Costi, and Y. Oreg, Phys. Rev. Lett. **84**, 3710 (2000).

[93] P. G. Silvestrov and Y. Imry, Phys. Rev. Lett. **85**, 2565 (2000).

[94] K. Kang and S. C. Shin, Phys. Rev. Lett. **85**, 5619 (2000).

[95] D. Boese, W. Hofstetter, and H. Schoeller, Phys. Rev. B **64**, 125309 (2001).

[96] J. König and Y. Gefen, Phys. Rev. Lett. **87**, 156803 (2001).

[97] W. Hofstetter, J. König, and H. Schoeller, Phys. Rev. Lett. **87**, 156803 (2001).

[98] J. König and Y. Gefen, Phys. Rev. B **65**, 045316 (2002).

[99] K. Kobayashi, H. Aikawa, S. Katsumoto, and Y. Iye, Phys. Rev. Lett. **88**, 256806 (2002).

[100] Y. Yi, M. Heiblum, and S. Shtrikman, Phys. Rev. Lett. **88**, 076601 (2002)

[101] B. Kubala and J. König, Phys. Rev. B **65**, 245301 (2002).

[102] B. Kubala and J. König, Phys. Rev. B **67**, 205303 (2003).

[103] M. Sigrist, A. Fuhrer, T. Ihn, K. Ensslin, S. E. Ulloa, W. Wegscheider, and M. Bichler, Phys. Rev. Lett. **93**, 066802 (2004).

[104] Z. Jiang, Q. Sun, X. C. Xie, and Y. Wang, Phys. Rev. Lett. **93**, 076802 (2004).

[105] Z. Jiang, Q. F. Sun, X. C. Xie, and Y. P. Wang, Phys. Rev. Lett. **94**, 179702 (2005).

[106] I. Weymann, J. König, J. Martinek, J. Barnaś, and G. Schön, Phys. Rev. B **72**, 113301 (2005).

[107] A. Hübel, J. Weis, W. Dietsche, and K. v. Klitzing, Appl. Phys. Lett. **91**, 102101 (2007).

[108] A. Hübel, J. Weis, and K. v. Klitzing, unpublished.

[109] T. Pohjola, H. Schoeller, and G. Schön, Europhys. Lett. **54**, 241 (2001).

[110] L. Borda, G. Zaránd, W. Hofstetter, B. Halperin, and J. v. Delft, Phys. Rev. Lett. **90**, 026602 (2003).

[111] A. W. Holleitner, A. Chudnovskiy, D. Pfannkuche, K. Eberl, and R. H. Blick, Phys. Rev. B **70**, 075204 (2004).

[112] D. T. McClure, L. DiCarlo, Y. Zhang, H.-A. Engel, and C. M. Marcus, Phys. Rev. Lett. **98**, 056801 (2007).

[113] A. Hübel, personal communication and yet unpublished data plots.

[114] S. Haupt and M. Hettler, unpublished.

[115] K. Held, A. Hübel, and J. Weis, unpublished.

Publications and Talks

Parts of this thesis have been published previously, are submitted, or are planned to be published elsewhere. Many results and intermediate working progress have been presented on conferences, workshops and schools on posters and in talks.

Publications

- S. Legel, J. König, G. Burkard, and G. Schön, *Generation of spin entanglement in nonequilibrium quantum dots*, Phys. Rev. B **76**, 085335 (2007).

- S. Legel, J. König, and G. Schön, *Generation and detection of spin entanglement in nonequilibrium quantum dots*, cond-mat/0712.3016, submitted to New Journal of Physics.

- S. Legel, J. König, and G. Schön, *Aharonov-Bohm interferometry with nonequilibrium quantum dots with on-site Coulomb interaction*, in preparation.

Talks

- S. Legel, J. König, and G. Schön, *Kohärenter und korrelierter Elektronentransport in Quantenpunkt Systemen mit gemeinsamen bzw. mehreren Zuleitungen*, Statusworkshop des Kompetenznetzes Funktionelle Nanostrukturen, Bad Herrenalb, September 2005.

- S. Legel, J. König, and G. Schön, *Aharonov-Bohm Interferometry with Quantum Dots*, DPG Frühjahrstagung, Dresden, March 2006.

- S. Legel, J. König, G. Burkard, and G. Schön, *Generation of Entanglement in Nonequilibrium Quantum Dots*, DPG Frühjahrstagung, Regensburg, March 2007.

- S. Legel, J. König, G. Burkard, and G. Schön, *Verschränkung von Elektronen als Nichtgleichgewichtseffekt in kohärent gekoppelten Quantenpunkten*, Statusworkshop des Kompetenznetzes Funktionelle Nanostrukturen, Bad Herrenalb, September 2007.

Acknowledgments

I would like to thank all the people who have contributed to this thesis in one or the other way.

At first, I would like to thank Gerd Schön for giving me the opportunity to work in his group. I am grateful for the advice, the support and the freedom I could enjoy during my time in Karlsruhe. I appreciate the promotion for attending conferences, workshops and scientific schools.

I sincerely thank Jürgen König for refereeing this thesis. Much more I have to thank for his support during the last years, for our collaboration, ,for many questions and answers.

Furthermore, I want to acknowledge many fruitful discussions with Dmitry Bagrets, Alessandro Braggio, Matthias Braun, Guido Burkard, Juan Carlos Cuevas, Göran Johansson, Elsa Prada, Pablo San Jose, Axel Thielmann, Daniel Urban, and Janne Viljas. In particular, I profited a lot from exchanging ideas with Jasmin Aghassi and Björn Kubala about our work and technical implementations of our calculations.

I also wish to thank Alexander Hübel and Jürgen Weis for interesting discussions and the collaboration within the Kompetenznetz Funktionelle Nanostrukturen.

The nice atmosphere and many debates which vitally enriched every day would not have been possible without my office mates Valentina Brosco, Tomas Löfwander, Michael Marthaler, Jan Martinek and Yasuhiro Utsumi.

I owe special thanks to Andreas Poenicke and Tobias Ulbricht for their commitment and invaluable help in any computer-related question.

Since I can not list all people who I would like to acknowledge at this place, it is the people of the TFP and the TKM who create the frame for a pleasant working atmosphere.

Moreover, I would like to take the opportunity to thank Michael Haefner, Ken-Ichiro Imura and Andreas Poenicke for some nice trips within Karlsruhe and its vicinity, their friendship, and all those things like Bratäpfel etc..

Finally I would like to thank my family and my friends for their trust and support throughout the years and especially Sandra for all the above, her endurance and the perfect wave.